2020-01-17

Laboratory Investigation of High Pressure Air Injection (HPAI) in a Dolomite Reservoir Core

Ruteaga-Romero, Selene

UNIVERSITY OF CALGARY

Laboratory Investigation of High-Pressure Air Injection (HPAI) in a Dolomite Reservoir Core

by

Selene Ruteaga Romero

A THESIS

SUBMITTED TO THE FACULTY OF GRADUATE STUDIES

IN PARTIAL FULFILMENT OF THE REQUIREMENTS FOR THE

DEGREE OF MASTER OF SCIENCE

GRADUATE PROGRAM IN CHEMICAL AND PETROLEUM ENGINEERING

CALGARY, ALBERTA

JANUARY, 2020

ABSTRACT

In this thesis an Enhanced Oil Recovery (EOR) process is presented, using thermal recovery by High Pressure Air Injection (HPAI) on a Mexican light oil reservoir. The main difference between HPAI and In Situ Combustion (ISC) is that the latter term is used to refer to air injection-based processes in heavy oil reservoirs, which require operation in the high temperature range (+350°C), for successful displacement of the oil by the oxidation zone. HPAI implies air injection into deep, light oil reservoirs, for which bond scission or combustion reactions are dominant in the 150 to 300°C or Low Temperature Range (LTR).

Two combustion tube tests were performed and analyzed, with the goal to evaluate the physical, chemical (kinetics) and fluid flow process behavior, as well as the rock and oil system's combustion characteristics, in a way to determine if this type of EOR would be suitable for the target reservoir, which is a Naturally Fractured Reservoir (NFR). The combustion tube tests were operated at the actual reservoir conditions of 2,213 psia (15.26 MPa) pressure and at the native temperature of 149°C with an air injection flux of 30 m3(ST)/m2h. For both tests, dolomite core plugs pre-saturated with dead oil were placed at specific intervals in the recombined core pack.

Currently, Mexico is starting to consider HPAI as an EOR in some of its reservoirs. Combustion tube tests are a method measuring the oil recovery, air requirement, fuel requirement and oxygen consumption. Such information is needed to design a field project and to estimate the economic parameter.

Based on the overall velocity of the combustion front, and produced gas composition history, there did not seen to be a strong effect on the burning performance between Test one which was initially fully saturated with liquids and Test two which had three different saturation regimes. The overall oil recovery based on the Original Oil in Place (OOIP) was 91.7% for Test one and 79.5% for Test two. For both tests, the oil saturation remaining in the core plugs was essentially zero.

ACKNOWLEDGMENTS

To my Parents, with whom I have always counted and whom always believe and encourage me, in all my dreams and goals. Thanks to their support and wise advice through my life. So, I am now able to accomplish this new success in my life. To my Father, who taught me how to solve problems beyond a narrow view, looking forward and questioning everything as an engineer should do. To my Mother, who taught me to be independent and a leader woman, to raise my voice and fight for my and your rights, where social success is to look for the wellness and equity of the majority instead of the minorities, to support the voice of my mates to be heard even though I am against their ideas, and to be the voice of those who are unlisten.

To my aunt Lilia, who sadly is no longer with us. She was a solid rock on my life, giving me love and advice, always cheered me up and prayed for me.

To Dr. Fluvio Ruiz and Dr. Alejandro Dieck, which always believed in my engineer talent and knowledge. They always encouraged me to grow professionally and without their support I would not be at this University.

To my friend Dr. Silvia Chávez, who was the main link between me and my supervisors, always helping me through the classes, providing the data required for the experiments and cheering me up through my home sickness.

To Dr. Sudarshan Mehta, which is a great and tough professor, but without his toughness I would not have been able to get out of my box. He always let me know I could count with him, and I hope to count with his mentoring and friendship for the rest of my life.

To Dr. Gordon Moore, who always guided me and helped me through my thesis. He always let me know that his door was open for me, giving me the confidence in myself, that does not matter how big a problem could be, between the both of us we would find a solution.

To Matthew Ursenbach, who always gave me a hand and with a lot of patience provided me the knowledge and guide that I required, to succeed in my calculations and experiments/tests. Without him this thesis would have not been accomplished.

To my friends Yolanda Villada, Luca Coppi, Patricia Apolinar and Thalia Hernández for all their encouragement.

To the In Situ Combustion Research Group at University of Calgary, for all the help and support provided to realize the experiments. In special to: Lucila Molinos, John Latino, Samuel F. Bartkiewicz and Mark Hancock, whom always helped me to reach successful experiments, and now more than co-workers are truly friends.

To CONACyT and PEMEX to sponsor my MSc at the University of Calgary, and hoping that it continues supporting and enriching the Mexican Talent.

INDEX

LIST OF FIGURES

LIST OF TABLES

LIST OF SYMBOLS AND ACRONYMS

AFR	Air/Fuel Ratio
A_r	Air Requirement
ARC	Accelerating Rate Calorimeter
BPR	Back Pressure Regulator
CHNS	Carbon, Hydrogen, Nitrogen and Sulfur
CT	Combustion Tube
DSC	Differential Scanning Calorimeter
DTA	Differential Thermal Analyzer
EGA	Effluent Gas Analysis
EOR	Enhanced Oil Recovery
F_r	Fuel Requirement
GC	Gas Chromatograph
GOR	Gas/Oil Ratio
H/C	Apparent Atomic Hydrogen to Carbon Ratio
HPAI	High Pressure Air Injection
HPHT	High Pressure and High Temperature
HPS	High Pressure Separator
HTO	High Temperature Oxidation
HTR	High Temperature Range
ILPC	Initial Liquid Production Collector
IS	Insufficient Sample
ISC	*In Situ* Combustion
ISCRG	*In Situ* Combustion Research Group
k	Absolute Permeability
k_i	Effective Permeability for Phase ***i***
k_{ri}	Relative Permeability for Phase ***i***
LPS	Low Pressure Separator
LTO	Low Temperature Oxidation

LTR	Low Temperature Range
∇P_i	Pressure Drop for Phase ***i***
μ_i	Viscosity for Phase ***i***
MFC	Mass flow Controller
MPF	Mesh Production Frac. Sand
MIF	Mesh Injection Frac. Sand
NFR	Naturally Fractured Reservoir
NS	No Sample was produced
NTGR	Negative Temperature Gradient Region
OOIP	Original Oil in Place
OS	Overflow Separator
PDSC	Pressurized Differential Scanning Calorimetry
PVT	Pressure – Volume – Temperature
q_i	Flux for phase ***i***
R	Oxygen/Nitrogen Ratio
RTO	Ramped Temperature Oxidation
SARA	Saturates, Aromatics, Resins and Asphaltenes
SI	International System of Units
ST	Standard Conditions (T = 15°C, Pressure = 101.325 KPa [1 standard atm])
TC	Centerline Thermocouple
TGA	Thermogravimetric Analyzer
TW	Wall Thermocouple
U	Air Flux
V_f	Burning Front Velocity
WTM	Wet Test Meter
Y	Fraction of Oxygen consumed/utilization

CHAPTER 1

INTRODUCTION

In this thesis an Enhanced Oil Recovery (EOR) process is presented, using thermal recovery by air injection/ *In Situ* Combustion (ISC), for reservoirs with light oil. The process is called High Pressure Air Injection (HPAI). The main topic of this thesis is the combustion tube tests performed on a Mexican light oil reservoir. As stated by Moore et al. 2002, HPAI is loosely defined as an EOR process, in which compressed air is injected into a high gravity, high pressure oil reservoir, with the expectation that the oxygen will react with a fraction of the reservoir oil, at an elevated temperature to produce flue gas. The produced flue gas usually comprises 10 to 14% CO_2, with the rest being N_2 primarily.

The air injection technique has been mainly used in reservoirs with conventional to heavy oil, Canada, Venezuela, USA, Rumania and India, or mature fields, where the heat generated by ISC is a necessary part of the recovery process. The major question is why this technique has not been implemented more in light oil reservoirs? It is due to a misconception that ISC is a thermal recovery process which is best suited for reducing oil viscosity, by increasing the temperature in the reservoir's oil. There is very little published data from combustion tube tests conducted at elevated pressures with light oil. Previous research has demonstrated that it is a very effective and efficient technique, when applied into deep light oil reservoirs with high pressure and high temperature, like exists in the Mexican target reservoir that is studied here. The process is simply initiated by injecting air, which will spontaneously ignite the Original Oil In Place (OOIP), due to the high temperature and pressure conditions in the reservoir.

To predict if this type of EOR would be successful in the field, it should be tested in the laboratory tests using a combustion tube and supporting thermal analysis tests. Experts for this type of EOR are associated in the *In Situ* Combustion Research Group (ISCRG) at University of Calgary, which have been doing research and applying the ISC and HPAI for 45 years. Currently, Mexico is starting to consider HPAI as an EOR in some of its reservoirs. In 2006 Mexico was the seventh largest oil producer in the world, producing 3.71 million barrels per day of petroleum products, of which 3.25 million barrels per day were crude oil. Mexican oil production has started to decline rapidly. The U.S. Energy Information Administration estimated that oil Mexican production would decline to 3.52 million barrels per day in 2007 and 3.32 million barrels per day in 2008 (Energy Information Administration et al. 2007).

Mexico was an important oil producer due to one of the biggest reservoirs (which used to be the second largest oil field worldwide) located in the South of the Gulf of Mexico, called Cantarell Field. This field started to be produced in 1979 and until 2007 most of the Mexican oil production came from it. In 1997 the National Oil Company (PEMEX) decided to start injecting nitrogen as a way to maintain the production. As a result, production increased from 1.1 million barrels per day in 1996 to 2.1 million barrels per day in 2004. After this date the production started to decline again in a dramatically way.

PEMEX is still seeking for ways to improve the oil production while more reservoirs are discovered. The combustion tube experiments reported in this thesis were performed using outcrop rock from a target field in the South of Mexico and light oil from the reservoir.

By 2014 the petroleum industry in Mexico made Mexico the eleventh largest producer of oil in the world and the thirteenth largest in terms of net exports. In 2019, Mexico has the twentieth largest oil reserves in the world, and it is the third largest oil producer in the Western Hemisphere behind the United States, Canada, and Brazil. (PEMEX et. al 2018)

Mexico produces three grades of crude oil: heavy, called Maya [<22°API] (accounting for more than half of the total production); light and low-sulfur, called Isthmus [34°API] (28% of production); and extra-light, called Olmeca [39°API] (20% of production) (Energy Information Administration et. al 2007).

The "South Zone" for PEMEX is comprised of the states of Chiapas, Tabasco, Campeche, Yucatán, Quintana Roo and the southern portions of Guerrero, Oaxaca and Veracruz. The target field in this thesis is located in Tabasco.

Mexico´s oil production by December 2018 and estimated reserves by January 2019 are shown in Tables 1.1 and 1.2. Pemex had divided Mexico in different zones/blocks for exploration and production. The field that was studied in this thesis belongs to what they called South Block which is the reason why only the reserves that belong to this zone/block are shown in Table 1.2.

Production [Units]	
Liquid and Condensates Hydrocarbons [10^3 bpd]	1,833
Gas [10^6 ft^3/d]	4,847

Source: Pemex Exploración y Producción at December 31st 2018

Table 1.1 Mexico´s Oil and Gas Production

	Crude Oil	Condensates	Dry Gas	Total
Total Reserves [10^6 barrels]	15,292	1,206	3,954	20,453
South Block	971	248	442	1,660
Proven Reserves [10^6 barrels]	5,333	453	1,224	7,010
South Block	611	158	279	1,048
Probable [10^6 barrels]	4,832	345	1,429	6,606
South Block	164	35	65	264
Possible [10^6 barrels]	5,128	408	1,300	6,837
South Block	196	54	98	348

Source: Pemex Exploración y Producción at January 1st 2019

Table 1.2 Mexico´s Reserves

In this thesis two combustion tube tests were operated and analyzed, with the goal to evaluate the physical, chemical (kinetics) and fluid flow process behavior, as well as the rock and oil system's combustion characteristics, in a way to determine if this type of EOR would be suitable for the target reservoir under the actual reservoir conditions. Combustion tubes are the traditional tool employed in the laboratories to investigate the performance of ISC processes. Combustion tubes are unscaled elemental physical simulators and represents a piece of the reservoir simulated at realistic temperatures and pressures in the laboratory with the constrains of one-dimensional flow (Prasad et al. 1986). Combustion tubes tests are a method for producing reliable data describing the ISC process, measuring the OOIP recovery at the start of the operation, air requirement, oxygen consumption and fuel requirement. Such information will help determine if the field project would be successful and which phenomena should be included in the ISC reservoir simulations and/or deserve additional research.

The performance prediction of the HPAI process in the field requires: 1) understanding of the physical and kinetic (chemical) reactions in the reservoir to determine the oil displacement efficiency in the portion of the reservoir that is swept by the combustion front, 2) understand displacement efficiency in the portions of the reservoir not swept by the combustion front, 3) type and conditions for the ignition, and 4) understanding how reservoir characteristics affects the overall EOR.

Other important aspect to be consider is the economic evaluation for any ISC project, which involves the cost of air compression. This factor was not studied in this thesis, because these are the first attempts to decide if HPAI is suitable with the reservoir under study. However, air is a low cost injectant and inside the reservoir air may be used as an agent of oxidation and heat release, pressurization, miscibility and gas stripping.

CHAPTER 2

LITERATURE REVIEW

2.1. IN SITU COMBUSTION (ISC)

It is also known as Air Injection or Fireflooding or High-Pressure Air Injection (HPAI), and it is an enhanced oil recovery process in which air is injected into an oil-bearing formation. This type of recovery involves the propagation of an energy generating reaction zone between oxygen and either original or modified fractions of the crude oil, which propagates through a reservoir so as to displace oil to production wells (Moore et al. 1988).

Oil is displaced by the resulting thermal front and combustion product gases. A small fraction of the oil and/or heavier components are burned as fuel by the advancing front. In some cases, water injection improves the energy efficiency and modifies the reaction kinetics. Normal, depleted or enriched air is injected as the oxidant (Mehta et al. 2018)

As reported by Mehta et al. (2018), dry combustion is not a true thermal process because oil is mobilized into the cold part of the reservoir.

2.2. THE COMBUSTION PROCESS

Enhanced Oil Recovery (EOR) by combustion is a method which provides energy and material transport through the porous media. The heat wave effectively reduces the viscosity of the driven oil and thus, for many crudes, dramatically increases its fluidity. The material transport ahead of the heat wave acts as a miscible fluid drive. The result is a very efficient sweep of residual oil from the area (Perry et al.1960).

All combustion processes require three elements: oxygen, temperature and fuel. In a reservoir, injection of normal or enriched air provides the oxygen, the fuel will be flammable hydrocarbon vapors and residual coke in place and the ignition could be spontaneous or by external agents (more details are described in section 2.2.1).

2.2.1. Forward *In Situ* Combustion

When the combustion front goes in the same direction as the air flow, the process is called Forward *In Situ* Combustion. The fuel required for the combustion is the residual coke from the in-place oil (Perry et al. 1960). If the reservoir does not have a sufficiently high temperature to generate a spontaneous ignition, it is initiated by heating the oil-bearing sand around an injection well with a gas burner, electric heater or by the injection of a hot fluid such as steam. Chemical agents are also used to promote spontaneous ignition. Air is injected to ignite the oil and to propagate the combustion zone outward from the injector. The elevated temperature zone displaces reservoir fluids which are advanced towards the production wells by a variety of mechanisms. Carbon dioxide is generated as a product of combustion and it has the potential to aid recovery through viscosity reduction and swelling of the oil (Moore et al. 1988).

2.2.2. Dry Forward *In Situ* Combustion

Air injection without the co-injection of water is called Dry In Situ Combustion. A schematic representation of this process (Figure 2.1) was described by Moore et al. (1988). The different regions formed during this process are:

Burned Zone. Area already swept by the combustion front, which would ideally result in a zone devoid of fuel. The bulk of the heat generated by the combustion remains in this region or is lost to the surroundings. Temperature in the burned zone rises in the direction of the combustion front.

Combustion Zone. In this area energy is generated. Hydrocarbon oxidation starts and carbon oxides and water are produced.

Cracking and Vaporization Zone. Assuming that all oxygen has been consumed in the combustion zone, oil in this area undergoes thermal cracking and vaporization. The generated light oil moves forward and is mixed with the oil ahead (native oil). The residual oil that remains behind will be the fuel source to sustain the combustion process.

Steam Zone. The water produced as a result of combustion reactions and mobilized connate water move forward from the high temperature area. The operating pressure and the concentration of combustion gases in the steam zone dictates the temperature in this zone. If unreacted oxygen passes through the combustion zone, it may react in the steam zone.

Condensation Front. The steam generated to form the steam zone moves forward and then condenses: the downstream edge of the steam bank where the temperature drops to a level approaching that of the native reservoir is called the condensation front.

The Altered Saturation Zone. It consists of a high water saturation zone or water bank downstream of the condensation front and an oil bank as a highly oil saturated zone, which forms downstream of the water bank. Note that the altered saturation zone tends to override the native reservoir as the combustion zone moves away from the injection well. The override behavior reflects the low density of the flowing gases.

Native reservoir. Area with original oil, which is changed by the presence of combustion gases.

Figure 2.2 presents schematic profiles illustrating the behavior of fluid saturations and temperatures, during a dry combustion process.

The most important cost in the operation is that of the air to oxidize the fuel. Fuel concentration is undoubtedly a function of many factors, not the least of which is the nature of the reservoir rock itself (Ramey, 1971).

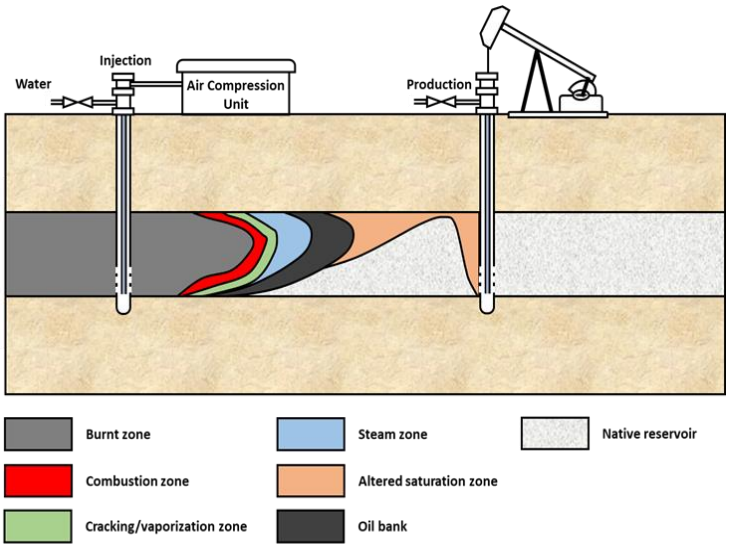

Figure 2.1 Forward *In Situ* Combustion (Fazlyeva et al. 2019)

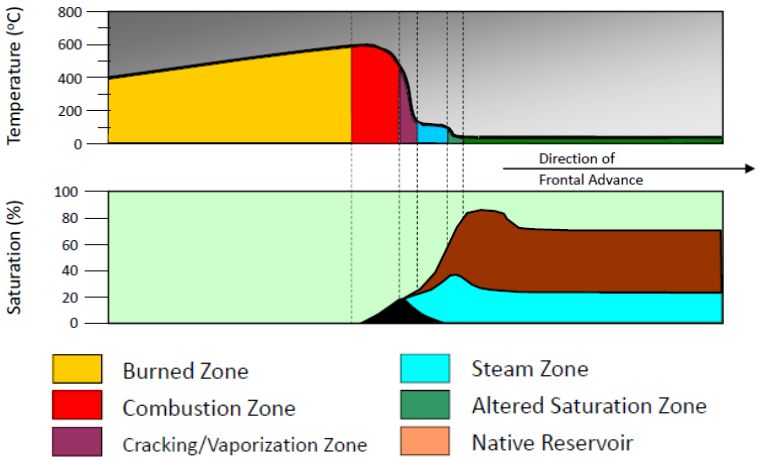

Figure 2.2 Schematic of Temperature and Saturation Profile for Dry Forward *In Situ* Combustion (Mehta et al. 2018).

2.2.3. Wet *In Situ* Combustion

The injection of water, alternately or simultaneously, with air can improve the energy efficiency of the process due to its high heat capacity when compared to air; the effective thermal conductivity of water is 100 times that of air, (Moore et al. 1988).

Wet *In Situ* Combustion can be classified according to the water/air ratio (WAR). At low WARs it is called Normal Wet Combustion. Figure 2.3 shows a schematic of the temperatures and saturations under this type of ISC. Assuming that all oxygen has been consumed in the combustion zone, oil in this area undergoes thermal cracking and vaporization. The generated light oil moves forward and is mixed with the oil ahead (native oil). The residual oil that remains behind will be the fuel source to maintain the combustion

process. Then the water injected passes through the combustion front as superheated steam. When the velocity of the vaporization front (trailing edge of the swept region that remains at temperatures above steam temperature) increases to the extent that liquid water enters the combustion zone, but vaporizes prior to passing all the way through the combustion/oxidation region is called Partially Quenched or Incomplete Wet Combustion. At high WARs, liquid water passes totally through the oxidation zone and it is called Superwet Combustion (Moore et al. 1988). Figure 2.4 shows a schematic of the temperatures and saturations under this type of ISC.

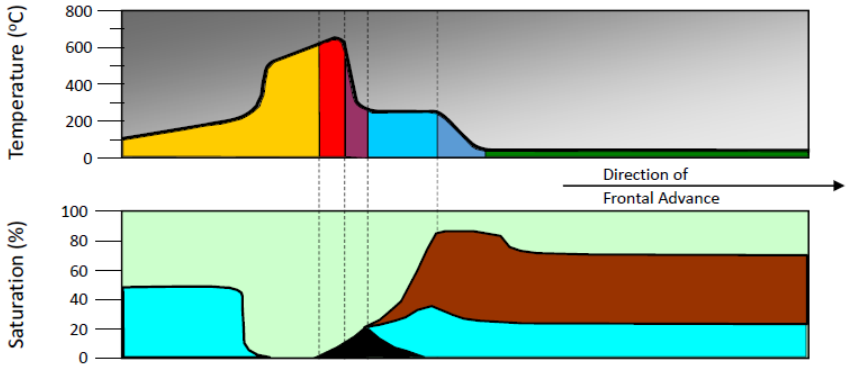

Figure 2.3 Schematic of Temperature and Saturation Profile for Normal Wet *In Situ* Combustion (Mehta et al. 2018).

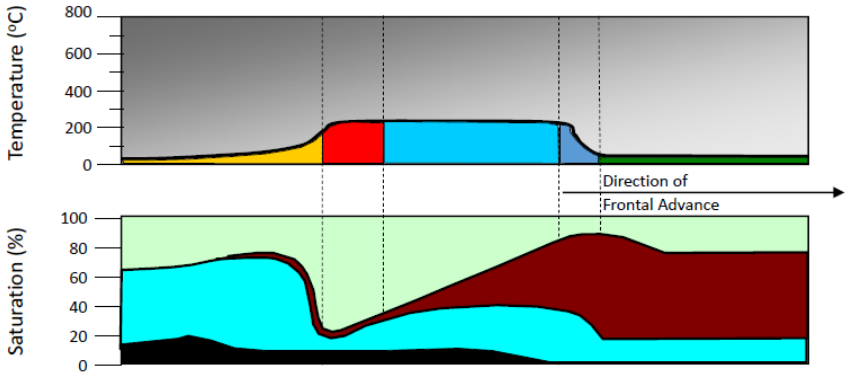

Figure 2.4 Schematic of Temperature and Saturation Profile for Super Wet *In Situ* Combustion (Mehta et al. 2018).

2.2.4. Reverse Combustion

When the combustion front advances in the opposite direction to the air flow, the process is called Reverse *In Situ* Combustion. During this process, the direction of the combustion zone movement is opposite to that of air flow. Thus, the formation may be ignited at a producing well, then the air injection location is switched to the injection well. In such cases, the combustion zone will move away from the producing well, toward the injection well, in the direction of increasing oxygen concentration. Meanwhile, the fluids displaced traverse the hot combustion zone, and are then produced (Farouq Ali et al. 2012).

In forward combustion, there are viscosity limitations that are not inherit in reverse combustion. With forward combustion, the products of combustion flow into a relatively cold region. With lower temperatures, problems of oil transport enter the picture when low-gravity or semi-solid oils are involved. In reverse combustion, the mobilized hydrocarbons enter a hot, pre-heated zone, which minimizes the problem of transporting oils having a prohibitive viscosity at ordinary reservoir temperatures (Perry et al. 1960).

The kinetics describing the reactions involving oxygen and hydrocarbons during reverse combustion are not well defined. Significant oxygen uptake by Low Temperature Oxidation (LTO) reactions in the region of the reservoir located between the air injectors and production wells would be expected to occur. The extent of modification of the original oil properties will be very dependent on the reservoir pressure and the temperature distribution in the region up stream (in terms of the direction of air flow) of the main reaction zone where combustion reactions are occurring. The residual hydrocarbon up stream (in terms or air flow) of the combustion zone would be expected to be an asphaltenes rich phase (especially for asphaltic crude oils) which then under goes thermal cracking and bond scission combustion reactions. Mobilized hydrocarbons displaced from the combustion zone have very different properties than those of the original oil due to the cracking of the asphaltenes and burning of the coke deposited as an end product of the LTO cracking reactions. A further difficulty associated with the LTO reactions is that they may result in the ignition of a secondary oxidation/combustion zone near the air injection well.

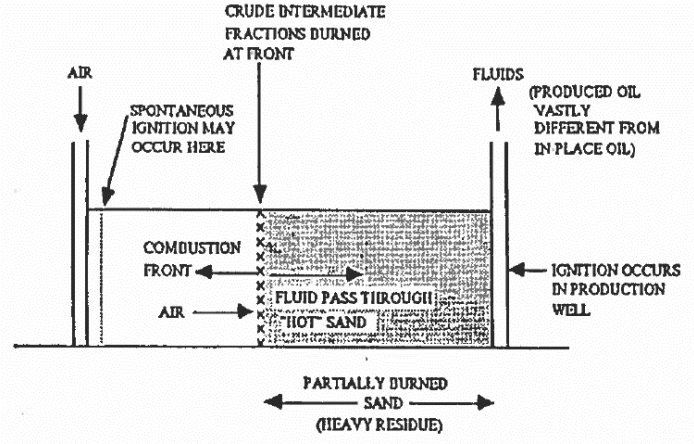

Figure 2.5 Schematic Reverse Combustion (Farouq Ali, 2012)

2.2.5. Enriched Air

It is a modification of the *In Situ* Combustion process, where oxygen content is greater than that of normal air [21% oxygen] (Mehta et al. 2018). Oxygen concentrations in enriched air can be as high as 100%, hence injection of enriched air reduces the volume of injection and vent gases which must be handled per unit volume of oxygen injected. As a result, it provides the opportunity to accelerate the oil recovery, in reservoir where the oxygen utilization efficiency is high. The produced carbon oxide concentrations will

increase and carbon dioxide will dissolve in the native oil increasing its mobility. Moore et al. (1987) conclude that oxygen and fuel requirements parameters for this technology are dependent on total pressure. Because of the direct effect of total pressure and total gas injection flux on oxygen storage, the oxygen flux at the burn front will be significantly lower for enriched air combustion compared with normal air combustion when the tests are conducted at equivalent injection fluxes and pressures.

“Enriched air injection is a modification of standard *In Situ* combustion technology with the potential to overcome a number of the problems that have hindered widespread field application of the process” (Moore et al. 1987).

2.2.6. High Pressure Air Injection (HPAI)

High Pressure Air Injection is an EOR process in which compressed air is injected into a high gravity (>25°API), high pressure, high temperature (>80°C), deep (>1,500 m) oil reservoir; bond scission or combustion reactions are dominant in the 150 to 300°C or what the ISCGR defines as the Low Temperature Range (LTR). The resulting flue gas mixture, which is primarily CO_2 and nitrogen, provides the mobilizing force to the oil downstream of the reaction region, sweeping it to production wells. The gas-oil mixture may be immiscible, or partly or completely miscible. In some situations, the elevated temperature reaction zone itself may provide a critical part of the sweep mechanism in terms of incremental recovery. (Moore et al. 2002).

HPAI is an economically viable alternative to gas injection on many deeper, low permeability reservoirs that are too tight for water injection. HPAI is also applicable as a tertiary recovery process on many of the larger, deeper, high gravity reservoirs, when the large volumes of medium BTU gases produced can be effectively utilized (Erickson et al. 1994). In reservoirs with high pressure and high temperature, self-ignition or spontaneous ignition will be generated (Mehta et al. 2018).

During the early life of an HPAI project, the air requirements per incremental barrel of oil are directly related to the water/oil ratios (Mace et al. 1975). At the same time, the composition of the produced gas stream is essentially the same as the reservoir solution gas, for a significant time following the start of air injection. Traces of nitrogen from the combustion gases begin to show up very early, within weeks after start of injection. CO_2 produced at the combustion wells, because of the higher solubility, lags behind the nitrogen by months or even years (Mace et al. 1975). HPAI could be a more attractive alternative than waterflooding in low permeability reservoirs where water injectivities are limited (Erickson et al. 1994).

2.3. DISCUSSION OF APPLICATION OF TERMS HTO AND LTO IN TRADITIONAL ISC AND HPAI LITERATURE

An evaluation of the historic literature on ISC and HPAI shows that the term Low Temperature Oxidation (LTO) is often used as an indicator of the temperature range in which oxidation reactions that do not result in the generation of significant carbon oxides are occurring. This temperature range is normally between room temperature (22°C) and 300°C. On the other hand, the term LTO is also used to describe the oxidation mode associated with oxygen addition reactions occurring in the liquid phase that generate energy and form oxidized hydrocarbon components.

The practice of using the term LTO interchangeably to describe either temperature range or reaction type results from the behavior of a number of heavy oils (normally <20°API) for which the dominant oxygen uptake mode at temperatures below 300°C involves oxygen addition reactions. The so called “heavy oils” do not generate significant carbon oxides or water of combustion when they undergo oxygen addition reactions and they clearly exhibit a “Negative Temperature Gradient Region (NTGR)” which, for a Canadian Bitumen from the Athabasca Oil Sands region, nominally extends over the temperature range of 280 to 350°C. The NTGR is a temperature range over which the oxygen uptake (or energy generation) rate decreases with increasing temperature.

On the other hand, so called light oils that are normally associated with a High Pressure Air Injection (HPAI) process exhibit a dominance of oxygen addition reactions at temperatures of less than nominally 180 to 200°C and combustion tube tests on these oils exhibit peak temperatures which are generally less than 300 to 350°C. In general, what are termed “light oils” by the *In Situ* Combustion Research Group (ISCRG) at University of Calgary, have an API gravity greater than 30° and while they exhibit a NTGR, the temperature range over which it occurs is greater than the temperature where bond scission reactions are effective at displacing light oils ahead of the leading edge of a combustion zone at reaction temperatures that are much less than those required for bond scission reactions to occur for a heavy oil.

Like the terminology LTO, the term “High Temperature Oxidation (HTO)” can be equally confusing. HTO reactions are assumed to be bond scission or carbon oxide and water forming reactions but one must understand that these reactions are not limited to high temperatures above 300 to 350°C. In fact, when high gravity light oils at elevated pressures (nominally greater than 7.0 MPa), HTO reactions are often the dominant oxygen consumption mode at temperatures as low as 180 to 200°C. This is particularly true for highly paraffinic crude oils.

In view of the possible confusion with the terms LTO and HTO, the *In Situ* Combustion Research Group at the University of Calgary has chosen to utilize the terminology Low Temperature Range (LTR) when the reactions temperature is between room temperature and the temperature corresponding to the upper temperature limit of the NTGR. This is the temperature where the oxygen uptake rate (Evolved Gas Analysis) or energy generation rate (Pressurized Differential Calorimeter (PDSC) or the Self-Heating Rate (Accelerating Rate Calorimeter (ARC), or Mass Loss Rate

(Thermogravimetric Analyzer) falls to a localized minimum level. It should be noted when using the ISCRG definition that the temperature marking the upper extent of the NTGR, which is considered to be the on-set of the High Temperature Range (HTR), is not exactly the same for each thermal analyzer, but as a first estimate it is approximately 350°C.

In order to avoid any confusion with regard to the nature of the oxidation reactions, the ISCRG prefers to use the terminology bond scission or combustion or carbon oxide forming reactions rather than HTO reactions and it uses the terminology oxygen addition or LTO when discussing liquid phase oxidation reactions that result in the generation of oxidized components. Burger et al. (1972) have provided an excellent discussion of the different types of oxidation reactions based on the nature of the products of the oxygen-hydrocarbons reactions. When produced oil samples or residual oil samples are analyzed following combustion tube, thermal cracking, or isothermal or ramped temperature oxidation tests using tubular or semi-batch reactors, the products of the reactions are often analyzed in terms of maltenes (toluene and pentane soluble fraction), asphaltenes (toluene soluble but pentane insoluble) and coke fractions (toluene and pentane insoluble). Organic acids are also formed, but they are generally observed through the pH of the produced water.

Figure 2.6 presents a cartoon that identifies the LTR, HTR and NTRG for a typical “heavy oil” and a typical “light oil”. Note that the NTGR is the temperature range between the temperature where the localized maximum in the oxygen uptake rate or energy generation rate occurs in the LTR and the temperature where the oxygen uptake/energy generation rates fall to a localized minimum. A temperature of 350°C is shown as the dividing temperature between the LTR and the HTR and it can be seen that the NTGR is assumed to fall in the LTR.

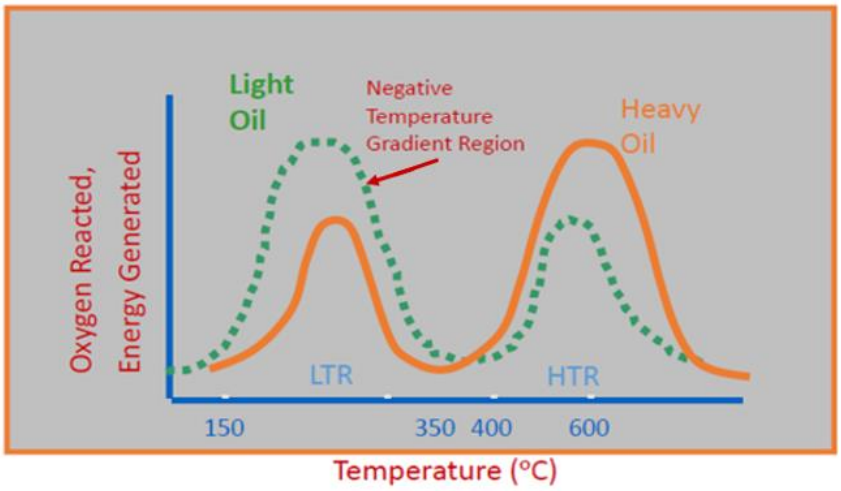

Figure 2.6 Oxidation Behavior for Light and Heavy Oils at Different Temperatures (Mehta, 2018)

Two oxygen uptake rate or heat flow traces are sketched on this figure. The trace labelled “heavy oil” is typical of the behavior of what is often associated with a candidate

reservoir for application of an ISC process while the “light oil” trace represents the typical behavior of a reservoir that is a candidate for a HPAI process. The actual shape of the traces is dependent on the thermal analyzer being used to finger print the crude oil. Similar, but not identical shapes are observed when evaluating mass loss rate (DTA), heat flow rate (DSC, PDSC) or oxygen uptake rate (Evolved Gas Analysis). For a given analyzer, the shapes of the traces are dependent on the crude oil composition, core matrix composition and surface area, reservoir pressure, absence or presence of connate water, and the heating rate employed by the apparatus used to generate the traces.

The “heavy oil” trace in Figure 2.6 illustrates the thermal behavior of a crude oils that requires bond scission reactions occurring in the HTR in order to achieve effective oil displacement from the combustion zone. While oxygen is consumed and energy is generated in the LTR, oxygen addition (LTO) reactions tend to immobilize the oil that is located in the region of the reservoir where these reactions are occurring. Depending on the reservoir pressure, this is often the steam bank region. Immobilization of the oil undergoing oxygen addition reactions is a result of the viscosity increase for the oxidized oil (Adegbesan et al. 1987) combined with the non-equal molar replacement of the gas phase components within the reservoir pores when oxygen is consumed without generating carbon oxides. The ISCRG is starting to conclude that the NTGR exhibit by heavy oils is caused by the inability of these oils to liberate sufficient quantities of flammable vapors (within a given temperature range) to support bond scission reactions in the vapor phase. The temperature range associated with the NTGR is therefore ultimately a function of the composition of the oil.

The “light oil” trace portrays the behavior of a crude oil that undergoes bond scission or combustion reactions within the LTR. The bond scission reactions that generate the maximum in the energy generation or heat flow traces that occurs in the LTR are very effective for displacing residual oil from the reaction zone. Peak temperatures, as seen during combustion tube tests are of a similar magnitude to the temperature corresponding to the localized maximum in the LTR, hence efficient oil displacement by the bond scission reactions occur without the requirement that the reaction temperature has to transcend the NTGR.

Figure 2.7 is a second cartoon that illustrates what is perhaps the most important implication arising from the differences in the physical properties and the oxidation/combustion kinetics for a typical “heavy oil” and a typical “light oil”.

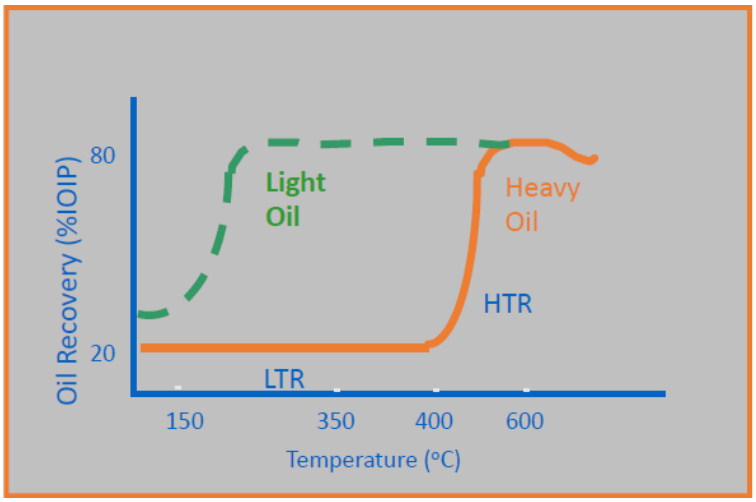

Figure 2.7 Recovery Performance for Light and Heavy Oils at Different Temperatures (Mehta et al. 2018).

Flue gas generated when “light oils” undergo oxygen addition reactions are effective for displacing oil from the region downstream of the reaction zone so there is often less concern about the nature of the oxygen uptake reactions so long as these reactions consume the injected oxygen. A further positive aspect of what the ISCRG defines as a light oil is that the NTGR occurs at higher temperature than the temperature at which most light oils exhibit peak temperatures (nominally in the range 250 to 350°C which falls in the LTR), hence there is no kinetics barrier (no NTGR) between the temperatures where oxygen addition reactions dominate and the temperatures where bond scission reactions, that can effectively mobilize oil, dominate.

This is not the case for a typical “heavy oil” as the flue gas generated is not very effective at displacing these generally viscous oils downstream of the heated (steam bank) zone. If the oxidation reactions involving a heavy oil are operating in the LTR, hot water will be generated and will recovery oil from downstream of the oxidation (steam bank) zone but the effectiveness of the generated hot water for displacing oil is much less than that of a combustion zone operating in the HTR. Hence, for a typical heavy oil, the reaction temperatures must be able to exceed the upper temperature limit of the NTGR in order for the oxygen consuming reactions to be in the bond scission mode which is required for effective displacement of the oil by the leading edge of the combustion zone (combustion front).

2.4. KINETICS REACTIONS

Oils that are potential candidates for In Situ Combustion recovery process are often screened by means of their oxidation characteristics; in particular, the kinetics of the ignition process and the transition temperature where LTO reactions dominate to the temperatures where HTO or bond scissions reactions dominate. For heavy oils, the transition is known as the “Negative Temperature Gradient Region (NTGR)” (Moore et

al. 1999). The NTGR is a temperature range over which the global oxygen uptake rates decrease with increasing temperature (Jia et al. 2003).

Thermal cracking (pyrolysis) is the modification of the native oil properties by thermal energy in the absence of oxygen (Mehta et al. 2018). These reactions involve dehydrogenation reactions (hydrogen stripping at constant carbon number), cracking reactions (carbon-carbon bond scissions) which generate lower carbon number molecules, and condensation reactions which result in the formation of molecules of greater carbon numbers. In an ideal combustion process, thermal cracking reactions happen instantly in front of the combustion zone and they might be the prime fuel laydown mechanisms (Burger et al. 1985).

The oxygen addition reactions happen when oxygen atoms are chemically bound into the molecular structure of the liquid hydrocarbons, producing various oxygenated compounds (hydro peroxides, aldehydes, ketones and acids). The compounds tend to further react and polymerize with each other, forming heavier fractions (Moore et al. 2002).

Bond scission reactions happen when oxygen breaks up the hydrocarbon molecules and produce CO_2, CO and water. For light oils, bond scission reactions can happen between 150 and 300°C and for heavy oils they occur when the maximum temperatures are higher than 450°C (Moore et al. 2002).

The importance of the transition from the low to high temperature regime; in particular, the “Negative Temperature Gradient Region” wherein the rate of oxidation decreases with increasing temperature, is that it may prevent the attainment of high temperate combustion (Moore et al. 1999).

The maximum oil recovery is the difference between the OOIP at the start of the operation and the oil consumed as fuel. If the fuel concentration is too low, the heat of combustion will not be sufficient to raise the temperature of the rock and the contained fluids to a level of self-sustained combustion (Fassihi et al. 1984).

In an ISC process a heterogeneous flow reaction occurs. Injected oxidant gas must pass through the burning zone, and four main transport process happen (Fassihi et al. 1984):

a) Oxygen diffuses from the bulk gas stream to the fuel interface.
b) The Oxygen absorbs and reacts with the fuel.
c) Then combustion products desorb, and
d) Products finally transfer into the bulk gas stream.

If any of these steps is inherently much slower than the remaining ones, the overall rate will be controlled by that step.

The study of *In Situ* combustion kinetics is undertaken for the following reasons (Sarathi, 1999):

- To characterize the reactivity of the oil,

- To determine the conditions required to achieve ignition and/or determine if self-ignition will take place in the reservoir upon air injection.
- To gain insight into the nature of fuel formed and its impact on combustion, and
- To establish parameter values for the kinetic (reaction rate) models used in the numerical simulation of ISC process.

Tadema et al. (1959) described the existence of two main reactions, one at low temperatures and one at high temperatures, which are quite common for any crude oils. Later work on kinetics (Burger et al. 1972) of crude oil oxidation in porous media confirmed the occurrence of three major reactions during ISC: (1) fuel deposition, (2) fuel combustion and (3) Low temperature oxidation.

2.4.1. Fuel Deposition

The residual hydrocarbon remaining after the crude oil displacement is considered as fuel. The amount of fuel available for in situ combustion varies with crude-oil and porous-medium characteristics, oil saturation, air flux and time-temperature relationships (Alexander et al. 1962). During a series of ramped-temperature oxidation experiments, Moore et al (1992) and colleagues observed a rapid fuel formation when oil was maintained in contact with an oxygen containing gas in a temperature range of 200°C and 300°C for an extended period of time.

Fuel deposition refers to the formation of fuel (mainly coke) as a result of the increase in the temperature. The fuel formed is deposited on the surface of the matrix. These reactions include pyrolysis/cracking of hydrocarbons. Oil pyrolysis reactions are mainly homogeneous and endothermic, and involve three kinds of reactions: dehydrogenation, cracking, and condensation (Sarati et al. 1999). Studies of Alexander et al. (1962) indicated that the amount of fuel deposited increased with increasing initial oil saturation as well as oil viscosity and decreased with increasing atomic hydrogen/carbon ratio and API gravity of the oil. Also, Vossoughi et al. (1982) showed that addition of clay particles increased the amount of fuel deposited.

The fuel content, if taken to be constant quantity, would depend on a variety of factors, related to the rock properties (permeability, porosity, and mineral content), the oil properties (viscosity, specific gravity, distillation characteristics, saturation), the water saturation, the gas saturation, and the air injection rate, oxygen concentration, and the prevailing temperature and pressure. It is, thus, a complex quantity, and is rather difficult to determine. Fuel content usually ranges from 1.5 to 2.5 lb_m/ft^3 (24 to 40 kg/m^3) (Farouq et al. 2012)

Bae et al. (1977) performed a thermogravimetric analysis (TGA) on 15 different samples. TGA measures weight change versus time or temperature curves. It was concluded that distillation has a great significance on the total fuel available. At higher pressures, distillation was lower which results in a higher fuel availability.

2.4.2. Fuel Combustion

The fuel combustion (HTO) reactions are heterogeneous and include reactions of oxygen with fuel producing carbon oxides and water. These reactions are exothermic and provide the thermal energy to sustain combustion (Cinar et al. 2008).

The combustion of the fuel deposited, which is a carbonaceous residue, having a composition CH_n (having an atomic ratio of H to C equal to n), can be described by the stoichiometric equation (2.1) presented by Farouq et al. (2012).

$$CH_n + \left\lfloor \frac{2m+1}{2m+2} + \frac{n}{4} \right\rfloor O_2 = \left\lfloor \frac{m}{m+1} \right\rfloor CO_2 + \left\lfloor \frac{1}{m+1} \right\rfloor CO + \frac{n}{2} H_2O \qquad (2.1)$$

Where:

n = atomic ratio of hydrogen to carbon,

m = mole ratio of CO_2 to CO produced,

m = infinity when complete combustion occurs producing only CO_2 and H_2O.

Benham et al. (1958) obtained the following equation for the air required to produce the oil in one cubic foot of reservoir.

$$\frac{\Phi_F}{V_F} = \frac{\left\lfloor \frac{2m+1}{m+1} + \frac{n}{2} \right\rfloor Z}{1.109x10^{-3}(12+n)Y} \qquad (2.2)$$

Where:

φ_F/V_F = Volume of air necessary to sweep the oil out of one cubic foot of reservoir volume behind the front, *i.e.* in the thesis will be used/referred as Air Requirement* (A_r).

Z = coke [lb/ft^3 of formation], *i.e.* in the thesis will be used/referred as to Fuel Requirement (F_r)*.

The previous equation for the SI units can be written as:

$$A_r = [AFR]\frac{F_r}{Y} \qquad (2.3)$$

Where:

A_r = Air requirement $\left\lfloor \frac{m^3(ST)}{m^3} \right\rfloor$

AFR = Air/fuel ratio $\left\lfloor \frac{m^3(ST)}{kg} \right\rfloor$

F_r = Fuel requirement [kg/m^3]

Y = Fraction of oxygen consumed/utilization

* More detailed in section 2.6

Penberthy et al. (1966) presented equation (2.4) to predict the rate of advance of the combustion front in terms of the fuel (C_f) and air requirement (A_r) parameters.

$$V_f = \frac{U}{C_f F_{af}} = \frac{U}{A_r} \quad (2.4)$$

Where:

V_f = burning front velocity [ft/h]; [m^3/h]

U = air flux or air flow rate per unit of area of combustion zone normal to air flow direction
[scf air/ h•ft^2]; [m^3(ST)/m^2 •h]

F_{af} = air/fuel ratio [scf air/lb_m fuel]; [m^3(ST)/kg]

C_f = coke [lb_m/ft^3 of formation]; [kg/m^3 of formation]

2.4.3. Oxidation Mechanisms

Combustion reactions involve the destructive oxidation of either the whole or a fraction of the native oil by bond scission reactions. The reactions products are combustion gases (carbon oxides) and water (Mehta et al. 2018).

Carbon dioxide is the dominant carbon oxide when oils are heated to temperatures where bond scission happen. The gas phase combustion parameters (H/C ratio, oxygen/fuel ratio and percent reacted oxygen converted to carbon oxides) are useful indicators of whether the oxidation kinetics are operating in the LTO (oxygen addition) or HTO (bond scission) modes (Moore et al. 1999).

The oil mobilization effectiveness of an oxidation/combustion zone during a dry combustion process is very dependent on the level of oxygen uptake by LTO reactions prior to the onset of HTO or bond scission reactions (Moore et al. 1999).

One of the main calculations during the oxidation is the air requirement, which is the amount of air needed for the combustion front to sweep a unit of volume of reservoir, and it can be predicted using equation (2.3) (Mehta et al. 2018).

2.4.3.1. Low Temperature Oxidation (LTO)

As discussed previously, LTO are oxygen addition reactions that happen between oxygen and oil at temperatures below 300°C (Moore et al. 1988). Moore et al. (1987) described that compositional changes occur in response to low temperature oxidation reactions in the steam bank region ahead of the main combustion front. The effect which this oxidation has on the overall process performance depends on the pressure, which

in turn controls the temperature of the steam bank, and on the time available for the oil to react within the steam bank.

For light oils (API>20°) bond scission reactions occur in the LTR and this is the temperature range where the major oil recovery happens (Figure 2.6, section 2.3). While for heavy oils (API<20°) in the LTR the oxidation is by oxygen addition reactions or LTO, which immobilize the oil due to the generation of a high asphaltenes concentration which results in a significant viscosity increase. Even if the reaction temperatures undergo the transition to the HTR, oil recoveries by the HTO reaction are low if the oil has undergone significant oxygen uptake by LTO reactions.

LTO takes place upon air injection either before or after ignition, when oxygen is available and reacts in the LTR. LTO reactions occurs with the oxygen dissolved in the whole volume of the dispersed oil phase. (Fassihi et al. 1984).

Hence, LTO reactions occur whenever oxygen reacts with oil but does not generate carbon oxides or water. They occur over a wide temperature range and can have a significant effect on the crude oil properties even at the native reservoir temperatures if the time period of contact is long. For both, light and heavy oils, the rate of oxygen uptake resulting in energy generation increases significantly at temperatures between 180 and 200°C. Because they occur at relatively low temperatures, LTO reactions are often credited with providing the energy required for spontaneous ignition. The negative aspect of LTO reactions is that they cause a significant increase in the apparent asphaltenes content of “heavy oils”. For these oils, viscosity increases with asphaltenes content, hence LTO reactions essentially immobilize the oxidized oil.

For some reactive oils, heat released in the LTR may lead to spontaneous ignition (Fassihi et al. 1984). It is worth mentioning that Fassihi never stated if the term reactive oil refers to oxygen uptake rate or heat generation rate.

2.4.3.2. High Temperature Oxidation (HTO)

It is in the High Temperature Range (above 350°C) where heavy oils must operate to consume oxygen by HTO or bond scission (destructive oxidation) reactions. It is in HTR where oxygen uptake (energy generation) rates are sufficiently rapid to provide effective mobilization of the crude oil by the combustion front (Figure 2.7, section 2.3). HTO reactions refer to bond scission reactions which result in the generation of carbon oxides and water. For light oils, these reactions occur in the LRT to the extent that the main energy generation responsible for oil mobilization by the elevated temperature reaction front are HTO reactions occurring in the LTR.

Since the Low Temperature Oxidation reactions occurring in the LTR can affect the composition and amount of fuel available for reaction in the High Temperature Range, and since oxygen utilization in the High Temperature Range dictates how much oxygen is available for reaction in the steam bank region, it is apparent that the LTO and HTO kinetics have a significant effect on the overall combustion performance (Moore et al. 1988).

The velocity of the burning front is controlled by the chemical reactions involved (Fassihi et al. 1984). It is not possible to operate in the high temperature combustion mode below a minimum oxygen flux (Moore et al. 1999). However, as suggested by Nelson and McNeil et al. (1961), it may be necessary to operate at low oxygen fluxes during the ignition phase.

As a rule of thumb, apparent atomic H/C ratios based on the produced gas composition should be less than 3.0 when an *In Situ* combustion process is operating in the high temperature combustion mode (Moore et al. 1999).

2.5. HIGH PRESSURE AIR INJECTION (HPAI) FOR LIGHT OILS

In Situ Combustion ISC is the process of injecting air into a reservoir to oxidize a small portion of the hydrocarbon present to generate heat and pressure. It suffers from fewer reservoir limitations than steam injection (Cinar et al. 2008).

In Situ Combustion in light oils is also called High Pressure Air Injection or HPAI. Fassihi et. al. (1994) mention that under appropriate conditions, when air is injected into the reservoir, a small amount of the OOIP is consumed while the rest is displaced, banked and eventually produced.

The combustion process for displacement of light oils is fundamentally different from the heavy oil combustion process. For heavier crude oils, heat and steam generation and subsequent viscosity reduction is the primary oil displacement mechanism. For this reason, it is important that the fuel for a heavy oil combustion is consumed in the High Temperature Oxidation (HTO) reaction regime. Flue gas benefits are minimal with heavy oils. For light oils, however, the heat generated is of secondary value, and flue gas generation is the primary factor in displacing oil. Burning in the High Temperature Range is of little consequence as long as the combustion front is self-sustaining and oxygen is consumed (Tiffin et al. 1997). Operating temperatures greater than 350°C are not required, but oxidation kinetics should be bond scission which historically is known as HTO reactions.

More description, details, advantages and disadvantages of this technology are covered in Chapter 3.

2.6. COMBUSTION PARAMETERS

The original purposes of the ISC tube tests carried out in the laboratory are to determine the self-sustaining ability of the combustion front propagation and to measure combustion design parameters for field projects, mainly oxygen/air and fuel requirements and air/fuel ratios. In addition to the above design parameters, combustion tube experiments also provide significant information on the reaction modes and properties of the produced fluids.

The key reaction that is required during ISC is the bond scission. This reaction is:

$$\text{Oil} + \text{Air} \rightarrow CO_2 + CO + H_2O \quad \text{(generic)} \tag{2.5}$$

$$C_xH_y + O_2 + N_2 \rightarrow CO_2 + CO + O_2 + H_2O + N_2 \quad \text{(detailed)} \tag{2.6}$$

From the composition of the produced gases, other combustion parameters are calculated. They include: apparent atomic H/C ratio, $(CO+CO_2)/CO$, $(CO+CO_2)/N_2$, air/fuel ratio, fraction of reacted oxygen converted to carbon oxides, and oxygen utilization.

CO_2 is the dominant carbon oxide when native or oxidized oils are heated to temperatures where bond scission reactions occur.

Fuel requirements in the traditional ISC literature were based on the mass of carbon and hydrogen consumed as the combustion zone sweeps a measured volume of reservoir. Carbon burned is calculated from the amount of carbon oxides produced and hydrogen burned is based on an oxygen balance. In view of the uncertainty in the fate of injected oxygen (water production, oxygen addition reactions), in the laboratory experiments performed by the ISCRG it is preferred to quote injection air requirements (the volume of injected air required to propagate a combustion zone through a unit of reservoir) and evaluate the fuel requirements (F_r) [kg/m^3] based on the observed air/fuel ratio (AFR) (Mehta et al. 2018).

$$Air\ Requirement\ (A_r) = \frac{Air\ Flux}{Combustion\ Front\ Velocity};\ \left[\frac{m^3(ST)}{m^3}\right] \tag{2.7}$$

$$Air\ Flux\ (U) = \frac{Volumetric\ Air\ Rate}{Area\ Normal\ to\ Flow};\ \left[\frac{scf\ air}{hr \cdot ft^2}\right];\ \left[\frac{m^3(ST)}{m^2 \cdot hr}\right] \tag{2.8}$$

$$AFR = \frac{23.64[1+R]\frac{[N_2]}{R}}{12.011([CO_2]+[CO])+4.032\left(\frac{[N_2]}{R}-[CO_2]-\frac{[CO]}{2}-[O_2]\right)};\ \left[\frac{m^3(ST)}{kg}\right] \tag{2.9}$$

Where R is the ratio of oxygen to nitrogen that is in the injected air. For normal air the composition is: 21% O_2, 78% N_2 and 1% Ar. Due to this:

$$R = \frac{y_{N_2}}{y_{O_2}} = {}^{78\%}/_{21\%} = 3.71 \tag{2.10}$$

y_{N_2}: $mole\ fraction\ or\ mole\ \%\ of\ N_2 injected\ gas$

y_{O_2}: $mole\ fraction\ or\ mole\ \%\ of\ O_2 injected\ gas$

[ ]: signifies normalized composition in mole fraction or number of moles of product gas (overall or incremental)

Most textbooks assume air is 21% O_2 and 79% N_2, therefore, the commonly quoted value of R is:

$$R = {}^{79\%}/_{21\%} = 3.76 \tag{2.11}$$

Laboratory tests performed by the ISCRG use premixed air which does not contain Argon, hence the R ratio is calculated for each test based on the actual O_2/N_2 ratio in the individual supply cylinders.

The apparent atomic H/C ratio is calculated using laboratory data (from combustion tube tests) to estimate it, as long as the laboratory test was conducted in the HTR for heavy oils where the bond scission reactions take place, and for light oils these reactions take place in the LTR.

$$Apparent\ {}^{H}/_{C}\ Ratio = \frac{4.0\left(\frac{[N_2]}{R} - [CO_2] - \frac{[CO]}{2} - [O_2]\right)}{[CO_2]+[CO]} \tag{2.12}$$

If the measured apparent H/C ratios are outside the range 1.0 to 2.0, it is recommended to use the actual H/C ratio for the original oil when estimating the amount of water generated by the combustion reaction.

The Air/Fuel ratio (AFR) is given by:

$$AFR = \frac{23.64\frac{[1+R]}{R}[N_2]}{\left(12.011+{}^{H}/_{C}\right)([CO_2]+[CO])} \tag{2.13}$$

The fractional conversion (f_{O2I}) of injected oxygen to carbon oxides is (Mehta et al. 2018):

$$f_{O_2 I} = \frac{([CO_2]+[CO])}{\frac{[N_2]}{R}} \tag{2.14}$$

The fractional conversion of reacted O_2 to CO_x (f_{O2R}):

$$f_{O_2 R} = \frac{\left([CO_2]+\frac{[CO]}{2}\right)}{\frac{[N_2]}{R} - [O_2]} \tag{2.15}$$

The fraction of oxygen utilization is calculated by (Mehta et. al 2018):

$$Y = \frac{\frac{[N_2]}{R} - [O_2]}{\frac{[N_2]}{R}} = 1 - R\frac{[O_2]}{[N_2]} = \frac{Reacted\ or\ consumed\ O_2}{Injected\ [O_2]} \tag{2.16}$$

And the excess of oxygen injected:

$$Excess\ O_2 = \frac{(1-Y)}{Y} = \frac{[Produced\ Oxygen]}{[Reacted\ Oxygen]} \quad (2.17)$$

There are many other parameters that can be provided by laboratory experiments, such as: liquid production history, stabilized and overall composition of produced gases, stabilized and overall burning time, peak temperatures, temperatures profiles (in time and by zone), and post burn residue.

All these combustion parameters provide important information on the behavior of the oil rock system during the combustion process. It is important to understand and monitor the gas phase combustion parameters as these provide the link between the laboratory combustion tube tests where temperatures are well known, and the field where temperature measurements are more difficult.

2.7. LABORATORY CONVENTIONAL ANALYSIS

2.7.1. Pressure – Volume - Temperature (PVT)

The main variable that determines the behavior of fluids, under reservoir conditions, during depletion is, the reservoir pressure. Hence, relatively simple tests which simulate recovery processes are conducted by varying the fluid pressure. The main emphasis is on the volumetric data at the reservoir pressure and on the reservoir surface temperatures, hence the name PVT data. In the simplest approach of predicting the PVT data, the reservoir oil is considered to be composed of two pseudo components (oil and gas). The effect of interstitial water on the phase behavior of hydrocarbons fluids is ignored in most PVT tests, hence the PVT tests are conducted in the absence of water. These pseudo components, are identified by flashing the reservoir fluid at the standard conditions (15°C and 101.325 kPa), and characterizing the separated gas and oil phases by their specific gravity and molecular weight values. Compositional data on the produced fluids are mainly determined for their applications in hydrocarbon processing.

The prime information from PVT tests are the ratio of phase volume at reservoir conditions to that at surface/standard conditions, and the solubility of gas in oil.

Reservoir fluids should be sampled as early as possible during the production life of a reservoir. When the reservoir pressure falls below the initial saturation pressure (bubble point pressure) the hydrocarbon phase forms two phases of gas and liquid. The mole ratio of the two phases flowing into the well is not generally equal to that formed in the reservoir. The sample can be collected either as a single phase at the bottom hole, when the pressure is still above the saturation value, or at the surface (Danesh et al. 2003).

2.7.2. Geology

Since practically all petroleum occurs in sedimentary rocks, sedimentary geology forms one of the main foundations of petroleum geology. Sedimentological models are used to predict the location of different facies in the sedimentary basins, and from that, where are the likely source rocks with a high content of organic matter as well as the nature of the reservoir rocks and cap rocks. The distribution and geometry of potential sandstones or carbonate reservoirs requires detailed sedimentological models, and sequence stratigraphy has been a useful tool in such reconstructions. Reservoir rocks are mostly sandstones and carbonates which are sufficiently porous to hold significant amounts of petroleum. The composition and properties of other rock types such as shales and salt are also important.

The sedimentary environments determine the distribution of reservoir rocks and their primary composition. Sediments do, however, alter their properties with increasing overburden due to diagenesis during burial. Diagenetic processes determine the porosity, permeability and other physical properties, in both sandstone and limestone reservoirs. Chemical processes controlling mineral reactions are important.

In general, a petroleum reservoir consists of source rock, reservoir rock, seal rock, trap, and fluid content. Source rock, or source environment, is believed to be responsible for the origin of petroleum. It is believed that the source rock is usually near the hydrocarbon reservoir, *i.e.*, that the petroleum was formed within that particular area (Aguilera et al. 1995). Snider et al. (1934) indicates that the main source rock is shale, followed by limestone.

Reservoir rock is characterized by porous and permeable beds. Precise determination of matrix and fracture porosity is important for accurate calculations of hydrocarbons in place. Matrix and fracture permeabilities are important parameters in calculating flow capacities. Most of the world's hydrocarbons accumulations occur in sandstones and carbonate rocks (Aguilera et al. 1995).

Seal rock confines hydrocarbons in the reservoir rock because of its extremely low level of permeability. Usually, seals have some plasticity, which allows them to deform rather than fracture during earth crust movements. The most important seal is shale, followed by carbonate rocks and evaporites (Aguilera et al. 1995).

A trap is formed by impervious material which surrounds the reservoir rock above a certain level. The trap holds the hydrocarbons in the reservoir. Traps are formed by a variety of structural and stratigraphic features (Aguilera et al. 1995).

Tectonics and structural geology provide an understanding of the subsidence, folding and uplift responsible for the creation and dynamic history of a basin. The timing of the folding and faulting that forms structural traps is very important in relation to the migration of hydrocarbons. Seismic methods have become the main tool for mapping sedimentary facies, stratigraphy, sequence stratigraphy and tectonic development (BjØrlykke et al. 2010).

Porosity represents the void space in a rock, and it can be classified as primary and secondary. Primary porosity is established when the sediment is first deposited. Thus, it is an inherent, original characteristic of the rock. Secondary porosity is the result of geologic processes after the deposition of sedimentary rock and has no direct relation to the form of the sedimentary particles. Most reservoirs with secondary porosity are either limestones or dolomites (Aguilera et al. 1995).

Permeability is a property of the porous medium and is a measure of the capacity of the medium to transmit fluids. Reservoirs can have primary and secondary permeability. Primary permeability is also referred to as matrix permeability by reservoir engineers. Secondary permeability can be either by fractures or solution vugs (Aguilera et al. 1995). The presence of unhealed, uncemented, open fractures greatly increases the permeability of a rock. Using Darcy's laws, Craft and Hawkins developed some models to estimate this permeability.

Fractures are usually formed in rocks which are brittle. Griggs et al. (1960) found that rock with very low ductility was characterized by a large strains (deformation caused by stress). For very ductile rocks, there is a large, permanent strain and a lack of fracturing.

Different types of fractures can be found. Nelson et al. (1985) classified them as open, deformed, mineral-filled and vuggy fractures.

Sound reservoir engineering studies should use as a base a combination of direct and indirect sources of information. Direct sources of information include cores, drill cuttings and downhole cameras. Indirect sources of information include all types of well logs (including mud logs), well testing data, inflatable packers and production history. These types of information can be mapped in many different ways and combined with reservoir engineering techniques that lead to estimates of hydrocarbons in place and recoveries under different depletion strategies (Aguilera et al. 1995).

2.7.3. Petrophysical Analysis

The term petrophysics was coined by G.E. Archie and J.H.M.A. Thomeer. By their definition, petrophysics is the study of physical and chemical properties of rocks and their contained fluids (Thomas et al. 1992).

This type of analysis is employed to understand the rock properties of the reservoir, particularly how pores in the subsurface are interconnected, controlling the accumulation and migration of hydrocarbons. Some of the key properties studied in petrophysics are lithology, porosity, water saturation, permeability (absolute), density, fluid saturation and pressures, fluid identification and characterization, fractional flow (oil, gas, water), and thickness (net pay). A key aspect of petrophysics is measuring and evaluating these rock properties by acquiring well logs, core and seismic measurements. These studies are then combined with geological and geophysical studies and reservoir engineering to give a complete picture of the reservoir (Tiabb et al. 2004).

Some petrophysicist use acoustic and density measurements of rocks to compute their mechanical properties and strength. They measure the compressional (P) wave velocity of sound through the rock and the shear (S) wave velocity and use these with the density of the rock to compute the rocks' compressive strength, which is the compressive stress that causes a rock to fail, and the rocks' flexibility, which is the relationship between stress and deformation for a rock. Converted wave analysis is also used to determine subsurface lithology and porosity (Tiabb et al. 2004).

Different methods of analysis exist, such as coring, fluid sampling (wireline and/or drill stem tests), and well logging. Coring or core analysis is a direct measurement of petrophysical properties, where rock samples are retrieved from subsurface and measured by core labs. This process is time consuming and expensive. Well logging is used as a relatively inexpensive method to obtain petrophysical properties downhole. Measurement tools are conveyed downhole using either wireline or LWD (logging while drilling) methods (Poupon et al. 1970).

In practical terms, petrophysics is used for two types of calculations: determination of original hydrocarbons in place and their distribution, and reservoir engineering dynamic flow calculations. For the development geoscientist, petrophysics means developing the detailed stratigraphic, depositional and diagenetic descriptions of the reservoir, both vertically and areally (Crain et al. 1986).

2.7.4. Relative Permeability Analysis

Relative permeability of rock to a reservoir fluid (oil, gas or water) is defined as the ratio of the effective permeability of the respective fluid phase to the absolute permeability of the rock. When two or more fluid phases are mobile in a reservoir, relative permeability is the single most important characteristic that controls the production of the flowing phases (Satter et al. 2016).

Relative permeability data should be obtained using experiments that best model the type of displacement that is thought to dominate reservoir flow performance. For example, water – oil imbibition curves are representative of waterflooding, while water – oil drainage curves describe the movement of oil into a water zone. Permeability and relative permeability describe the flow of a particular fluid in a particular rock type. If the fluid system changes or the rock type changes, the appropriate values of permeability and relative permeability must be measured. For example, if a waterflood is planned for an oil reservoir that is being depleted, laboratory measured permeabilities need to represent the injection of water into a core with reservoir oil and connate water (Fanchi et al. 2010).

Relative permeability data are often measured and reported for laboratory analysis of several core samples from one or more wells in a field. The set of relative permeability curves should be sorted by lithology and averaged to determine a representative set of curves for each rock type. Several procedures exist for normalizing or averaging relative

permeability data (Fanchi et al. 2010). The values of relative permeability range between 0 and 1 (Satter et al. 2016).

Darcy's law to multiphase flow, is used to calculate the relative permeabilities:

$$q_i = -\frac{k_i}{\mu_i}\nabla P_i \qquad \text{for } \boldsymbol{i} = 1, 2 \tag{2.18}$$

Subscript ***i*** indicates that the parameters are for phase ***i***

Where:

q_i is the flux [cm^3/cm^2s]
∇P_i is the pressure gradient [atm/m]
μ_i is the viscosity [cp]
k_i is the phase permeability (effective permeability for phase ***i***) [Darcy]

Relative permeability, k_{ri}, for phase ***i*** is then defined from $k_i = k_{ri}k$, as:

$$k_{ri} = {k_i}/{k} \tag{2.19}$$

Where k is the permeability of the porous medium in single phase flow, *i.e.*, the absolute permeability.

2.8. THERMAL ANALYSIS TECHNIQUES

2.8.1. Differential Thermal Analyzer (DTA)

DTA is a thermal technique in which the temperature of a sample, compared with the temperature of a thermally inert material, is recorded as a function of the sample, inert material, or furnace temperature as the sample is heated or cooled at a uniform rate. Generally speaking, phase transitions, dehydration, reduction, and some decomposition reactions produce endothermic effects, whereas crystallization, oxidation, and some decomposition reactions produce exothermic effects. The temperature changes occurring during these chemical or physical changes are detected by a differential method, such as illustrated in Figure 2.9. If the sample and reference temperatures are T_s and T_r, respectively, then the difference in temperature, $T_s - T_r$, is the function recorded. Small temperature changes occurring in the sample are generally not detected by this method (Wendlandt et al. 1974).

DTA analyzers operate at near-atmospheric pressure and are operated at high heating rates; hence, they provide very little information concerning the low temperature liquid phase reactions (Bhattacharya et al. 2017).

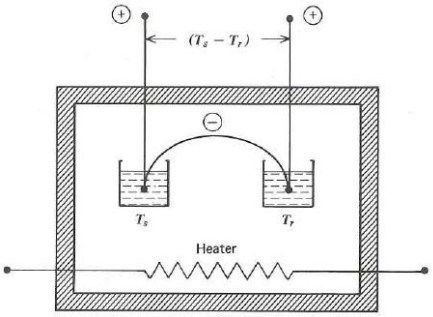

Figure 2.8 Basic DTA System (Wendlandt, 1974).

2.8.2. Thermogravimetric Analyzer (TGA)

The thermal analysis technique of thermogravimetry (TGA) is one in which the change in sample mass is recorded as function of temperature. Three modes of thermogravimetry exist: (a) isothermal or static thermogravimetry, in which the sample mass is recorded as a function of time at constant temperature; (b) quasistatic thermogravimetry, in which the sample is heated to constant mass at each of a series of increasing temperatures; and (c) dynamic thermogravimetry, in which the sample is heated in an environment whose temperature is changing in a predetermined manner, preferably at a linear rate (Wendlandt et al. 1974).

The resulting mass-change versus temperature curve provides information concerning the thermal stability and composition of the initial sample, the thermal stability and composition of any intermediate compounds that may be formed, and the composition of the residue, if any. Except for the mass-changes, much of the information obtained from the TGA curve is of an empirical nature in that the transition temperatures are dependent on the instrumental and sample parameters. The thermal stability indicates the ability of substance to maintain its properties as nearly unchanged as possible on heating (Wendlandt et al. 1974).

A high pressure TGA named TherMax 500 which was manufactured by ThermoCahn Co, and it can handle pressures up to 1,000 psig and temperatures up to 1,000°C, using heating rates of up to 25°C/min.

2.8.3. Pressurized Differential Scanning Calorimetry (PDSC)

The PDSC is a differential scanning calorimeter under either high or low-pressure conditions. Raw materials and finished products are often processed or intended for use at elevated temperature and pressure. Conventional calorimetry characterizes well the changes in physical and chemical properties of materials. Now, pressure DSC extends characterization of materials to extreme pressures. A calorimeter measures phase changes, reactions or processes that absorb or release heat. A PDSC measures the effects of pressure on these measurements. PDSC results are often different for

samples analyzed in open versus hermetically sealed pans due to changes in pressure inside sealed pans. PDSC controls pressure to study and understand the reason for those differences. Materials processed at conditions other than ambient temperature or products designed for extreme end use conditions can be better characterized at operating conditions using a controlled pressure DSC. The heart of the PDSC is a heat flux plate designed to measure small energy changes with reliability versus not just temperature but also versus pressure (Instruments Specialists Incorporated).

This test provides fingerprinting of oils and combustion kinetics using oil or oil plus core. It is useful to identify dominant reaction regimens, providing activation energies. It allows comparison of different oils or oils fractions (*e.g.* SARA) (Mehta et al. 2018).

2.8.4. Differential Scanning Calorimeter (DSC)

In order to estimate the relative ratio of free (bulk) and emulsified (dispersed) water in an emulsion, DSC is used. The use of this technique is based on the different water solidification (freezing) temperatures between dispersed and bulk aqueous phases. Thus, depending on the relative energy released at the different temperatures, during the solidification process upon cooling, the ratio bulk/dispersed water could be estimated in the synthetic emulsions when using different diluents (Balsamo et al. 2013).

DSC operates at near-atmospheric pressure and are operated at high heating rates; hence, they provide very little information concerning the low temperature liquid phase reactions (Bhattacharya et al. 2017).

2.8.5. Accelerating Rate Calorimeter (ARC)

The ARC is unique for its exceptional adiabaticity, its sensitivity, and its sample universality. ARC is one of the screenings tests used to determine the suitability for air injection enhanced oil recovery. These tests show oil reactivity and exothermicity over a broad range of temperatures: low temperature range, negative temperature gradient region, and high temperature range to 500°C (Bhattacharya et al. 2017).

ARC is used to assess the oil oxidation properties. It is designed to assess the oil ability to self-sustain a heat generating process under adiabatic conditions in the presence of oxygen at reservoir conditions (Germain et al. 1997).

The ARC consists of a small (1-inch diameter) spherical sample holder connected to auxiliary flowlines, into which the reactants are placed under very accurate temperature and heat supply control so that rapid exothermic reactions can be followed and held under adiabatic conditions (Bhattacharya et al. 2017). Figure 2.9 shows a schematic of an ARC.

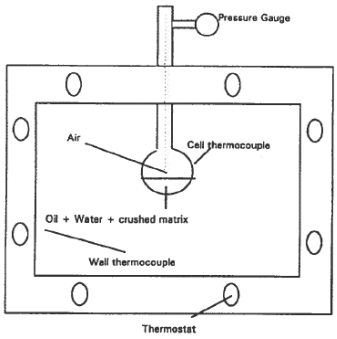

Figure 2.9 ARC Description. dT/dt, Pressure and Temperature are Recorded. (Germain et al. 1997)

An ARC can handle high operating pressures (designed to operate to 41.5 MPa) and reservoir temperatures up to 500°C (Yannimaras, 1995). Because of its pressure capability, the ARC is generally used to evaluate light oil (HPAI) candidate reservoirs (Bhattacharya et al. 2017)

ARC tests are run to obtain the Arrhenius activation energy, pre-exponential factor, and order of reaction, along with the starting temperature and extent of the main exotherms (Yannimaras et al. 1995).

Two types of ARC tests exit (Yannimaras et al. 1995):

- "Closed" ARC system testing, where fixed amount of air, is initially charged to the reactor. When testing light oils from high pressure reservoirs, the initial charge pressure is the original reservoir pressure. If tests are performed on low pressure reservoirs, the initial pressure is often set at a level which provides enough oxygen to consume the mass of oil sample. The test is performed at near adiabatic operation.
- "Flowing" type ARC testing, where the oil sample is maintained under a continuously replenished stream of air at reservoir pressure and quasiadiabatic operation.

The ARC differs from other commonly used thermal analyzers in that it only is heated in a near linear with time schedule when exothermic reaction are not occurring. When an exotherm is detected, the heating rate depends on the rate of heat generation.

2.8.6. Ramped Temperature Oxidation Apparatus (RTO)

RTO tests allow for a comprehensive understanding of the ISC behavior in the LTR, HTR and the Negative Temperature Gradient Region (NTGR), and the experimental results can be used to investigate the kinetic parameters for combustion reactions. RTO experiments involve the controlled heating of re-combined, oil-saturated cores in a plug flow reactor under a flowing gas stream using a range of oxygen concentrations. Figure 2.10 shows a schematic of RTO (Chen et al. 2014).

The parameters normally measured are oxygen uptake, oxygen utilization, apparent atomic hydrogen/carbon ratio, fraction of reacted oxygen converted to carbon oxides, $(CO_2+CO)/CO$ ratio, CO_2/N_2 ratio, and apparent air/fuel ratio. These parameters may be calculated on an instantaneous basis (based on product gas composition only), incremental basis (based on moles of the individual components over a given time period) or on an overall basis (based on cumulative mole of the individual produced gases).

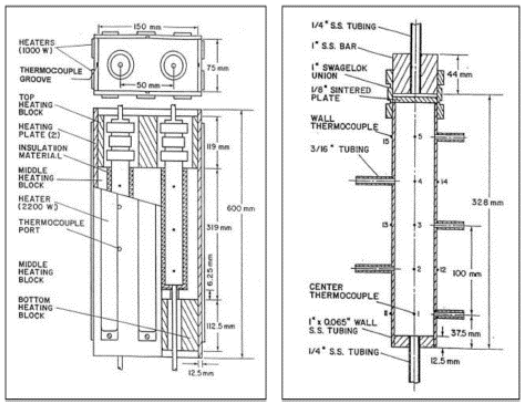

Figure 2.10 Schematic of RTO Apparatus (Chen, 2014).

2.8.7. Combustion Tube (CT)

Combustion tube tests are designed to simulate the nature of the propagating combustion front and the resulting dynamic reaction kinetics in conditions closely approximating those in a reservoir (Tiffin et al. 1997).

Information on some of the mechanism governing the air injection process can be obtained from combustion tube tests. A properly designed and operated combustion tube test can provide much useful information about the test rock/oil system's combustion characteristics. The air and fuel requirements are the key parameters which show the best agreement with properly operating field projects. Following are the parameters normally measured:

- Equivalent apparent atomic H/C ratio of the burned fuel
- Air/fuel ratio
- Oxygen/fuel ratio
- Oxygen requirement, discussed above
- Fraction of reacted oxygen converted to CO_xs
- Effect of the injected water-air ratio on the process parameters
- Characteristics of the produced fluids
- Peak combustion temperatures
- Potential H_2S generation

- pH of produced water

Many of these parameters are strongly influenced by, amongst other factors, the properties of the test fluid, the test pressure and temperature and the nature of the rock matrix (permeability, porosity, and how much clay and pyrite it contains) (Prasad et al. 1986).

With the information obtain it is possible to know the stability of the combustion reactions, the economic parameters (air, fuel requirements), monitoring parameters (composition of product gases and properties of liquids produced) and operating strategies (Mehta et al. 2018).

Figure 2.11 Combustion Tube for 21 MPa Tests (Mehta et. al 2018)

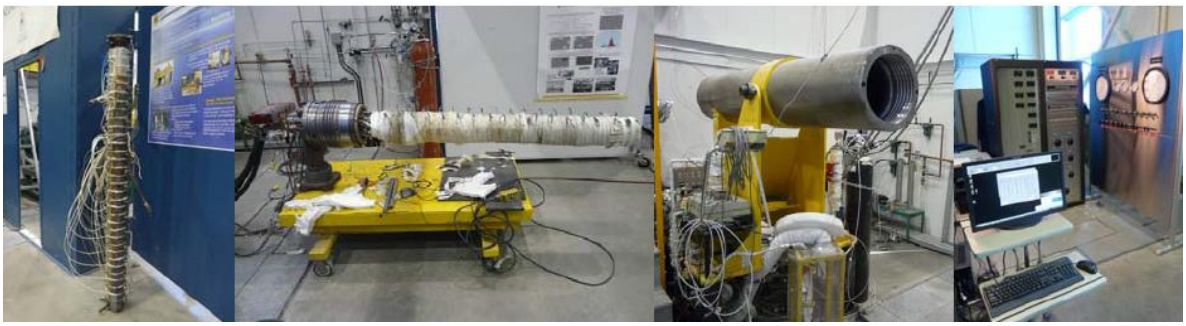

Figure 2.12 Combustion Tube for 42 MPa Tests (HPAI) (Mehta et al. 2018)

2.8.8. Effluent or Evolved Gas Analysis (EGA)

Effluent or Evolved Gas Analysis involves measuring the product gas composition and product gas volumetric flow rates associated with combustion tube tests, Ramped Temperature Oxidation (RTO) tests and any thermal analysis apparatus for which product gas is generated.

CHAPTER 3

HIGH PRESSURE AIR INJECTION (HPAI)

As discussed in the previous chapter ISC or fireflooding is for heavy oils which require operation in the high temperature range (+350°C), for successful displacement of the oil by the oxidation zone, and HPAI is for light oils reservoirs, for which bond scission or combustion reactions are dominant in the 150 to 300°C or Low Temperature Range (Moore et al. 2002). HPAI is also an economically viable alternative to gas injection, for deeper high gravity reservoirs, when the large volume of medium BTU gases produced can be effectively utilized (Erickson et al. 1994).

HPAI is defined as an enhanced oil recovery process in which compressed air is injected into a high gravity, high pressure, deep oil reservoir, with the expectation that the oxygen in the injected air will react with a fraction of the reservoir oil at an elevated temperature to produce carbon dioxide (Moore et al. 2002). The resulting flue gas mixture, which is primarily CO_2 and nitrogen, provides the mobilizing force to the oil downstream of the reaction region, sweeping it to production wells. The gas-oil mixture may be immiscible, or partly or completely miscible. In some situations, the elevated temperature reaction zone itself may provide a critical part of sweep mechanism in terms of incremental recovery. Prasad et al. (1986) mentioned that immiscible displacement of oil by carbon dioxide is an important mechanism at these pressures, assisting in displacing oil more rapidly.

Air injection into high pressure reservoirs is an emerging technology for the enhanced recovery of light oils. It is probably the best hope for improved recovery from the world's ever declining reserves of conventional oil and profitable enhanced recovery of the enormous quantities of residual oil trapped in depleted and matured water flooding light oil reservoirs (Shokoya et al. 2001).

In the simplest implementation, the process is initiated by injecting air, which will spontaneously ignite the in-place oil due to the high temperature and pressure conditions in the reservoir. In situations where spontaneous ignition of the native reservoir oil is not likely to occur, the ignition must be aided with the injection of a chemical mixture capable of spontaneous ignition at the reservoir conditions, or by an initial input of energy, usually provided by a downhole heater or a burner. Air injection is achieved using compressors that are specifically designed for air at the pressure levels that are required to inject the desired volumes (Moore et al. 2002).

To interpret and optimize field performance of the front combustion generated by the HPAI, dominant chemical and physical mechanism of the displacement process must be understood, and the influence of reservoir characteristics and operating procedures in determining swept areas of the reservoir must be established.

During the early life of a HPAI project, the air requirements per incremental barrel of oil are directly related to the water/oil ratios (Erickson et al. 1994).

Chemically there are some critical factors to consider in order to have a successful HPAI, which are:

- Bond scission reactions, where oxygen breaks up the hydrocarbon molecules and produce CO_2 and water. For light oils these reactions primarily happen between 150 and 300°C.

  Hydrocarbon + Oxygen → Carbon Oxides + Water

- Oxygen addition reactions, where oxygen atoms are chemically bond into the molecular structure of the liquid hydrocarbon, producing various oxygenated compounds (hydroperoxides, aldehydes, ketones and acids). The compounds tend to further react and polymerize with each other, forming heavier oil fractions. These reactions appear to dominate temperatures below 150°C for light oils.

  Hydrocarbon + Oxygen → Oxygen addition products

Tadema et al. (1959) performed several combustion tests with a transparent combustion tube. Figure 3.1 shows the process with a simplified diagram. It was observed that most of the oil in place is not consumed in the combustion zone but is transported away from the injection well, at the front of the reaction zone, in a constantly growing region of high oil saturation. The high oil saturation results from the combined effects of gas drive, water drive, steam drive, and vaporization of the virgin oil. Oil production is not expected until the edge of this oil bank reaches the production sand face or well. It is theorized that the oil within the oil bank is lighter than the virgin oil and becomes more volatile as the burn progresses. The reasoning is that heavy fractions tend to be burned, whereas lighter fractions tend to be vaporized in the steam bank and vaporization regions, which subsequently are transported downstream to the oil zone. As a result of this reflux of lighter components, the concentration of lighter ends in the oil zone is expected to increase continually (Lerner et al. 1985). The oil is subjected to water and steam drives. The water and steam zones are produced from water initially in place plus water produced by combustion reaction.

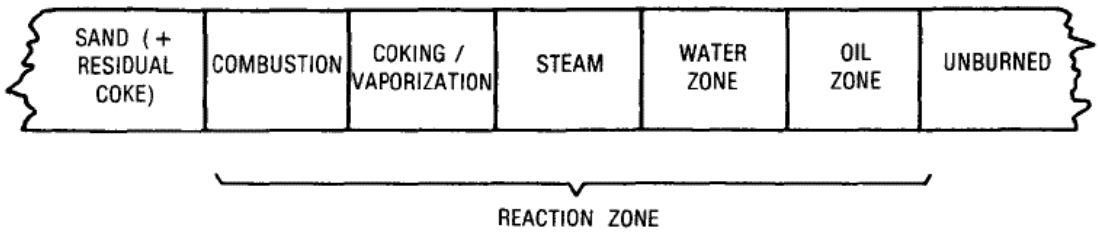

Figure 3.1 Simplified Picture of the Reaction Zone for a ISC Process (Lerner et al. 1985).

Avoiding operations in an oxygen addition reaction mode is highly desirable for essentially all air injection-based process, by ensuring operation in the bond scission mode.

In the combustion zone, oil that has not been displaced is consumed and the majority of heat is released. The primary products from combustion are CO_2 and water. From stoichiometry, the hydrogen/carbon ratio of the fuel determines the mass of oxygen consumed per mass of fuel, the amount of CO_2 produced per mass of fuel, and the total produced gas flux for given oxygen and nitrogen flux. Produced CO_2 is typically highly soluble in the oil, usually called “oil swell”. Indeed, one proposed advantage of 100% oxygen injection is that higher concentrations of CO_2 expected downstream of the burn zone should reduce fuel consumption and required oxygen (Lerner et al. 1985).

The main recovery factors of the HPAI applied to light oil reservoirs are (Clara et al. 1999):

1. Flue gas sweeping
2. Field re-pressurization allowing a faster oil production,
3. Oil swelling, mainly by the *in situ* generated CO_2 dissolution
4. Stripping of the light components of the oil by the flue gas,
5. Later thermal effects.

Laboratory studies and cores taken from post burn regions of fields show that approximately 5 to 10 percent of the OOIP is consumed as fuel for the process; the rest is mobilized and can be available for capture (Moore et al. 2002).

The key parameters to have a successful HPAI which is initiated by spontaneous ignition are (Moore et al. 2002):

- The amount of OOIP at the start of air injection and the ability of the oil to spontaneously ignite and sustain stable oxygen uptake reactions (bond scission) over the life of the injectors.
- Air compressors
    - ✓ The pressure and volume rating of the units.
    - ✓ Successful ignition can result in a significant rise in the injection pressure.
    - ✓ Specify the volume of the reservoir that they desire to service with a given injector and the operating life they desire for that injector.
- Laboratory screening of candidate reservoirs
    - ✓ Provides an indication of whether the oil will react in the desired oxidation mode at reservoir conditions.
    - ✓ Provides parameters such as air and fuel requirements, and air/oil ratios that can be used for conducting preliminary economic assessments of field projects.
    - ✓ Supplies kinetic data that can be used for numerical simulations.
    - ✓ Provides produced gas compositions and water composition.
- Air injection rate must be able to sustain the combustion reactions
    - ✓ Sufficient air must be injected to maintain the oxidation reactions in the bond scission or combustion mode.

Finally, kinetics depend on:

- Composition of the oil

- Solid core matrix
- Connate brine

One of the unique features of HPAI is the self-correcting nature of the combustion zone, due to the rapid mobilization of oil into the downstream pores, which temporarily reduces the gas permeability and redirects the air flow (Moore et al. 2002).

Before arrival of the combustion zone, portions of the oil undergo vaporization and the extent of vaporization depends on oil volatility, the gas flux available to displace the oil that does vaporize, peak combustion temperatures attained, and distance between injection and production wells (since oil bank volatility continually increases). The flue gases displace the oil in a forward contacting extraction process, resembling a multi-contact vaporizing gas drive mechanism (Shokoya et al. 2001).

Shokoya et al. (2001) mentioned that the improvement in recovery of light oil by HPAI involves a combination of reservoir pressurization, oil swelling, immiscible gas displacement, super critical extraction (operating above the critical point of water), spontaneous ignition, complete oxygen utilization, near miscibility of the *in situ* generated flue gases with the reservoir oil.

The composition of the produced gas stream early in the life of a HPAI project is essentially the same as the reservoir solution gas. Traces of nitrogen from the combustion gases begin to show up very early, within weeks after start of injection. CO_2, because of the higher solubility, lags behind the nitrogen by months or even years (Mace et al. 1975).

The combustion process is a highly coupled problem that involves three phase fluid flow with heat, mass and momentum transport, and chemical reaction. Because of this coupled nature, it is difficult to isolate contributions of any one mechanism experimentally.

HPAI in light oil reservoirs can be divided in two principal modes; a) the conventional drive process, in which a combustion front displaces the oil horizontally, and b) a drainage process, in which the injection of air into a dipping reservoir causes gravity drainage (Fassihi et al. 1996).

HPAI is more than a simple gas flood, and it should be treated as a thermal process (Gutiérrez et al. 2007). For light oils, the heat generated is of secondary value and flue gas generation is the primary factor in displacing oil (Fassihi et al. 1996).

Light oils exhibit a negative temperature gradient region (NTGR) over the approximate temperature range from 280 – 350°C. This behavior is characterized by a decreasing rate of oxygen uptake as the temperature is increased. The oxygen uptake rates fall to levels which provide insufficient energy generation. Note for the light oils that the maximum temperatures in the LTR marks the beginning of the NTGR. This can be appreciated in Figure 3.2, where an ARC test for a light oil was performed and the bond scission reaction occurred in a temperature range of 200 to 260°C, and the NTGR took place between 260 to 320°C. In this figure the self-heat rate represents the energy generation rate divided by the heat capacity of the reactor, and self-heat rates are plotted

against the inverse of the corresponding absolute temperatures (in Kelvin). For purposes of clarity, the corresponded temperatures (in Celsius) are also indicated.

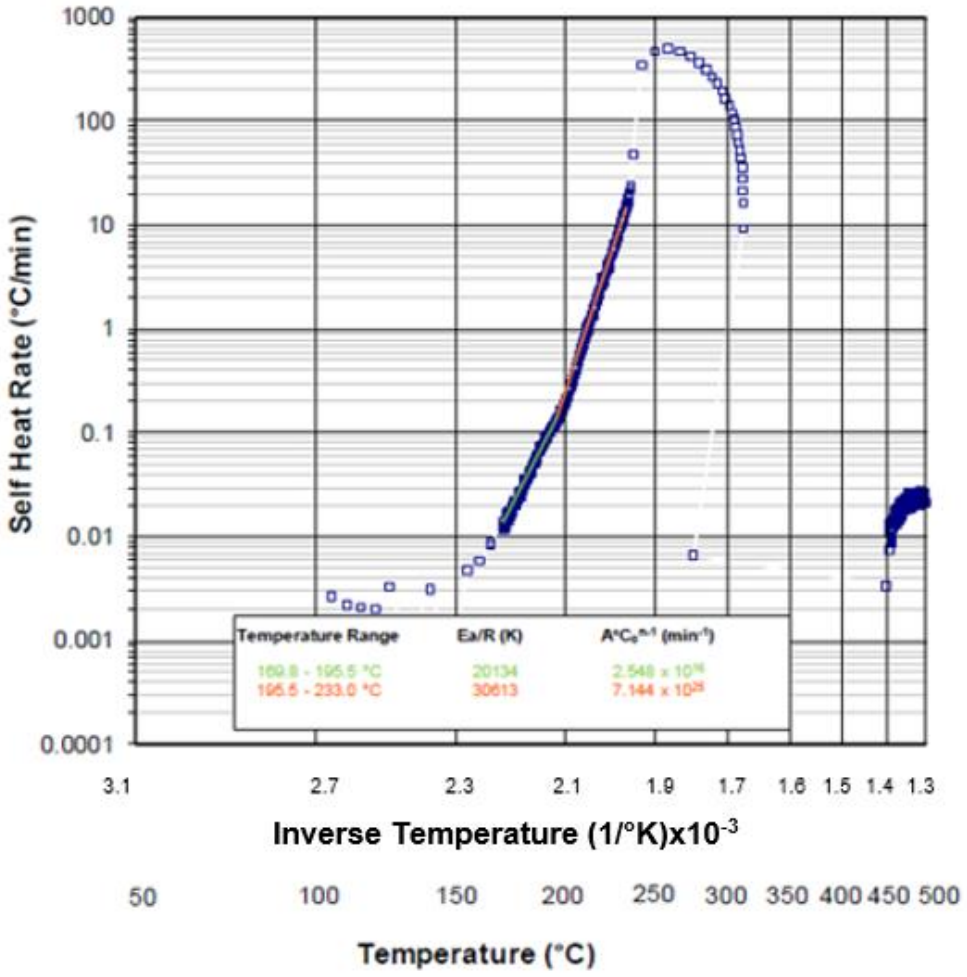

Figure 3.2 Oxidation Behavior for a Mexican Light Oil from the target Reservoir (Mallory et al. 2019)

The temperature difference between the temperature when the localized maximum rate occurs and the localized maximum or peak temperature in the LTR will depend on the composition of the crude oil as well as the effective heat capacity and heat loss characteristics of the reservoir (Moore et al. 1998).

For HPAI, since temperatures do not have to exceed those corresponding to the upper limit of the NTGR (<350°C), efficient light oil displacement can be maintained at relatively low oxygen fluxes (Moore et al. 1998).

Lerner et al. (1985) explained that for some light oils it could be assumed that some oxygen bypasses the combustion zone, LTO reactions may occur in the steam, water, oil, or virgin sand zones. Oxygen bypass can result from either insufficient combustion

rates (*i.e.* insufficient residence time) to consume all the oxygen in the high temperature burn zone or high permeability streaks that enable oxygen to travel so rapidly through the high temperature zone that it contacts insufficient fuel for complete utilization.

Table 3.1 summarizes the nominal temperature ranges in which oxygen addition and bond scission reactions are important for the model light oils. Light oil data are primarily based on the results of a number of combustion tube and ramped temperature oxidation experiments performed at the University of Calgary by the *In Situ* Combustion Research Group (Moore et al. 1998). It is noticed that Table 3.1 has been modified from the original table published in 1998.

Temperature Range (°C)	Dominant Oxidation Mode	Secondary Oxidation Mode	Reactant
<150	Oxygen Addition		
150 -300	Bond Scission	Oxygen Addition	
350 -700	Bond Scission		Gas Phase, solid residual
700 +	Bond Scission		Gas Phase

Table 3.1 Summary of Oxidation Kinetic Regimes for Model Light Oils (Moore et al. 1998)

Light oils have fewer operational problems, likelihood of autoignition and better oxygen utilization, and economics, light oils commanding a substantial financial premium over heavy oils (Fassihi et al. 1994).

HPAI process should improve under field conditions (high pressure) as the oil becomes more reactive (Gutiérrez et al. 2007).

The combustion process requires a minimum air flux to maintain the bond scission reactions; hence, it is preferable to inject into fewer injectors at higher rates than to operate a large number of injectors at lower rates. Operating a HPAI project at lower rates could result in oxygen addition reactions dominating the process and hence, reduced performance (Gutiérrez et al. 2007).

With HPAI the combustion gas drive displacement efficiencies are higher than for ISC projects. This is a result of several factors (Erickson et al. 1994):

a) Pressures are considerably higher hence, the product gases are more miscible;
b) Mobility ratios of displacing gas and oil are more favorable because of lower viscosity oil;
c) Higher reservoir temperatures improve oxygen utilization so there is less channeling of air, resulting in higher vertical and areal displacement efficiencies.

The composite effects of the previous three factors, are the ability to produce more oil with less air, and the effective elimination of heat and corrosion problems at the producing wells, at least during the early life. Also, produced gas per incremental barrel is less.

In light oils due to the miscibility of the carbon dioxide generated by the combustion reactions the oil swells, which enhances its displacement from the pores (Yannimaras et al. 1991).

A significant enhancement for the HPAI process could occur for reservoir above the critical pressure of water (22.1MPa), because the temperature of the steam generated by dry combustion could exceed water's critical temperature (374.1°C). Such super critical steam conditions are achievable only in HPAI. Extraction of hydrocarbons from the oil by supercritical steam could increase process efficiency substantially and lead to generation of miscibility (Yannimaras et al. 1991).

3.1. ADVANTAGES AND DISADVANTAGES OF HPAI

Some benefits in light oil are (Erickson et al. 1994, Fassihi et al. 1994, Gutiérrez et al. 2007, Moore et al. 1998 and Tiffin et al. 1997):

- Excellent displacement efficiency and mobilization of extra combustion oil.
- Rapid reservoir pressurization
- Flue-gas sweeping
- Flue gas stripping of the reservoir oil
- Oil swelling mainly by the *in situ* generated carbon dioxide
- Excellent displacement efficiency
- Mobilization of extra combustion oil
- Injection gas substitution
- Spontaneous oil ignition and complete oxygen utilization for HPHT reservoirs
- Operation above the critical point of water with possible super-extraction benefits
- Near miscibility and associated enhanced hydrocarbons extraction capability of the flue gas
- Air availability
- Salt precipitation from the formation water in the steam zone, which promotes better volumetric sweep of the reservoir
- When compared to ISC process, HPAI could be more attractive alternative than waterflooding in many cases, since the response would be six to ten times that expected from waterflooding. This is certainly true in low permeability reservoirs where water injectivities are limited.
- HPAI is a unique method of conserving natural resources by increasing the recovery of clean burning petroleum hydrocarbons.
- Fuel requirements are substantially less for HPAI than ISC as the operating temperature at which bond scission reactions occur are significantly lower for a successful HPAI than for a successful ISC project.
- The average BTU content of the produced gases from higher gravity HPAI projects is substantially higher than for ISC. Utilization of the higher BTU gases can significantly improve the overall economics of HPAI.

- Light oils generally have good mobility in the cold portion of the reservoir; thus, the combination of the cold zone mobility and capability of effective displacement at low fluxes means that a single injector can service a much greater volume of light oil reservoir.
- Oxidation reactions in light oils are much less sensitive to air flux, they can be maintained in the bond scission mode while operating with moderate air injection rates on reservoirs which have been developed on large spacings. Even if the air flux is not sufficient to sustain operation in the bond scission mode, an air injection project involving the light oil will continue as a gas flood within the regions not affected by the oxidation reactions.
- Air is a low cost injectant, compared with methane or nitrogen
- The operating conditions associated with HPAI candidates result in higher density of the flowing gas phase (pressure effect), lower viscosity of the oil phase (temperature and pressure effect), increased solubility of gas phase components, lower residual oil saturation and lower residual water saturation (temperature effect).

Some disadvantages are:

- The reservoir should have sufficient temperature to generate the spontaneous ignition when air is injected.
- Air flux depends of air injection capacity and well spacing.
- Extrapolation of the GOR suggested by Fassihi et al.1994, is not appropriate to estimate recovery factors of HPAI projects; its application could lead to the underestimation of reserves and more importantly, to the mismanagement of the project (Gutiérrez et al. 2007).
- High capital and operating cost of compressors compared to water injection pumps.
- The general misconception that HPAI is a thermal recovery process which is best suited for reducing oil viscosity by increasing the temperature (Moore et al. 1998).
- The major concern with spontaneous ignition and low air flux operation is the formation of hydroperoxides in the region of the injection well. Great care must be taken during the early air injection period to ensure that air is continuously supplied to the air injectors so as to prevent burn back into the injection well (Moore et al. 1998).

As a way to having a successful HPAI project the following stops are required:

- Perform tests with the reservoir fluids at reservoir conditions.
- Provide technical parameters resulting from these experiments.
- Build appropriate numerical models to simulate lab experiments and obtain field rate and recovery predictions.
- Design and operate field projects efficiently and safely.

CHAPTER 4

TARGET RESERVOIR

The reservoir under study is located in the south of Mexico in Tabasco State. The south area of Mexico is well known for being an oil zone which is very complex due to the geology, depth of the hydrocarbons and the high pressure – high temperature conditions that predominate in that area.

The rocks from the late Jurassic are the oil producers in the states of Tamaulipas, Veracruz, Tabasco, Campeche in Mexico and in the south of the United States. Geologically, they are the oldest oil reservoirs and deepest in this regions, located between 3,000 and 5,000 meters. The layers in this age are potentially the storage of oil in the Gulf of Mexico (plays).

The south portion of the Gulf of Mexico produces more than 65% of the oil in Mexico, in the region several oil and gas source horizons are present: Oxfordian and Tithonian. Both periods match with source intervals around the world. The most prolific horizon is the Tithonian, and the differences between the types of oil from these rocks are the level of maturity that the source rocks had reached.

The target reservoir is a carbonate (dolomite) light oil reservoir which is a naturally fractured reservoir and it is in an anticlinal, and limited by faults and a saline dome. For a better understanding, the main concept about naturally fractured reservoir and saline dome are discussed below, as well as the impact of these conditions in the target reservoir.

4.1. NATURALLY FRACTURED RESERVOIRS (NFR)

A definition reported by Nelson et al. (1985) is “A reservoir fracture is a naturally occurring macroscopic planar discontinuity in rock due to deformation or physical diagenesis”. Aguilera et al. (1995) defines a NFR as “a reservoir which contains fractures created by mother nature. These natural fractures can have a positive or negative effect on fluid flow”. He defines positive/negative effect in flow when open uncemented or partially cemented fractures can connect oil flow (positive) or gas and water (negative due to coning effects). Totally cemented fractures may create seals to all types of flow. In Aguilera´s et al. opinion (1995), Aguilera says that for him all reservoirs have a certain amount of fractures, hence all reservoirs are NFR.

The importance for looking into fractures is because they could delineate the reservoir structure, define the mechanism of the fracture and predict the reservoir properties (porosity and permeability) and potential. Also, when studying the fractures, the morphology, intensity, width and fracture/matrix communication can be predicted. It is important to remember that the fractures influence the displacement of oil, so recovery

is affected by them and fractures are usually formed in rocks which are brittle (Aguilera et al. 1995).

In a NFR two types of porosity are present: primary and secondary porosity. Aguilera et al. (1995) defines primary porosity as the porosity that is established when the sediments are first deposited. Thus, it is an inherent, original characteristic of the rock. The value of primary porosity depends on many factors, such as arrangement and distribution, cementation and degree of interconnection among the voids. Therefore, it is necessary to differentiate between total primary porosity and effective porosity. Total primary porosity is the ratio between the total primary void spaces and the bulk volume of the rock. Whilst, the effective primary porosity is the ratio between the interconnected void space and the bulk volume of the rock.

Secondary porosity is the result of geologic processes after the deposition of sedimentary rock and has no direct relation to the form of the sedimentary particles. In general, secondary porosity is due to solution, recrystallization, dolomitization and fractures (Aguilera et al. 1995).

Developing NFR has led to numerous economic failures. Reservoir engineers usually make two key assumptions: 1) the fractures have a negligible storage capacity and are only channels of high permeability that allows fluids to flow; and 2) the matrix has an important storage capacity, but a very small permeability. The first assumption creates a big fiasco due to the fact that many reservoirs that produce at high initial rates decline drastically after a short period of time. This occurs because the producible oil has been stored in the fracture system. The second assumption must be studied carefully. If the permeability of the matrix is very low, then the oil bleed-off from the matrix into the fractures might be very slow and only the oil originally within the fractures will be produced in a reasonable span of time. If the matrix has a reasonable permeability, then the storage capacity of the matrix becomes of paramount importance, Figure 4.1 (Aguilera et al. 1995).

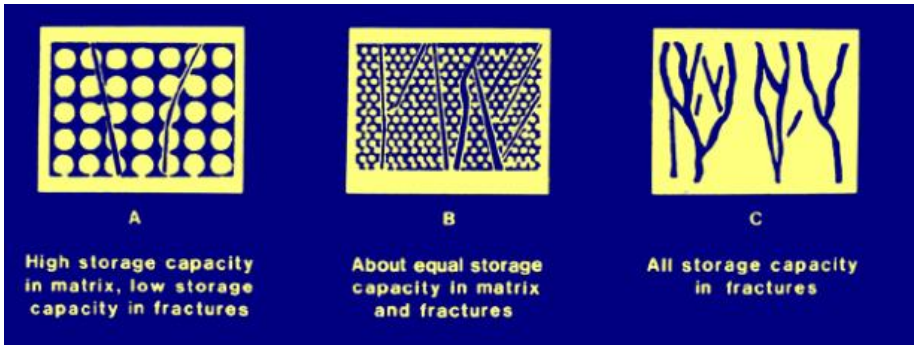

Figure 4.1 Schematic Sketches Showing Porosity Distribution in Fractured Reservoir Rocks (McNaughton et al. 1975).

Other parameters that play an important role on how quickly oil moves from the matrix into the fractures include matrix porosity, total matrix compressibility, fracture spacing or

distance between fractures and oil viscosity. Because of its low viscosity, gas movement from the matrix into the fractures is faster than oil movement (Aguilera et al. 1995).

Permeability is another important property and it is defined as the measure of the capacity of the medium to transmit fluids. Reservoirs can have primary and secondary permeability. Primary permeability is also referred to as matrix permeability by reservoir engineers. Secondary permeability can be either by fractures or solution vugs (Aguilera et al. 1995). The presence of unhealed, uncemented, open fractures greatly increases the permeability of a rock/reservoir. Effective or net confining pressure, *i.e.*, the difference between confining and pore fluid pressure, plays an important role in generation of fractures (Aguilera et al. 1995).

To study the fractures in a reservoir there are different sources of information that we can resort to, and they are classified as direct and indirect sources. Direct sources are core analysis, oriented cores, drill cuttings, and downhole cameras. The indirect sources are: drilling history, log analysis, well testing, inflatable packers, and production history (Aguilera et al. 1995).

4.2. SALINE DOME

It is important to understand the formation and behavior of saline domes because important resources of sulphur, oil and gas, around the world, are associated with saline domes.

The salts deposits form as an effect of evaporation. There are two mainly environments to generate salt layers. In the marine environment due to the evaporation of the water and the precipitation of the salt from the water and on land due to the evaporation in brackish lagoons, also known as evaporite rocks (Figure 4.2).

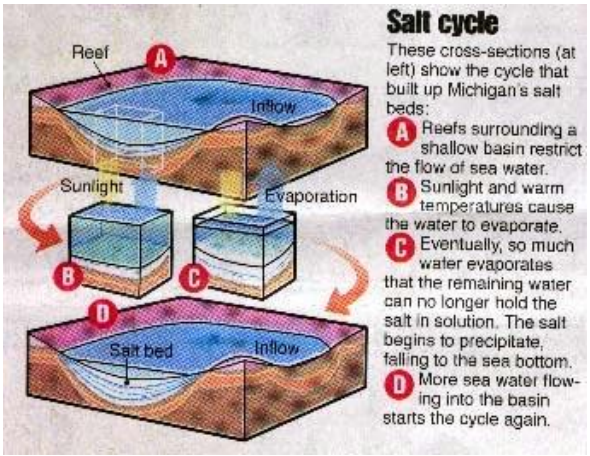

Figure 4.2 Salt Cycle (Source: Michigan State University - Geography)

Around the world several salt deposits are known. The total thickness of these deposits can be 1,000 meters, mainly from the Precambrian and Tertiary. It is been stated that in

a marine environment, relatively closed and for the big amount of water evaporation the salts concentration increases. With more evaporation the salts precipitate in a relation with its solubility capacity.

The largest extension and thickness of evaporite deposits are from marine origin. It has been calculated that from a water column 427 meters height, 6.7 meters of halite precipitate and 0.3 meters of cast (Baños et al. 2009). The halite is present in uniform stratified deposits, generating different textures and sedimentary structures. The cast is a non-uniform mass or in layers with some deformation due to the volume increase that the salt suffers during the hydration, showing different fibrous textures or crystals and sediments crisscrossed.

The halite is frequently associated with other evaporates and it can form saline domes, where the halite is found at the central portion of the dome (core) and it is surrounded by sediments. In the top of the dome it has cast, limestone or anhydrite indistinctly. These saline domes are actually sedimentary intrusions, which were generated due to density difference present. The evaporites, in this case the halite, is less dense than the sediments on top, that is why when it has some lithostatic pressure, it tends to emerge at zones with less pressure, usually upwards, causing the salt intrusion in the overburden layers (which are weaker than the salt). In Figure 4.3 it is shown the relation between density and depth.

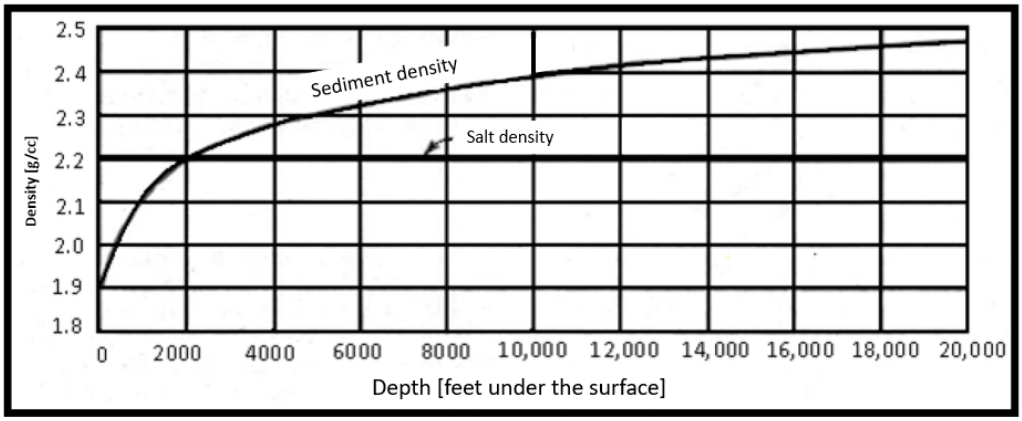

Figure 4.3 Plot of the Behavior of Salt and Sediments Against Depth (Baños et al. 2009)

The salt layers (saline domes) move/behave depending on temperature. When the salt layer is near the surface, it means, at low temperature, its own internal resistance impedes its flow. On the other hand, salt is highly mobile when it is hot, but to increase the temperature it has to gain depth, and this implies that several kilometers of sediments have to deposit on top of it.

The evaporite rocks are classified based on their mineralogy composition and chemistry. Hence, these rocks are divided in four main groups: carbonates, sulfates, chlorides, and bromides.

- Carbonates: calcite ($CaCo_3$), dolomite ($CaMg(CO_3)_2$) and magnesite ($MgCO_3$)

- Sulfates: anhydrite ($CaSO_4$) and cast ($CaSO_4\ 2H_2O$)
- Chlorides: halite (regular salt) (NaCl), silvite (KCl) and carnallite ($KMgCl_3\ 6H_2O$)
- Bromides: borax ($Na_2B_4O_5\ (OH)_4\ 8H_2O$)

The evaporites can be developed in continental, marine and mixed environments. The principal factor to generate them is the climate condition: dry and arid. The salt in layers is generated due to the evaporation in extended rock beds and where the environmental conditions allowed the salt masses to precipitate on layers which reached thickness of 1,000 meters.

The saline domes are present when pre-existent sedimentary layers press vertically or laterally, due to the low density of compacted salt (2.16 g/cc), the salt behaves like a plastic or like an extremely viscous fluid (but salt's viscosity is really low if it is compared with other sedimentary rocks, except for the clays) and creates reservoirs of cylindrical shape with a ellipsoid or circular diameter surrounded/covered by anhydrite or a cast of calcite rock.

There are two main types of domes as shown in Figure 4.4

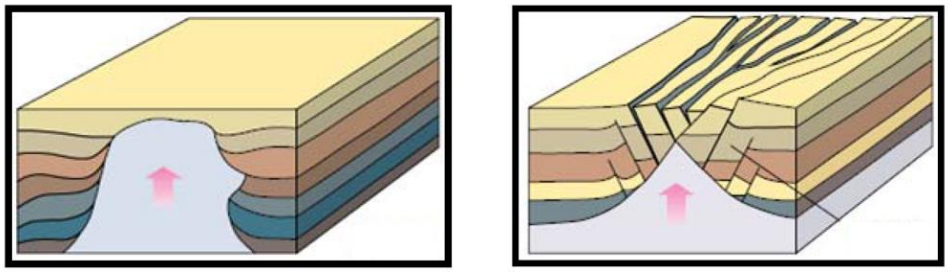

Figure 4.4 Different Types of Salt Structures (Baños et al. 2009)

For a long time, the saline structures where explored, due to their high potential related with the hydrocarbons, because salt is a rock that presents a great seal to trap the oil and gas. Now days, the challenge is to identify the oil and gas reservoirs under these domes. Figure 4.5. The sub-saline plays (a stratigraphic unit which contain hydrocarbons) have the characteristic of being aloctones formations (away from their original deposit) (Baños et al. 2009).

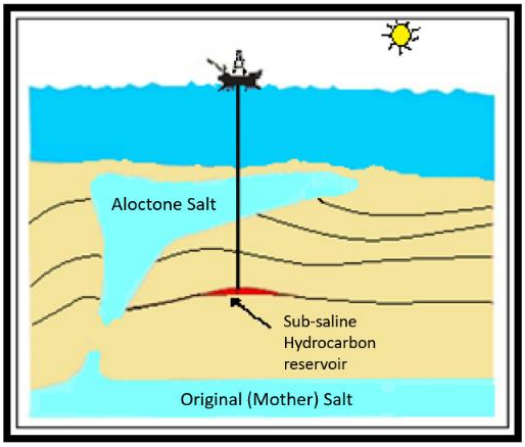

Figure 4.5 Example of a Sub-Saline Reservoir (Baños et al. 2009)

Based on several studies made in the South East of Mexico, in the area included by the east of the Itsmo de Tehuantepec, west of the Yucatan Peninsula, and the marine area of the Gulf of Mexico, it is understood that during the Middle Jurassic an extended oceanic basin was formed, where a deep sequence of evaporites (salt, cast and anhydrite) was deposited for more than 1,500 meters, product of a transgression (movement of the ocean plate over the continental plate) that generated the ancestral Gulf of Mexico.

When the sinking of the Gulf's bottom increased, the environmental conditions changed, hence the evaporites accrued in high sequences of more dense minerals (sandstones and shales), that later with the saline tectonic were affected during the late Oligocene and early Miocene, due to this the formation of important domes, diapirs and faults generated the geologic structures that have a huge economic oil interest.

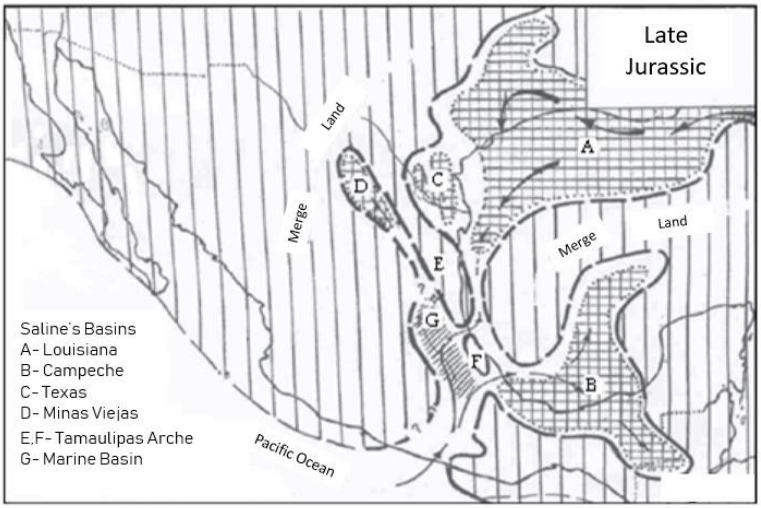

Figure 4.6 Formation of Saline Structures in Mexico (Baños et al. 2009)

4.3. GEOLOGY AND LITHOLOGY OF THE TARGET RESERVOIR

The principal field structure is an asymmetric anticlinal, elongate and is bounded by two inverse faults, with a slight NW-SE inclination, divided into two major blocks by an inverse fault in the North. Figure 4.7. The first block is bounded by two inverse faults with North-South orientation, with a West-East inclination, with the water contact in the North at 5,500 meters. The field where the reservoir is located has a high incidence of faults due to the tectonic and saline movements of the area. These faults are impregnated with light oil. The petrophysical properties interpreted by the geophysical and core logs show an average porosity of 5 percent, permeability of 5mD, and a water saturation of 12 percent. The average depths are: 3,400 – 3,800 meters for the Tertiary, 5,500 – 6,200 meters for the Jurassic, and 5,300 – 5,900 meters for the early and middle Cretaceous. The formation that is producing now in the field has 53 meters thickness, with an area of 51 km^2, and belongs to the Late Cretaceous and Middle Cretaceous, formed mostly by limestone and dolomitic limestone. The top of the reservoir is located at 5,328 meters depth and the base is at 5,640 meters. Finally, the presence of a salt body in the deeper structures and in the neighboring region is present. It is believed that the salt body in the field is currently still an active mechanism (Salazar et al. 2009).

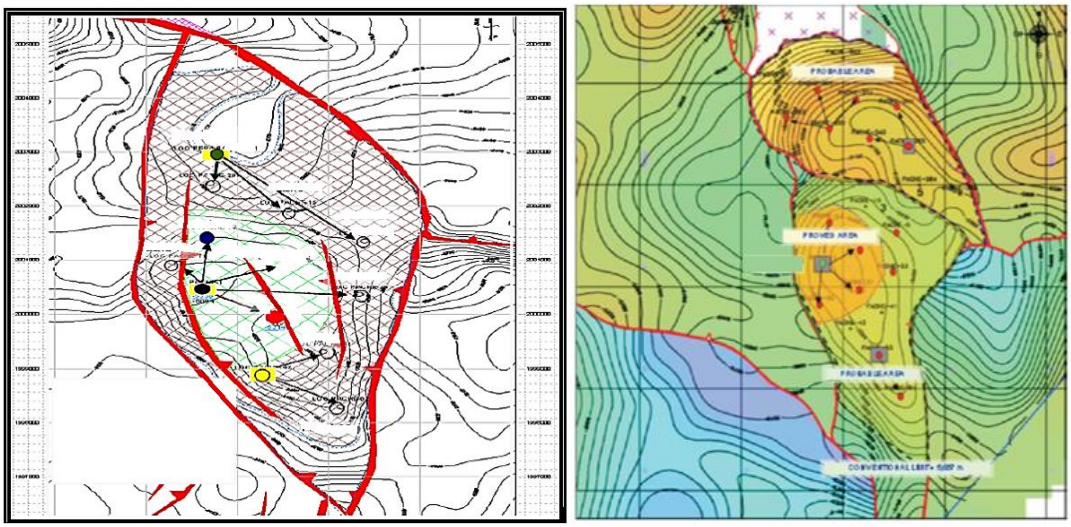

Figure 4.7 Structural Configuration of the Target Reservoir (Gómez et al. 2014).

The sedimentary model locates the reservoir in a marine platform from the Cretaceous. The regional stratigraphy of the target field is similar to the rest of the fields located in the south of Mexico (Tabasco seaboard, Chiapas and Marine area of Campeche). The sedimentary environments in the Southeast basin have an evolution from a continental environment to a marine environment. During the late Jurassic, a marine transgression produced shallow water environments generating a carbonate deposition with high energy. During the Thitonian, the transgression processes, combined with the subsidence, produced carbonated shales, which are the most important source rock in

the basin. During the early Cretaceous, several subsidence and extension processes occurred generating Horst and Graben; Figure 4.8 diagrams this phenomena. The rocks from the Thitonian Jurassic comprises dark brown mudstone with dolomites and/or dolomitic limestone inserted, whereas that in the Kimmeridgian characterized by light gray fractured dolomites, with caverns made by dissolution or evaporites. The early Cretaceous is also a sequence of carbonates with some fine grain dolomites (mudstone) and some layers of coarse grains (packstone to grainstone) of light brown to beige with fractures and micro cavities.

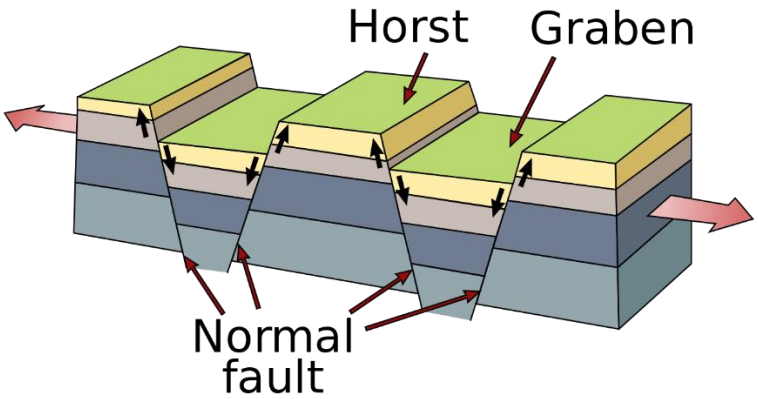

Figure 4.8 Horst and Graben Phenomena (© United States Geological Survey)

The Middle Cretaceous has the characteristic of crystalline dolomites with a sequence of beige to light brown color, with fractures and micro-cavities, and a fractured trail of dolomitic limestone inserted. The fractures present dissolution cavities, which are partially closed by calcite, organic material and hydrocarbons, and some of which are open.

The Late Cretaceous is the most complex section because it contains detritus and turbidites, with insertions of mudstone – wackestone and limestone slightly dolomitized (new water formation). Sometimes laminar bentonite limestone with slim shales are present, and in the base, some dolomites are found. The cap rock has compacted limestone and marl that belongs to the Late Cretaceous. Figure 4.9 shows the geology column of the field.

Age [Mil years]	Stratigraphic unit		Thickness [m]	Lithology
5.3	Pliocene		2256	Limestone and Sand
23	Miocene	Late Cretaceous	300	Limestone and Sand
		Early Cretaceous	458	
		Encanto	85	
		Deposit	35	
34	Oligocene	Late	210	Shale and Sand
		Middle		
		Early		
56	Eocene	Late	220	Shale and Sand
		Middle		
		Early		
66	Paleocene		1256	Shale
135	Cretaceous	Late	318	Limestone and marl
		Middle	160	Dolomite and limestone
		Early	131	Dolomite and limestone
141	Jurassic	Late	300	limestone

Figure 4.9 Geology Column of the Target Field

The seismic image shown in Figure 4.10 demonstrates how fractured and complex the reservoir is.

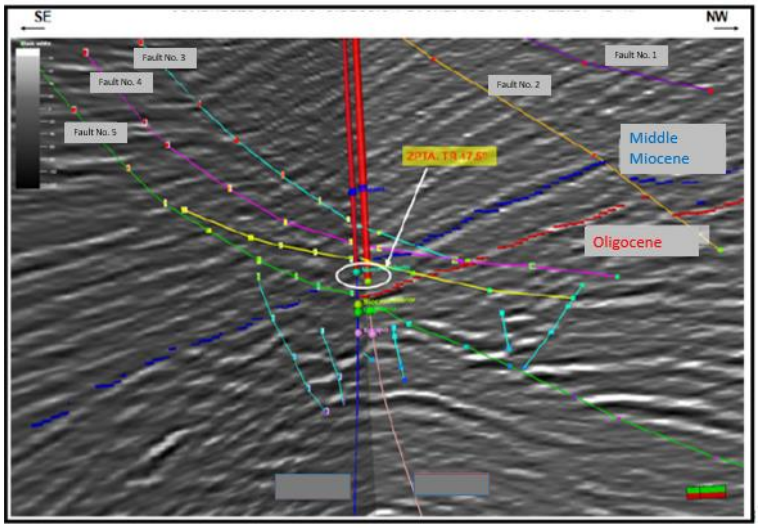

Figure 4.10 Seismic Section with SE – NW Direction (Gómez et al. 2014)

4.4. PRODUCTION HISTORY AND RESERVES OF THE TARGET RESERVOIR

As mention above, the petrophysical properties interpreted by the geophysical and core logs show an average porosity of 5 percent, permeability of 5mD, and a water saturation of 12 percent. The formation that is producing now in the field has 53 meters thickness,

with an area of 51 km^2, and belongs to the Late Cretaceous and Middle Cretaceous, formed mostly by limestone and dolomitic limestone. The top of the reservoir is located at 5,328 meters depth and the base is at 5,640 meters.

The initial conditions of the reservoir were: pressure of 59.6MPa (608 kg/cm^2) and temperature of 140°C, with a GOR of 593 $(ST)m^3/m^3$. From the PVT the oil density registered is 43.7°API (light oil), saturation pressure of 43.5 MPa (342.87 kg/cm^2) and a GOR of 443.29 $(ST)m^3/m^3$ at bubble pressure and 149°C.

Table 4.1, shows the reserves that were estimated at January 2014.

Reserve	Oil [10^6 STB]	Gas [10^9 cc(St)]
1P	3.64	4.19
2P	10.75	21.01
3P	10.75	21.01

Table 4.1 Oil and Gas Reserves of the Reservoir at January 2014 (PEMEX Exploración y Producción)

The declination in production is due to the low pressure at the reservoir and water cut. Figure 4.11, shows the oil, water and gas rate against time.

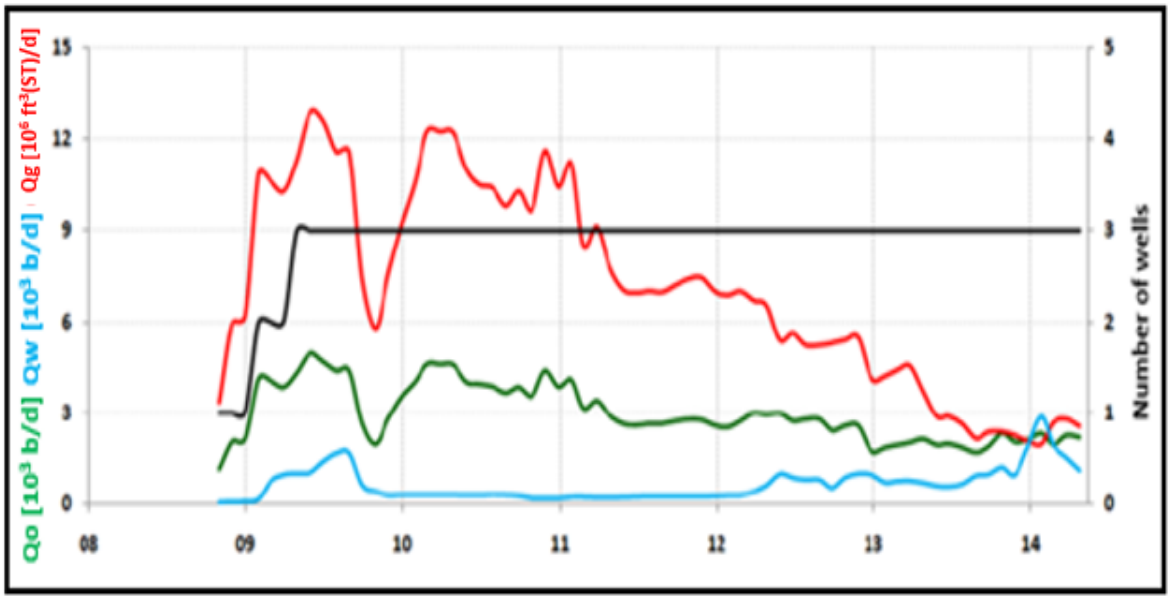

Figure 4.11 Production History of the Target Field @ Standard Conditions (PEMEX Exploración y Producción)

CHAPTER 5

TARGET RESERVOIR EXPERIMENT/TEST

Two experiments were performed for a Mexican light oil reservoir which is an NFR. The goal was to use the combustion tube facilities at University of Calgary, using the experience of the ISCRG, to assess the burning characteristics of the Mexican reservoir materials under conditions that would be encountered in the field. Both tests were designed to model an NFR (low permeability in the matrix and high permeability in the fractures) with HPAI. The material used to represent the reservoir were:

- Dolomite outcrop rock, which was crushed and used to simulate the fractures due to its high permeability.
- Dolomite core plugs, which represent the core matrix, due to its low permeability.
- Light oil from the reservoir.
- Synthetic brine.
- Methane

The two experiments were designed to advance a combustion front through the saturated crushed core, past the embedded plugs, and observe the behavior of the combustion front, the burning characteristics of the core and fluids in the presence of embedded low permeability core plugs, the combustion parameters, as well of the changes in the fluid saturations of the crushed core, and the core plugs.

Information from some of the mechanisms governing the fireflooding process can be obtained from the combustion tube tests. A properly designed and operated combustion tube test and the analysis of the composition of the produced gas, oil and brine is a guideline for the combustion front behavior and an economic projection of a field test's performance.

A combustion tube test is not a scaled experiment. On the contrary, it represents a piece of the reservoir simulated in the laboratory with the constraint of one-dimensional flow. Some general observations that can be made about the combustion tube experiments are:

- The stoichiometry of the reactions are controlled by the temperature, pressure and chemical characteristics of the reactants. It will not be affected by the configuration of the testing apparatus.
- The combustion tube´s heat losses are considerably different from that of the reservoir. The reservoir is naturally well insulated by the overburden and the underburden. On the other hand, a laboratory tube´s heat losses, due to its metal construction, are relatively high compared to the limited amount of heat generated. However, this problem is overcome by using 33 wall heaters, controlled by corresponding thermocouples, which maintain a temperature between the centerline and the wall at 5 to 10°C in order to minimize heat losses in the surroundings.

5.1 EXPERIMENTAL EQUIPMENT

The test was performed by the ISCRG at the University of Calgary using their High-Pressure Combustion Tube system. The core holder used for this test series was a 4-inch (10 cm) outer diameter, 5.5 feet (1.69 m) long, thin walled (2 mm) type 600 Inconel tube. The tube is approximately 12 liters volume, allowing for significant sample sizes and operating time. The tube is equipped with 33 (1,000 W clamshell type) heaters, forming 33 heating zones, each 2-inch (5 cm) in length, thus allowing for near adiabatic operation of the combustion test. Associated with each heating zone is a pair of fixed location thermocouples, one that extends radially into the centerline of the tube, and one that is fastened to the outer tube wall at the same axial position. As the centerline thermocouple (TC) senses the approach of the combustion front by the increased difference with the corresponding wall thermocouple (TW), the heater is activated in order to bring the wall temperature within 5 to 10°C of the centerline, in order to minimize heat losses to the surroundings.

The combustion tube is operated in a pressure jacket system, capable of operation at pressures up to 6,000 psig (42 MPa) in order to match most reservoir pressures of the oil samples being tested. The thin wall combustion tube is simultaneously pressured from the inside and outside. It is generally operated vertically so as to minimize gravity segregation effects, with injection at the top and production at the bottom.

This High-Pressure Combustion Tube system is optimized for testing conventional and light oil reservoirs for air injection-based recovery processes. The production system is equipped with a large, 3-liter trap, capable of collecting the first flush of light oil and brine that is always mobilized by the early gas injection period. Once gas break through, production is switched to a high/low pressure gas separator system. The gas stream is then directed to the back-pressure controller which maintains reservoir pressure in the system. Liquids (oil and brine) are manually withdrawn from the low-pressure separator in sample jars and stored for later analyses. A schematic drawing of the combustion tube is given in Figure 5.1. Some photos from the combustion tube and the pressure jacket are shown in Appendix A.

5.2 TEST MATERIALS

5.2.1 Gas

The hydrocarbon gas used for Test two was pure methane. Test one was not saturated with gas.

5.2.2 Oil

The oil used was provided by a Mexican company from the actual Mexican Oil Field, located in the south of Mexico. The oil sample was tested and established to contain a small amount of brine, so the oil was used as received in the tests. The original oil properties were measured in the laboratory and are shown in Table 5.1.

Temperature [°C]	15	25	40	55
Density [g/cm³]	0.8309	0.8238		
Viscosity [cp]		4.14	2.93	2.09

Mass Percent				H/C ratio
Carbon	Hydrogen	Nitrogen	Sulfur	
85.61	13.66	0.05	0.55	1.90

Table 5.1. Properties of Test Oil

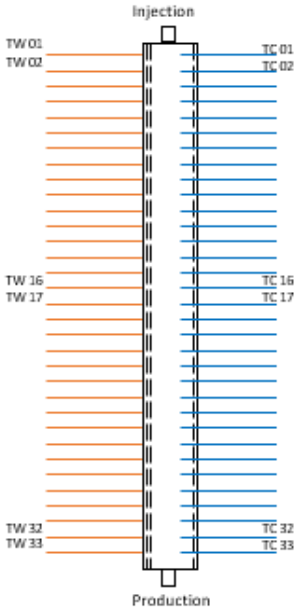

Figure 5.1 High Pressure Combustion Tube, Showing the Position of the Centerline Thermocouples (TC_i) and the Wall Thermocouples (TW_i)

5.2.3 Brine

A synthetic brine was used. It was made using the specifications, shown in Table 5.2, based on water analysis of a well provided by the Mexican company.

Compounds	Molar Mass [g/mol]	Conc. (mol/l)	Conc. (g/l)	Conc. (g/10l)
$MgCl_2 \cdot 6\ H_2O$	203.3	0.029617	6.021	60.212
$MnCl_2 \cdot 4\ H_2O$	197.91	0.000000	0.000	0.000
$CaCl_2 \cdot 2\ H_2O$	147.01	0.149701	22.007	220.075
$FeCl_3 \cdot 6\ H_2O$	270.3	0.000005	0.001	0.014
KCl	74.55	0.000000	0.000	0.000
$BaCl_2 \cdot 2\ H_2O$	244.26	0.000000	0.000	0.000
$SrCl_2 \cdot 6\ H_2O$	266.62	0.000000	0.000	0.000
LiCl	42.39	0.000000	0.000	0.000
$NaHCO_3$	84.01	0.001500	0.126	1.260
Na_2SO_4	142.04	0.000458	0.065	0.651
Na_2CO_3	105.99	0.000000	0.000	0.000
NaI	149.89	0.000000	0.000	0.000
NaBr	102.89	0.000000	0.000	0.000
NaCl	58.44	0.776705	45.391	453.906

Table 5.2 Synthetic Brine Composition Used in the Combustion Tube Tests

5.2.4 Core

The core used in the tests belonged to an outcrop in the studied Mexican field that belongs to the same Cretaceous Era as the reservoir rock. It was received as a rock and was crushed into smaller pieces in the laboratory. These pieces were extracted with toluene, then were placed in the oven and fired at 350°C (662°F) for 16 hours, the goal was to remove all the organic material that was attached to the surface of the sand grains. After the heating period in the oven, the rock pieces were crushed into fine grains (sand size) and sieved, the material bigger than #150 mesh was used in the tests. During the thesis the word “core” or “crushed core” will be used to refer to this material. This crushed core was used on both tests simulated the fractures on the reservoir due to its higher permeability than the core plugs. Figure 5.2 shows the rock outcrop as received (left side) and the crushed core after being extracted, crushed and sieved (right side).

Figure 5.2 Outcrop Core (left) and Crushed Core (right)

5.2.5 Core Plugs or Plugs

The reservoir under study was a NFR and conformed basically by dolomites. During the test the goal was to represent and study the combustion front’s behavior through the matrix and the fracture. Due to this, core plugs with specific porosity and mainly dolomite composition from a Silurian formation that belong to the Paleozoic were bought from Kocurek Industries (Caldwell, Texas). The core plugs in the test simulated the matrix rock, because it has a lower permeability than the crushed core. The average porosity of the core plugs was 13 percent. The permeability for the core plugs used for Test one was not measured, owing to the non-standard plug sizes. Similar core plugs used in Test two have shown a permeability of 250 - 300 mD. Appendix A presents photos of some of the core plugs. Some characteristics of the core plugs are shown in Table 5.3.

For Test one, the core plugs were saturated with dead oil. To achieve this oil saturation a pressure vessel was used, where the core plugs were put inside. When the vessel was closed all the air inside was displaced with CO_2. Then the plugs were submerged in oil for 93 hours at 5,000 psig (34.5 MPa) pressure. The vessel was de-pressured and the cores remained submerged in oil until being packed in the core holder. Table 5.4 shows the oil concentration in each core plug.

Plug No.	Length [inches]	Outer Diameter [inches]	Volume [cm^3]	Porosity [%]	Permeability [mD]	Test Number
#1 - #3	1.5	2	77.22	13.1		1
#4	1.5	3	154.44	12.8		1 *
#5	1.5	0.7	9.46	10.8	--	1
#6	3	2	154.44	13.1		1
#7a	1.5	2	77.22	11.8		1
#7					262	2
#9					284	2
#10	1.5	2	77.22	13.1	280	2
#11					312	2
#13					270	2
#16					287	2

* this core plug has a center hole of 1" diameter x 1.5" length. The volume is without the center hole.

Table 5.3 Characteristics of the Core Plugs Used in Test One and Two

Plug No.	Mass before saturation [g]	Mass after saturation [g]	Mass of oil in the core [g]
#1	184.49	193.05	8.56
#2	184.35	192.95	8.60
#3	183.64	192.67	9.03
#4	370.67	389.27	18.60
#5	23.54	24.46	0.92
#6	369.92	386.76	16.84
#7a	187.91	193.63	7.72

Table 5.4 Oil Mass in Oil Saturated Core Plugs for Test One

For Test two, the core plugs were saturated with oil. To achieve this oil saturation a pressure vessel was used, where the core plugs were put inside. When the vessel was closed, the air was vacuum during two days. After vacuum, CO_2 was injected for a day. Then the plugs were submerged in oil for 24 hours at 5,000 psig pressure. The vessel was de-pressured and the cores waited submerged in oil until being packed in the core holder. Table 5.5 shows the oil concentration in each core plug.

Plug No.	Mass before saturation [g]	Mass after saturation [g]	Mass of oil in the core [g]
#7	184.55	193.07	8.52
#9	187.00	194.76	7.76
#10	187.35	194.95	7.60
#11	182.57	190.83	8.26
#13	184.31	192.64	8.33
#16	184.63	192.99	8.36

Table 5.5 Oil Mass Saturation in Core Plugs for Test Two

5.3 TEST ONE

5.3.1 Tube Packing and Flooding

The packing procedure of the combustion tube was through the production end. The top and bottom of the combustion tube was filled with 500 grams of 16 mesh silica frac sand followed by 500 grams of 20/30 mesh silica frac sand. Both sands were wetted with 30 grams of synthetic brine and tamped in the combustion tube. The frac sand were placed with the intention of avoiding any sand grain migration into the injection/production system. Between the silica frac sand sections of one-kg samples of crushed core saturated with nominal 70 grams of synthetic brine where placed in the tube. All the crushed core and frac sand sections were inserted and tamped manually. Along the combustion tube the saturated core plugs were embedded in the crushed core. Figure 5.3 shows the location of the thermocouples and the core plugs. In Table 5.6 (the packing notes), the crushed core and brine masses in terms of the packing depth are shown. In the hole of Core Plug #4, Core Plug #5 was inserted and centered. The gap between the two core plugs was filled with crushed core. Core Plug #6 was drilled with a side radial hole to insert Thermocouple 22 to the centerline of the plug.

When the combustion tube was fully packed, it was closed, sealed, insulated and inserted in the combustion tube jacket and oriented with the injection end at the top. Then the combustion tube was connected to a vacuum pump for 30 minutes to reduce the amount of air that was trapped during the packing. The short time for evacuation was to avoid altering the oil and/or water saturation in the core plugs. At atmospheric pressure, dead oil was injected into the packed combustion tube upward thorough the production end, while the injection end was open. Oil was injected until it broke through. This was followed by a brine injection through the production end until it broke through. Finally, a second oil flood was injected downward through the injection end. Table 5.7 shows a summary of the individual core samples and fluid masses, fluid saturation of the crushed core and fluids in lines after the second oil flood and prior to the actual test.

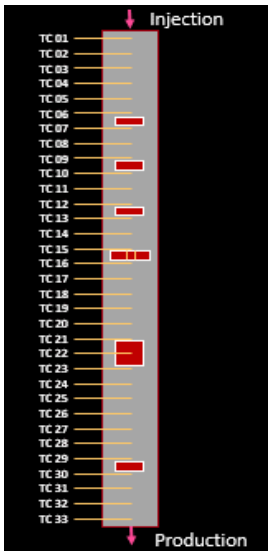

Figure 5.3 Schematic Drawing of the Combustion Tube with the Thermocouples and Location of the Embedded Core Plugs. Test One

Sample	Embedded Core Plug	Mass of Crushed Core [g]	Mass of Brine [g]	Incremental Depth [mm]	Depth from Production End [mm]
16 m Inj. Frac		500	30.02	47	1,707
20/30 m Inj. Frac		500	30.07	39	1,668
Core 1		1,000	70.34	79	1,589
Core 2		1,000	70.60	80	1,509
Core3A	Plug #1	1,000	71.42	46	1,463
Core 3B				46	1,417
Core 4		1,000	70.21	79	1,338
Core 5A	Plug #2	1,000	70.45	25	1,313
Core 5B				64	1,249
Core 6		1,000	70.28	80	1,169
Core 7A	Plug #3	1,000	70.37	11	1,158
Core 7B				78	1,080
Core 8A	Plug #4 + 5	1,000	69.98	74	1,006
Core 8B				2	1,004
Core 9		1,000	70.49	103	901
Core 10		1,000	70.01	80	821
Core 11		1,000	70.00	79	742
Core 12A	Plug #6	1,000	70.47	47	695
Core 12B				40	655
Core 13		1,000	70.20	94	561
Core 14		1,000	70.17	76	485
Core 15		1,000	71.52	80	405
Core 16		1,000	70.01	80	325
Core 17A	Plug #7a	1,000	70.04	30	295
Core 17B				57	238
Core 18		1,000	70.05	79	159
Core 19		216.12	15.29	17	142
20/30 m Prod Frac		500	30.45	37	105
16 m Prod Frac		500	30.01	46	59

Table 5.6 Packing Masses. Test One

	Packed Masses [g]		Mass of liquid [g]
Crushed Core	18,216.1	Oil in Crushed Core	2,740.9
Frac Sand	2,000.0	Brine in Crushed Core	1,704.5
Core Plugs	1,504.5	Oil in Core Plugs	70.3
	Saturations in Crushed Core [%]	Oil in Lines	25.9
		Water in Lines	0.0
Oil	67.3		
Water	32.7	Oil in Total System	2,837.1
Gas	0.0	Water in Total System	1,704.5
Calculated Porosity of the Crushed Core Pack [%]		41.6	
Crushed Core Pore Volume [cm^3]		5,013	

Table 5.7 Masses and Saturations after Packing and Flooding the Combustion Tube. Test One

5.3.2 Set Up/Pre-Test

The following activities were realized in a way to ensure a good test. For more reference see Figure 5.4

- The injected air mass flow controllers were calibrated at test conditions (reservoir conditions).
- The Gas Chromatograph (GC) was calibrated and a test sequence was realized.
- The liquid BPR (Back Pressure Regulator) initially was manually set at 500 psig.
- The Kamer valve controller regulator used to back pressure the flowing produced gas was set at the desired operating pressure for the test, once the production stream was directed to the high-pressure trap.
- Production lines and the high-pressure trap were pressurized with helium to the liquid BPR that controls the flow to the primarily liquid flow to the Initial Liquid Production Collector (ILPC).

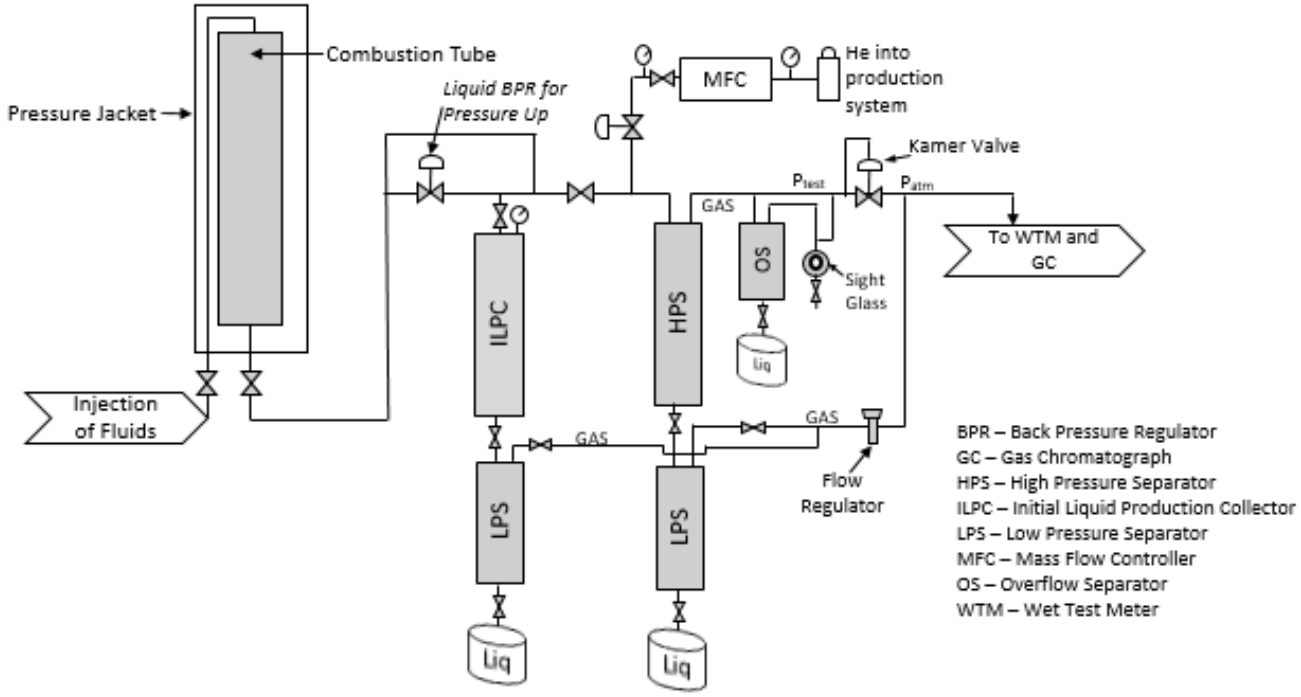

Figure 5.4 Back Pressure Regulator and Production Separator System

5.3.3 Combustion Test

The pressure jacket was oriented vertically with the injection end at the top so flow is downward. The core was pressurized to the reservoir pressure of 2,200 psig with injection of dead oil and heating expansion, this was realized 2.48 hours prior air injection. At the same time helium was injected in annular space (space between combustion tube and pressure jacket), keeping the annulus pressure 100 psig above the injection pressure inside the combustion tube to avoid tube deformation resulting

from a high differential pressure across the tube wall and to prevent air from flowing to the annulus in the case of a leak developing in the core holder wall.

Once the reservoir pressure (2,200 psig) and reservoir temperature (149°C) were reached, Helium flow to the production trap and associated flow lines was started to ensure that the Kamer valve was operating and capable of maintaining back pressure control once the production gases from the combustion tube broke through and all production was directed to the high pressure separator.

Next, Zones 1, 2 and 3 were heated up to 175°C (ignition temperature). When the first three zones reached the ignition temperature, air ignition started at time zero. Time zero was defined when air injection started, and it was declared as Day 0 of the test, happening at 12:26 PM, 24 October 2018. The air injected was a synthetic air with composition of oxygen of 21.82 mole percent and the rest nitrogen. Injection started at a rate of 224 liter(ST)/h (flux of 30 m^3(ST)/m^2h). The centerline thermocouples at the start of air injection for Zone 1, 2 and 3 registered a temperature in the core of 184, 173 and 178°C respectively, and the wall thermocouples were maintained at 175°C for the first three zones. After 12 minutes of air injection the first sign of ignition was observed when the temperature in Zones 2 and 1 increased, reaching a temperature of 387°C.

After ignition, air injection continued pushing the combustion front through the core pack. At 5.83 hours the combustion front passed Zone/TC 26, located at 76 percent of the core length, then air injection was switched to helium at the same rate of 224 liter(ST)/h. The air that was inside the combustion tube at the moment of the switch, was displaced by the helium and continued reacting/consuming at the combustion front. The purpose of injecting helium was to purge the core pack of the combustion/production gases (for mass balance calculation), to have a portion of the core that could be evaluated for the nature of the residual hydrocarbons and to evaluate the post-test masses of oil and water in the core. Safety reasons also required that the production flange seal not to be heated above 300°C. The wall heaters were operated on differential control during the whole test (air and helium injection). The injection of helium lasted until 14.55 hours. When the injection of helium was turned off, the system was de-pressured.

During the entire test the produced liquids (oil and water) were collected intermittently in sample bottles for a subsequent separation and analysis. The gas produced was sent to the GCs and monitored on a cycle of 8 minutes (Helium GC) and 22 minutes (product gas GC). After the tube cooled down, it was removed from the pressure jacket and unpacked in incremental sections of crushed core and core plugs, which were sent for analysis. Some photos are presented in Appendix A. Table 5.8 shows a summary of the injected and produced gases.

Parameter [units]	Value
Helium in Production System Following Pressure Up [liters (ST)]	219.9
Time of Air Injection [run hours]	0.0
Time of Helium Injection (Purge) [run hours]	5.83
Oxygen Injected [liters (ST)]	284.4
Nitrogen Injected [liters (ST)]	1,019.3
Helium Injected (Purge) [liters (ST)]	1,987.5
Helium Injected to Production Systems [liters (ST)]	302.9
Total Volume of Injected Gas [liters (ST)]	3,814.0
Total Volume of Produced Gas [liters (ST)]	3,539.8
Volume Out – Volume In [liters (ST)]	-274.2

Table 5.8 Summary of Injected and Produced Gases-Test One

5.3.4 Results

5.3.4.1 Temperatures Profiles

The tube was positioned vertically with the injection end at the top. At the start of the test, after reaching the reservoir conditions, zones one to three were consider the “ignition zones”, which were heated up to 175°C with the objective of generating the ignition. During the whole test the temperatures at the centerline were recorded. The highest temperature registered by each thermocouple is shown in Table 5.9, the distances where the thermocouples are located is from the injection end.

The temperatures recorded by the centerline and wall thermocouples against their axial locations are shown in Figures 5.5 and 5.6 respectively. At 220°C a horizontal line is drawn, which is the temperature where the front velocity was calculated. During the first 21 zones the combustion front advanced at a stable velocity, after this a slowdown in velocity can be appreciated. It is good to remember that after Zone/TC 26, the air injection was shut down and switched for helium, called the “Helium Purge”, which pushed the remaining air in the tube all the way to the production end, and this air kept reacting with part of the hydrocarbons stored in the combustion tube.

In Figure 5.5, it is seen that at some zones the thermocouples reached a “peak temperature”, then the zone temperatures decreased, and then again started to increase and reach the highest or maximum zone temperature recorded. The first localized maximum temperature is called the “peak temperature” while the highest temperature is called the maximum temperature. The residual energy generation that occurs after the peak temperature has been observed at a given thermocouple location is believe to be related to the counter diffusion of volatile hydrocarbon components, whose composition was in the flammable range. One explanation of this behavior is that it is related to the vapor steam phase. Depending on the relative permeability of the water phase in the

region of the reaction zone, where bond scission or combustion reactions generate energy at a sufficient rate to form the leading edge, vapor steam will form in the rapidly heated pores and while it may flow downstream with the combustion gases, given the low molecular mass of water, it may convect in a direction counter to the air flow. Light non condensable gases like hydrogen and methane are also candidates for counter diffusion, but it is recognized that heavier condensable hydrocarbons components may also be transported counter to the air flow once a convective roll cell develops.

An important point to note is that the energy generation rate during the time that a zone temperature increases from the “peak temperature” to a maximum temperature is very low and the reaction can be terminated by inducing a greater temperature differential between the centerline and wall temperature for the zone in question.

It can be argued that a solid residual hydrocarbon (*e.g.* coke like phase) could also support the residual energy generation. This argument is the reason that the ISCRG unpacks and analyzes the post-test core after every test. Ignition of the toluene extracted post-test core samples almost always shows that the core in the region where residual heat generation is observed does not contain residual hydrocarbon or coke.

In Figure 5.7, the combustion front velocity slope at 220°C (from the centerline thermocouples) is appreciated. From 0 to 5.86 hours, time period of air injection, the velocity was 0.283 m/h. At 5.86 hours run time, when air was switch to helium, the front velocity was 0.124 m/h. The change in front velocity occurred at approximately 3.8 hours, during the air injection period and the velocity during the helium purge remained at the same level until helium broke through.

Zone	Distance from Injection End (mm)	Peak Temperature		Maximum Temperature	
		Time [hours]	[°C]	Time [hours]	[°C]
1	29	0.37	387	0.37	387
2	80	0.60	443	0.60	443
3	131	0.84	466	2.97	475
4	181	1.01	415	6.93	500
5	232	1.18	384	7.67	521
6	283	1.40	299	7.78	519
7	334	2.17	453	8.03	524
8	385	1.84	306	7.33	503
9	435	1.99	287	7.33	472
10	486	2.29	293	7.30	412
11	537	2.16	285	5.82	344
12	588	2.50	286	4.57	309
13	639	2.80	279	3.85	311
14	689	3.01	282	4.73	296
15	740	3.31	287	4.68	334
16	791	3.41	295	4.07	345
17	842	3.58	289	5.02	320
18	893	3.65	299	3.65	299
19	943	3.65	305	3.65	305
20	994	3.85	311	3.85	311
21	1,045	4.03	287	4.03	287
22	1,096	4.47	267	4.47	267
23	1,147	4.85	295	4.85	295
24	1,197	5.02	286	5.02	286
25	1,248	5.57	271	5.57	271
26	1,299	5.72	286	5.72	286
27	1,350	6.18	296	6.18	296
28	1,401	6.33	267	6.33	267
29	1,451	6.85	227	6.85	227
30	1,502	7.18	214	7.18	214
31	1,553	7.48	191	7.48	191
32	1,604	7.63	173	7.63	173
33	1,655	----	---	3.85	149

Table 5.9. Maximum Temperatures Summary in Test One

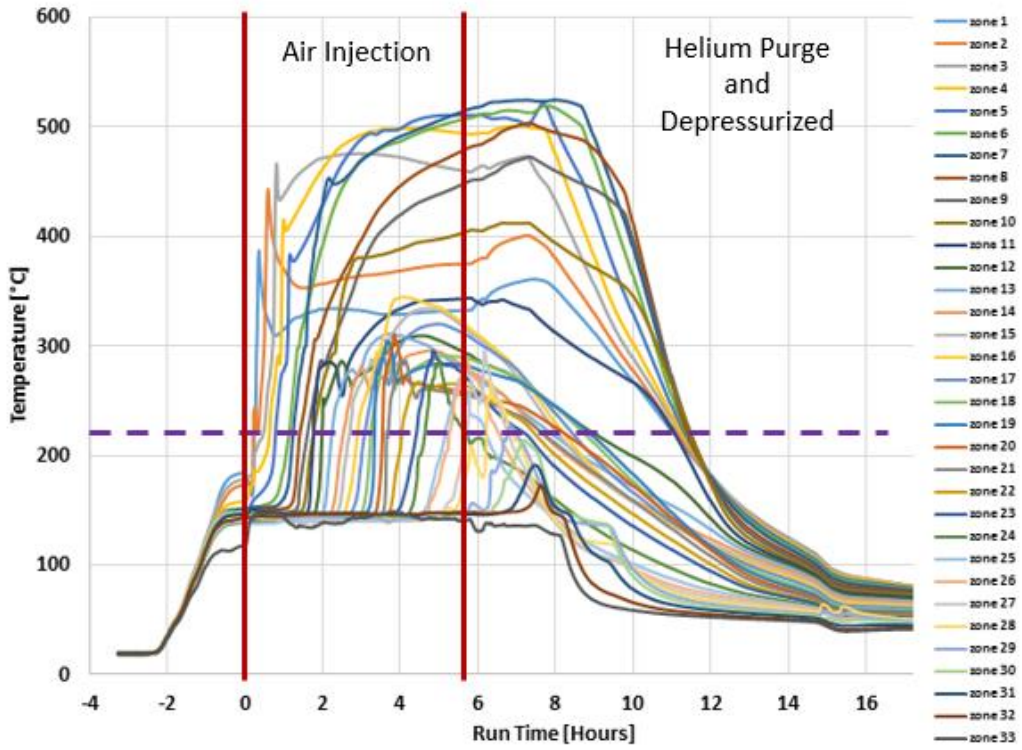

Figure 5.5. Center Line, Temperatures Profiles. Test One

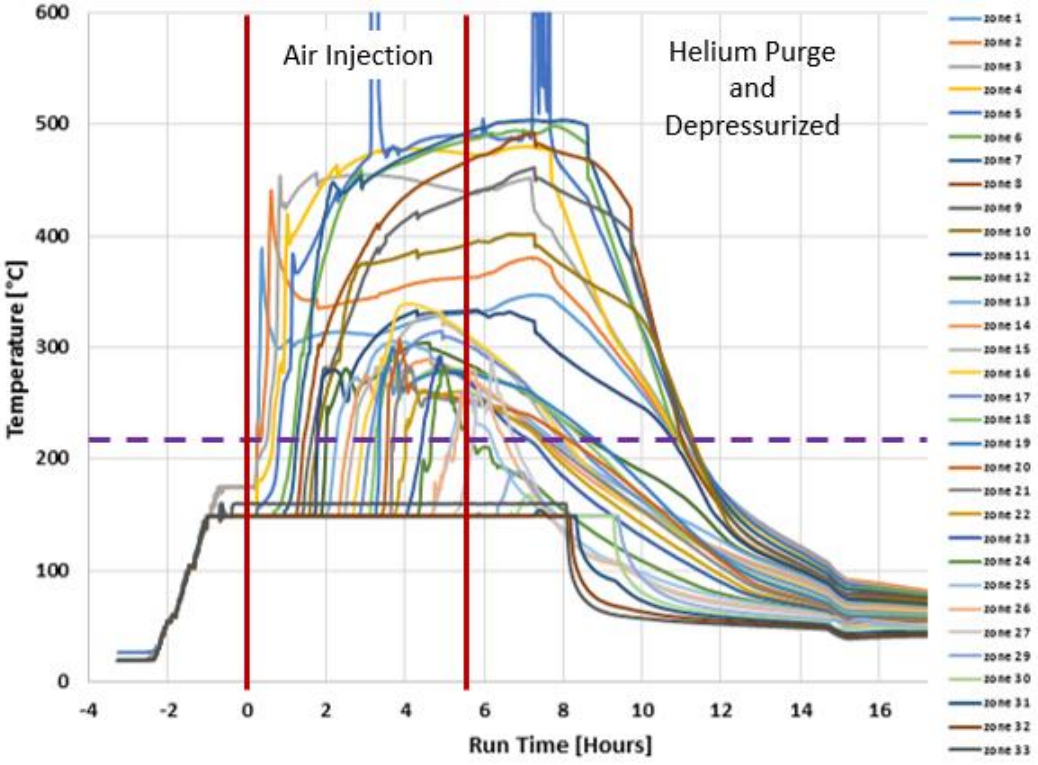

Figure 5.6. Wall Temperatures Profiles, Test One

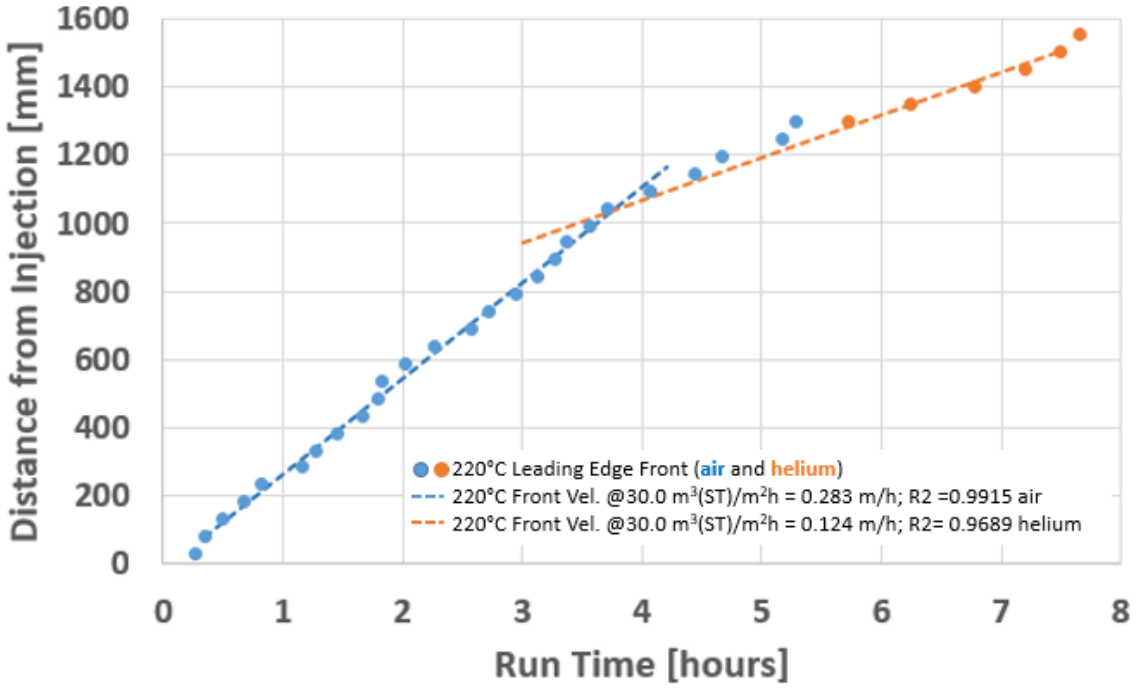

Figure 5.7. Velocity Plot of the 220°C. Test One

5.3.4.2 Overall Run

Once the test started with the injection of air, the injection pressure increased and some liquid was produced. Then ignition occurred and the combustion front was generated. The combustion front started to push the liquids towards the production end and generated some combustion gases. All the produced liquids were collected for a post-test analysis. When the gases from combustion broke through, the production fluids were sent to the main separator and the gases were analyzed in real time by the two Gas Chromatographs (GC). In Table 5.10 the production gas compositions versus time are tabulated. The helium dilution reported in the right-hand column of Table 5.10 and Figure 5.8 corresponds to the percentage of the produced gas stream that was helium. Note from 0.0 to 1.21 hours run time, the gas flowing to the GC constitutes essentially 100% helium, which was injected downstream of the core to pressurize the production system. No helium had entered the core by that time. During the same period, normal air contamination was present in the production system. The amount of contaminant air was sufficiently low that the GC only detected the nitrogen peak. At final stages helium was injected to purge the core and displace all the mobile hydrocarbons and air in the tube that remained after the air injection was shut down. During the HPAI run, light hydrocarbons were produced. This type of hydrocarbons may generate significant revenue if they are recovered.

The air used for the test was a synthetic air with an oxygen:nitrogen ratio of 21.815:78.185, Hence, the R value was 3.584 (ratio of mole fraction N_2/mole fraction O_2 in the injected air). Nitrogen as an inert gas did not react during the combustion test. In

Figure 5.8 it can be said that the product gas N_2 concentration was close to 80%. Nitrogen mass balance shows good agreements as seen by comparing Tables 5.12 and 5.13. Carbon dioxide has the quality to be miscible in light oils, due to this when CO_2 started to be produced at the beginning it was being absorbed by the oil. Once the oil approached saturation, the CO_2 broke out and was produced and quantified. Water also carries dissolved CO_2, and significant changes in the produced gas CO_2 content can be seen if fluids are produced from the high-pressure trap at the same time that the GC samples the gas.

Figure 5.8 shows a stable composition over time indicating that the oxidation reactions were operating in the bond scission mode in the LTR as light oils do. It was also observed that there were two stable periods based on the concentrations of the produced combustion gases, the first one between 3.5 to 5.0 hours and the second at 6.2 to 8.0 hours. Figure 5.9 graphically represents the composition of the produced gas against time. Observing Figure 5.9 at around 3.9 run hour, the light hydrocarbons concentration is approaching to zero for many of the components.

From Table 5.9 it is appreciated that the peak and maximum temperatures are the same after 3.58 hours, this relates to the termination of the reaction that supported the residual energy generation in Zones 3 to 17. Figure 5.9 shows that light hydrocarbons (n-C_3, n-C_4 and n-C_5) are present in the product gas, reaching a maximum at about 1.59 hours, helium dilution is very high at this time so the absolute value of the individual component concentrations may be uncertain due to the impact of the high helium dilution on the shape of the individual hydrocarbons and hydrogen peaks.

The incremental and cumulative air injection during Test One is summarized in Table 5.11 with respect to run time, as well as the air/fuel ratio and the apparent H/C ratio. An important thing to observe is in the incremental H/C ratio at some times are negative. This implies that for the time period corresponding to the gas sample more oxygen was produced as CO_x's than oxygen was injected. This behavior could result from: a) The residual hydrocarbon being burn was pre-oxidized earlier in the test, or b) Due to the presence of dolomites, which could be reacting and forming CO_2 and c) Due to dissolved CO_2 being released from the produced fluids.

Nitrogen oxidation was neglected because all the combustion performance was lower than 1,000°C. No H_2S was produced during the test. The stabilized air and fuel requirement parameters were based on a tube cross sectional area of 7.472×10^{-3} m^2 and on an air injection flux of 30.0 m^3/m^2h.

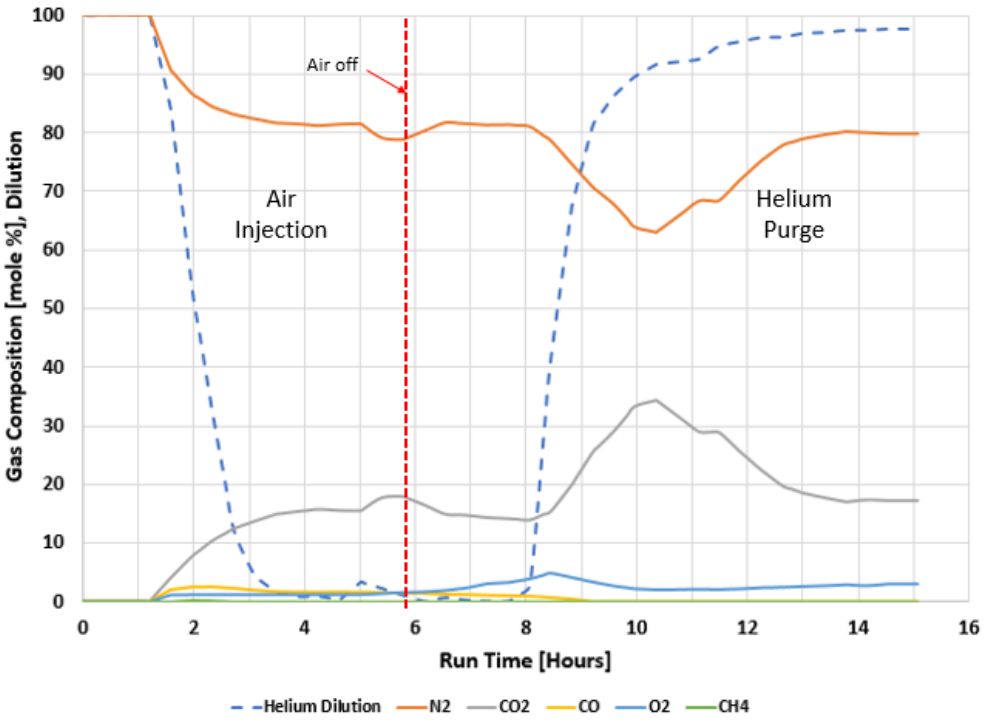

Figure 5.8. Produced Combustion Gas Composition. Test One

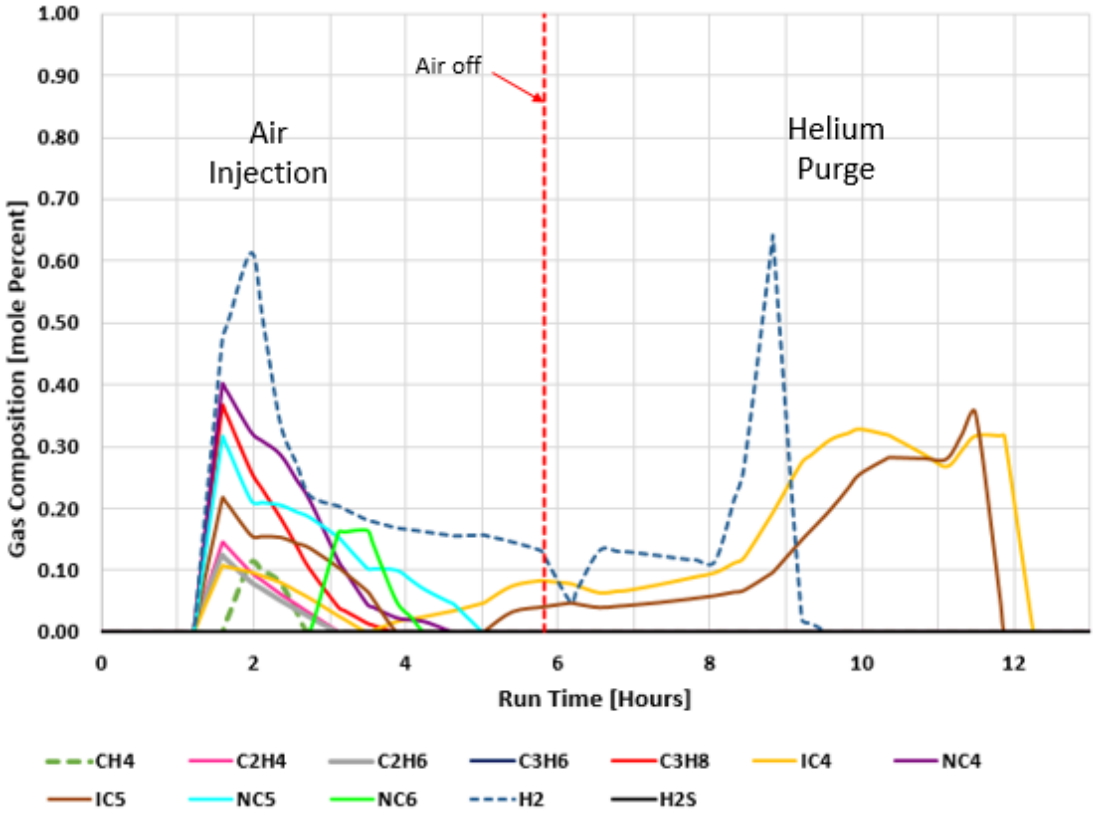

Figure 5.9. Produced Light Hydrocarbons Gas Composition. Test One

Table 5.10 Produced Gas Composition. Test One

Runtime [hours]	Mole percentage																He Dilution [%]
	N_2	CO_2	CO	O_2	CH_4	C_2H_4	C_2H_6	C_3H_6	C_3H_8	iC_4	nC_4	iC_5	nC_5	nC_6	H_2	H_2S	
-0.70	100.00	0.00	0.00	0.00	0.00	0.00	0.00	0.00	0.00	0.00	0.00	0.00	0.00	0.00	0.00	0.00	99.84
0.00	100.00	0.00	0.00	0.00	0.00	0.00	0.00	0.00	0.00	0.00	0.00	0.00	0.00	0.00	0.00	0.00	99.85
0.06	100.00	0.00	0.00	0.00	0.00	0.00	0.00	0.00	0.00	0.00	0.00	0.00	0.00	0.00	0.00	0.00	99.86
0.43	100.00	0.00	0.00	0.00	0.00	0.00	0.00	0.00	0.00	0.00	0.00	0.00	0.00	0.00	0.00	0.00	99.98
0.45	100.00	0.00	0.00	0.00	0.00	0.00	0.00	0.00	0.00	0.00	0.00	0.00	0.00	0.00	0.00	0.00	99.98
0.67	100.00	0.00	0.00	0.00	0.00	0.00	0.00	0.00	0.00	0.00	0.00	0.00	0.00	0.00	0.00	0.00	99.98
0.83	100.00	0.00	0.00	0.00	0.00	0.00	0.00	0.00	0.00	0.00	0.00	0.00	0.00	0.00	0.00	0.00	99.98
1.00	100.00	0.00	0.00	0.00	0.00	0.00	0.00	0.00	0.00	0.00	0.00	0.00	0.00	0.00	0.00	0.00	99.96
1.07	100.00	0.00	0.00	0.00	0.00	0.00	0.00	0.00	0.00	0.00	0.00	0.00	0.00	0.00	0.00	0.00	99.96
1.13	100.00	0.00	0.00	0.00	0.00	0.00	0.00	0.00	0.00	0.00	0.00	0.00	0.00	0.00	0.00	0.00	99.95
1.15	100.00	0.00	0.00	0.00	0.00	0.00	0.00	0.00	0.00	0.00	0.00	0.00	0.00	0.00	0.00	0.00	99.95
1.21	100.00	0.00	0.00	0.00	0.00	0.00	0.00	0.00	0.00	0.00	0.00	0.00	0.00	0.00	0.00	0.00	99.95
1.32	97.30	1.14	0.61	0.33	0.00	0.04	0.04	0.00	0.10	0.03	0.11	0.06	0.09	0.00	0.14	0.00	95.34
1.59	90.60	3.99	2.12	1.14	0.00	0.15	0.12	0.00	0.37	0.11	0.40	0.22	0.31	0.00	0.48	0.00	83.86
1.62	90.30	4.26	2.15	1.15	0.01	0.14	0.12	0.00	0.36	0.11	0.39	0.21	0.31	0.00	0.49	0.00	81.62
1.67	89.78	4.73	2.22	1.15	0.02	0.14	0.12	0.00	0.34	0.11	0.38	0.20	0.29	0.00	0.50	0.00	77.64
1.68	89.61	4.89	2.24	1.16	0.03	0.13	0.11	0.00	0.34	0.11	0.38	0.20	0.29	0.00	0.51	0.00	76.31
1.97	86.63	7.64	2.60	1.20	0.11	0.10	0.08	0.00	0.26	0.10	0.32	0.16	0.21	0.00	0.61	0.00	53.52
2.12	85.75	8.70	2.60	1.20	0.10	0.08	0.07	0.00	0.23	0.09	0.31	0.15	0.21	0.00	0.51	0.00	45.08
2.35	84.34	10.40	2.61	1.21	0.08	0.06	0.05	0.00	0.18	0.08	0.29	0.15	0.20	0.00	0.34	0.00	31.64
2.57	83.62	11.53	2.47	1.21	0.04	0.04	0.04	0.00	0.14	0.07	0.25	0.14	0.19	0.00	0.27	0.00	20.51
2.73	83.07	12.38	2.36	1.21	0.00	0.03	0.03	0.00	0.10	0.06	0.21	0.14	0.19	0.00	0.22	0.00	11.99
3.11	82.30	13.68	2.01	1.20	0.00	0.00	0.00	0.00	0.04	0.03	0.11	0.10	0.15	0.16	0.20	0.00	4.18
3.18	82.17	13.90	1.97	1.20	0.00	0.00	0.00	0.00	0.04	0.02	0.10	0.10	0.14	0.16	0.20	0.00	3.72
3.49	81.62	14.85	1.76	1.20	0.00	0.00	0.00	0.00	0.02	0.00	0.05	0.07	0.10	0.16	0.18	0.00	1.64
3.57	81.58	14.94	1.75	1.20	0.00	0.00	0.00	0.00	0.01	0.00	0.04	0.05	0.10	0.14	0.18	0.00	1.49
3.88	81.45	15.30	1.68	1.20	0.00	0.00	0.00	0.00	0.00	0.02	0.02	0.00	0.10	0.05	0.17	0.00	0.86
4.07	81.31	15.49	1.68	1.20	0.00	0.00	0.00	0.00	0.00	0.02	0.02	0.00	0.08	0.03	0.17	0.00	0.88

Table 5.10 Produced Gas Composition. Test One

Runtime [hours]	Mole percentage																He Dilution [%]
	N_2	CO_2	CO	O_2	CH_4	C_2H_4	C_2H_6	C_3H_6	C_3H_8	iC_4	nC_4	iC_5	nC_5	nC_6	H_2	H_2S	
4.26	81.17	15.69	1.67	1.20	0.00	0.00	0.00	0.00	0.00	0.03	0.02	0.00	0.07	0.00	0.16	0.00	0.90
4.57	81.36	15.51	1.69	1.20	0.00	0.00	0.00	0.00	0.00	0.03	0.00	0.00	0.05	0.00	0.16	0.00	0.45
4.64	81.40	15.48	1.69	1.20	0.00	0.00	0.00	0.00	0. 00	0.0 4	0.00	0.00	0.05	0.00	0.16	0.00	0.35
5.02	81.46	15.46	1.66	1.21	0.00	0.00	0.00	0.00	0.00	0.05	0.00	0.00	0.00	0.00	0.16	0.00	3.33
5.07	81.16	15.74	1.66	1.23	0.00	0.00	0.00	0.00	0.00	0.05	0.00	0.00	0.00	0.00	0.16	0.00	3.19
5.40	79.08	17.67	1.61	1.38	0.00	0.00	0.00	0.00	0.00	0.08	0.00	0.03	0.00	0.00	0.15	0.00	2.25
5.78	78.79	17.87	1.50	1.58	0.00	0.00	0.00	0.00	0.00	0.08	0.00	0.04	0.00	0.00	0.13	0.00	1.08
5.82	78.93	17.73	1.49	1.59	0.00	0.00	0.00	0.00	0.00	0.08	0.00	0.04	0.00	0.00	0.12	0.00	0.98
6.16	80.28	16.43	1.44	1.68	0.00	0.00	0.00	0.00	0.00	0.08	0.00	0.05	0.00	0.00	0.05	0.00	0.05
6.23	80.54	16.13	1.42	1.73	0.00	0.00	0.00	0.00	0.00	0.08	0.00	0.04	0.00	0.00	0.07	0.00	0.17
6.25	80.60	16.06	1.41	1.74	0.00	0.00	0.00	0.00	0.00	0.08	0.00	0.04	0.00	0.00	0.07	0.00	0.19
6.54	81.69	14.84	1.31	1.92	0.00	0.00	0.00	0.00	0.00	0.06	0.00	0.04	0.00	0.00	0.13	0.00	0.67
6.78	81.57	14.72	1.27	2.20	0.00	0.00	0.00	0.00	0.00	0.07	0.00	0.04	0.00	0.00	0.13	0.00	0.41
6.92	81.50	14.65	1.25	2.36	0.00	0.00	0.00	0.00	0.00	0.07	0.00	0.04	0.00	0.00	0.13	0.00	0.26
7.30	81.27	14.25	1.12	3.11	0.00	0.00	0.00	0.00	0.00	0.08	0.00	0.05	0.00	0.00	0.12	0.00	0.08
7.32	81.27	14.25	1.12	3.11	0.00	0.00	0.00	0.00	0.00	0.08	0.00	0.05	0.00	0.00	0.12	0.00	0.08
7.68	81.32	14.08	1.05	3.29	0.00	0.00	0.00	0.00	0.00	0.09	0.00	0.05	0.00	0.00	0.12	0.00	0.10
7.82	81.22	14.00	1.01	3.51	0.00	0.00	0.00	0.00	0.00	0.09	0.00	0.05	0.00	0.00	0.12	0.00	1.05
8.06	81.02	13.85	0.94	3.91	0.00	0.00	0.00	0.00	0.00	0.10	0.00	0.06	0.00	0.00	0.12	0.00	2.81
8.32	79.44	14.82	0.79	4.56	0.00	0.00	0.00	0.00	0.00	0.11	0.00	0.06	0.00	0.00	0.22	0.00	28.32
8.44	78.64	15.31	0.71	4.89	0.00	0.00	0.00	0.00	0.00	0.12	0.00	0.07	0.00	0.00	0.27	0.00	41.20
8.82	74.71	19.77	0.43	4.17	0.00	0.00	0.00	0.00	0.00	0.19	0.00	0.10	0.00	0.00	0.63	0.00	66.82
8.82	74.62	19.87	0.42	4.15	0.00	0.00	0.00	0.00	0.00	0.19	0.00	0.10	0.00	0.00	0.64	0.00	67.37
9.20	70.71	25.48	0.00	3.37	0.00	0.00	0.00	0.00	0.00	0.28	0.00	0.15	0.00	0.00	0.02	0.00	81.17
9.32	69.84	26.53	0.00	3.17	0.00	0.00	0.00	0.00	0.00	0.29	0.00	0.16	0.00	0.00	0.02	0.00	82.65
9.59	67.75	29.05	0.00	2.69	0.00	0.00	0.00	0.00	0.00	0.31	0.00	0.20	0.00	0.00	0.00	0.00	86.19
9.82	65.40	31.65	0.00	2.40	0.00	0.00	0.00	0.00	0.00	0.32	0.00	0.23	0.00	0.00	0.00	0.00	88.20
9.97	63.89	33.31	0.00	2.21	0.00	0.00	0.00	0.00	0.00	0.33	0.00	0.25	0.00	0.00	0.00	0.00	89.50

Table 5.10 Produced Gas Composition. Test One

Runtime [hours]	Mole percentage																He Dilution [%]
	N_2	CO_2	CO	O_2	CH_4	C_2H_4	C_2H_6	C_3H_6	C_3H_8	iC_4	nC_4	iC_5	nC_5	nC_6	H_2	H_2S	
10.32	63.08	34.27	0.00	2.05	0.00	0.00	0.00	0.00	0.00	0.32	0.00	0.28	0.00	0.00	0.00	0.00	91.39
10.35	63.01	34.35	0.00	2.04	0.00	0.00	0.00	0.00	0.00	0.32	0.00	0.28	0.00	0.00	0.00	0.00	91.55
10.82	66.28	31.06	0.00	2.10	0.00	0.00	0.00	0.00	0.00	0.29	0.00	0.28	0.00	0.00	0.00	0.00	92.10
11.11	68.31	29.01	0.00	2.13	0.00	0.00	0.00	0.00	0.00	0.27	0.00	0.28	0.00	0.00	0.00	0.00	92.44
11.32	68.40	28.88	0.00	2.10	0.00	0.00	0.00	0.00	0.00	0.30	0.00	0.32	0.00	0.00	0.00	0.00	93.68
11.49	68.47	28.78	0.00	2.08	0.00	0.00	0.00	0.00	0.00	0.32	0.00	0.35	0.00	0.00	0.00	0.00	94.71
11.82	71.52	25.93	0.00	2.18	0.00	0.00	0.00	0.00	0.00	0.32	0.00	0.05	0.00	0.00	0.00	0.00	95.38
11.87	72.01	25.47	0.00	2.20	0.00	0.00	0.00	0.00	0.00	0.32	0.00	0.00	0.00	0.00	0.00	0.00	95.49
12.25	75.27	22.34	0.00	2.39	0.00	0.00	0.00	0.00	0.00	0.00	0.00	0.00	0.00	0.00	0.00	0.00	96.18
12.32	75.71	21.88	0.00	2.41	0.00	0.00	0.00	0.00	0.00	0.00	0.00	0.00	0.00	0.00	0.00	0.00	96.19
12.63	77.85	19.67	0.00	2.48	0.00	0.00	0.00	0.00	0.00	0.00	0.00	0.00	0.00	0.00	0.00	0.00	96.22
12.82	78.39	19.07	0.00	2.55	0.00	0.00	0.00	0.00	0.00	0.00	0.00	0.00	0.00	0.00	0.00	0.00	96.53
13.01	78.96	18.42	0.00	2.62	0.00	0.00	0.00	0.00	0.00	0.00	0.00	0.00	0.00	0.00	0.00	0.00	96.86
13.32	79.49	17.80	0.00	2.71	0.00	0.00	0.00	0.00	0.00	0.00	0.00	0.00	0.00	0.00	0.00	0.00	96.98
13.40	79.63	17.64	0.00	2.73	0.00	0.00	0.00	0.00	0.00	0.00	0.00	0.00	0.00	0.00	0.00	0.00	97.01
13.78	80.15	16.94	0.00	2.90	0.00	0.00	0.00	0.00	0.00	0.00	0.00	0.00	0.00	0.00	0.00	0.00	97.39
13.82	80.13	16.98	0.00	2.89	0.00	0.00	0.00	0.00	0.00	0.00	0.00	0.00	0.00	0.00	0.00	0.00	97.39
14.16	79.97	17.29	0.00	2.74	0.00	0.00	0.00	0.00	0.00	0.00	0.00	0.00	0.00	0.00	0.00	0.00	97.41
14.54	79.80	17.16	0.00	3.04	0.00	0.00	0.00	0.00	0.00	0.00	0.00	0.00	0.00	0.00	0.00	0.00	97.60
14.55	79.80	17.16	0.00	3.04	0.00	0.00	0.00	0.00	0.00	0.00	0.00	0.00	0.00	0.00	0.00	0.00	97.60
14.57	79.80	17.16	0.00	3.04	0.00	0.00	0.00	0.00	0.00	0.00	0.00	0.00	0.00	0.00	0.00	0.00	97.60
15.07	79.80	17.16	0.00	3.04	0.00	0.00	0.00	0.00	0.00	0.00	0.00	0.00	0.00	0.00	0.00	0.00	97.60

Table 5.10 Produced Gas Composition. Test One

Table 5.11 Incremental Fuel ad Air Parameters. Test One

Run Time	Air Injection		Air/Fuel		Apparent H/C		Cumulative Production for the Gases					
	Cum	Inc.	Inc.	Cum.	Inc.	Cum.	N_2	CO_2	CO	O_2	H_2S	CH_4
hours	l (ST)	l (ST)/h	m^3/kg	m^3/kg			l (ST)	l (ST)	l (ST)	l (ST)	l (ST)	l (ST)
1.13	254.04	14.94	26.88	26.88	-	-	0.08	0.00	0.00	0.00	0.00	0.00
1.15	257.77	3.74	26.88	26.88	-	-	0.08	0.00	0.00	0.00	0.00	0.00
1.21	270.66	12.89	26.88	26.88	-	-	0.09	0.00	0.00	0.00	0.00	0.00
1.32	295.13	24.47	23.85	24.00	57.91	61.54	1.61	0.02	0.01	0.01	0.00	0.00
1.59	356.09	60.96	18.22	18.70	12.50	13.93	15.08	0.61	0.32	0.18	0.00	0.00
1.62	362.38	6.29	17.91	18.63	11.68	13.69	16.65	0.68	0.36	0.20	0.00	0.00
1.67	373.58	11.21	17.37	18.41	10.39	13.06	19.87	0.85	0.44	0.24	0.00	0.00
1.68	377.32	3.74	17.20	18.40	10.00	13.03	20.04	0.86	0.44	0.24	0.00	0.00
1.97	441.51	64.19	14.59	16.10	5.49	7.86	44.21	2.98	1.16	0.57	0.00	0.03
2.12	474.45	32.94	13.86	15.48	4.50	6.80	58.72	4.45	1.59	0.78	0.00	0.05
2.35	526.94	52.49	12.81	14.45	3.26	5.26	89.17	8.19	2.52	1.21	0.00	0.08
2.57	575.32	48.38	12.28	13.80	2.68	4.40	121.52	12.63	3.47	1.68	0.00	0.10
2.73	612.37	37.05	11.90	13.45	2.28	3.95	145.59	16.20	4.14	2.03	0.00	0.10
3.11	697.92	85.55	11.47	12.80	1.80	3.18	205.53	26.13	5.59	2.91	0.00	0.10
3.18	713.54	15.63	11.39	12.72	1.73	3.09	216.51	27.98	5.85	3.07	0.00	0.10
3.49	783.34	69.80	11.06	12.34	1.41	2.67	272.90	38.19	7.05	3.89	0.00	0.10
3.57	799.47	16.13	11.03	12.27	1.38	2.60	285.95	40.57	7.33	4.09	0.00	0.10
3.88	868.71	69.24	10.91	12.06	1.27	2.36	334.43	49.64	8.32	4.80	0.00	0.10
4.07	911.54	42.84	10.83	11.94	1.20	2.25	364.37	55.32	8.93	5.24	0.00	0.10
4.26	954.19	42.65	10.75	11.84	1.14	2.15	394.12	61.05	9.54	5.68	0.00	0.10
4.57	1,023.62	69.42	10.82	11.72	1.20	2.03	442.88	70.31	10.54	6.40	0.00	0.10
4.64	1,039.50	15.88	10.84	11.70	1.21	2.01	452.12	72.06	10.73	6.53	0.00	0.10
5.02	1,124.86	85.36	10.86	11.62	1.22	1.93	500.32	81.16	11.70	7.25	0.00	0.10
5.07	1,135.69	10.83	10.74	11.60	1.11	1.91	506.43	82.34	11.82	7.34	0.00	0.10
5.40	1,210.29	74.59	9.94	11.41	0.46	1.72	564.72	95.31	13.00	8.36	0.00	0.10
5.78	1,295.71	85.43	9.93	11.23	0.37	1.54	632.04	110.52	14.26	9.71	0.00	0.10

Table 5.11 Incremental Fuel ad Air Parameters. Test One

Run Time	Air Injection		Air/Fuel		Apparent H/C		Cumulative Production for the Gases					
	Cum	Inc.	Inc.	Cum.	Inc.	Cum.	N_2	CO_2	CO	O_2	H_2S	CH_4
hours	l (ST)	l (ST)/h	m^3/kg	m^3/kg			l (ST)	l (ST)	l (ST)	l (ST)	l (ST)	l (ST)
5.82	1,303.81	8.09	9.99	11.22	0.41	1.53	638.43	111.95	14.38	9.84	0.00	0.10
6.16	1,303.81	0.00	10.60	11.19	0.80	1.50	660.76	116.50	14.78	10.31	0.00	0.10
6.23	1,303.81	0.00	10.75	11.19	0.89	1.49	669.76	118.29	14.94	10.50	0.00	0.10
6.25	1,303.81	0.00	10.79	11.19	0.91	1.49	670.38	118.41	14.95	10.52	0.00	0.10
6.54	1,303.81	0.00	11.45	11.20	1.33	1.49	705.18	124.71	15.50	11.34	0.00	0.10
6.78	1,303.81	0.00	11.57	11.21	1.30	1.48	733.81	129.85	15.94	12.11	0.00	0.10
6.92	1,303.81	0.00	11.65	11.23	1.28	1.47	753.83	133.44	16.25	12.69	0.00	0.10
7.30	1,303.81	0.00	12.05	11.28	1.24	1.46	807.95	142.89	16.99	14.76	0.00	0.10
7.32	1,303.81	0.00	12.06	11.28	1.24	1.46	809.73	143.20	17.01	14.82	0.00	0.10
7.68	1,303.81	0.00	12.23	11.33	1.27	1.45	858.13	151.54	17.63	16.78	0.00	0.10
7.82	1,303.81	0.00	12.34	11.35	1.24	1.44	875.38	154.50	17.84	17.53	0.00	0.10
8.06	1,303.81	0.00	12.54	11.39	1.18	1.44	910.28	160.44	18.24	19.21	0.00	0.10
8.32	1,303.81	0.00	12.18	11.41	0.61	1.41	936.07	165.23	18.50	20.70	0.00	0.10
8.44	1,303.81	0.00	12.01	11.41	0.35	1.40	944.75	166.92	18.57	21.23	0.00	0.10
8.82	1,303.81	0.00	9.85	11.39	-0.66	1.36	958.35	170.50	18.65	21.99	0.00	0.10
8.82	1,303.81	0.00	9.81	11.39	-0.67	1.36	958.69	170.59	18.65	22.01	0.00	0.10
9.20	1,303.81	0.00	7.94	11.34	-1.43	1.32	967.54	173.77	18.65	22.43	0.00	0.10
9.32	1,303.81	0.00	7.61	11.33	-1.54	1.30	969.92	174.67	18.65	22.54	0.00	0.10
9.59	1,303.81	0.00	6.89	11.30	-1.77	1.27	974.12	176.46	18.65	22.71	0.00	0.10
9.82	1,303.81	0.00	6.25	11.27	-2.00	1.25	977.10	177.90	18.65	22.82	0.00	0.10
9.97	1,303.81	0.00	5.88	11.25	-2.13	1.24	978.76	178.76	18.65	22.88	0.00	0.10
10.32	1,303.81	0.00	5.68	11.22	-2.18	1.21	981.92	180.47	18.65	22.98	0.00	0.10
10.35	1,303.81	0.00	5.66	11.21	-2.19	1.20	982.22	180.63	18.65	22.99	0.00	0.10
10.82	1,303.81	0.00	6.38	11.18	-1.89	1.17	986.78	182.76	18.65	23.13	0.00	0.10
11.11	1,303.81	0.00	6.89	11.16	-1.67	1.16	989.21	183.79	18.65	23.21	0.00	0.10
11.32	1,303.81	0.00	6.92	11.15	-1.65	1.15	990.66	184.40	18.65	23.25	0.00	0.10
11.49	1,303.81	0.00	6.94	11.14	-1.63	1.14	991.69	184.83	18.65	23.28	0.00	0.10

Table 5.11 Incremental Fuel ad Air Parameters. Test One

Run Time	Air Injection		Air/Fuel		Apparent H/C		Cumulative Production for the Gases					
	Cum	Inc.	Inc.	Cum.	Inc.	Cum.	N_2	CO_2	CO	O_2	H_2S	CH_4
hours	l (ST)	l (ST)/h	m^3/kg	m^3/kg			l (ST)	l (ST)	l (ST)	l (ST)	l (ST)	l (ST)
11.82	1,303.81	0.00	7.76	11.13	-1.26	1.13	993.49	185.48	18.65	23.34	0.00	0.10
11.87	1,303.81	0.00	7.91	11.13	-1.19	1.13	993.77	185.58	18.65	23.35	0.00	0.10
12.25	1,303.81	0.00	8.99	11.13	-0.67	1.13	995.57	186.11	18.65	23.41	0.00	0.10
12.32	1,303.81	0.00	9.16	11.13	-0.58	1.13	995.88	186.20	18.65	23.42	0.00	0.10
12.63	1,303.81	0.00	10.04	11.12	-0.09	1.13	997.48	186.60	18.65	23.47	0.00	0.10
12.82	1,303.81	0.00	10.30	11.12	0.05	1.12	998.35	186.81	18.65	23.49	0.00	0.10
13.01	1,303.81	0.00	10.60	11.12	0.21	1.12	999.21	187.01	18.65	23.52	0.00	0.10
13.32	1,303.81	0.00	10.90	11.12	0.38	1.12	1,000.50	187.30	18.65	23.57	0.00	0.10
13.40	1,303.81	0.00	10.98	11.12	0.42	1.12	1,000.83	187.37	18.65	23.58	0.00	0.10
13.78	1,303.81	0.00	11.34	11.12	0.59	1.12	1,002.26	187.67	18.65	23.63	0.00	0.10
13.82	1,303.81	0.00	11.32	11.12	0.59	1.12	1,002.41	187.70	18.65	23.64	0.00	0.10
14.16	1,303.81	0.00	11.15	11.12	0.53	1.12	1,003.66	187.97	18.65	23.68	0.00	0.10
14.54	1,303.81	0.00	11.25	11.12	0.48	1.12	1,004.95	188.25	18.65	23.73	0.00	0.10
14.55	1,303.81	0.00	11.25	11.12	0.48	1.12	1,004.98	188.26	18.65	23.73	0.00	0.10
14.57	1,303.81	0.00	11.25	11.12	0.48	1.12	1,005.03	188.27	18.65	23.73	0.00	0.10
15.07	1,303.81	0.00	11.25	11.12	0.48	1.11	1,019.96	191.46	18.65	24.30	0.00	0.10

Table 5.11. Incremental Fuel and Air Parameters. Test One

The overall air and fuel calculations, as well as the volume balances for the major components are shown in Table 5.12 and 5.13:

Total Air Required	1,305 l(ST)
Measured Air Feed	1,304 l(ST)
Measured Oxygen Feed	284.5 l(ST)
Measured Nitrogen Feed	1,020 l(ST)
Total Volume of Produced Gas (He free)	1,260 l(ST)
Total Volume of Produced Gas (He included)	3,540 l(ST)
Air/Fuel Ratio	11.1 m^3(ST)/kg
O_2/Fuel Ratio	2.42 m^3(ST)/kg
Air Requirement*	129.70 m^3(ST)/m^3
Fuel Requirement*	11.66 kg/m^3
Apparent H/C	1.11
Oxygen Utilization	91.46%
(CO_2+CO)/CO Ratio	11.18
(CO_2+CO)/N_2 Ratio	0.21
Reacted Oxygen forming CO_x	77.49%
Total Hydrocarbon's Gas Production	10.6 g
Total Oil Consumed as Fuel	117.2 g
Total Mass of Oil Produced as Gas	127.8 g

*Based on a burned volume of 10.1 x 10^{-3} m^3 (76% of the CT)

Table 5.12 Overall Air-Fuel Calculations. Test One

Most of the above gas phase combustion parameters were calculated using the stoichiometric equation:

$$C_xH_y + aO_2 + (R)a\ N_2 \rightarrow b\ CO_2 + d\ CO + f\ O_2 + j\ H_2O + (R)a\ N_2$$

where, $R = \frac{N_2 mole\ fraction}{O_2\ mole\ fraction}$ in the feed gas.

a, b, d, f and j are the stoichiometric coefficients based on the individual volume (or moles) of the components in the produced gases, and are defined as:

Carbon: x = b + d

Hydrogen: y= 2j

$$a = b + \frac{d}{2} + f + \frac{j}{2}$$

Component Production [l (ST)]	
O_2	24.29
N_2	1,019.97
CO	18.65
CO_2	191.48
CH_4	0.09
C_2H_4	0.11
C_2H_6	0.11
C_3H_6	0.00
C_3H_8	0.40
C_{4+}	3.22
H_2	2.08
H_2S	0.00

Table 5.13 Volume of Produced Gases. Test One

5.3.4.3 Stabilized Combustion Period

The combustion performed in this test was a dry combustion (no water injection), therefore the combustion front velocity was based on the rate of advance downstream of a specific temperature at the leading edge of the high temperature region. The selected temperature is based on the range where oxidation/combustion reactions occur, which are primarily responsible for the oil mobilization. Usually for light oils, the peak temperatures are in the range of 300 to 400°C, but the temperature where the energy generation rate occurs is in the range of 200 to 280°C. The selected temperature to establish the location of the combustion front was 220°C, where the combustion reactions were occurring. In this test, two stable combustion front velocities were observed (see Figure 5.7).

Table 5.14 presents the stable product gas composition corresponding to the portion of the test where the combustion tube front propagation rate and the product gas composition were stable. As shown in Figure 5.8, the composition of the produced gas was stable during the period 3.5 to 5.1 GC hours and again for the period of 6.2 to 8.0 GC hours. Table 5.15 provides the stabilized combustion parameters corresponding to the advance of the 200°C leading edge over the two stable velocity periods.

The first combustion front velocity over the period of 0.5 to 3.7 run hours was 0.279 m/h, which for an average air flux of 30.0 m^3(ST)/m^2h translates to an air requirement of 107 m^3(ST)/m^3 of reservoir. The later 220°C combustion front advance was over the period between 4.1 to 7.5 run hours as shown by the dotted orange line in Figure 5.7. The velocity of that latter combustion front was 0.123 m/h, giving a stable air requirement of 244 m^3(ST)/m^3 of reservoir.

	Stabilized Period 1	Stable Period 2
Air Flux [m^3(ST)/m^2•h], [scf/ft^2•h]	30.0	---
Time Interval by 220°C Front Velocity [hour]	0.5 to 3.7	4.1 to 7.5
Gas Chromatograph Interval [hour]	3.5 to 4.7	6.5 to 7.8
Component	**Stabilized Composition [mole percent]**	
CO_2	15.42	14.40
CO	1.69	1.16
O_2	1.20	2.79
N_2	81.49	81.46
CH_4	0.00	0.00
C_2H_4	0.00	0.00
C_2H_6	0.00	0.00
C_3H_8	0.00	0.00
C_4+	0.03	0.02
H_2S	0.00	0.00
H_2	0.17	0.17

Table 5.14 Stable Product Gas Composition. Test One

Combustion Front	220°C Leading Edge	220°C Leading Edge
Air Flux [m^3(ST)/m^2•h], [scf/ft^2•h]	30.0	----
Time Interval by Velocity [hour]	0.5 to 3.7	4.1 to 7.5
Gas Chromatograph Interval [hour]	3.5 to 4.7	6.5 to 7.8
Air Flux Location	Inlet	Inlet
Air/Fuel Ratio [m^3(ST)/kg]	10.87	11.91
Combustion Front Velocity [m/h]	0.279	0.123
Air Required [m^3(ST)/m^3]	107.14	243.90
Fuel Required [kg/m^3]	9.86	20.49
Apparent Atomic H/C Ratio	1.23	1.27
Percent Oxygen Utilization	94.72	87.72
Percent Conversion of Reacted O_2 to Carbon Oxides	75.52	75.13
(CO_2 + CO)/CO Ratio	10.12	13.41
(CO_2 + CO)/N_2 Ratio	0.21	0.19
N_2/O_2 Ratio	3.58	3.58

Table 5.15 Summary of Stabilized Combustion Parameters. Test One

5.3.4.4 Liquid Production History

During the entire test all the liquids produced were collected in sample bottles and stored for subsequent separation and analysis. The liquids separation process was to firstly remove the free water (by gravity segregation) contained in the jars by pipetting, which was quantified and analyzed. The remaining oil and water were centrifuged at 10°C and 2,500 rpm for 15 to 30 minutes. The oil samples collected from the centrifugation were

analyzed by Karl Fischer technique to ensure that no water remained in the oil. Once the liquids were completely separated, the masses were measured and tested for property analyses.

Table 5.16 summarizes the liquid production history. It is noticed that the large liquid sample recorded at 1.08 hours corresponds to the contents of the ILPC Figure 5.10 shows the cumulative water and oil productions during the test, as well as the location of the combustion front while those liquids were produced. Table 5.16 shows that 147.3 g of water and 185.8 g of oil were produced prior the start of air injection. These liquids were produced due to the pressurization and pre-heating to reach the reservoir conditions (2,200 psig and 149°C). At the end of the test (helium purge) 2,600.7 g of oil and 1,554.8 g of water were produced. With this information it was calculated that 91.67% of the OOIP was recovered, noting that the volume swept by the 220°C front (combustion zone/air injection) was 76% of the core.

An interesting observation from Figure 5.10 is that the water production rate increased significantly at 3.22 hours, hence the period where the 200°C front velocity was 0.124 m/h corresponds to the production of the water bank.

At 14.55 hour run time the system was turned off and the combustion tube de-pressured, reporting the last liquid sample on Table 5.16 under the line of 14.57 hours run time.

Sample	Run Time [hours]	Mass Oil [g]	Cum. Oil [g]	H_2O Free [g]	H_2O Emul. [g]	Total H_2O [g]	Cum. H_2O [g]
1	0.00	185.81	185.81	146.68	0.57	147.25	147.25
2	1.08	1,683.57	1,869.38	49.60	137.60	187.20	334.45
3	2.03	174.70	2,044.08	62.10	2.85	64.95	399.40
4	3.22	209.01	2,253.09	142.43	6.96	149.39	548.79
5	4.05	29.16	2,282.25	280.04	0.81	280.85	829.64
6	4.83	83.73	2,365.98	233.35	2.33	235.68	1,065.32
7	5.85	124.12	2,490.10	231.17	6.77	237.94	1,303.26
8	14.57	110.56	2,600.66	251.22	0.28	251.50	1,554.76
Lines		--	--	---	36.00	36.00	1,590.36

Table 5.16. Liquid Production History. Test One

5.3.4.5 Extraction and Analysis of Post-Test Core and Core Plugs

After the test, the combustion tube was unpacked, removing the core plugs and crushed core in segments, which were deposited in airtight bags for their analysis. Visual observation indicated that the volume covered by the combustion front during the air injection period (0.0 to 5.82 run time) was clean, while the section swept during the helium flood showed a slight oil content in the crushed core and core plugs. Table 5.17

shows the core pack properties after the burn and Table 5.18 a visual description of the post-burn core during the unpacking.

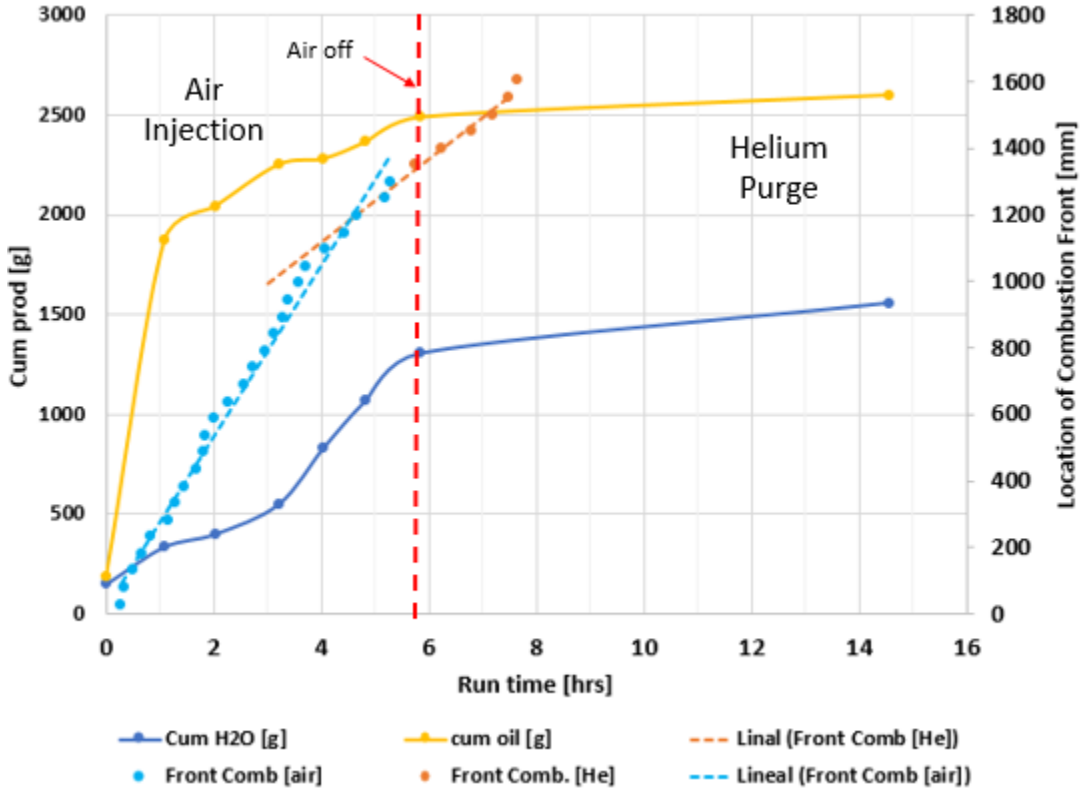

Figure 5.10.Cumulative Production Masses of Oil and Water and Location of Combustion Front. Test One

The methodology used to measure the fluid content in post-test cores was:

- The samples, or a portion of the samples depending on the size, were placed in a pre-weighted Soxhlet thimble
- After weighting, the samples where set into the Soxhlet extraction device. The extraction took between 16 to 36 hours, depending on the size and saturation of the core, using toluene as the extracting solvent. The water extracted was collected in Dean-Stark traps and transferred into graduated cylinders for quantification.
- The core that was left in the Soxhlet thimble was placed in the fume hood to evaporate the toluene. Next it was put in the furnace at 120°C overnight to remove any remaining toluene and weighted.
- The mass of oil from the extracted core was calculated by difference.
- Finally, extracted and dried samples were weighted again and heated to 600°C for 16 hours. Each sample was cooled in a desiccator and weighted. If any mass loss about the blank was measured, it was assumed to equal the coke mass (toluene insoluble) deposited on the core during the combustion.

Figure 5.11 shows the percent of oil, water and coke remaining the Core Plugs and crushed core after the combustion test, taken from Table 5.17, as well as the maximum temperature registered by each center line thermocouple during the test (from Table 5.9).

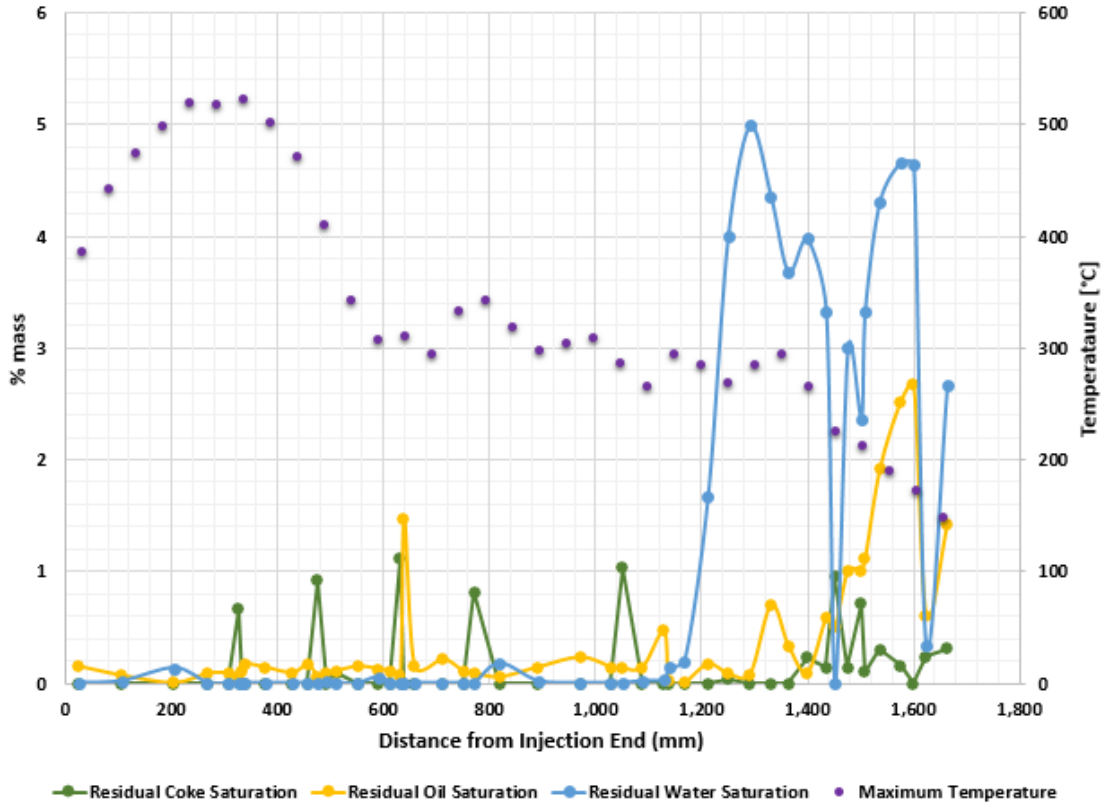

Figure 5.11. Residual Oil, Water and Coke in the Post-Burn Core. Test One

Table 5.17- Core Pack Properties after the Run. Test One

Sample	Sample Number	Distance from Injection end Midpoint [mm]	Mass of Sample [g]	Mass oil [%]	Mass water [%]	Mass coke [%]	Mass oil [g]	Mass water [g]	Mass coke [g]
16 MPF	1	1,663.00	567.33	1.422	2.661	0.310	8.067	15.097	1.759
20/30 MFP	2	1,623.00	458.16	0.607	0.332	0.240	2.782	1.520	1.100
Core 1	3	1,599.50	300.50	2.669	4.646	0.000	8.020	13.961	0.000
Core 2-1	4	1,574.50	407.57	2.515	4.661	0.160	10.249	18.997	0.652
Core 2-2	5	1,535.50	597.30	1.917	4.307	0.306	11.448	25.725	1.826
Core 3-1a	6	1,508.00	204.51	1.117	3.332	0.105	2.284	6.814	0.214
Core 3-1b	7	1,500.50	65.34	1.000	2.365	0.714	0.654	1.545	0.466
Core 3-2	8	1,475.50	368.75	1.013	2.998	0.139	3.735	11.055	0.514
Core Plug #7a	9	1,451.00	190.24	0.510	0.000	0.950	0.970	0.000	1.807
Core 3-3	10	1,434.50	370.77	0.585	3.329	0.145	2.171	12.341	0.539
Core 4-1	11	1,399.00	713.00	0.094	3.977	0.231	0.671	28.358	1.649
Core 4-2	12	1,363.00	407.31	0.333	3.685	0.000	1.357	15.010	0.000
Core 5-1	13	1,330.50	505.40	0.701	4.357	0.000	3.543	22.019	0.000
Core 5-2	14	1,290.50	505.97	0.079	4.991	0.000	0.400	25.250	0.000
Core 6-1	15	1,249.50	540.31	0.083	3.995	0.035	0.446	21.586	0.189
Core 6-2	16	1,211.50	518.60	0.172	1.666	0.000	0.891	8.639	0.000
Core 7-1	17	1,167.50	604.72	0.009	0.200	0.000	0.055	1.209	0.000
Core 7-2	18	1,138.00	264.85	0.031	0.138	0.000	0.081	0.366	0.000
Core 8-1	19	1,128.00	77.84	0.468	0.029	0.000	0.365	0.023	0.000
Core 8-2	20	1,088.00	537.60	0.142	0.017	0.000	0.765	0.090	0.000
Core Plug #6	21	1,051.00	371.03	0.130	0.000	1.030	0.482	0.000	3.822
Core 8-3	22	1,028.50	585.95	0.144	0.000	0.000	0.844	0.000	0.000
Core 9	23	970.50	908.70	0.233	0.000	0.000	2.115	0.000	0.000
Core 10	24	890.50	1,070.69	0.143	0.018	0.000	1.528	0.190	0.000
Core 11	25	818.00	804.32	0.055	0.176	0.000	0.442	1.414	0.000
Core Plug #4+5	26	770.50	407.84	0.090	0.000	0.820	0.367	0.000	3.344
Core 12-1	27	751.00	209.44	0.102	0.000	0.000	0.214	0.000	0.000
Core 12-2	28	711.00	1,003.50	0.219	0.000	0.000	2.193	0.000	0.000
Core 13-1	29	658.00	470.58	0.149	0.000	0.000	0.701	0.000	0.000
Core 13-2	30	638.00	5.99	1.474	0.000	0.000	0.088	0.000	0.000
Core Plug #3	31	631.00	183.68	0.070	0.000	1.110	0.129	0.000	2.039

Table 5.17- Core Pack Properties after the Run. Test One

Sample	Sample Number	Distance from Injection end Midpoint [mm]	Mass of Sample [g]	Mass oil [%]	Mass water [%]	Mass coke [%]	Mass oil [g]	Mass water [g]	Mass coke [g]
Core 13-3	32	612.00	344.62	0.110	0.000	0.000	0.379	0.000	0.000
Core 13-4	33	589.50	92.13	0.128	0.055	0.000	0.118	0.051	0.000
Core 14-1	34	551.00	877.10	0.151	0.000	0.000	1.327	0.000	0.000
Core 14-2	35	511.00	176.09	0.111	0.000	0.096	0.195	0.000	0.169
Core 15-1	36	491.00	277.71	0.095	0.017	0.000	0.264	0.048	0.000
Core Plug #2	37	475.00	183.92	0.065	0.000	0.920	0.120	0.000	1.692
Core 15-2	38	456.00	417.38	0.167	0.000	0.000	0.697	0.000	0.000
Core 15-3	39	427.50	243.05	0.094	0.000	0.000	0.228	0.000	0.000
Core 16-1	40	377.00	871.00	0.140	0.000	0.000	1.221	0.000	0.000
Core 16-2	41	337.50	62.50	0.175	0.000	0.000	0.109	0.000	0.000
Core 17-1	42	332.00	160.81	0.109	0.000	0.000	0.176	0.000	0.000
Core Plug #1	43	326.00	183.52	0.060	0.000	0.660	0.110	0.000	1.211
Core 17-2	44	307.00	339.02	0.090	0.000	0.000	0.304	0.000	0.000
Core 17-3	45	267.50	454.01	0.087	0.000	0.000	0.396	0.000	0.000
Core 18	46	204.50	868.80	0.003	0.134	0.000	0.024	1.164	0.000
20/30 MIF	47	106.50	1,845.12	0.068	0.018	0.000	1.254	0.329	0.000
16 MIF	48	24.50	356.86	0.150	0.000	0.000	0.537	0.000	0.000
Total							**75.515**	**232.803**	**22.992**

Table 5.17 Core Pack Properties after the Run. Test One

Table 5.18 Description of Post Burn Core. Test One

Sample	Distance from Injection [mm]	Distance from Production [mm]	Description
16MFP-1	1,579	115	Wet, Oily frac sand
20/30 MFP	1,549	145	Wet, Oily frac sand, with dark regions
Core 1	1,532	162	Oily core
Core 2-1	1,499	195	Oily core
Core 2-2	1,454	240	Oily core, a bit drier
Core 3-1a	1,444	250	Oily core, unconsolidated
Core 3-1b	1,439	255	Oily core, consolidated
Core 3-2	1,394	300	Core around Plug #7; less oily
Plug #7a	1,390	304	Damp plug
Core 3-3	1,361	333	Oily core, drier
Core 4-1	1,319	375	Damp core; oily smell
Core 4-2	1,289	405	As above
Core 5-1	1,254	440	As above
Core 5-2	1,209	485	As above
Core 6-1	1,172	522	As above
Core 6-2	1,133	561	Transition to dry, clean core
Core 7-1	1,084	610	Dry, clean burned core
Core 7-2	1,074	620	As above
Core 8-1	1,064	630	Hard consolidated from end of Core Plug #6
Core 8-2	994	700	Core around Plug #6
Plug #6	990	704	Dry plug
Core 8-3	949	745	Dry, clean burned core
Core 9	874	820	As above
Core 10	789	905	As above
Core 11	729	965	As above
Plug #4+5	694	1,000	Concentric plug, including sand between plugs
Core 12-1	690	1,004	Core around Plug #4+5
Core 12-2	614	1,080	Dry, clean burned core
Core 13-1	584	1,110	Unconsolidated core from below Plug #3
Core 13-2	574	1,120	Consolidated core from below Plug #3
Plug #3	570	1,124	Dry plug
Core 13-3	536	1,158	Core around Plug #3
Core 13-4	525	1,169	Core above Plug #3
Core 14-1	459	1,235	Dry, clean burned core
Core 14-2	445	1,249	Consolidated core stuck to wall
Core 15-1	419	1,275	Core from below Plug #2
Plug #2	413	1,281	Dry plug
Core 15-2	381	1,313	Core around Plug #2
Core 15-3	356	1,338	Core above Plug #2
Core 16-1	280	1,414	Dry, clean burned core
Core 16-2	277	1,417	Consolidated core
Core 17-1	269	1,425	Core from below Plug #1
Plug #1	265	1,429	Dry plug

Table 5.18 Description of Post Burn Core. Test One

Sample	Distance from Injection [mm]	Distance from Production [mm]	Description
Core 17-2	231	1,463	Core around Plug #1
Core 17-3	186	1,508	Core above Plug #1
Core 18	105	1,589	Dry, clean burned core
20/30mFrac	3	1,704	Dry clean frac sand and core
16mFrac	0	1,707	Dry clean frac sand

Table 5.18. Description of Post-Burn Core. Test One

From the cores collected and analyzed after the combustion test, it can be appreciated that the test was highly effective sweeping/pushing the hydrocarbons out of the crushed core and core plugs. The total amount of residual hydrocarbon in the post test core(s) was 75.5 g and 22.7 g of coke, from an original volume of 2,741 g, leading is to a successful test. The coke amount after the test is not precisely known for dolomite cores, due to the decomposition of dolomite, which can alter/modify the “mass loss on ignition” used to measured it. After the dried core and plugs samples were heated to 600°C for 16 hours, and the mass difference in the core plugs before and after burning them at 600°C was around 23% mass lost and for the crushed cores was 22.5% mass lost. As will be discussed in Chapter 6, the mass loss on heating dolomites has been studied by Olszak et al. (2015).

Based in Olzark et al (2015) studies then the total mass loss measured cannot be assumed to be all due to coke. Based on Olzark’s study, and on test in the ISCRG is laboratory it was assumed that 22.5% of the mass lost was associated with rock decomposition and the difference was the remaining coke in the crushed core and core plugs.

In our post- test analysis, the mass of water left in the core and plugs after the test was 232.8 g.

For the seven core plugs, which were representing the matrix (low permeability) in the reservoir and were originally saturated with dead reservoir oil, it was observed that the post-test cores had with a very low amount of residual oil. When they were removed from the combustion tube, they were weighted and then cut approximately in half using a diamond saw with no fluid during the cutting process. In Appendix A, Photo 5 shows some of the core plugs during the combustion tube’s unpacking process. Photo 6 presents the cutting process. Half of each plug was crushed and the fluid contents were measured following the same procedure as the crushed core, described previously. Table 5.19 summarizes the initial and final content of fluids in the core plugs. As a reminder, air injection was shut down when air reached Zone 26 (Thermocouple 26) located 1,299 mm from injection end, therefore the core plugs that were located upstream of Zone/TC 26 came out quite clean showing a good oil swept. Figure 5.3, shows the schematic location of the core plugs. From Table 5.9 it can be inferred that when maximum temperatures were around 300°C (high-temperatures zones) the

combustion front had a good performance pushing/removing the oil. On the other hand, the last core plug, which the combustion front reached during the helium purge, showed increased mass of remaining oil.

With this observations and measurements of the initial and final fluids saturations it can be suggested that an EOR with HPAI for this Mexican reservoir has good potential.

Core Plug	Mass of Oil [g]		Oil Displaced [mass %]	Max. Temp. [°C]	Oil Concentration in Adjacent Crushed Core [mass %]		
	Initial	Post-Test			Above	Beside	Below
#1	8.56	0.11	98.7	522	0.09	0.09	0.11
#2	8.60	0.13	98.5	422	0.09	0.17	0.09
#3	9.03	0.13	98.6	310	0.13	0.11	0.15
#4+5	19.52	0.36	98.2	340	0.22	0.10	0.05
#6	16.84	0.48	97.1	267	0.14	0.14	0.47
#7a	7.72	0.97	87.4	221	0.59	1.01	1.10

Table 5.19. Summary of Oil Displacement in Core Plugs for Test One.

5.3.4.6 Material Balance

All fluids going in and out of the system were measured in a way to keep a material balance. Table 5.20 presents a summary of the fluids injected and produced during the run. The mass of water generated during combustion was calculated from the computed hydrogen consumption, and water produced as vapor was based on the assumption that the product gas was saturated with water at 0°C (the cold trap temperature).

The density, viscosity and asphaltenes (C_{5+} which are soluble in toluene and pentane), properties in the original oil and the oil samples collected during production are shown in Table 5.21. An elemental analysis of the oil including carbon, hydrogen, nitrogen and sulfur (CHNS) are shown in Table 5.22. Table 5.23 presents the water properties of the produced water.

Oil Balance	[g]
Initial Oil in System	2,837.1
Oil Produced as liquid	2,600.7
Oil Produced as gas	117.2
Fuel Produced as gas	10.6
Residual Hydrocarbon in pack	83.0
Total Produced	2,811.5
Difference	25.6
Percent error	0.9
Water Balance	**[g]**
Initial Water in System	1,704.5
Water injected	0.0
Water generated by Combustion	90.4
Total In	1,794.9
Water Produced as liquid	1,554.8
Water Produced as gas	22.0
Residual Water in Pack	232.8
Difference	-14.7
Percent Error	-0.8

Table 5.20. Liquid Mass Balance. Test One

Sample	Time [hours]	Viscosity 25°C [cp (mPa•s)]	Density 25°C [g/cm^3]	Asphaltenes Mass %
Original Oil	--	4.14	0.8238	0.01
Produced Oil				
1	0.00	3.38	0.8283	0.16
2	1.07	2.89	0.8147	0.13
3	2.02	3.20	0.8202	0.14
4	3.20	3.00	0.8198	0.14
5	4.03	3.40	0.8240	0.13
6	4.82	5.63	0.8235	0.25
7	5.83	8.59	0.8347	0.34
8	14.55	3.73	0.8247	0.09

Table 5.21 Oil Properties Pre and Post Burn. Test One

Sample	Time [hours]	Mass Percent				H/C ratio
		Carbon	Hydrogen	Nitrogen	Sulfur	
Original Oil	--	85.61	13.66	0.05	0.55	1.9015
Produced Oil						
1	0.0	86.35	13.88	0.05	0.58	1.9155
2	1.07	84.81	13.86	0.04	0.59	1.9475
3	2.02	85.56	13.86	0.04	0.51	1.9304
4	3.20	85.65	13.91	0.03	0.55	1.9354
5	4.03	85.90	13.87	0.04	0.52	1.9242
6	4.82	86.75	13.97	0.04	0.55	1.9191
7	5.83	86.50	13.98	0.04	0.49	1.9260
8	14.55	84.71	13.55	0.03	0.43	1.9062

Table 5.22 CHNS of Oil Samples. Test One

Sample	Time	pH	CO_3^{2-}	HCO^{3-}	Cl^-	SO_4^{2-}	Total solids	Ca^{2+}	Fe^{3+}	Mg^{2+}	K^+	Na^+
	[hours]		(mg/L)	(mg/L)	(mg/L)	(mg/L)	(mg/L)	(mg/L)	(mg/L)	(mg/L)	(mg/L)	(mg/L)
Original Water	---	7.34	0.00	92	42,552	40	72,900	6,100	<3.0	750	<15	19,000
Produced water during water flood	---	3.96	0.00	0	40,779	550	74,600	4,500	15	1,800	70	19,000
Produced water from oil flood	---	3.95	0.00	0	39,006	39	77,100	5,800	<3.0	850	<15	19,000
Free Water:												
1	0.0	6.62	0.00	21	39,006	76	74,500	5,300	<3.0	1,200	<15	18,000
2	1.07	7.10	0.00	39	40,779	89	72,100	IS	IS	IS	IS	IS
3	2.02	7.43	0.00	67	40,779	89	69,500	5,300	<3.0	1,100	32	18,000
4	3.20	7.50	0.00	311	40,779	215	71,400	5,400	<3.0	940	43	18,000
5	4.03	7.69	0.00	397	37,233	370	74,300	5,400	<3.0	1,100	69	18,000
6	4.82	4.65	0.00	696	37,233	465	72,700	4,700	16	1,100	67	15,000
7	5.83	4.51	0.00	1355	31,914	521	65,900	4,700	5.7	1,100	63	13,000
8	14.55	4.39	0.00	1641	40,779	530	58,400	4,600	<3.0	1,100	51	11,000

*IS- Insufficient Sample to conduct the analysis

Table 5.23 Produced Water Analysis. Test One

5.4 TEST TWO

5.4.1 Tube Packing and Flooding

As was described for test one, the packing procedure of the combustion tube was thorough the production end. The injection and production ends of the combustion tube were filled with approximately 500 grams of 16 mesh silica frac sand followed by 500 grams of 20/30 mesh silica frac sand. The frac sand at the injection end was wetted with 18 grams (approximately) of dead oil from the reservoir and less than 5 grams for the frac sands near the production end. Both sands were tamped in the combustion tube. As for test one, these frac sands, were placed with the intention of avoiding any sand grain migration into injection/production system. Between the silica frac sand sections, individual bags of one-kg samples of crushed core saturated with different amounts of dead oil and synthetic brine where placed in the tube. The design of different saturations was because in this experiment it was intended to represent three different zones (gas cap, oil and aquifer) as the actual reservoir state. The amounts of synthetic brine and dead oil used during packing the different zones is summarized in Table 5.24. All the crushed core and frac sand sections were inserted and tamped manually. Along the combustion tube the saturated core plugs were embedded in the crushed core, with two core plugs in each saturation zone. Figure 5.12 shows schematically the location of the thermocouples, the core plugs and the three different zones.

When the combustion tube was fully packed, it was closed, sealed, insolated and inserted in the combustion tube jacket and oriented with the injection end at the top. At atmospheric pressure, synthetic brine was injected into the packed combustion tube upward through the production end, connecting a line/hose through TC 23, to vent air and collect brine. The synthetic brine was injected until it broke through. Water injection through production line to reconstitute the aquifer in the combustion tube. Table 5.25 shows a summary of the masses of the frac sand, crushed core, core plugs, fluids and the fluids saturations in the crushed core, after the water flood of the aquifer zone.

5.4.2 Set Up/Pre-Test

The same procedure as described for Test one was realized to set up the combustion tube test. For more reference see section 5.3.2.

Table 5.24 Packing Masses. Test Two

Sample	Embedded Core Plug/ Zone	Mass of Crushed core/Core Plug [g]	Mass of Brine [g]	Mass of Oil [g]	Incremental Depth [mm]	Depth from Production End [mm]
16 m Inj Frac		498.56	0.00	18.28	42	1,711
20/30 m Inj Frac		495.74	0.00	18.38	44	1,667
Core 1		1,004.44	0.00	36.47	81	1,586
Core 2		1,000.25	0.00	36.69	81	1,505
Core 3A		999.89	0.00	36.52	89	1,464
	Plug #7	184.55	0.00	8.52	--	1,427
Core 3B		--	--	--	--	1,416
Core 4		1,000.14	0.00	35.70	82	1,334
Core 5A		1,000.29	0.00	37.15	88	1,311
	Plug #9	187.00	0.00	7.76	--	1,270
Core 5B		--	--	--	--	1,246
Core 6	End of Gas Cap Zone	694.19	0.00	25.29	56	1,190
Core 7		997.64	12.08	177.49	79	1,111
Core 8A		998.08	12.68	177.38	94	1,056
	Plug #10	187.35	0.00	7.60	--	--
Core 8B		--	--	--	--	1,017
Core 9		1,001.51	12.14	178.16	81	936
Core 10		1,000.61	12.14	178.17	82	854
Core11A		997.73	12.11	177.21	91	804
	Plug #11	182.57	0.00	8.26	--	766
Core 11B		--	--	--	--	763
Core 12		1,000.44	12.11	177.57	81	682
Core 13	End of Oil Zone	603.26	7.31	107.83	49	633
Core 14		1,000.51	0.00	8.55	81	552
Core 15A		1,000.99	0.00	8.43	87	499
Core 15B		--	--	--	--	465
	Plug #13	184.31	0.00	8.33	--	460
Core 16		1,000.39	0.00	8.66	79	386
Core 17A		1,000.39	0.00	8.61	88	346

Table 5.24 Packing Masses. Test Two

Sample	Embedded Core Plug/ Zone	Mass of Crushed core/Core Plug [g]	Mass of Brine [g]	Mass of Oil [g]	Incremental Depth [mm]	Depth from Production End [mm]
	Plug #16	184.63	0.00	8.36	--	305
Core 17B		--	--	--	--	298
Core 18		1,000.32	0.00	8.51	80	218
Core 19	End of Water Zone	1,000.11	0.00	8.63	79	139
20/30 m Prod Frac		499.10	0.00	4.28	44	95
16 m Prod Frac		364.73	0.00	2.87	33	62

Table 5.24 Packing Masses. Test Two

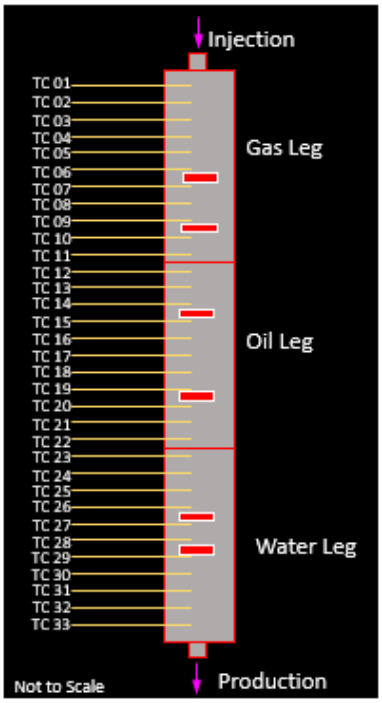

Figure 5.12 Schematic Drawing of Combustion Tube with the Thermocouples, Saturation Zones and Location of the Embedded Core Plugs. Test Two

	Packed Masses [g]		Mass of Fluids [g]
Crushed Core	18,301.2	Gas in Crushed Core	146.3
Frac Sand	1,858.1	Oil in Crushed Core	1,476.8
Core Plugs	1,110.4	Brine in Crushed Core	1,575.3
	Over all Saturations in Crushed Core [%]	Oil in Core Plugs	48.83
Oil	35.1	Oil in Total System	1,525.63
Brine	29.5	Brine in Total System	1,575.3
Gas	35.4		
Calculated Porosity of the Crushed Core Pack [%]		41.8	
Crushed Core Pore Volume [cm^3]		5,103.4	

Saturations for Each Zone			
	Gas Zone	**Oil Zone**	**Water Zone**
Oil [%]	17.5	83.0	4.2
Water [%]	0.0	4.5	84.3
Gas [%]	82.5	12.5	11.5
Pore Volume [cm^3]	1,694	1,712	1,697

Table 5.25 Masses and Saturations after Packing and Flooding the Combustion Tube. Test Two

5.4.3 Combustion Test

The pressure jacket was oriented vertically with the injection end at the top so air flow was downward. The core was pressurized up to 1,500 psig with methane and heating expansion, this was realized 2.78 hours prior to air injection. At the same time helium was injected in the annular space (space between combustion tube and pressure jacket), keeping 100 psig above the injection pressure inside the combustion tube, to prevent air or methane entering the annulus if a leak developed through the core holder or Swagelok fittings and to avoid tube deformation resulting from a high pressure differential across the tube.

When the pressure of 1,500 psig was reached, Helium flow to the production trap and associated flow lines was started to ensure that the Kamer valve was operating and capable of maintaining back pressure control once the production gases from the combustion tube broke through and all production was directed to the high-pressure separator. The heaters were turned on to heat the core up to 149°C (reservoir pressure) and with fluid expansion aiming for the reservoir pressure of 2,200 psig. The reservoir temperature was reached 1.5 hours prior air injection, registering a pressure inside the combustion tube of 1,791 psig. Then Zone/TC 33 was heated to 160°C to compensate for heat losses at the production flange. More methane was injected to compress and reach the 2,200 psig (reservoir pressure).

When the reservoir pressure and temperature were reached Zones 1, 2 and 3 were heated up to 175°C (ignition temperature). When the first three zones reached the ignition temperature, air ignition started at time zero. Time zero was defined when the air injection started, and it was designated as Day 0 of the test happening at 11:52 AM, 25 June 2019.

The air injected was a synthetic air with composition of oxygen of 23.00 mole percent and the rest nitrogen. Injection started at a rate of 149.44 liter(ST)/h (flux of 20 m^3(ST)/m^2h). The wall thermocouples were maintained at 175°C for the first three zones. After 28 minutes of air injection the first sign of ignition was observed when the temperature in Zones 1, 2 and 3 increased, reaching a temperature of 499°C. After ignition, at 34 minutes of air injection, the air flux was increased to 224 liter(ST)/h (flux of 30 m^3(ST)/m^2h).

After ignition and increasing the air injection rate, the injected air continued pushing the combustion front through the core pack. At 7.13 hours the combustion front passed Zone/TC 26, located at 76 percent of the combustion tube length, then air injection was switched to helium at the same rate of 224 liter(ST)/h. The air and product gases that were inside the combustion tube at the moment of the switch, were displaced by the helium and continued reacting/consuming in the combustion zone. The purpose of injecting helium, the same as in Test One, was to purge the core pack of the combustion/production gases, for mass balance calculations. Stopping air injection at TC 26 was to leave a portion of the core un-swept by the combustion zone that could be evaluated for the nature of the residual hydrocarbons. Safety reasons also required that the production flange seal not be heated above 300°C. The wall heaters were

operated on differential control during the entire test (air and helium injection). The injection of helium lasted until 14.48 hours. When the injection of helium was turned off, and the system was de-pressured.

During the whole test the produced liquids (oil and water) were collected intermittently in sample bottles for subsequent separation and analysis. The gas produced was sent to the GCs and monitored on a cycle of 8 minutes (Helium GC) and 22 minutes (product gas GC). After the tube cooled down, it was removed from the pressure jacket and unpacked in incremental sections of crushed core and core plugs, which were sent for analysis. Table 5.26 shows a summary of the injected and produced gases.

Parameter [units]	Value
Helium in Production System Following Pressure Up [liters (ST)]	219.9
Time of Air Injection [run hours]	0.0
Time of Helium Injection (Purge) [run hours]	7.13
Methane Injected [liters (ST)]	186.18
Oxygen Injected [liters (ST)]	357.45
Nitrogen Injected [liters (ST)]	1,196.66
Helium Injected (Purge) [liters (ST)]	1,647.51
Helium Injected to Production System [liters (ST)]*	164.00
Total Volume of Injected Gas [liters (ST)]	3,771.70
Total Volume of Produced Gas [liters (ST)]	3,571.88
Volume Out – Volume In [liters (ST)]	-199.82

*The measured since start of air injection [run time = 0.0]

Table 5.26 Summary of Injected and Produced Gases. Test Two

5.4.4 Results

5.4.4.1 Temperatures Profiles

The tube was positioned vertically with the injection end at the top, the same as Test One. During the entire test the temperatures at the centerline were recorded. The maximum temperature registered by each thermocouple is shown in Table 5.27. The distance where the thermocouples are located from the injection end are also presented. The first localized maximum temperature in a given zone is called the “peak temperature” while the highest temperature is called the maximum temperature. After 0.56 hours of injecting air the first signs of ignition were noted based on the temperature profiles, and it was decided to increase the air flux from 20 to 30 m^3/m^2h.

The temperatures recorded by the centerline and wall thermocouples against the location of them are shown in Figures 5.13 and 5.14 respectively. At 220°C a horizontal line is drawn, which is the temperature where the front velocity is calculated. During the whole test the combustion front advanced at a stable velocity. It is good to remember that after Zone/TC 26, the air injection was shut down and switched to helium, called the “Helium Purge”, which pushed the remaining air and product gases in the tube all the

way to the production end. The stored air kept reacting with the residual hydrocarbons remaining in the combustion tube.

Zone	Distance from Injection End [mm]	Time [hours]	Max Temp [°C]
1	28.9	0.75	475.43
2	79.7	1.03	362.82
3	130.5	1.30	499.28
4	181.3	1.57	385.19
5	232.1	3.58	350.98
6	282.9	3.35	397.84
7	333.7	3.13	446.67
9	435.3	3.88	320.48
10	486.1	3.93	359.70
11	536.9	3.98	328.87
12	587.7	3.90	302.34
13	638.5	4.13	293.73
14	689.3	4.43	299.02
15	740.1	4.50	294.37
16	790.9	4.53	293.38
17	841.7	4.50	307.79
19	943.3	5.00	304.27
20	994.1	5.18	312.86
22	1,095.7	5.77	306.57
23	1,146.5	5.90	302.98
24	1,197.3	6.52	293.22
25	1,248.1	7.15	307.52
26	1,298.9	7.35	291.41
27	1,349.7	7.15	288.40
28	1,400.5	9.15	300.78
29	1,451.3	8.83	282.28
30	1,502.1	9.73	291.24
31	1,552.9	9.95	288.88
33	1,654.5	9.63	172.17

Table 5.27 Maximum and Peak Temperatures Summary in Test Two

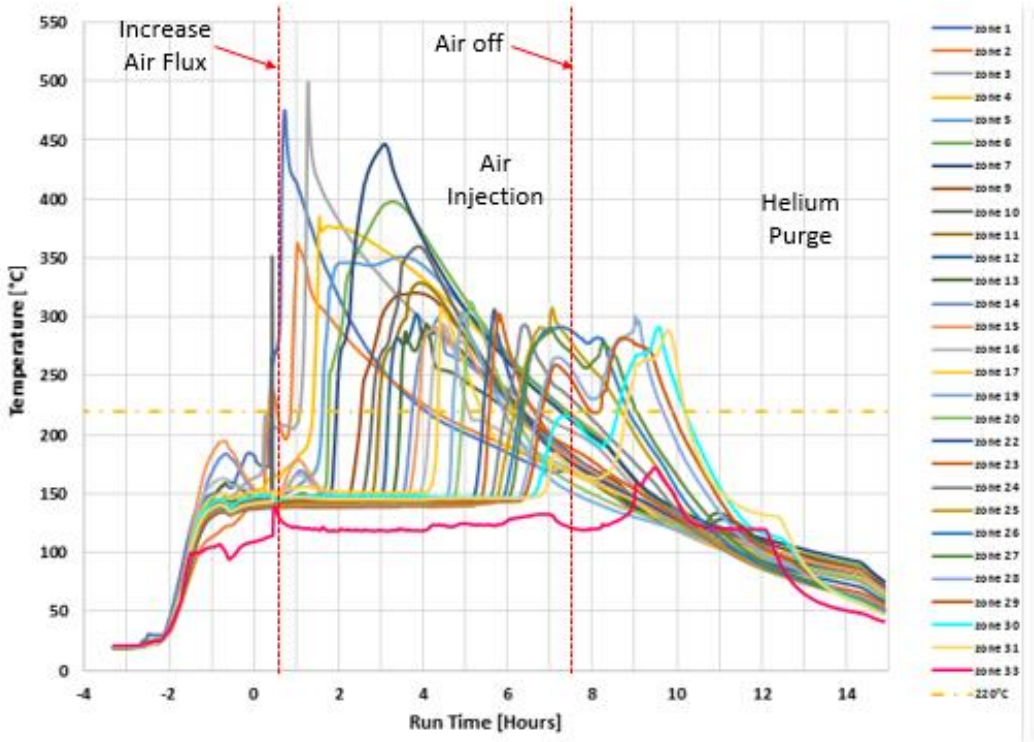

Figure 5.13 Center Line, Temperatures Profiles. Test Two

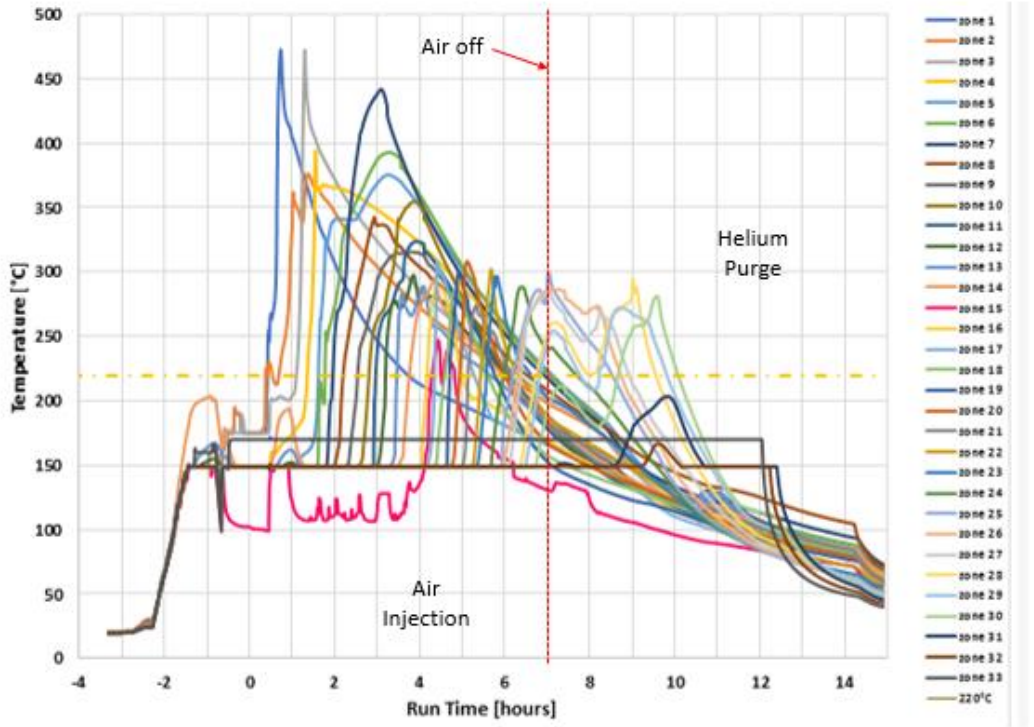

Figure 5.14 Wall Temperatures Profiles, Test Two.

In Figure 5.15, the combustion front velocity slope at 220°C (from the centerline thermocouples) is presented. The combustion front's velocity was 0.211 m/h, over the total air injection portion of the test, with a R^2 = 0.9852. The front velocity decreased after the helium purge was started (7.13 hours) but this observation is based on very limited data.

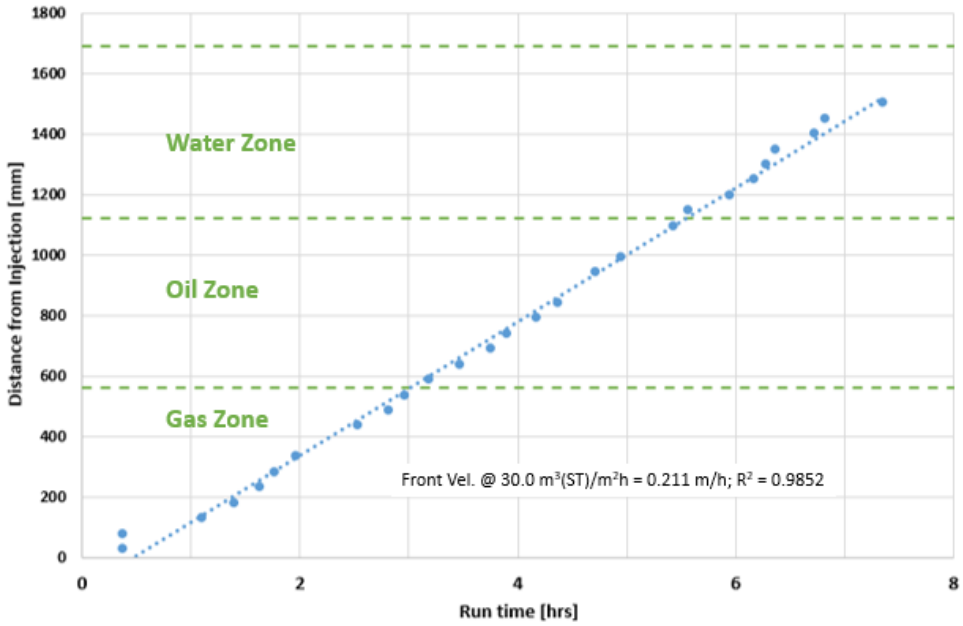

Figure 5.15 Velocity Plot of the 220°C. Test Two

5.4.4.2 Overall Run

Once the test started with the injection of methane, then air, the injection pressure increased and some liquid was produced. Then ignition occurred and the combustion front was generated. The combustion front started to push the liquids towards the production end and generated some combustion gases. All the produced liquids were collected for a post-test analysis. When the combustion gases were detected in the ILPC, the production fluids were sent to the main high-pressure separator and the gases were analyzed in real time by two Gas Chromatographs (GCs). In Table 5.28 the production gas compositions versus time are tabulated. The helium dilution reported in the right-hand column of Table 5.28 and Figure 5.16 corresponds to the percentage of the produced gas stream that was helium. Note from 0.0 to 0.64 hours run time, the gas flowing to the GCs was essentially 100% helium, which was injected downstream to pressurize the production system. No helium had entered the core by that time. Methane that was injected to pressurize the core broke through at about one hour run time. All the methane was produced in the first 5 hours of run time. Due to the methane flowing through the GC sample loop, no initial contamination of nitrogen and oxygen were detected, nitrogen was first detected at about one hour, starting to increase, while the methane decrease between one and two hours. At the final stages of the test, helium

was injected to purge the core and displace all the mobile hydrocarbons, air and product gases in the tube that remained after the air injection was shut down. During the HPAI run, light hydrocarbons were produced. This type of hydrocarbons may generate significant revenue if they are recovered.

The air used for the test was a synthetic air with an oxygen:nitrogen ratio of 23.00:77.00, Hence, the R value was 3.3478 (ratio of mole fraction N_2/mole fraction O_2 in the injected air). Nitrogen as an inert gas did not react during the combustion. In Figure 5.16 it can be seen that the product gas N_2 concentration was close to 80%. Nitrogen mass balance shows good agreements as seen by comparing Tables 5.29 and 5.28. Carbon dioxide has the quality to be miscible in light oils, due to this when CO_2 started to be produced at the beginning it was absorbed in the oil until the oil was approaching saturation, then CO_2 broke out and was produced and quantified. Water also carries dissolved CO_2, and significant changes in the produced gas CO_2 content can be seen if fluids are produced from the high-pressure trap at the same time that the GC samples the product gas.

Figure 5.16 shows a stable composition over time indicating that combustion was operating in the bond scission mode in the LTR as light oils do. It was also appreciated that the stable period during the produced combustion gases, was between 5.5 to 9.5 GC hours. Figure 5.17 graphically represents the composition of the produced light hydrocarbon gas against time.

The incremental and cumulative air injection during the test is summarized in Table 5.29 with respect the run time, as well as the air/fuel ratio and the apparent H/C ratio. An important thing to observe is in the incremental H/C ratio at some times are negative. This occurs during periods where more oxygen was produced as CO_x's than oxygen was injected. This behavior can be generated by: a) The oxidizing period last a while before going into a good combustion and bond scission period, or b) Due to the presence of dolomites, which could be reacting and forming CO_2 and c) Due to dissolved CO_2 being released from the produced fluids.

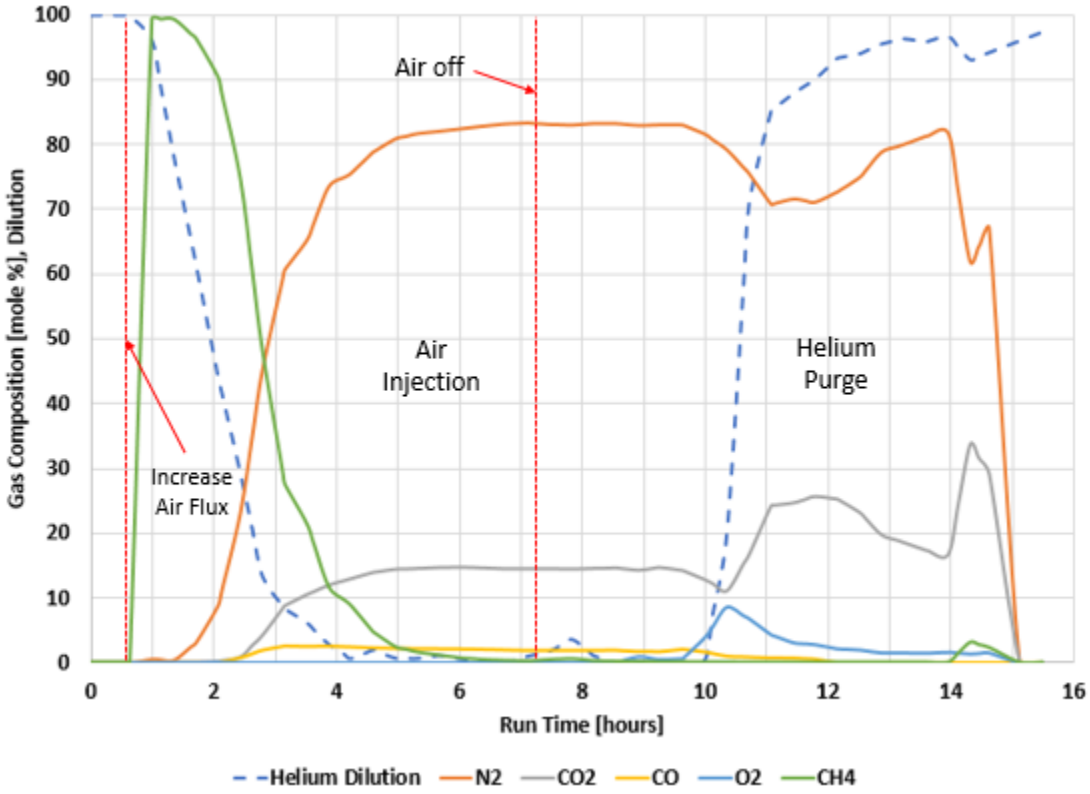

Figure 5.16 Produced Combustion Gas Composition. Test Two

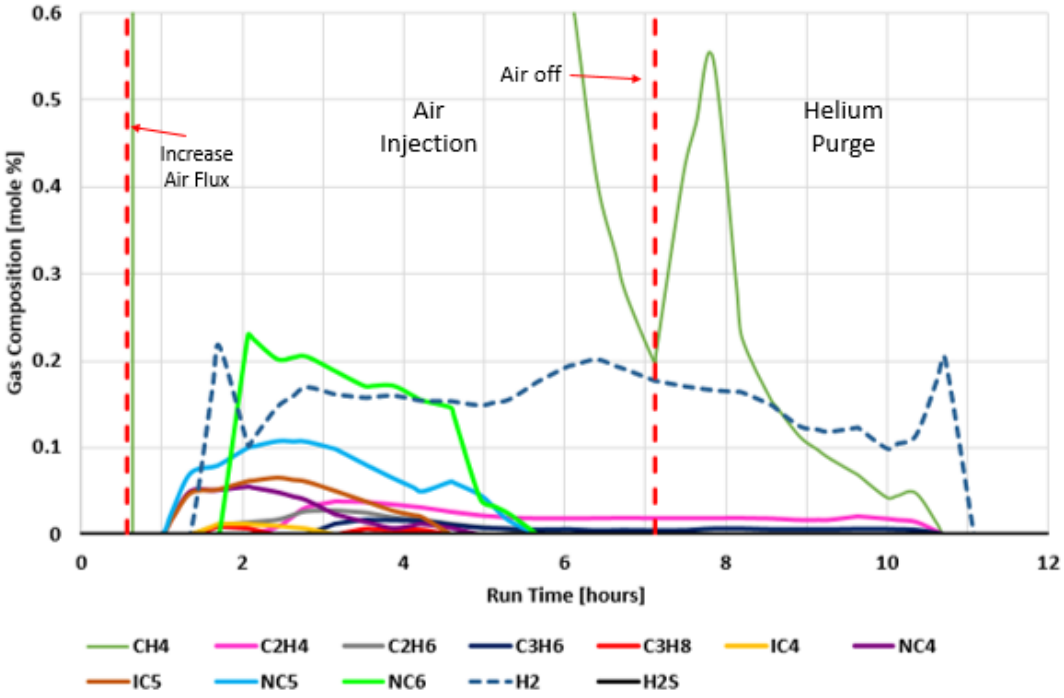

Figure 5.17 Produced Light Hydrocarbons Gas Combustion. Test Two

Table 5.28 Produced Gas Composition. Test Two

Runtime [hours]	Mole Percentage																He Dilution [%]
	N_2	O_2	CO	CO_2	CH_4	C_2H_4	C_2H_6	H_2S	C_3H_6	C_3H_8	iC_4	nC_4	iC_5	nC_5	nC_6	H_2	
-0.03	0.00	0.00	0.00	0.00	0.00	0.00	0.00	0.00	0.00	0.00	0.00	0.00	0.00	0.00	0.00	0.00	100.00
-0.02	0.00	0.00	0.00	0.00	0.00	0.00	0.00	0.00	0.00	0.00	0.00	0.00	0.00	0.00	0.00	0.00	100.00
0.00	0.00	0.00	0.00	0.00	0.00	0.00	0.00	0.00	0.00	0.00	0.00	0.00	0.00	0.00	0.00	0.00	100.00
0.02	0.00	0.00	0.00	0.00	0.00	0.00	0.00	0.00	0.00	0.00	0.00	0.00	0.00	0.00	0.00	0.00	100.00
0.13	0.00	0.00	0.00	0.00	0.00	0.00	0.00	0.00	0.00	0.00	0.00	0.00	0.00	0.00	0.00	0.00	100.00
0.28	0.00	0.00	0.00	0.00	0.00	0.00	0.00	0.00	0.00	0.00	0.00	0.00	0.00	0.00	0.00	0.00	100.00
0.37	0.00	0.00	0.00	0.00	0.00	0.00	0.00	0.00	0.00	0.00	0.00	0.00	0.00	0.00	0.00	0.00	100.00
0.38	0.00	0.00	0.00	0.00	0.00	0.00	0.00	0.00	0.00	0.00	0.00	0.00	0.00	0.00	0.00	0.00	100.00
0.40	0.00	0.00	0.00	0.00	0.00	0.00	0.00	0.00	0.00	0.00	0.00	0.00	0.00	0.00	0.00	0.00	100.00
0.55	0.00	0.00	0.00	0.00	0.00	0.00	0.00	0.00	0.00	0.00	0.00	0.00	0.00	0.00	0.00	0.00	100.00
0.57	0.00	0.00	0.00	0.00	0.00	0.00	0.00	0.00	0.00	0.00	0.00	0.00	0.00	0.00	0.00	0.00	100.00
0.58	0.00	0.00	0.00	0.00	0.00	0.00	0.00	0.00	0.00	0.00	0.00	0.00	0.00	0.00	0.00	0.00	100.00
0.64	0.00	0.00	0.00	0.00	0.00	0.00	0.00	0.00	0.00	0.00	0.00	0.00	0.00	0.00	0.00	0.00	99.93
1.00	0.64	0.00	0.00	0.00	99.36	0.00	0.00	0.00	0.00	0.00	0.00	0.00	0.00	0.00	0.00	0.00	96.18
1.13	0.58	0.00	0.00	0.01	99.34	0.00	0.00	0.00	0.00	0.00	0.00	0.02	0.02	0.03	0.00	0.00	89.29
1.36	0.49	0.00	0.00	0.03	99.31	0.00	0.00	0.00	0.00	0.00	0.00	0.05	0.05	0.07	0.00	0.00	78.14
1.63	2.57	0.00	0.00	0.05	97.01	0.00	0.01	0.00	0.00	0.01	0.01	0.05	0.05	0.08	0.00	0.17	65.29
1.72	3.19	0.00	0.00	0.05	96.32	0.00	0.01	0.00	0.00	0.01	0.01	0.05	0.05	0.08	0.00	0.22	61.45
2.08	8.93	0.07	0.00	0.12	90.30	0.00	0.01	0.00	0.00	0.01	0.01	0.06	0.06	0.10	0.23	0.10	44.08
2.13	11.16	0.07	0.12	0.22	87.84	0.00	0.01	0.00	0.00	0.01	0.01	0.05	0.06	0.10	0.23	0.11	41.75
2.44	23.13	0.06	0.74	0.79	74.67	0.01	0.02	0.00	0.00	0.00	0.01	0.05	0.07	0.11	0.20	0.15	29.35
2.63	34.92	0.05	1.33	2.58	60.48	0.02	0.02	0.00	0.00	0.00	0.01	0.04	0.06	0.11	0.20	0.16	20.76
2.80	45.18	0.04	1.85	4.15	48.13	0.03	0.03	0.00	0.00	0.00	0.01	0.04	0.06	0.11	0.20	0.17	13.38
3.13	59.45	0.03	2.43	8.35	29.13	0.04	0.03	0.00	0.01	0.00	0.00	0.02	0.05	0.10	0.19	0.16	8.78
3.16	60.62	0.03	2.48	8.70	27.58	0.04	0.03	0.00	0.01	0.00	0.00	0.02	0.05	0.10	0.19	0.16	8.41
3.52	65.17	0.03	2.41	10.41	21.42	0.04	0.03	0.00	0.02	0.01	0.00	0.01	0.04	0.08	0.17	0.16	6.25
3.63	67.77	0.03	2.42	10.87	18.36	0.04	0.02	0.00	0.02	0.01	0.00	0.01	0.04	0.08	0.17	0.16	5.20
3.88	73.47	0.03	2.45	11.90	11.64	0.04	0.02	0.00	0.02	0.01	0.00	0.01	0.03	0.07	0.17	0.16	2.90
4.13	74.92	0.04	2.37	12.59	9.61	0.03	0.02	0.00	0.02	0.01	0.00	0.01	0.02	0.05	0.16	0.16	1.36

Table 5.28 Produced Gas Composition. Test Two

Runtime [hours]	Mole Percentage																He Dilution [%]
	N_2	O_2	CO	CO_2	CH_4	C_2H_4	C_2H_6	H_2S	C_3H_6	C_3H_8	iC_4	nC_4	iC_5	nC_5	nC_6	H_2	
4.24	75.53	0.04	2.34	12.88	8.75	0.03	0.02	0.00	0.02	0.01	0.00	0.01	0.02	0.05	0.15	0.15	0.71
4.60	78.79	0.04	2.22	13.85	4.69	0.03	0.01	0.00	0.01	0.00	0.00	0.01	0.00	0.06	0.15	0.15	2.06
4.63	78.97	0.04	2.21	13.89	4.49	0.03	0.01	0.00	0.01	0.00	0.00	0.01	0.00	0.06	0.14	0.15	1.94
4.96	80.81	0.04	2.13	14.33	2.42	0.02	0.01	0.00	0.01	0.00	0.00	0.00	0.00	0.05	0.04	0.15	0.78
5.13	81.21	0.04	2.10	14.39	2.01	0.02	0.01	0.00	0.01	0.00	0.00	0.00	0.00	0.03	0.03	0.15	0.76
5.32	81.63	0.04	2.08	14.46	1.56	0.02	0.01	0.00	0.01	0.00	0.00	0.00	0.00	0.02	0.02	0.16	0.73
5.63	81.96	0.04	2.06	14.58	1.16	0.02	0.00	0.00	0.01	0.00	0.00	0.00	0.00	0.00	0.00	0.17	1.13
5.68	82.01	0.04	2.05	14.60	1.10	0.02	0.00	0.00	0.01	0.00	0.00	0.00	0.00	0.00	0.00	0.18	1.19
6.04	82.40	0.04	2.02	14.66	0.66	0.02	0.00	0.00	0.01	0.00	0.00	0.00	0.00	0.00	0.00	0.19	0.62
6.13	82.51	0.04	2.01	14.63	0.59	0.02	0.00	0.00	0.01	0.00	0.00	0.00	0.00	0.00	0.00	0.20	0.53
6.40	82.80	0.04	1.97	14.55	0.41	0.02	0.00	0.00	0.00	0.00	0.00	0.00	0.00	0.00	0.00	0.20	0.26
6.63	83.02	0.06	1.92	14.46	0.32	0.02	0.00	0.00	0.00	0.00	0.00	0.00	0.00	0.00	0.00	0.19	0.14
6.76	83.14	0.07	1.89	14.41	0.28	0.02	0.00	0.00	0.00	0.00	0.00	0.00	0.00	0.00	0.00	0.19	0.07
7.12	83.29	0.08	1.82	14.40	0.20	0.02	0.00	0.00	0.00	0.00	0.00	0.00	0.00	0.00	0.00	0.18	1.07
7.13	83.28	0.08	1.82	14.41	0.21	0.02	0.00	0.00	0.00	0.00	0.00	0.00	0.00	0.00	0.00	0.18	1.10
7.15	83.27	0.08	1.82	14.41	0.22	0.02	0.00	0.00	0.00	0.00	0.00	0.00	0.00	0.00	0.00	0.18	1.14
7.48	83.06	0.07	1.84	14.42	0.42	0.02	0.00	0.00	0.00	0.00	0.00	0.00	0.00	0.00	0.00	0.17	1.89
7.63	83.03	0.07	1.83	14.40	0.47	0.02	0.00	0.00	0.01	0.00	0.00	0.00	0.00	0.00	0.00	0.17	2.62
7.84	82.98	0.07	1.83	14.38	0.55	0.02	0.00	0.00	0.01	0.00	0.00	0.00	0.00	0.00	0.00	0.17	3.65
8.13	83.17	0.07	1.83	14.45	0.29	0.02	0.00	0.00	0.01	0.00	0.00	0.00	0.00	0.00	0.00	0.16	1.61
8.20	83.21	0.07	1.83	14.47	0.23	0.02	0.00	0.00	0.01	0.00	0.00	0.00	0.00	0.00	0.00	0.16	1.12
8.56	83.19	0.11	1.84	14.54	0.16	0.02	0.00	0.00	0.01	0.00	0.00	0.00	0.00	0.00	0.00	0.15	0.00
8.63	83.13	0.27	1.80	14.47	0.15	0.02	0.00	0.00	0.01	0.00	0.00	0.00	0.00	0.00	0.00	0.14	0.06
8.92	82.91	0.97	1.66	14.20	0.11	0.02	0.00	0.00	0.01	0.00	0.00	0.00	0.00	0.00	0.00	0.12	0.31
9.13	82.96	0.70	1.66	14.43	0.10	0.02	0.00	0.00	0.01	0.00	0.00	0.00	0.00	0.00	0.00	0.12	0.23
9.28	82.99	0.52	1.66	14.60	0.09	0.02	0.00	0.00	0.01	0.00	0.00	0.00	0.00	0.00	0.00	0.12	0.18
9.63	82.98	0.66	1.98	14.15	0.07	0.02	0.00	0.00	0.01	0.00	0.00	0.00	0.00	0.00	0.00	0.12	0.09
9.64	82.98	0.66	1.99	14.14	0.07	0.02	0.00	0.00	0.01	0.00	0.00	0.00	0.00	0.00	0.00	0.12	0.09
10.00	81.57	3.94	1.60	12.73	0.04	0.02	0.00	0.00	0.01	0.00	0.00	0.00	0.00	0.00	0.00	0.10	0.51

Table 5.28 Produced Gas Composition. Test Two

Runtime [hours]	Mole Percentage																He Dilution [%]
	N_2	O_2	CO	CO_2	CH_4	C_2H_4	C_2H_6	H_2S	C_3H_6	C_3H_8	iC_4	nC_4	iC_5	nC_5	nC_6	H_2	
10.13	80.69	5.65	1.37	12.11	0.04	0.02	0.00	0.00	0.01	0.00	0.00	0.00	0.00	0.00	0.00	0.10	7.61
10.36	79.15	8.68	0.97	11.02	0.05	0.02	0.00	0.00	0.00	0.00	0.00	0.00	0.00	0.00	0.00	0.11	20.16
10.63	76.41	7.33	0.88	15.19	0.01	0.00	0.00	0.00	0.00	0.00	0.00	0.00	0.00	0.00	0.00	0.18	58.21
10.72	75.50	6.88	0.85	16.57	0.00	0.00	0.00	0.00	0.00	0.00	0.00	0.00	0.00	0.00	0.00	0.20	70.85
11.08	70.74	4.37	0.74	24.15	0.00	0.00	0.00	0.00	0.00	0.00	0.00	0.00	0.00	0.00	0.00	0.00	85.28
11.13	70.86	4.20	0.73	24.21	0.00	0.00	0.00	0.00	0.00	0.00	0.00	0.00	0.00	0.00	0.00	0.00	85.64
11.44	71.56	3.15	0.70	24.58	0.00	0.00	0.00	0.00	0.00	0.00	0.00	0.00	0.00	0.00	0.00	0.00	87.91
11.63	71.31	2.98	0.60	25.10	0.00	0.00	0.00	0.00	0.00	0.00	0.00	0.00	0.00	0.00	0.00	0.00	89.10
11.80	71.09	2.83	0.52	25.56	0.00	0.00	0.00	0.00	0.00	0.00	0.00	0.00	0.00	0.00	0.00	0.00	90.18
12.13	72.53	2.23	0.04	25.19	0.00	0.00	0.00	0.00	0.00	0.00	0.00	0.00	0.00	0.00	0.00	0.00	93.12
12.16	72.67	2.18	0.00	25.15	0.00	0.00	0.00	0.00	0.00	0.00	0.00	0.00	0.00	0.00	0.00	0.00	93.39
12.52	74.90	2.00	0.00	23.10	0.00	0.00	0.00	0.00	0.00	0.00	0.00	0.00	0.00	0.00	0.00	0.00	94.07
12.63	76.09	1.87	0.00	22.05	0.00	0.00	0.00	0.00	0.00	0.00	0.00	0.00	0.00	0.00	0.00	0.00	94.53
12.88	78.81	1.56	0.00	19.63	0.00	0.00	0.00	0.00	0.00	0.00	0.00	0.00	0.00	0.00	0.00	0.00	95.58
13.13	79.62	1.56	0.00	18.82	0.00	0.00	0.00	0.00	0.00	0.00	0.00	0.00	0.00	0.00	0.00	0.00	96.13
13.24	79.98	1.56	0.00	18.46	0.00	0.00	0.00	0.00	0.00	0.00	0.00	0.00	0.00	0.00	0.00	0.00	96.37
13.60	81.23	1.50	0.00	17.26	0.00	0.00	0.00	0.00	0.00	0.00	0.00	0.00	0.00	0.00	0.00	0.00	95.91
13.63	81.28	1.52	0.00	17.21	0.00	0.00	0.00	0.00	0.00	0.00	0.00	0.00	0.00	0.00	0.00	0.00	95.97
13.96	81.78	1.65	0.00	16.57	0.00	0.00	0.00	0.00	0.00	0.00	0.00	0.00	0.00	0.00	0.00	0.00	96.70
14.13	72.46	1.53	0.00	24.56	1.45	0.00	0.00	0.00	0.00	0.00	0.00	0.00	0.00	0.00	0.00	0.00	95.03
14.32	61.90	1.40	0.00	33.60	3.10	0.00	0.00	0.00	0.00	0.00	0.00	0.00	0.00	0.00	0.00	0.00	93.12
14.45	64.05	1.46	0.00	31.72	2.76	0.00	0.00	0.00	0.00	0.00	0.00	0.00	0.00	0.00	0.00	0.00	93.59
14.47	64.33	1.47	0.00	31.48	2.72	0.00	0.00	0.00	0.00	0.00	0.00	0.00	0.00	0.00	0.00	0.00	93.65
14.48	64.61	1.48	0.00	31.23	2.68	0.00	0.00	0.00	0.00	0.00	0.00	0.00	0.00	0.00	0.00	0.00	93.71
14.63	67.07	1.55	0.00	29.09	2.29	0.00	0.00	0.00	0.00	0.00	0.00	0.00	0.00	0.00	0.00	0.00	94.25
15.13	0.00	0.00	0.00	0.00	0.00	0.00	0.00	0.00	0.00	0.00	0.00	0.00	0.00	0.00	0.00	0.00	96.07
15.50	0.00	0.00	0.00	0.00	0.00	0.00	0.00	0.00	0.00	0.00	0.00	0.00	0.00	0.00	0.00	0.00	97.42

Table 5.28 Produced Gas Composition. Test Two

Table 5.29 Incremental Fuel and Air Parameters. Test Two

Runtime	Air Injected		Air/Fuel		Apparent H/C		Cumulative Production for the Gases					
	Inc.	Cum.	Inc.	Cum.	Inc.	Cum.	N_2	CO_2	CO	O_2	H_2S	CH_4
hours	l(ST)/h	l(ST)	m^3/kg	m^3/kg			l(ST)	l(ST)	l(ST)	l(ST)	l(ST)	l(ST)
0.00	149.44	0.00	0.00	0.00	--	--	0.00	0.00	0.00	0.00	0.00	0.00
0.02	149.44	2.49	0.00	0.00	--	--	0.00	0.00	0.00	0.00	0.00	0.00
0.13	149.44	19.93	0.00	0.00	--	--	0.00	0.00	0.00	0.00	0.00	0.00
0.28	149.44	41.22	0.00	0.00	--	--	0.00	0.00	0.00	0.00	0.00	0.00
0.37	149.44	54.79	0.00	0.00	--	--	0.00	0.00	0.00	0.00	0.00	0.00
0.38	149.44	57.29	0.00	0.00	--	--	0.00	0.00	0.00	0.00	0.00	0.00
0.40	149.44	59.78	0.00	0.00	--	--	0.00	0.00	0.00	0.00	0.00	0.00
0.55	149.44	82.19	0.00	0.00	--	--	0.00	0.00	0.00	0.00	0.00	0.00
0.57	224.15	85.93	0.00	0.00	--	--	0.00	0.00	0.00	0.00	0.00	0.00
0.58	224.15	89.66	0.00	0.00	--	--	0.00	0.00	0.00	0.00	0.00	0.00
0.64	224.15	101.49	0.00	0.00	--	--	0.00	0.00	0.00	0.00	0.00	0.00
1.00	224.15	182.19	25.49	25.49	--	--	0.03	0.00	0.00	0.00	0.00	4.51
1.13	224.15	212.95	22.70	24.03	60.37	126.38	0.06	0.00	0.00	0.00	0.00	9.33
1.36	224.15	262.82	18.46	21.23	16.79	35.47	0.11	0.00	0.00	0.00	0.00	18.26
1.63	224.15	325.02	22.79	22.49	62.73	55.30	0.59	0.01	0.00	0.00	0.00	35.53
1.72	224.15	343.64	23.04	22.60	70.32	57.84	0.74	0.01	0.00	0.00	0.00	39.82
2.08	224.15	424.33	24.09	23.75	85.74	77.49	3.35	0.05	0.00	0.02	0.00	65.05
2.13	224.15	437.10	21.31	23.38	35.38	66.84	3.89	0.06	0.01	0.02	0.00	69.08
2.44	224.15	504.96	17.21	18.35	14.93	18.66	16.50	0.49	0.40	0.06	0.00	107.89
2.63	224.15	548.42	14.14	16.18	7.28	11.50	30.08	1.49	0.91	0.08	0.00	130.31
2.80	224.15	585.78	13.10	15.02	5.59	8.85	44.81	2.83	1.51	0.09	0.00	145.28
3.13	224.15	660.50	11.24	12.95	3.03	5.20	85.30	8.50	3.15	0.11	0.00	164.18
3.16	224.15	666.54	11.14	12.87	2.92	5.09	88.62	8.97	3.28	0.11	0.00	165.63
3.52	224.15	747.23	10.79	12.05	2.44	3.93	137.35	16.72	5.06	0.14	0.00	180.90
3.63	224.15	772.57	10.81	11.90	2.44	3.74	153.42	19.29	5.63	0.14	0.00	185.05
3.88	224.15	827.86	10.86	11.67	2.45	3.43	194.44	25.90	6.98	0.16	0.00	191.25
4.13	224.15	884.65	10.74	11.48	2.29	3.19	238.05	33.20	8.35	0.18	0.00	196.58
4.24	224.15	908.68	10.69	11.42	2.23	3.12	256.12	36.27	8.90	0.19	0.00	198.58

Table 5.29 Incremental Fuel and Air Parameters. Test Two

Runtime	Air Injected		Air/Fuel		Apparent H/C		Cumulative Production for the Gases					
	Inc.	Cum.	Inc.	Cum.	Inc.	Cum.	N_2	CO_2	CO	O_2	H_2S	CH_4
hours	l(ST)/h	l(ST)	m^3/kg	m^3/kg			l(ST)	l(ST)	l(ST)	l(ST)	l(ST)	l(ST)
4.60	224.15	989.31	10.64	11.26	2.13	2.90	318.38	47.16	10.63	0.22	0.00	202.12
4.63	224.15	996.72	10.64	11.25	2.13	2.88	324.13	48.17	10.79	0.23	0.00	202.43
4.96	224.15	1,070.01	10.66	11.15	2.12	2.75	387.02	59.28	12.43	0.26	0.00	204.22
5.13	224.15	1,108.80	10.68	11.11	2.13	2.69	420.47	65.18	13.28	0.27	0.00	205.01
5.32	224.15	1,150.76	10.70	11.08	2.14	2.65	450.84	70.54	14.04	0.29	0.00	205.56
5.63	224.15	1,220.87	10.69	11.04	2.12	2.60	501.56	79.53	15.30	0.31	0.00	206.24
5.68	224.15	1,231.58	10.68	11.03	2.12	2.59	509.63	80.96	15.50	0.31	0.00	206.35
6.04	224.15	1,312.34	10.71	11.00	2.14	2.54	571.13	91.85	17.00	0.35	0.00	206.81
6.13	224.15	1,332.95	10.73	10.99	2.16	2.53	586.86	94.63	17.37	0.35	0.00	206.92
6.40	224.15	1,393.03	10.80	10.98	2.22	2.50	635.60	103.15	18.52	0.38	0.00	207.15
6.63	224.15	1,445.02	10.88	10.97	2.28	2.49	677.93	110.50	19.49	0.41	0.00	207.31
6.76	224.15	1,473.85	10.92	10.97	2.31	2.48	702.13	114.67	20.03	0.43	0.00	207.38
7.12	224.15	1,554.11	10.97	10.97	2.34	2.47	768.92	126.17	21.48	0.49	0.00	207.54
7.13	0.00	1,554.11	10.97	10.97	2.34	2.47	771.40	126.60	21.53	0.50	0.00	207.54
7.15	0.00	1,554.11	10.97	10.97	2.33	2.47	774.43	127.12	21.60	0.50	0.00	207.55
7.48	0.00	1,554.11	10.94	10.97	2.31	2.46	789.18	129.67	21.92	0.51	0.00	207.62
7.63	0.00	1,554.11	10.94	10.97	2.32	2.46	795.87	130.83	22.06	0.52	0.00	207.66
7.84	0.00	1,554.11	10.95	10.97	2.33	2.46	803.16	132.09	22.22	0.52	0.00	207.70
8.13	0.00	1,554.11	10.94	10.97	2.31	2.46	813.49	133.87	22.45	0.53	0.00	207.74
8.20	0.00	1,554.11	10.93	10.97	2.31	2.46	820.97	135.17	22.61	0.54	0.00	207.76
8.56	0.00	1,554.11	10.91	10.96	2.27	2.45	859.69	141.91	23.46	0.59	0.00	207.83
8.63	0.00	1,554.11	10.98	10.96	2.26	2.45	867.21	143.21	23.62	0.61	0.00	207.84
8.92	0.00	1,554.11	11.27	10.98	2.21	2.44	918.92	152.03	24.64	1.22	0.00	207.91
9.13	0.00	1,554.11	11.13	10.99	2.19	2.43	956.42	158.52	25.38	1.54	0.00	207.95
9.28	0.00	1,554.11	11.03	10.99	2.18	2.42	978.00	162.31	25.81	1.67	0.00	207.97
9.63	0.00	1,554.11	11.08	10.99	2.23	2.41	1,028.54	170.89	27.00	2.07	0.00	208.01
9.64	0.00	1,554.11	11.08	10.99	2.23	2.41	1,030.14	171.16	27.04	2.09	0.00	208.01
10.00	0.00	1,554.11	12.53	11.06	1.92	2.39	1,088.18	180.18	28.16	4.89	0.00	208.04

Table 5.29 Incremental Fuel and Air Parameters. Test Two

Runtime	Air Injected		Air/Fuel		Apparent H/C		Cumulative Production for the Gases					
	Inc.	Cum.	Inc.	Cum.	Inc.	Cum.	N_2	CO_2	CO	O_2	H_2S	CH_4
hours	l(ST)/h	l(ST)	m^3/kg	m^3/kg			l(ST)	l(ST)	l(ST)	l(ST)	l(ST)	l(ST)
10.13	0.00	1,554.11	13.41	11.10	1.68	2.38	1,107.42	183.06	28.49	6.24	0.00	208.05
10.36	0.00	1,554.11	15.38	11.18	1.15	2.35	1,137.63	187.25	28.85	9.55	0.00	208.07
10.63	0.00	1,554.11	12.19	11.20	-0.03	2.31	1,155.55	190.79	29.06	11.27	0.00	208.07
10.72	0.00	1,554.11	11.37	11.20	-0.30	2.30	1,159.76	191.71	29.10	11.65	0.00	208.07
11.08	0.00	1,554.11	8.11	11.17	-1.25	2.25	1,167.78	194.44	29.19	12.15	0.00	208.07
11.13	0.00	1,554.11	8.09	11.16	-1.22	2.25	1,168.86	194.80	29.20	12.21	0.00	208.07
11.44	0.00	1,554.11	7.94	11.14	-1.06	2.22	1,173.58	196.42	29.24	12.42	0.00	208.07
11.63	0.00	1,554.11	7.81	11.13	-1.10	2.21	1,176.18	197.33	29.26	12.53	0.00	208.07
11.80	0.00	1,554.11	7.70	11.12	-1.14	2.20	1,178.46	198.15	29.28	12.62	0.00	208.07
12.13	0.00	1,554.11	7.96	11.11	-0.92	2.18	1,181.62	199.24	29.28	12.72	0.00	208.07
12.16	0.00	1,554.11	7.98	11.11	-0.90	2.18	1,181.85	199.32	29.28	12.72	0.00	208.07
12.52	0.00	1,554.11	8.63	11.11	-0.47	2.17	1,184.32	200.08	29.28	12.79	0.00	208.07
12.63	0.00	1,554.11	8.98	11.10	-0.21	2.17	1,185.02	200.28	29.28	12.81	0.00	208.07
12.88	0.00	1,554.11	9.87	11.10	0.48	2.17	1,186.56	200.66	29.28	12.84	0.00	208.07
13.13	0.00	1,554.11	10.20	11.10	0.72	2.17	1,187.92	200.98	29.28	12.86	0.00	208.07
13.24	0.00	1,554.11	10.35	11.10	0.84	2.17	1,188.34	201.08	29.28	12.87	0.00	208.07
13.60	0.00	1,554.11	10.87	11.10	1.27	2.16	1,189.89	201.41	29.28	12.90	0.00	208.07
13.63	0.00	1,554.11	10.89	11.10	1.29	2.16	1,190.02	201.43	29.28	12.90	0.00	208.07
13.96	0.00	1,554.11	11.21	11.10	1.50	2.16	1,191.36	201.70	29.28	12.93	0.00	208.07
14.13	0.00	1,554.11	8.03	11.10	-0.72	2.16	1,192.27	202.01	29.28	12.95	0.00	208.09
14.32	0.00	1,554.11	5.64	11.08	-1.97	2.14	1,194.71	203.33	29.28	13.00	0.00	208.21
14.45	0.00	1,554.11	6.06	11.06	-1.77	2.12	1,196.29	204.11	29.28	13.04	0.00	208.27
14.47	0.00	1,554.11	6.12	11.06	-1.75	2.12	1,196.44	204.19	29.28	13.04	0.00	208.28
14.48	0.00	1,554.11	6.18	11.06	-1.72	2.12	1,196.59	204.26	29.28	13.05	0.00	208.28
14.63	0.00	1,554.11	6.71	11.06	-1.46	2.12	1,196.66	204.29	29.28	13.05	0.00	208.28
15.13	0.00	1,554.11	0.00	11.06	0.00	2.12	1,196.66	204.29	29.28	13.05	0.00	208.28
15.50	0.00	1,554.11	0.00	11.06	0.00	2.12	1,196.66	204.29	29.28	13.05	0.00	208.28

Table 5.29 Incremental Fuel and Air Parameters. Test Two

The overall air and fuel calculations, as well as the volume balances for the major components are shown in Table 5.30 and 5.31.

Total Air Required	1,554 l(ST)
Measured Air Feed	1,554 l(ST)
Measured Oxygen Feed	357.4 l(ST)
Measured Nitrogen Feed	1,197 l(ST)
Total Volume of Produced Gas (He free)	1,655 l(ST)
Total Volume of Produced Gas (He included)	3,572 l(ST)
Air/Fuel Ratio	11.0 m^3(ST)/kg
O_2/Fuel Ratio	2.53 m^3(ST)/kg
Air Requirement*	160.57 m^3(ST)/m^3
Fuel Requirement*	14.52 kg/m^3
Apparent H/C	2.05
Oxygen Utilization	96.26%
(CO_2+CO)/CO Ratio	8.17
(CO_2+CO)/N_2 Ratio	0.20
Reacted Oxygen forming CO_x	64.68%
Total Oil Consumed as Fuel	143.19 g
Total Hydrocarbon's Gas Production**	152.67 g
Total Mass of Oil Produced as Gas**	295.86 g

*Based on a burned volume of 10.1 x 10^{-3} m^3 (76% of the CT)
**Contains the volume of CH_4 injected (131 g)

Table 5.30 Overall Air Fuel Calculations. Test Two

Component Production [l (ST)]	
O_2	13.34
N_2	1,196.66
CO	28.68
CO_2	207.19
CH_4	204.27*
C_2H_4	0.31
C_2H_6	0.13
C_3H_6	0.10
C_3H_8	0.02
C_{4+}	1.90
H_2	2.25
H_2S	0.00

*Includes Methane that was injected at the start of the test.
Table 5.31 Volume of Produced Gases. Test Two

Nitrogen oxidation was neglected because all the combustion performance was lower than 1,000°C. No H_2S was produced during the test. The stabilized air and fuel

requirement parameters were based on a tube cross sectional area of 7.472 x 10^{-3} m^2 and on an air injection flux of 30.0 m^3/m^2h.

5.4.4.3 Stabilized Combustion Period

The combustion performed in this test was a dry combustion (no water injection), same as Test One, therefore the combustion front velocity was based on the rate of advance downstream of a specific temperature at the leading edge of the high temperature region. The selected temperature is based on the range where oxidation/combustion reactions occur, which are primarily responsible for the oil mobilization. Usually for light oils, the peak temperatures are in the range of 300 to 400°C, but the temperature where the energy generation rate occurs is in the range of 200 to 280°C. The selected temperature to establish the location of the combustion front was 220°C, where the combustion reaction were occurring. In this test, one stable combustion front velocity was observed (see Figure 5.15).

Table 5.32 presents the stable product gas composition corresponding to the portion of the test where the combustion tube front propagation rate and the product gas composition were stable. As shown in Figure 5.16, the composition of the produced gas was stable during the period 5.5 to 9.5 GC hours. Table 5.33 provides the stabilized combustion parameters corresponding to the advance of the 220°C leading edge over the stable velocity period.

The combustion front velocity over the period of 1.1 to 6.2 run hours was 0.211 m/h, which for an average air flux of 30.0 m^3(ST)/m^2h translates to an air requirement of 136.09 m^3(ST)/m^3 of reservoir.

	Stabilized Zone
Air Flux [m^3(ST)/m^2•h], [scf/ft^2•h]	30.0
Time Interval by 220°C Front Velocity [hour]	1.1 to 6.2
Gas Chromatograph Interval [hour]	5.5 to 9.5
Component	**Stabilized Composition [mole percent]**
CO_2	14.46
CO	1.86
O_2	0.20
N_2	82.93
CH_4	0.37
C_2H_4	0.00
C_2H_6	0.01
C_3H_8	0.00
C_4+	0.00
H_2S	0.00
H_2	0.17

Table 5.32 Stable Product Gas Composition. Test Two

Combustion Front	220°C Leading Edge
Air Flux [m^3(ST)/m^2•h], [scf/ft^2•h]	30.0
Time Interval by Velocity [hour]	1.1 to 6.2
Gas Chromatograph Interval [hour]	5.5 to 9.5
Air Flux Location	Inlet
Air/Fuel Ratio [m^3(ST)/kg]	10.92
Combustion Front Velocity [m/h]	0.211
Air Required [m^3(ST)/m^3]	136.09
Fuel Required [kg/m^3]	12.46
Apparent Atomic H/C Ratio	2.25
Percent Oxygen Utilization	99.19
Percent Conversion of Reacted O_2 to Carbon Oxides	62.64
(CO_2 + CO)/CO Ratio	8.77
(CO_2 + CO)/N_2 Ratio	0.20
N_2/O_2 Ratio	3.35

Table 5.33 Summary of Stabilized Combustion Parameters. Test Two

5.4.4.4 Liquid Production History

During the entire test all the liquids produced were collected in sample bottles and stored for subsequent separation and analysis. The liquids separation process was to firstly remove the free water (due to gravity segregation) contained in the jars by pipetting, which was quantified and analyzed. The remaining oil and water were centrifuged at 10°C and 2,500 rpm for 15 to 30 minutes. The oil samples collected from the centrifugation were analyzed by Karl Fischer technique to ensure that no water remained in the produced oil. Once the liquids were completely separated, the masses were measured and tested for property analyses.

Table 5.34 summarizes the liquid production history. Figure 5.18 shows the cumulative water and oil productions during the test, as well as the location of the combustion front while those liquids were produced. Table 5.34 shows that 574 g of water and 424 g of oil (run time of 0.55 hours) were produced, in the ILPC. Air injection had commenced at the time this collection was isolated. The liquids produced to the ILPC were due to the methane injection to reach the gas saturation for the gas zone, and pressurization and pre-heating to reach the reservoir conditions (2,200 psig and 149°C). At the end of the test, followed the helium purge and de-pressuring, 1,213 g of oil and 1,405 g of water were produced. With this information it was calculated that 79.54% of the OOIP was recovered, noting that the volume swept by the 220°C front (combustion zone) was 76% of the core.

The core was de-pressured at 14.48 run hour, and the last liquids sample was collected and reported on Table 5.34 under the line for 14.55 run hour.

Figure 5.19 shows a period of reduced pressure in the core as evident by the saw tooth shaped pressure trace between 7.2 and 8.3 hours. The time of the initial drop in pressure corresponds to the switch from air injection to helium injection which happened at 7.13 hours run time. It is not believed that the switch in injection gas had anything to do with the pressure reduction other than it was at this time that the operators noted that liquid was entering the sight glass cell that is mounted just upstream of the produced gas back pressure valve. Liquid at this location indicated that the main production trap as well as the liquid carry over trap were close to full of liquid. The volume of the combined traps is 1.5 liters, and while it is not possible to exactly specify the volume of produced liquid that was actually in the combined traps, it was certainly enough to result in liquid carryover from the liquid carryover trap to the sight glass cell. After evaluating the liquid production history as presented in Table 5.34 and Figure 5.18, it is most probable that the liquid collected in the glass sample bottles at 7.13, 12.22 and 13.30 hours had been displaced from the combustion tube by 7.13 hours. This assumption is shown graphically in Figure 5.18 by the dashed lines.

The problem with draining the high-pressure collector was associated with the manual flow control valve that is in the line connecting the high-pressure separator with the low pressure separator. The valve was removed after completion of the test and no solids were found to be in the valve. Emulsions have been observed to cause a blockage problem and this is the best guess as to what happened on this test. It is noted that after the pressure was drawn down between 7.2 and 7.9 hours, the rate of withdrawn of fluids from the high to low pressure separator was controlled by the rate that the fluid could be withdrawn while maintaining gas flow through the back-pressure valve. This meant that the volume of the injected helium as measured at reservoir conditions had to exceed the rate of volume withdrawal of liquid from the trap.

Sample	Run time [hours]	Mass Oil [g]	Cum. Oil [g]	Mass H_2O Free [g]	Mass H_2O Emul. [g]	Total H_2O [g]	Cum. H_2O [g]
1	0.55	424.03	424.03	551.99	21.68	573.67	573.67
2	5.60	195.01	619.04	204.61	15.20	219.81	793.48
3	7.13	52.92	671.96	73.04	7.70	80.74	874.22
4	12.22	0.48	672.44	484.98	1.22	486.20	1,360.42
5	13.30	374.41	1,046.85	4.82	24.20	29.02	1,389.44
6	14.55	165.86	1,212.71	0.00	15.63	15.63	1,405.07
Lines	--	10.59	1,223.30	23.03	12.00	35.03	1,440.10

Table 5.34 Liquid Production History. Test Two

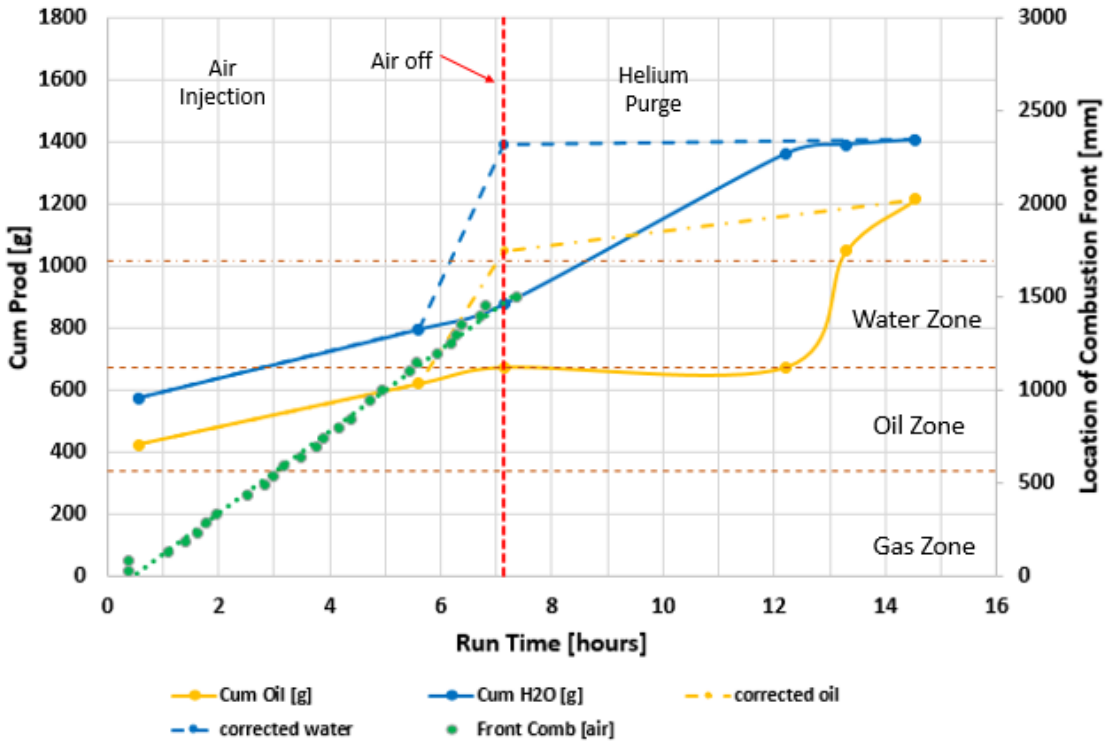

Figure 5.18 Cumulative Production Masses of Oil and Water and Location of Combustion Front. Test Two

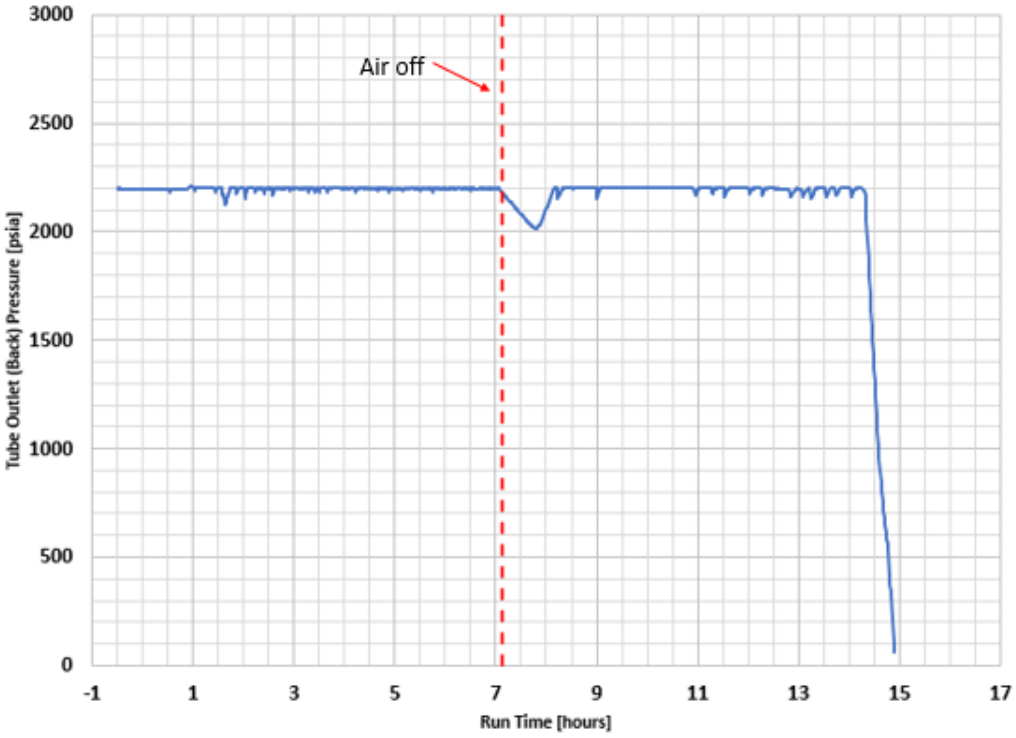

Figure 5.19 Combustion Tube Outlet Pressure. Test Two

5.4.4.5 Extraction and Analysis of Post-Test Core and Core Plugs

After the test, the combustion tube was unpacked, removing the core plugs and crushed core in segments, which were deposited in airtight bags for their analysis. Visual observation indicated that a length of about 0.80 meters (TC 18) covered by the combustion front during the air injection period (0.0 to 7.13 run time) was clean, while the rest of the length during the air injection and helium flood showed a slight oil content in the crushed core and core plugs. Table 5.35 shows a visual description of the post-burn core during the unpacking and Table 5.36 the core pack properties after the burn.

The methodology used to measure the fluid content in post-test cores was the same used and described for Test one, for more reference see section 5.3.4.5.

Figure 5.20 shows the percent of oil, water and coke remaining the Core Plugs and crushed core after the combustion test, taken from Table 5.36, as well as the maximum temperature registered by each center line thermocouple during the test (from Table 5.27).

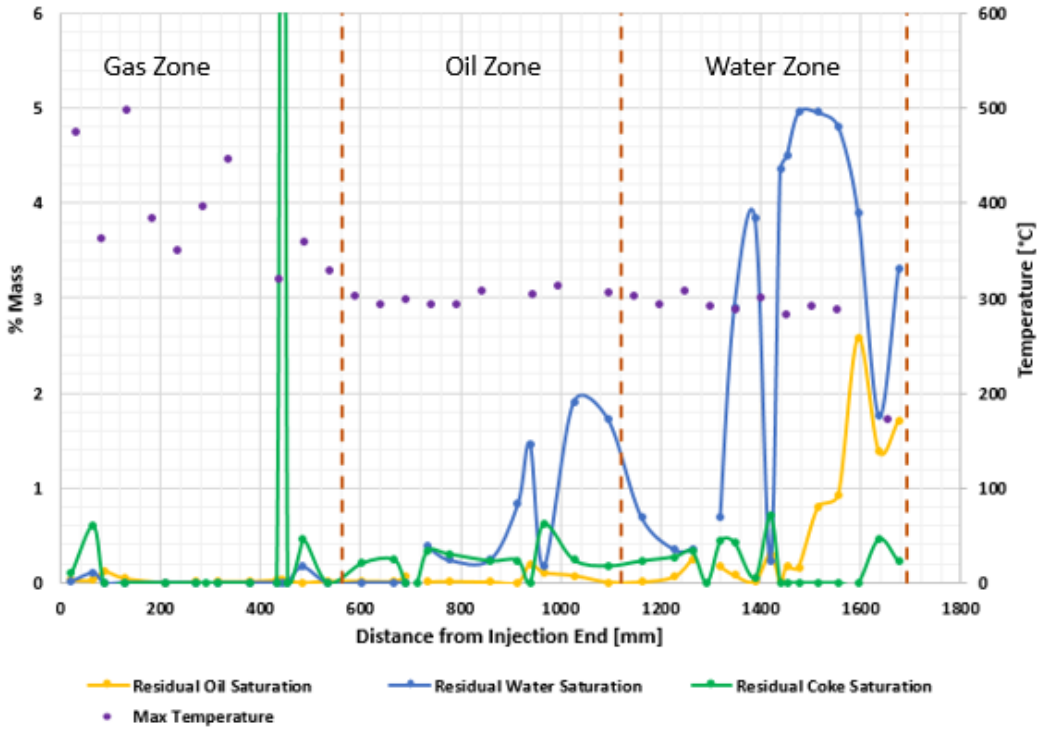

Figure 5.20 Residual Oil, Water and Coke in the Post Burn Core. Test Two

From the core samples collected and analyzed after the combustion test, it can be appreciated that the test was highly effective sweeping/pushing the hydrocarbons out of the crushed core and core plugs. The total amount of residual hydrocarbon in the post-test cores and plugs were 45 g and 37 g of coke, respectively from an original volume of 1,477 g, leading is to a successful test. The coke amount after the test is not precisely known for dolomite cores, due to the presence of brine can alter/modify the “mass loss on ignition” used to measure it. As per the discussion in Chapter 6, the blanks for the core plugs and crushed core were 23 and 22.5 mass percent, respectively.

Sample	Distance from Injection [mm]	Distance from Production [mm]	Description
16MFP-1	1,676.5	95	Oily damp frac sand with oil smell
20/30 MFP	1,637.0	139	Oily frac sand with transition to burn region
Core 1-1	1,595.5	178	Damp crushed core with oily smell
Core 1-2	1,556.0	218	Same as above
Core 2-1	1,516.0	258	Damp crushed core, less saturation, oil smell
Core 2-2	1,476.0	298	Same as above
Core 3-1	1,452.5	305	Bottom of Core Plug #16
Core 3-2	1,439.5	324	Crushed Core around Plug #16
Plug #16	1,420.0	344	Damp
Core 3-3	1,389.0	386	Crushed Core above the Plug #16. Clean burned channel
Core 4-1	1,347.5	427	Transition to dry burned sand
Core 4-2	1,319.5	442	Below Plug #13. Mostly dry Burned Core
Plug #13	1,293.0	480	Partially damp
Core 5-1	1,264.0	500	Crushed Core around Plug #13
Core 5-2	1,228.0	552	Clean Burned Core
Core 6	1,161.5	633	Damp clean core
Core 7	1,095.0	685	Noticeable damp
Core 8	1,026.5	770	As above
Plug #11	966.5	805	Burn Plug
Core 9-1	939.0	825	Crushed Core alongside Plug #11
Core 9-2	914.5	854	Transition to dap core to dry core
Core 10	859.0	936	Dry burned core
Core 11a	776.0	1,020	Same as above
Core 11b	734.0	1,020	Consolidated material stuck to the wall
Plug #10	712.0	1,064	Burn and dry Plug
Core 12-1	690.0	1,064	Crushed core around Plug #10
Core 12-2	666.5	1,111	Dry burned core
Core #13	603.5	1,190	Same as above
Core 14-1	534.0	1,250	Same as above
Plug #9	484.0	1,290	Burn and dry Plug
Core 14-2a	454.0	1,310	Crushed Core around the Plug #9
Core 14-2b	444.0	1,310	Consolidated crushed core around Plug #9
Core 14-3	432.0	1,334	Top of Core Plug #9
Core 15	379.0	1,416	Dry burned core
Core 16-1	314.5	1,463	Crushed core around Plug #7
Plug #7	291.0	1,463	Burn and dry Plug
Core 16-2	270.0	1,505	Crushed Core above Plug #7. Dry clean burn
Core 17	208.5	1,586	Dry burned core
Core 18a	127.5	1,667	Dry burned core
Core 18b	87.0	1,667	Consolidated crushed core
20/30mFrac	65.0	1,711	Mixed with some pack core
16mFrac	21.5	1,754	Dry frac sand

Table 5.35 Description of Post-Burn Core. Test Two

Table 5.36 Core Pack Properties after the Run. Test Two

Sample	Sample Number	Distance from Injection End Midpoint [mm]	Mass of Sample [g]	Mass Oil [%]	Mass Water [%]	Mass Coke [%]	Mass Oil [g]	Mass Water [g]	Mass Coke [g]
16MFP-1	1	1,676.50	393.64	1.707	3.318	0.222	6.720	13.062	0.874
20/30 MFP	2	1,637.00	496.20	1.382	1.762	0.462	6.855	8.741	2.292
Core 1-1	3	1,595.50	513.36	2.578	3.894	0.000	13.235	19.988	0.000
Core 1-2	4	1,556.00	565.45	0.928	4.811	0.000	5.246	27.206	0.000
Core 2-1	5	1,516.00	537.18	0.808	4.960	0.000	4.341	26.642	0.000
Core 2-2	6	1,476.00	518.56	0.164	4.961	0.000	0.853	25.728	0.000
Core 3-1	7	1,452.50	145.98	0.174	4.498	0.000	0.254	6.566	0.000
Core 3-2	8	1,439.50	343.50	0.012	4.353	0.000	0.040	14.954	0.000
Core Plug #16	9	1,420.00	186.87	0.305	0.224	0.703	0.571	0.419	1.314
Core 3-3	10	1,389.00	576.73	0.014	3.841	0.054	0.082	22.152	0.310
Core 4-1	11	1,347.50	558.88	0.079	2.901	0.429	0.443	16.212	2.397
Core 4-2	12	1,319.50	413.25	0.172	0.690	0.436	0.710	2.851	1.802
Core Plug #13	13	1,293.00	185.31	NT	NT	NT	NT	NT	NT
Core 5-1	14	1,264.00	369.10	0.256	0.351	0.328	0.945	1.297	1.212
Core 5-2	15	1,228.00	696.80	0.064	0.348	0.274	0.446	2.422	1.913
Core 6	16	1,161.50	984.55	0.008	0.695	0.230	0.079	6.838	2.264
Core 7	1	1,095.00	709.56	0.007	1.726	0.178	0.051	12.248	1.266
Core 8	2	1,026.50	974.28	0.078	1.911	0.242	0.758	18.618	2.356
Core Plug #11	3	966.50	183.75	0.110	0.168	0.619	0.202	0.309	1.137
Core 9-1	4	939.00	342.60	0.198	1.467	0.000	0.679	5.024	0.000
Core 9-2	5	914.50	709.51	0.005	0.828	0.238	0.034	5.874	1.686
Core 10	6	859.00	921.89	0.008	0.239	0.233	0.072	2.205	2.144
Core 11a	7	776.00	910.72	0.014	0.241	0.305	0.131	2.199	2.774
Core 11b	8	734.00	91.00	0.010	0.386	0.338	0.009	0.351	0.307

Sample	Sample Number	Distance from Injection End Midpoint [mm]	Mass of Sample [g]	Mass Oil [%]	Mass Water [%]	Mass Coke [%]	Mass Oil [g]	Mass Water [g]	Mass Coke [g]
Core Plug #10	9	712.00	187.79	NT	NT	NT	NT	NT	NT
Core 12-1	10	690.00	378.78	0.064	0.000	0.000	0.241	0.000	0.000
Core 12-2	11	666.50	692.24	0.017	0.000	0.248	0.117	0.000	1.715
Core 13	12	603.50	868.19	0.017	0.000	0.208	0.151	0.000	1.807
Core 14-1	13	534.00	953.35	0.018	0.000	0.000	0.174	0.000	0.000
Core Plug #9	14	484.00	186.75	0.000	0.169	0.457	0.001	0.315	0.853
Core 14-2a	15	454.00	494.13	0.024	0.000	0.000	0.119	0.000	0.000
Core 14-2b	16	444.00	15.50	0.038	0.000	26.393	0.006	0.000	4.091
Core 14-3	1	432.00	304.87	0.028	0.000	0.000	0.087	0.000	0.000
Core 15	2	379.00	1,083.46	0.014	0.000	0.000	0.156	0.000	0.000
Core 16-1	3	314.50	421.99	0.012	0.000	0.000	0.051	0.000	0.000
Core Plug #7	4	291.00	184.24	NT	NT	NT	NT	NT	NT
Core 16-2	5	270.00	494.35	0.010	0.000	0.000	0.049	0.000	0.000
Core 17	6	208.50	1,050.78	0.002	0.000	0.000	0.024	0.000	0.000
Core 18a	7	127.50	819.47	0.046	0.000	0.000	0.380	0.000	0.000
Core 18b	8	87.00	57.68	0.120	0.000	0.000	0.069	0.000	0.000
20/30mFrac	9	65.00	395.63	0.027	0.105	2.668	0.108	0.416	2.374
16mFrac	10	21.50	672.35	0.028	0.017	0.776	0.186	0.115	0.672
Total	**--**	**--**	**21,590.22**	**--**	**--**	**--**	**44.674**	**242.754**	**37.559**

NT- Not Tested Samples

Table 5.36 Core Pack Properties after the Run. Test Two

About the six core plugs, which were representing the matrix (low permeability) in the reservoir and were originally saturated with dead reservoir oil, it was observed that the first four (gas and oil zone) came out with a very low oil saturations, while the last two, located in the water zone, showed more signs of remaining oil saturation, because the core plugs were reached by the combustion front during the helium purge. When they were removed from the combustion tube, they were weighted, then the second core plug of each zone was cut approximately in half using a diamond saw with no fluid during the cutting process. In Appendix A, photo 7 shows some of the core plugs after the combustion tube´s unpacking process. Of the cores that were cut (Appendix A Photo 8), one half was crushed and measured for fluid contents. It was assumed and recorded that the measured fluids contents in each core plug was the same as in the mate portion of the core plug that was not cut nor analyzed. Table 5.37 summarized the initial and final content of fluids in the core plugs. As a reminder, air injection was shut down when the heading edge of the combustion zone reached Zone 26 (TC 26) located 1,295 mm from injection end, therefore the core plugs that were located above Zone/TC 26 came out quite clean showing a good oil swept. Figure 5.12, shows the schematic location of the core plugs. The core plugs located in the water zone were reached after air injection was shut down. From Table 5.27 it can be inferred that when maximum temperatures were around 300°C (high temperatures zones) the combustion front had a good performance displacing/removing the oil.

Core Plug	Mass of Oil [g]		Oil Displaced [mass %]	Max. Temp. [°C]	Oil Concentration in Adjacent Crushed Core [mass %]		
	Initial	Post-Test			Above	Beside	Below
#7	8.52	NT	--	446	0.010	0.012	0.014
#9	7.76	0.00	100	320	0.020	0.030	0.018
#10	7.60	NT	--	299	0.017	0.064	0.014
#11	8.26	0.20	97.58	312	0.005	0.198	0.078
#13	8.33	NT	---	307	0.064	0.256	0.172
#16	8.36	0.57	93.18	300	0.174	0.012	0.014

NT – Not Tested Sample

Table 5.37 Summary of Oil Displacement in Core Plugs at Test Two

5.4.4.6 Material Balance

All fluids going in and out of the system were measured in a way to keep a material balance. Table 5.38 presents a summary of the fluids injected and produced during the run. The mass of water generated during combustion was calculated from the computed hydrogen consumption, and water produced as vapor was based on the assumption that the product gas was saturated with water at 0°C (the cold trap temperature).

Oil Balance	[g]
Initial Oil in System	1,524.6
Oil Produced as liquid	1,212.7
Oil Produced as gas	142.6
Fuel Produced as gas	155.7
Residual Hydrocarbon in pack	90.9
Total Produced	1,601.9
Difference	-77.3
Percent error	-5.0
Water Balance	**[g]**
Initial Water in System	1,575.3
Water injected	0.0
Water generated by Combustion	140.3
Total In	1,715.6
Water Produced as liquid	1,405.1
Water Produced as gas	18.9
Residual Water in Pack	241.7
Difference	50
Percent Error	2.9

Table 5.38 Liquid Mass Balance. Test Two

The density, viscosity and asphaltenes (C_{5+} which are soluble in toluene and pentane) properties in the original oil and the oil samples collected during production are shown in Table 5.39. An elemental analysis of the oil collected in the individual samples, including carbon, hydrogen, nitrogen and sulfur (CHNS) are shown in Table 5.40. Table 5.41 presents the water properties of the produced water.

Sample	Time [hours]	Viscosity 25°C [cp (mPa•s)]	Density 25°C [g/cm^3]	Asphaltenes Mass %
Original Oil	--	4.14	0.82	0.01
Produced Oil				
1	0.55	4.55	0.84	0.45
2	5.60	2.27	0.81	0.24
3	7.13	4.42	0.84	0.31
4	12.22	IS	IS	IS
5	13.30	4.14	0.84	0.32
6	14.55	4.17	0.84	0.28

*IS – Insufficient sample to conduct the analysis

Table 5.39 Oil Properties Pre and Post Burn. Test Two

Sample	Time [hours]	Mass Percent				H/C ratio (mol/mol)
		Carbon	Hydrogen	Nitrogen	Sulfur	
Original Oil		85.61	13.66	0.05	0.55	1.9015
Produced Oil						
1	0.55	86.09	13.44	0.03	0.55	1.8604
2	5.60	85.48	13.72	0.02	0.42	1.9127
3	7.13	86.04	13.33	0.02	0.43	1.8463
4	12.22	IS	IS	IS	IS	IS
5	13.30	85.78	13.35	0.01	0.53	1.8546
6	14.55	85.40	13.26	0.02	0.55	1.8503

*IS – Insufficient sample to conduct the analysis

Table 5.40 CHNS of Oil Samples. Test Two

Sample	Time [hours]	pH	CO_3^{2-} (mg/L)	HCO^{3-} (mg/L)	Cl^- (mg/L)	SO_4^{2-} (mg/L)	Total solids (mg/L)	Ca^{2+} (mg/L)	Fe^{3+} (mg/L)	Mg^{2+} (mg/L)	K^+ (mg/L)	Na^+ (mg/L)
Original Water		7.34	0.00	92	42,552	40	72,900	6,100	<3.0	750	<15	19,000
Produced Water												
1	0.55	5.95	0.00	15	39,006	51	92,000	5,000	1.6	1,000	8.5	16,000
2	5.60	6.51	0.00	218	33,687	61	93,900	5,200	1.6	960	12	17,000
3	7.13	7.05	0.00	183	28,368	78	87,500	5,200	<1.2	760	15	12,000
4	12.22	4.24	0.00	442	28,368	240	85,900	4,500	8.4	780	31	13,000
5	13.30	4.05	IS	IS	17,730	IS	19,500	IS	IS	IS	IS	IS
6	14.55	NS	NS	NS	IS	NS	NS	NS	NS	NS	NS	NS

*NS – No sample was produced

Table 5.41 Produced Water Analysis. Test Two

CHAPTER 6

RESULTS AND DISCUSSION

6.1 TEST ONE VS. TEST TWO

6.1.1 Tube Packing and Flooding

The main difference between the two combustion tube experiments was the size and the number of core plugs used and the initial fluid saturations. Test One used seven core plugs of different sizes and the CT was saturated as a restored state crushed core with oil and brine (liquids), hence no gas saturation, while Test Two used six core plugs of the same size and the crushed core was pre-mixed to have three distinct saturation zones (representing gas cap, oil interval and aquifer). Table 6.1, Table 6.2 and Figure 6.1, summarize the characteristics and conditions for both CT tests prior to the experiment.

Core Plug No.	Length [inches]	Outer Diameter [inches]	Volume [cm^3]	Porosity [%]	Permeability [mD]	Test Number
#1 - #3	1.5	2	77.22	13.1	--	1
#4	1.5	3	154.44	12.8		1 *
#5	1.5	0.7	9.46	10.8		1
#6	3	2	154.44	13.1		1
#7a	1.5	2	77.22	11.8		1
#7	1.5	2	77.22	13.1	262	2
#9					284	2
#10					280	2
#11					312	2
#13					270	2
#16					287	2

* this core plug has a center hole of 1” diameter x 1.5” length. The volume is without the center hole.

Table 6.1 Characteristics of the Core Plugs Used in Test One and Two

Packed Masses [g]	Test One	Test Two
Crushed Core	18,216.1	18,301.2
Frac Sand	2,000.0	1,858.1
Core Plugs	1,504.5	1,110.4

Overall Saturations in Crushed Core [%]	Test One	Test Two
Oil	67.3	35.1
Brine	32.7	29.6
Gas	0.0	35.3

Mass of Liquid [g]	Test One	Test Two
Oil in Crushed Core	2,740.9	1,476.8
Brine in Crushed Core	1,704.5	1,575.3
Oil in Core Plugs	70.3	47.8
Oil in Lines	25.9	0.0
Water in Lines	0.0	0.0
Oil in Total System	2,837.1	1,524.6
Brine in Total System	1,704.5	1,575.3
Calculated Porosity of the Crushed Core Pack [%]	41.6	41.8
Crushed Core Pore Volume [cm^3]	5,013	5,103.4

Saturations for Each Zone in Test Two [%]	Gas Zone	Oil Zone	Water zone
Gas	82.5	12.6	11.5
Oil	17.5	82.9	4.2
Water	0.0	4.5	84.3
Pore Volume [cm^3]	1,694	1,712	1,697

Table 6.2 Masses and Saturations after Packing and Flooding the CT for Test One and Two

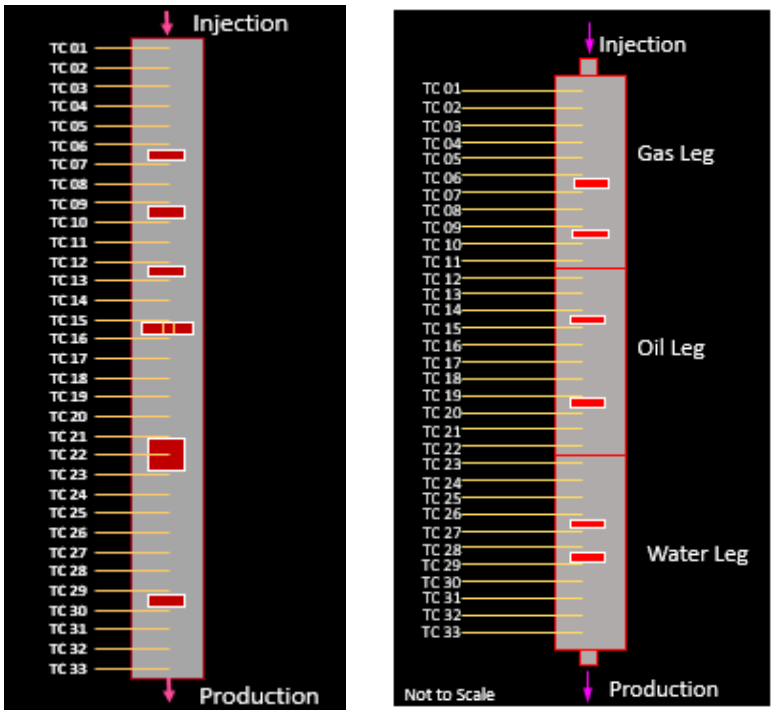

Test One Test Two

Figure 6.1 Schematic Drawing of the Combustion Tube with the TC and Location of the Embedded Core Plugs (Not to Scale)

6.1.2 Combustion Test

Both tests were performed at reservoir conditions: 15.26 MPa pressure (2,213 psia) and pre-heat to the initial reservoir temperature of 149°C. For Test one the operating pressure was reached through dead oil injection and heating expansion. For Test two the pressure was established through methane injection and heating expansion. Table 6.3 shows a summary for the principal characteristics for both tests.

Parameter [units]	Test One	Test Two
Helium in Production System Following Pressure Up [liters (ST)]	219.9	219.9
Time of Air Injection [run hours]	0.0	0.0
Time of Helium Injection (Purge) [run hours]	5.83	7.13
Methane Injected [liters (ST)]	0.0	186.18
Oxygen Injected [liters (ST)]	284.4	357.45
Nitrogen Injected [liters (ST)]	1,019.3	1,196.66
Helium Injected (Purge) [liters (ST)]	1,987.5	1,647.51
Helium Injected to Production System [liters (ST)]	302.9	164.00
Total Volume of Injected Gas [liters (ST)]	3,814.0	3,771.70
Total Volume of Produced Gas [liters (ST)]	3,539.8	3,571.88
Volume Out – Volume In [liters (ST)]	-274.2	-199.82

Table 6.3 Summary of Injected and Produced Gases for Test One and Two

6.1.3 Results

6.1.3.1 Temperature Profiles and Overall Run

Both tests were positioned vertically with the injection end at the top. At the start of the tests, after reaching the reservoir conditions, zones one to three were consider “ignition zones”, which were heated up to 175°C with the objective of generating the ignition. During both tests the temperatures at the centerline were recorded. The centerline temperatures against the location of the TCs are shown in Figure 6.2. At 220°C a horizontal line is drawn, which is the temperature where the front velocity was calculated. For both tests air injection was terminated when the combustion front reached TC 26.

The maximum temperature for the first TC during Test one was just over 500°C, while for Test two just one TC registered 500°C, being the highest (Figure 6.2). For Test two, the effect of the zone temperature rising to a “Maximum Temperature” after the “Peak Temperature” occurred is barely seen. What is believed to be the cause of this behavior that there is no water and a low oil saturation in the gas zone and the initial gas saturation associated with the pre-mixed core in Test two. Due to of the absence of connate water, there was no steam formation associated with the vaporization of connate water in this zone. Because of its low molecular weight, steam is believed to be the cause of the development of a convective roll cell which transfers vapor fuel to the upstream zones. From Figure 6.2 for Test two at 7.13 run hours (when the injection gas change from air to helium), the temperatures profiles show that Zones/TCs 28, 29, 30 and 31 exhibited decreasing followed by increasing temperatures. These four zones were exhibiting

leading edge temperatures that were increasing towards their peak temperatures at the time that air injection was switched to helium. As explained previously, a problem with drawing liquid production from the high-pressure trap was identified and the remedial actions applied to address this problem dropped the pressure within the production system and caused the back-pressure valve controlling product gas flow from the production system to restrict the flow of product gas. Primarily liquid was withdrawn from the high-pressure trap until about 8.6 hours (see pressure profile in Figure 5.19), when gas was again continuously produced. It is the re-establishment of gas flow out of the core that was responsible for the temperatures in Zones/TCs 28 to 31 to ultimately increase and exhibit peak temperatures similar to those in Zones/TCs 12 to 27. It is noted that the same behavior was observed during Test one, when the liquid sample corresponding to the end of air injection was withdrawn. In the case of Test one, the gas flow upset was for a much shorter duration.

It should be noted during Test two that while the peak temperatures in zones/TCs 10 to 31 are typical of those associated with a propagating steam bank during a wet combustion process, the thermal wave at a given zone only exists for a short duration. The shape of the thermal wave at Zones/TCs 10 to 31 have a similar shape to the heat wave during many dry combustion tests except for the low levels of the peak temperatures.

During Test two, the TCs in zones 10 to 31 achieved peak temperatures that were in the range of 300°C, hence, as stated previously, the heat wave in those zones are more typical of the temperatures within the steam bank of a wet combustion test conducted at the pressure of Tests one and two. For both Tests one and two, the peak temperatures were controlled by the energy generation rate and the partial pressure of water in the flowing gas phase. It is noted that the saturation temperature of pure water at an absolute pressure of 2,213 psia is 343.5°C. The peak temperature in what appears as the steam bank is approximately 300°C at which the partial pressure of the water vapor is 1,246 psia, hence assuming ideal gas behavior and Dalton's law, the mole fraction water in the vapor (flowing gas) phase is 1,246 psia/2,213 psia x 100 or 56 mole percent. The presence of this concentration of steam in the vapor phase and the resulting reduction in the oxygen partial pressure will reduce the rate of oxygen uptake at the leading edge of the combustion zone.

The combustion process examined in both tests was dry combustion (no water injection), therefore the combustion front velocity was based on the rate of advance downstream of a specific temperature at the leading edge of the elevated temperature region. The selected temperature is based on the range where oxidation/combustion reactions occur, which are primarily responsible for the oil mobilization. Usually for light oils, the peak temperatures may fall in the range of 300 to 400°C, but the temperature in the LTR where the maximum energy generation rate occurs is in the range of 200 to 280°C (*i.e.* in the LTR). This is the reason that the selected temperature to establish the location of the combustion front was selected as 220°C.

When the combustion front velocity plot (Figure 6.3) is analyzed, it is appreciated that for Test one the combustion front velocity changes around 3.9 hours, from 0.283 to

0.124 m/h. This change in the combustion front velocity occurred prior to the switch from air to helium, so this velocity change is not related to the changeover in the injection gas. Figure 6.3 shows that for Test two a constant velocity of 0.211 m/h was observed during the air injection period. Therefore, the combustion front velocity for Test two did not vary to a significant extent as the front moved through the gas, oil and water zones.

Figure 6.4 shows for Test one that the change in the combustion front velocity occurred at the time (3.9 hours) when the light hydrocarbons concentration approached zero and the peak temperatures fell into the LTR. Figure 6.2 shows for Test one that TCs one to five and seven exhibited peak temperatures in excess of 350°C while TCs three to ten exhibited maximum temperatures between 400 and 530°C. It was not until 3.67 hours when the leading edge showed a peak temperature of 299°C that the residual energy generation up stream of the leading edge was no longer sufficient to sustain a temperature rise after the peak temperature occurred. It is noted again that 3.9 hours is when the front velocity decreased for Test one.

Figure 6.4 shows that hydrogen and C_{4+} continued to be produced over the total gas injection periods for both Tests one and two. Note also that plots at Figure 6.4 have different gas composition scales.

Figure 6.5 shows the combustion gases and nitrogen produced for both tests. The amount of CH_4 for Test one was produced in response of the combustion reactions, while for Test two, CH_4 was produced as a result of the oxidation and cracking reactions in addition to the CH_4 injected during the pressure up. Methane does not appear to react to a significant extent, which means that the majority of the injected CH_4 was produced. The assumption made about methane not being consumed to a significant extent is due to its ignition point. Theoretically it is 540°C, but in experiments made by Robinson et al. (1984) no values with firm verification of ignition were below 600°C. When reviewing Figure 6.5, note that helium associated with the helium purge broke through at 8 run hours for Test one and 10 run hours for Test two.

It is also noted from Figure 6.5 that the nitrogen response is different for both tests. For Test one, it started to be measured at GC time zero as 100% and then decreasing to around 80% by 3 GC hours. While for Test two, nitrogen was not detected until after 1.5 GC hours and reached 80% around 5 GC hours. This different behavior was due to the fluids used to pressure up, for Test One dead oil was used, while for Test Two methane was injected for pressure up so it broke through first followed by the nitrogen contained in the air.

Due to the differences in the average combustion front velocities, which for Test two was slower, the times when air was turned off were 5.83 run hours for Test one and 7.13 run hours for Test two. Based on these times the inverse combustion front velocities for the two tests are in the range of 7.13/5.83 or 1.34.

The overall air and fuel calculations, as well as the volume balances for the major components are shown in Table 6.4 and 6.5. From these tables it is appreciated that the overall air and fuel requirements were higher for Test two compared to Test one, and this is reflected in the time that air was injected for the two tests. The overall air/fuel

ratios were similar, but the overall apparent H/C ratio was higher for test two than test one. Both tests exhibited good combustion based on the $(CO_2+CO)/N_2$ ratio, being greater than 0.20. Based on the $(CO_2+CO)/N_2$ ratio it can be stated that both tests exhibited a high level of conversion of reacted oxygen to carbon oxides. The overall $(CO_2+CO)/CO$ ratios for both tests are high when compared to a “rule of thumb” value of 4 for heavy oil, low pressure tests. But they are comparable to other dry light oil combustion tests reported by Mehta et. al (2018).

Figure 6.6 shows the cumulative injected and produced gas volumes. From this plot it is appreciated that even though both tests had different combustion front velocities, the overall gas injected and produced, showed similar trends. Note the reduction in gas production rate for Test two at 7.2 hours which was due to the problem with liquid withdraw from the High-Pressure Separator (HPS) as described in Chapter 5.

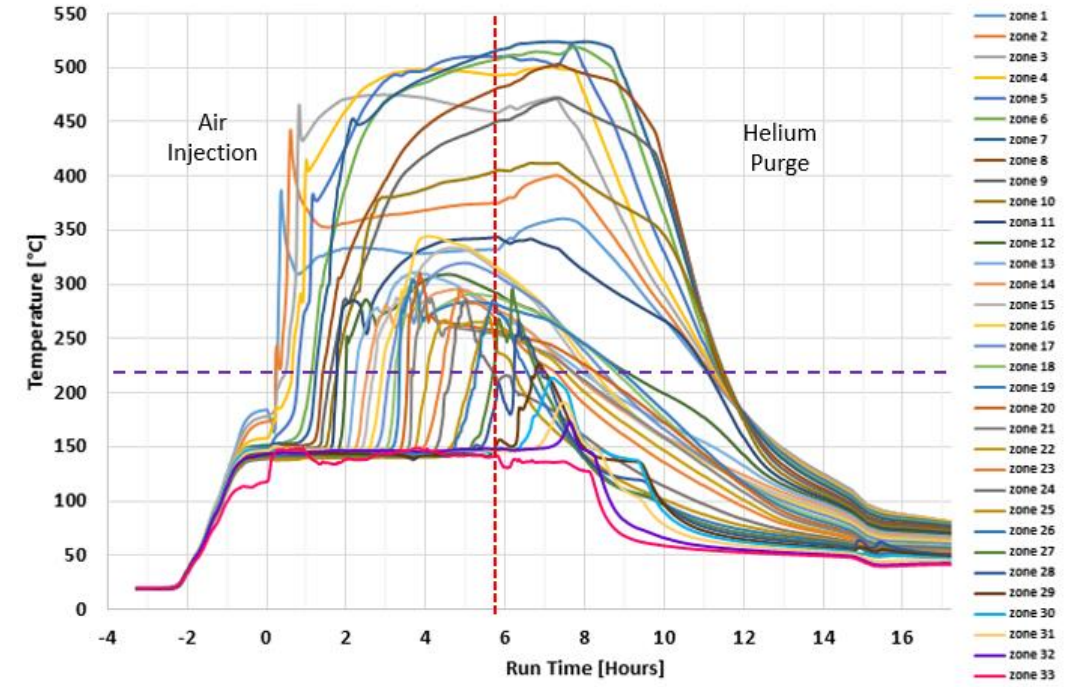

Test One

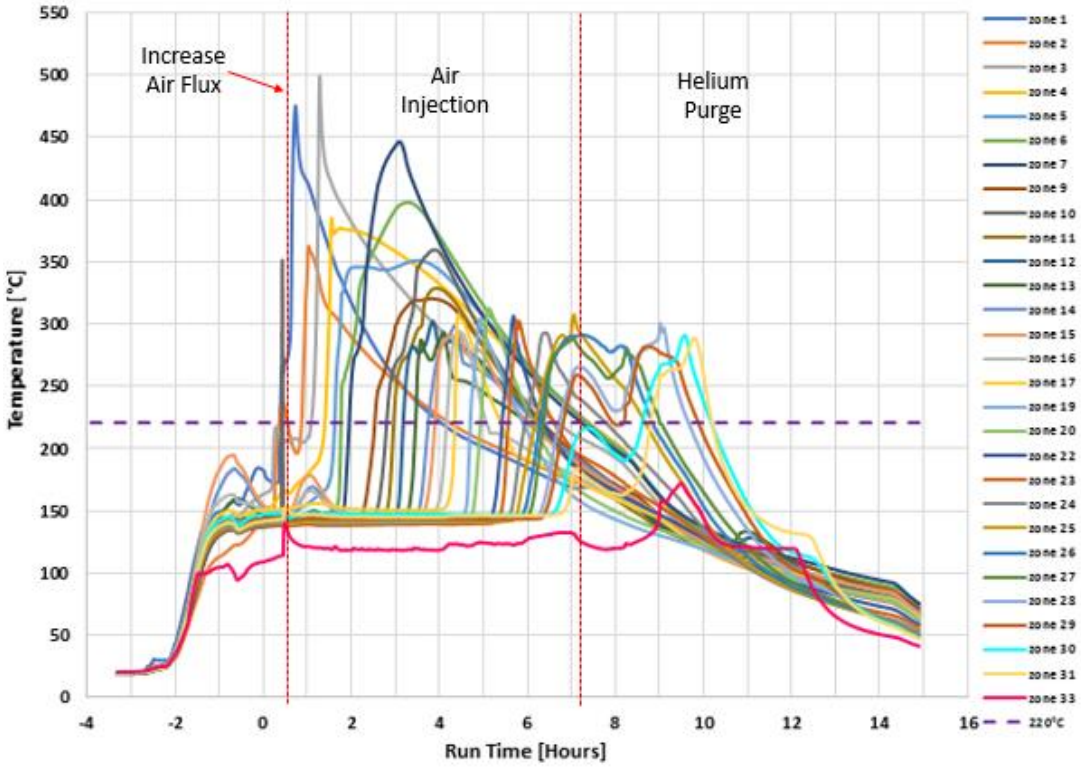

Test Two

Figure 6.2 Centerline, Temperatures Profiles for Test One and Two

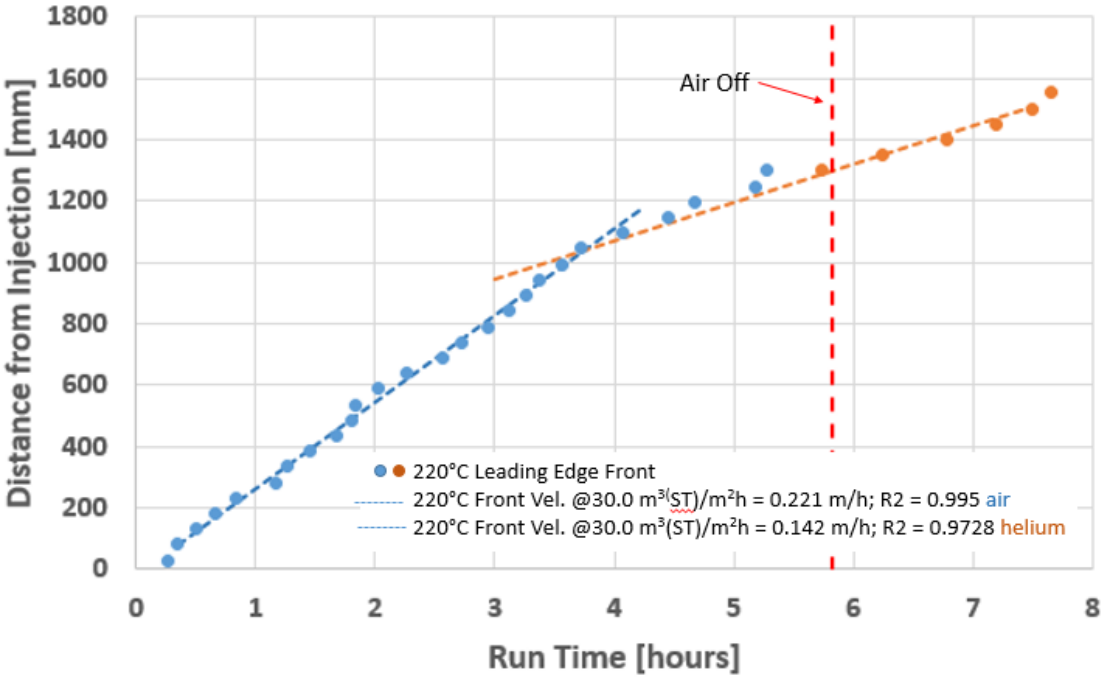

Test One

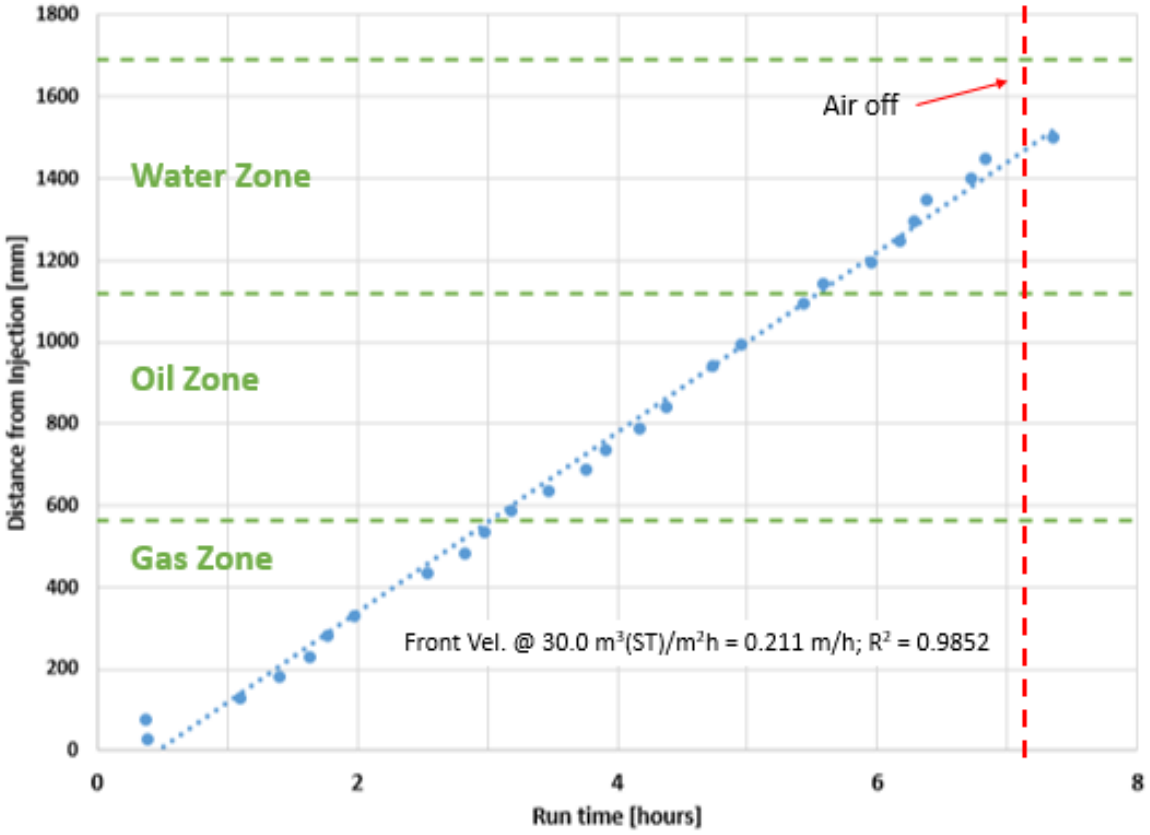

Test Two

Figure 6.3 Velocity Plot of the 220°C

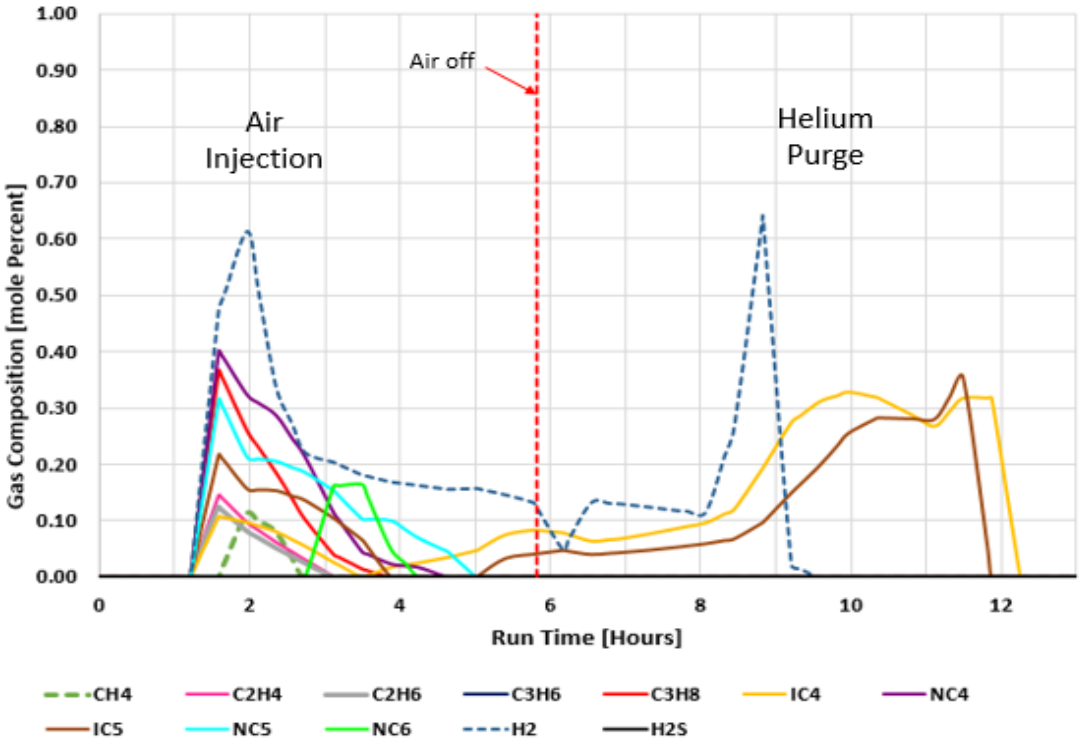

Test One

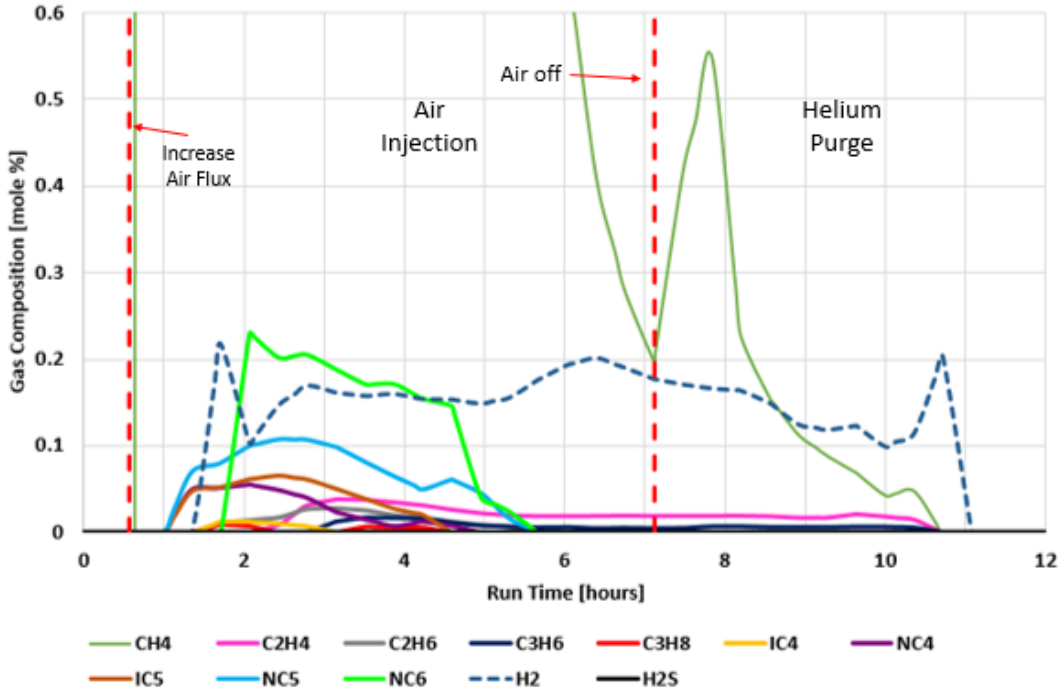

Test Two

Figure 6.4 Produced Light Hydrocarbons Gas Combustion.

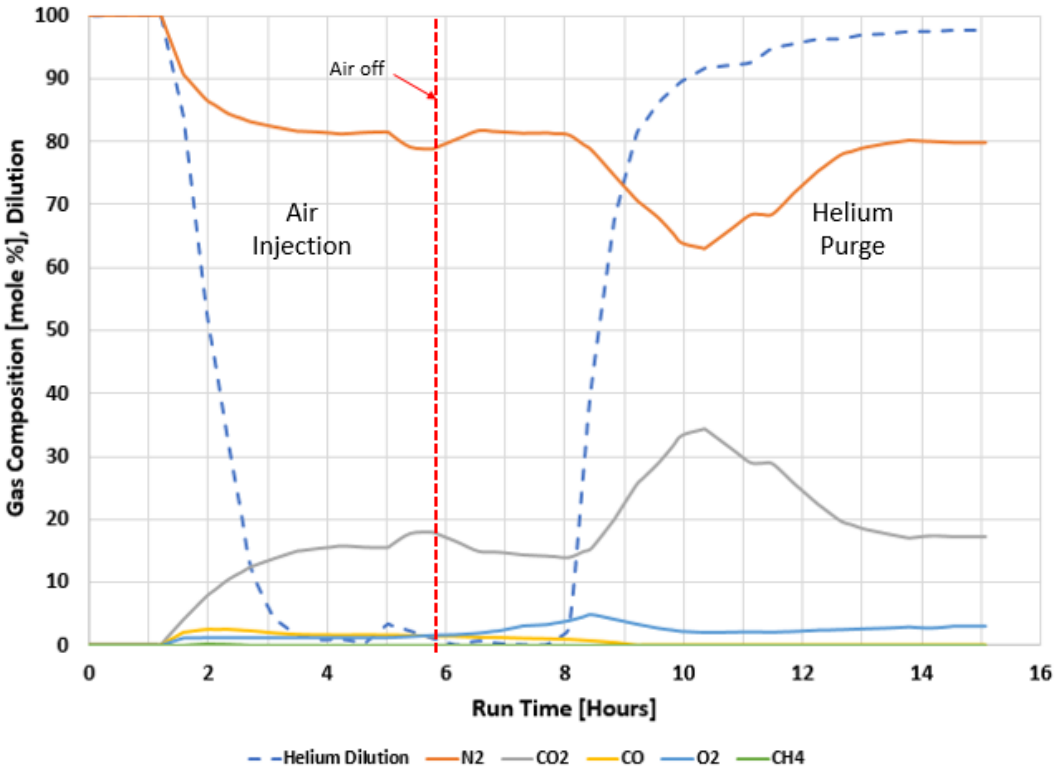

Test One

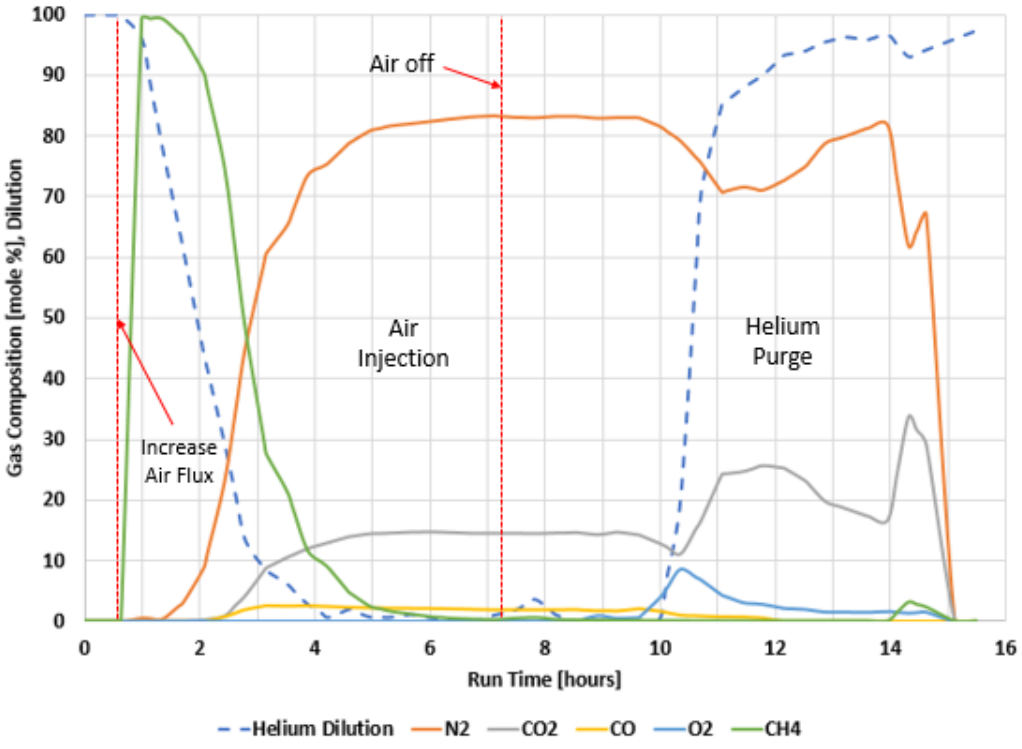

Test Two

Figure 6.5 Produced Combustion Gas Composition.

Parameter [Units]	Test One	Test Two
Total Air Required [l(ST)]	1,305	1,554
Measured Air Feed [l(ST)]	1,304	1,554
Measured Oxygen Feed [l(ST)]	284.5	357.4
Measured Nitrogen Feed [l(ST)]	1,020	1,197
Total Volume of Produced Gas (He free) [l(ST)]	1,260	1,655
R	3.58	3.35
Total Volume of Produced Gas (He included) [l(ST)]	3,540	3,572
Air/Fuel [m^3(ST)/kg]	11.1	11.0
O_2/Fuel [m^3(ST)/kg]	2.42	2.53
Air Requirement [m^3(ST)/m^3]*	129.70	160.57
Fuel Requirement [kg/m^3]*	11.66	14.52
Apparent H/C	1.11	2.05
Oxygen Utilization [%]	91.46	96.26
(CO_2+CO)/CO	11.18	8.17
(CO_2+CO)/N_2	0.21	0.20
Reacted Oxygen forming CO_x [%]	77.49	64.68
Total Hydrocarbon's Gas Production [g]	10.60	152.67**
Total Oil Consumed as Fuel [g]	117.20	143.19
Total Mass of Oil Produced as Gas [g]	127.80	295.86**

*Based on a burned volume of 10.1 x 10^{-3} m^3 (76% of the CT)
**Contains the volume of CH_4 injected (131 g)

Table 6.4 Overall Air-Fuel Calculations

where, $R = \frac{N_2 mole\ fraction}{O_2\ mole\ fraction}$ in the feed gas.

Component Production [l (ST)]		
	Test One	Test Two
O_2	24.29	13.34
N_2	1,019.97	1,196.66
CO	18.65	28.68
CO_2	191.48	207.19
CH_4	0.09	*204.27
C_2H_4	0.11	0.31
C_2H_6	0.11	0.13
C_3H_6	0.00	0.10
C_3H_8	0.40	0.02
C_{4+}	3.22	1.90
H_2	2.08	2.25
H_2S	0.00	0.00

* Contains the volume of CH_4 injected.

Table 6.5 Volume of Produced Gases.

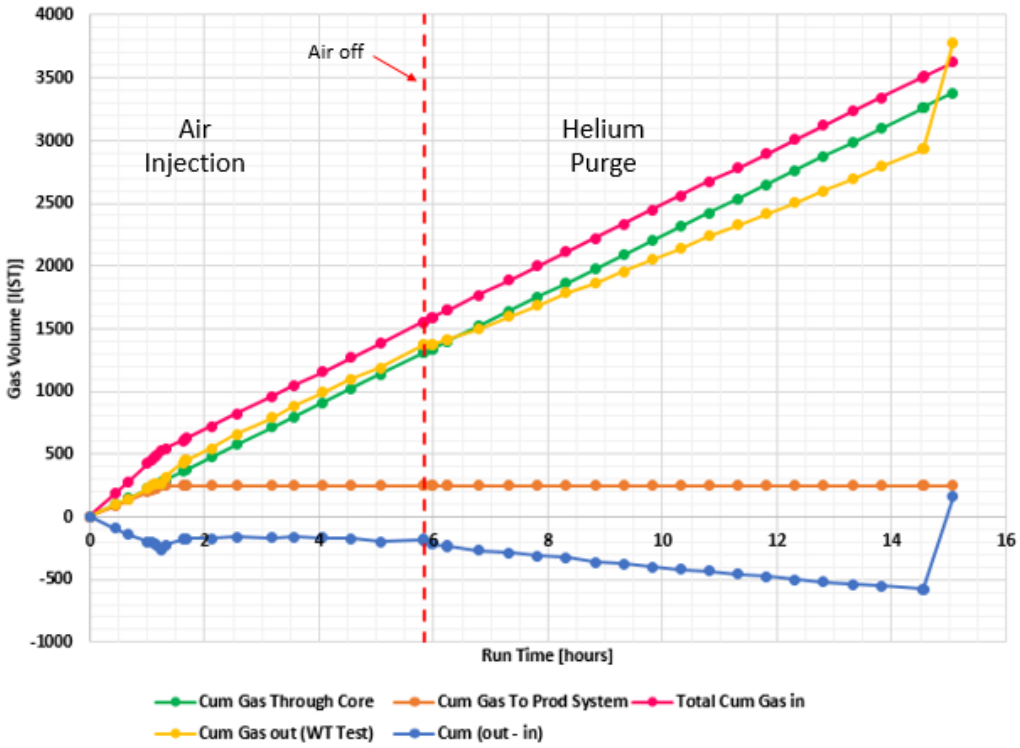

Test One

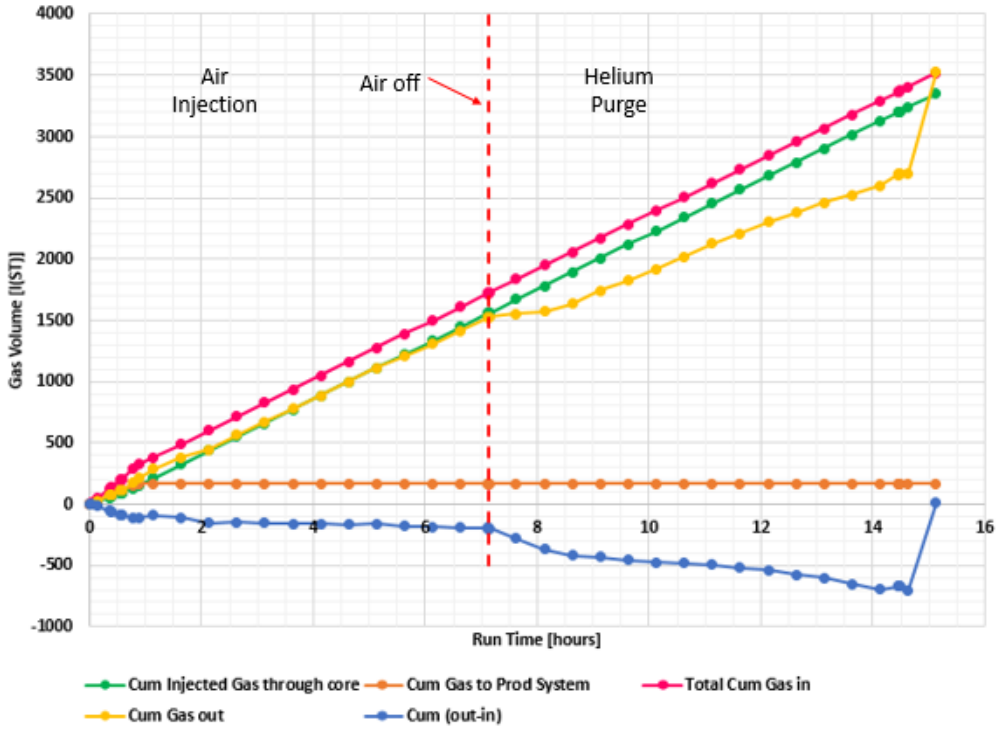

Test Two

Figure 6.6 Gas Balance. Cumulative Volumes

The liquid production after the helium purge for Test one was 2,600 g of oil and 1,590 g of water, while for Test two it was 1,223 g of oil and 1,440 g of water. Figure 6.7, shows the summary for both tests. As has been described previously, there was a problem draining the high-pressure production trap for Test two. The high-pressure trap was flooded when a slug of liquid was displaced from the core prior to 7.2 run hour, and it was not possible to produce this liquid without totally interrupting the flow of gas through the back-pressure valve. For Test two, the fluid sample masses for the samples collected in glass bottles at 7.13, 12.22 and 13.30 run hours were all assigned a time of 7.13 for arrival in the high-pressure production traps. The modified production profiles for Test two are shown in Figure 6.7 with dotted lines while the observed production profiles are shown with solid lines. The, as measured, curves for cumulative liquid production for Test one and the modified production curve for Test two are plotted against the pore volume of gas injected at reservoir conditions in Figure 6.8.

Analyzing Figure 6.8, it is appreciated that for Test one, which had a higher content of oil and water, most of the liquids were produced before the air was shut down. After the air was switched for helium, the content of oil left in the core was less. This was the expected behavior, while for Test Two, as it has mentioned before, there was a problem draining the HPS, so the dashed lines are the assumption of how the liquid production was expected, which would have been before switching the air off. Due to this the oil and water bank cannot be reported as accurate representation. Actually, the precise location and time of when the oil bank broke through is unknown, but the corrected oil production number at three pore volumes (7.13 hours) is qualitatively correct based on the observed flooding of the production traps.

Table 6.6 presents the stable product gas composition corresponding to the portion of the test where the combustion tube front propagation rate and the product gas composition were stable. As shown in Figure 6.5, for Test one the composition of the produced gas was stable during the GC period 3.5 to 5.1 hours and again for the GC period of 6.2 to 8.0 hours, as for Test two the stable product gas composition period was between 5.5 to 9.5 GC hours. Note that the times reported for the gas compositions are GC sample times and they have not been adjusted for the delay time between when the gas is produced within the core (assumed to be the time that the reaction front is at the location of the leading edge of the combustion zone) and the time that the gas produced in the core is analyzed by the GC. For combustion tube tests, the delay time is very difficult to predict, but the time between when the injection gas is switch from air to helium and the time that helium is then detected by the GC is used to estimate the stabilized run period from a combustion front velocity perspective that corresponds to a stabilized product gas composition. The run time periods assumed to represent periods of stabilized combustion front velocities are shown in Tables 6.6 and 6.7 as are the GC time periods corresponding to the stabilized product gas compositions.

The stable parameters reported in Tables 6.6 and 6.7 indicate that both tests exhibited good burning characteristics. As the injection air flux was 30.0 $m^3(ST)/m^2h$ for both tests, the stabilized air and fuel requirements are proportional to the inverse of the combustion front velocity. Even though the average oil saturation for Test two was much less than

that for Test one, the stabilized velocity for Test two was only 27% higher than the front velocity for Test one during what is denoted as the stabilized period one. The combustion front velocity during stable period two of Test one was 0.124 m/h. This is not considered as the stabilized velocity for Test one, however indicated by the significant change in the front velocity, there was a change in the burn kinetics at 3.9 hours.

The parameters reported for stabilized period one for Test one are considered to be more representative of the parameter that will be experienced in a field project. The basis for making this recommendation is outlined in the following paragraph.

From Figure 6.9 it can be seen for Test one that oxygen break through occurred at approximately two hours and that it continued to be produced over the course of the test. The change in oxygen utilization can be seen from the differences in average oxygen concentration for stabilized periods one and two. It can also be seen from the change in stabilized oxygen utilization for the two periods. It is noted from Figure 6.7 for Test one that the time of the velocity change occurred was when the water bank was being produced. This suggest that the fluid saturation in the portion of the core swept during stable period two for Test one, would have been high and this may have contributed to the change in oxygen uptake kinetics that is reflected by the difference in gas phase parameters for stabilized period one and stable velocity period two of Test one. It is noted from the CO_2 production profile shown in Figure 6.9 for Test one that there was an increase in CO_2 production rate between 5 and 6 hours.

The change in the combustion kinetics cannot be overlooked, but the increased CO_2 production is believed to primarily associated with CO_2 dissolved in the produced water being released when the water was transferred from the high pressure to the low-pressure separator.

The air and fuel requirement parameters are the economic parameters that show the best comparison with field processes that are operating under conditions where bond scission or combustion reactions are the dominant mode of oxygen uptake. Based on the overall air requirements of 130 and 160 $m^3(ST)/m^3$ for Test one and two respectively, the highly fluid saturated core of test one performed better than the composite core for Test two. The higher overall air requirements for Test two is reflective of the total burn time for Test two being one and a half hours longer than that for Test one. When one compares the stabilized air requirements for stabilized period one for Test one (107 $m^3(ST)/m^3$) with the stabilized value for Test two (136 $m^3(ST)/m^3$), the 27 percent increase in air requirements (as indicated previously based on the stabilized front velocities) is not an unexpected difference based on the significant difference in the nature of the core pack fluid saturations.

It is noted from Table 6.7 that stabilized air/fuel ratios for Test one (stable period one) and Test two are similar, hence the fuel requirements for the two tests of 9.9 and 12.5 for Test One and Two, respectively directly reflect the difference in air requirements.

Additional difference between the stabilized parameters for the two tests are seen in the oxygen utilization and in the apparent atomic H/C ratios (1.23 for Test one and 2.25 for

Test two) which are reflected in the percent conversion of reacted oxygen converted to carbon oxides (75.5% for Test one and 62.64% for Test two). The apparent H/C ratios and percent reacted oxygen converted to carbon oxides provide essentially the same information which is that more oxygen was consumed during Test two by oxygen addition (LTO) reactions. It is recognized that LTO reactions are not as effective at mobilizing oil as compared to HTO reactions. Although Test two took 1.5 hours more to reach TC 26, both Tests showed good oxygen utilization during the air injection periods.

The CO_2 production curve for Test one as shown in Figure 6.9, shows three slopes. As indicated previously, the CO_2 production rate changed around hour five, and again when the switch from air to helium occurred. During the helium purge, the rate of production of product gas dropped in response to increased storage of gas within the core associated with cooling temperatures (Figure 6.6). Once helium broke through (see Figure 6.5), the rate of CO_2 production dropped in response to the reduction in total produced gas flow rate, the increasing helium dilution, and the decreasing oxygen concentration, as helium invaded the reaction zone. For Test two, the cumulative CO_2 production versus time curve is linear, hence there is no apparent change in the reaction kinetics. The CO_2 production rate is lower after the switch to helium injection. The low production CO_2 rate, immediately following the switch injection gas to helium relates to the problem with the valve withdrawing liquid production from the high-pressure trap.

For Test one around 7 to 8.5 hours of run time the production of unreacted O_2 increased. The reduction in O_2 utilization is one of the reasons why the apparent air requirements for stable period two is higher than that for stabilized one. The other reason is that once helium injection commenced and the subsequent reduction in the product gas flow rate, the O_2 flux within the reaction zone will be significantly lower than the injection O_2 flux. Since the stabilized oxygen requirement are based on the injection air flux (rather than the effective, because of possible change in the O_2 concentration, air flux in the reaction zone), the change in oxygen storage within the swept zone of the core will significantly impact the apparent air requirements when they are based on the injection gas flux.

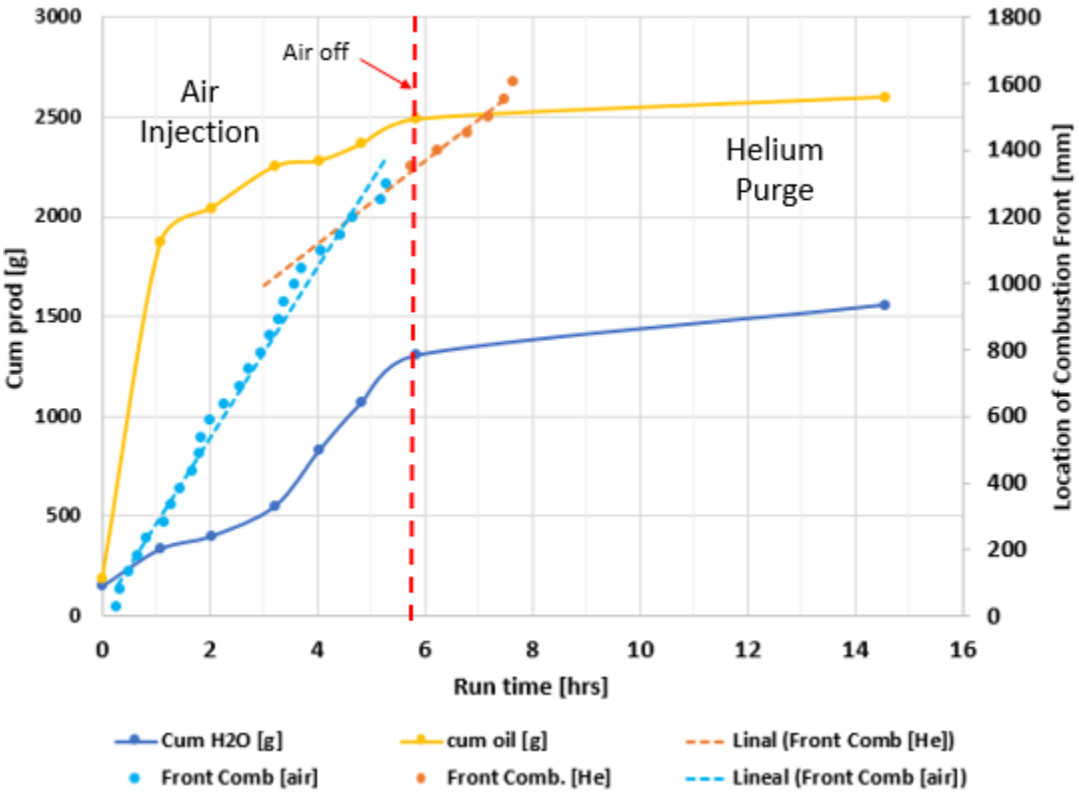

Test One

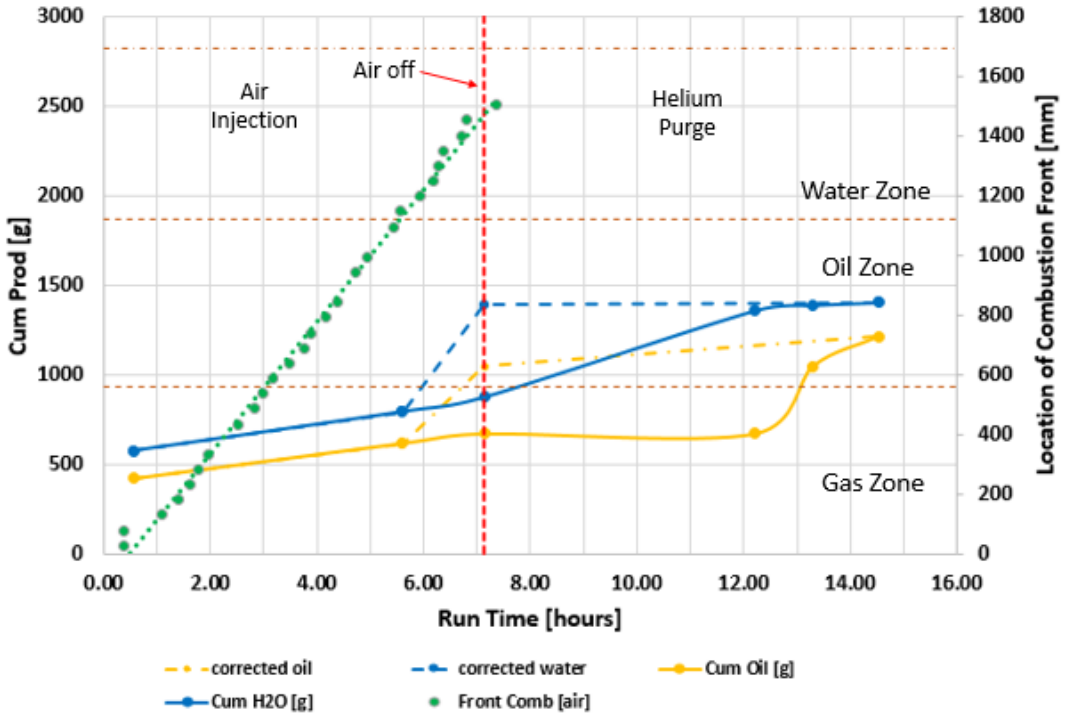

Test Two

Figure 6.7 Cumulative Production Masses of Oil and Water and Location of Combustion Front

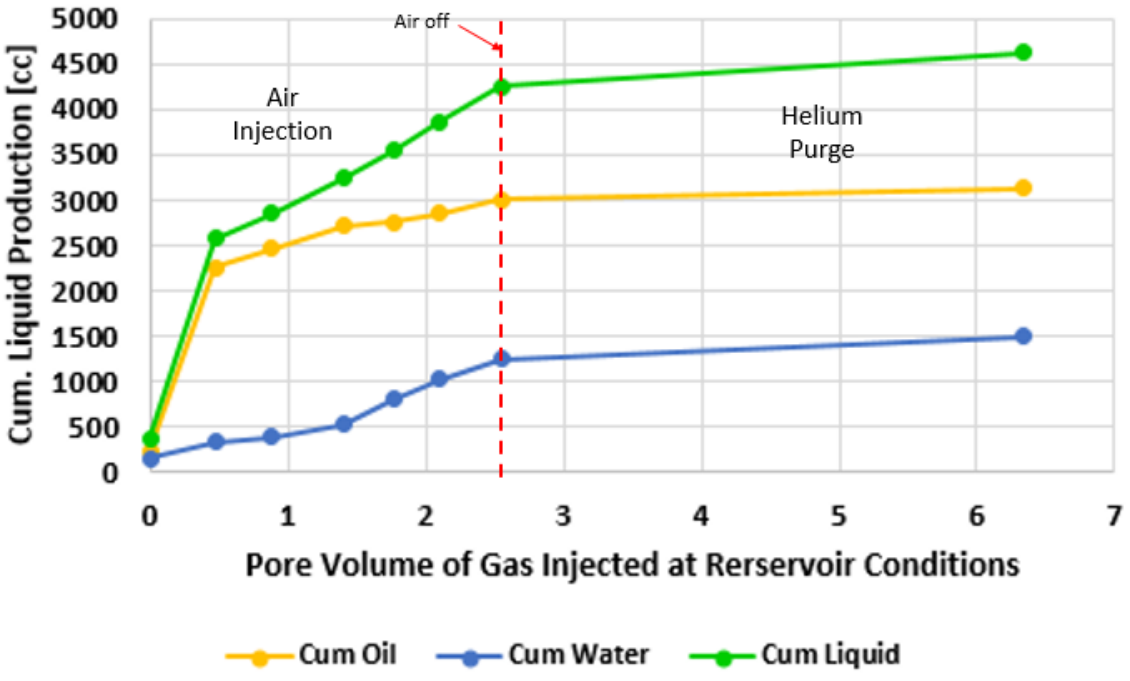

Test One

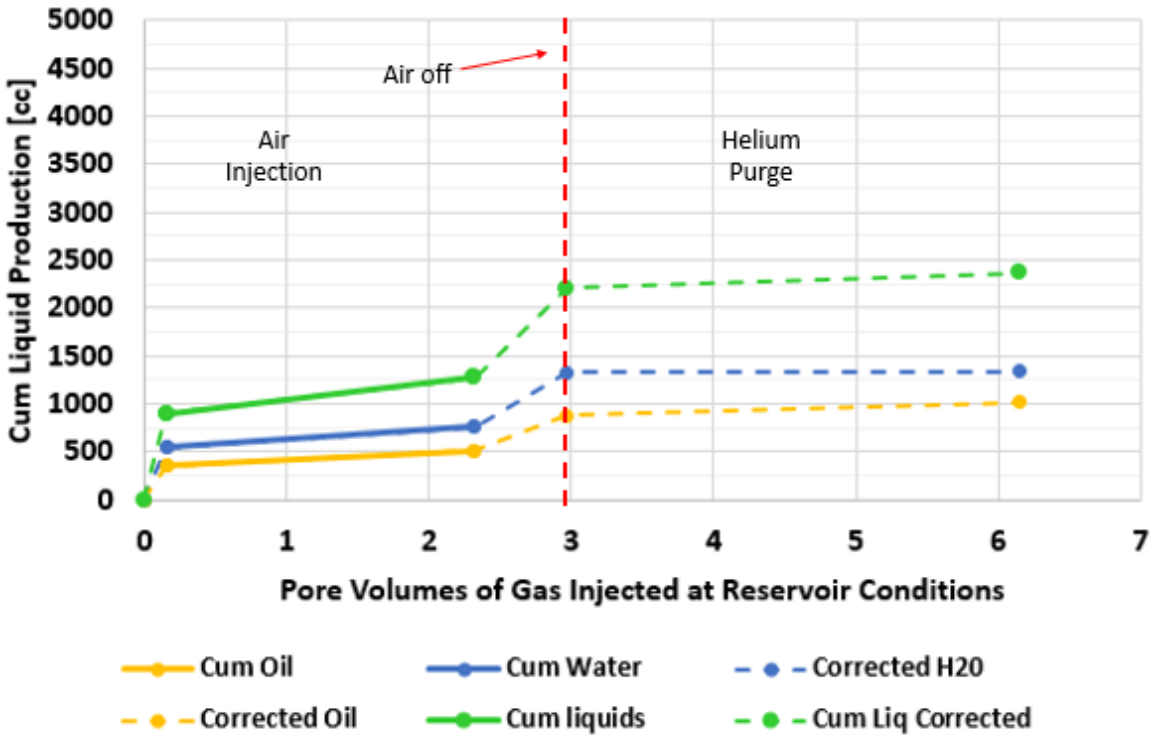

Test Two

Figure 6.8 Cumulative Liquid Production Based on Pore Volumes Injected

	Test One		Test Two
	Stabilized Period 1	Stable Period 2	Stabilized Period
Air Flux [$m^3(ST)/m^2•h$], [$scf/ft^2•h$]	30.0	----	30.0
Time Interval by 220°C Front Velocity [hour]	0.5 to 3.7	4.1 to 7.5	1.1 to 6.2
Gas Chromatograph Interval [hour]	3.5 to 4.7	6.5 to 7.8	5.5 to 9.5
Component	**Stabilized Composition [mole percent]**		
CO_2	15.42	14.40	14.46
CO	1.69	1.16	1.86
O_2	1.20	2.79	0.20
N_2	81.49	81.46	82.93
CH_4	0.00	0.00	0.37
C_2H_4	0.00	0.00	0.00
C_2H_6	0.00	0.00	0.01
C_3H_8	0.00	0.00	0.00
C_4+	0.03	0.02	0.00
H_2S	0.00	0.00	0.00
H_2	0.17	0.17	0.17

Table 6.6 Stable Product Gas Composition. Test One and Two

Combustion Front 220°C Leading Edge	Test One		Test Two
	Stabilized Zone 1	Stable Zone 2	Stabilized Period
Air Flux [$m^3(ST)/m^2•h$], [$scf/ft^2•h$]	30.0	----	30.0
Time Interval by Velocity [hour]	0.5 to 3.7	4.1 to 7.5	1.1 to 6.2
Gas Chromatograph Interval [hour]	3.5 to 4.7	6.5 to 7.8	5.5 to 9.5
Air Flux Location	Inlet	Inlet	Inlet
Air/Fuel Ratio [$m^3(ST)/kg$]	10.87	11.91	10.92
Combustion Front Velocity [m/h]	0.279	0.123	0.211
Air Required [$m^3(ST)/m^3$]	107.14	243.90	136.09
Fuel Required [kg/m^3]	9.86	20.49	12.46
Apparent Atomic H/C Ratio	1.23	1.27	2.25
Percent Oxygen Utilization	94.72	87.72	99.19
Percent Conversion of Reacted O_2 to Carbon Oxides	75.52	75.13	62.64
$(CO_2 + CO)/CO$ Ratio	10.12	13.41	8.77
$(CO_2 + CO)/N_2$ Ratio	0.21	0.19	0.20
N_2/O_2 Ratio	3.58	3.58	3.35

Table 6.7 Summary of Stabilized Combustion Parameters for Test One and Two

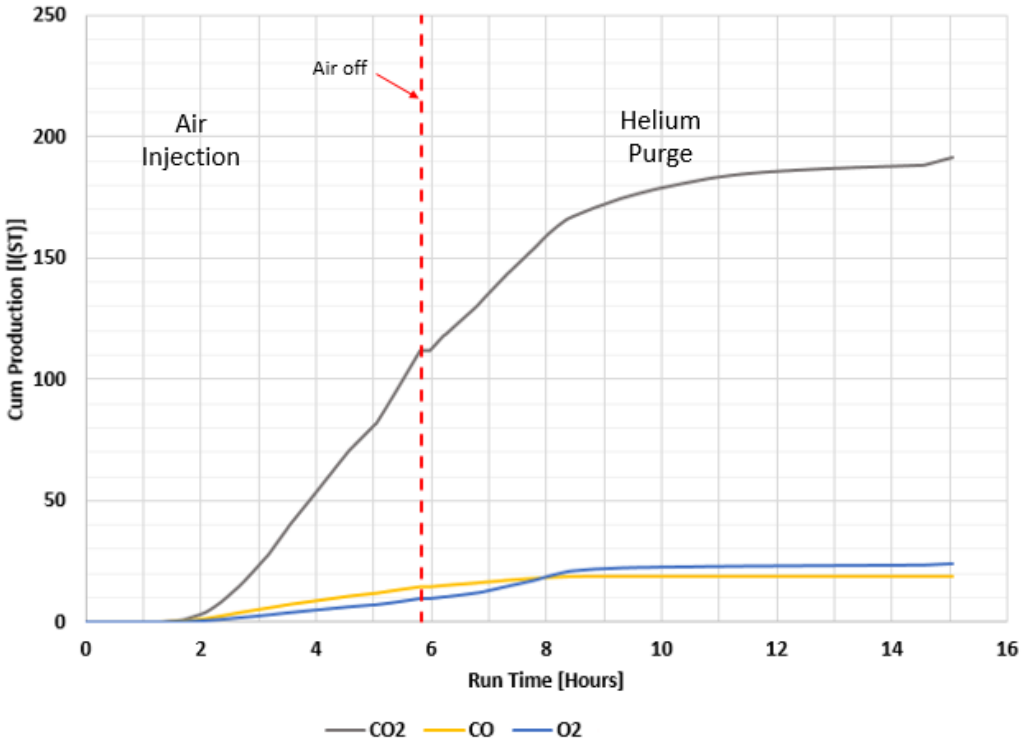

Test One

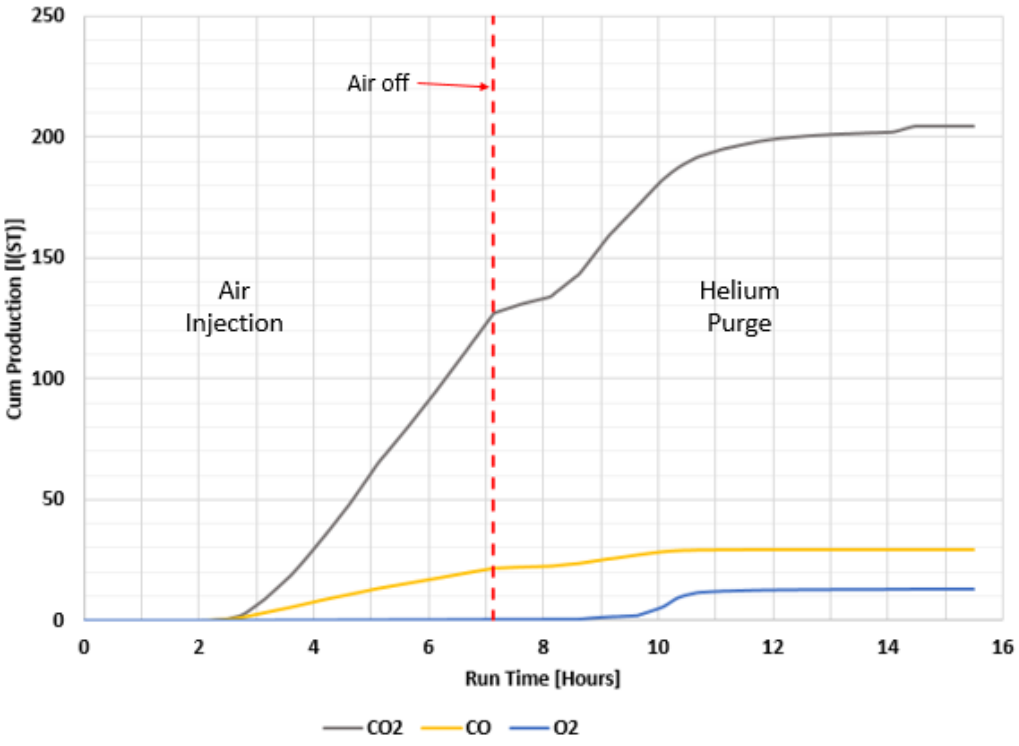

Test Two

Figure 6.9 Cumulative Combustion Gases for Test One and Two

6.1.3.2 Post Test Analysis and Material Balance

Figure 6.10 summarizes the residual mass concentrations in the post test crushed core samples showed in Tables 5.17 and 5.36, where it can be noted that the residual mass percentages were, from an overall point of view, very similar for both tests. Figure 6.11 shows the initial mass percentage of oil in the core plugs showed in Tables 5.4 and 5.5, as well as the final mass percentage of oil, water and coke in the post test core plugs showed in Tables 5.17 and 5.36, and the maximum temperatures to which they were exposed. Figure 6.10 and 6.11, show that the combustion front was highly effective at removing the hydrocarbons out of the core plugs and displacing the oil from the crushed core. For both tests, at the time when air injection was terminated and helium injection commenced, the leading edge of the combustion front reached TC 26 which was 1,295 mm from the injection end of the core. For Test one residual oil concentrations, up to 2.6 mass percent, were present from 1,397 mm (TC 28) to the core outlet, while residual water concentration up to 5 mass percent were present from 1,1944 mm (TC 24) to the core outlet. Coke concentrations present downstream from TC 28 were up to 0.67 mass percent. Residual oil remained on the core in those zones where the maximum temperatures were less than 300°C. For Test two a water bank between the locations of TC 18 (889 mm), and TC 25 (1,245 mm) had water concentrations up to 1.9 mass percent and a second water bank between TC 26 (1,295 mm) and the end of core with maximum levels approaching 5 mass percent. An oil bank from TC 29 (1,448 mm) to the core outlet had a maximum residual oil saturation of 2.6 mass percent. No coke was observed in the post test crushed core upstream of TC 12 (584mm). A maximum level of coke of 0.4 mass percent was located close to TC 26 where air injection was terminated. One exception to low coke concentration was observed in TC 9, but this was a very small sample (15.5 g) which was visually identified during unpacking.

The coke concentration after the test are not precisely known for dolomite cores, due to the presence of brine, which can alter/modify the “mass loss on ignition test” used to measure it. After the dried and extracted core and core plug samples were heated to 600°C for 16 hours, if any mass loss above the pre-determined blank was measured, it was assumed to be equal to the coke mass (toluene insoluble residual hydrocarbon) deposited on the core during combustion. For the current tests, which involved dolomite core the mass difference in the core plugs before and after ignition was around 23% and for the crushed cores was 22.5%. This type of behavior in dolomites has been studied by Olszak et al. (2015). He stated that when investigating the kinetics of thermal decomposition of minerals, as dolomites, the thermal decomposition can proceed in one endothermic step in air, nitrogen or CO_2 atmospheres. After calcination, the resultant oxides have lower molar volumes, larger surface area, and greater porosities than the calcium carbonate form. For a synthetic-ordered dolomite, the decomposition occurred in a two-stage process, the thermal decomposition of dolomite proceeds as follows:

$$CaMg(CO_3)_2 \leftrightarrow CaCO_3 + MgO + CO_2$$

$$CaCO_3 \leftrightarrow CaO + CO_2$$

Olszak et al. 2015 found that the mass loss is 23.87% in the first stage, and 43.97% in the second stage of calcium carbonate decomposition. The second stage of decomposition is reversible. The extent of the reversibility depends on the temperature.

Based in Olszak's studies, it was assumed that 22.5% of mass loss in the core was due to loss associated with the rock mineral in the crushed core and 23 mass percent loss for the plug cores, and the remaining difference was the coke reported. Figures 6.8 and 6.9 shows the schematic location of the core plugs, as well as the oil, water and coke mass percentages in each core plug for each test. As a reminder, air injection was shut down when air reached TC 26, located 1,299 mm from injection end.

Calculations were made of estimating how much CO_2 could be produced, assuming that 1 kg mole of $CaMg(CO_3)_2$ produces 1 kg mole of CO_2, then:

$$1kgmole\ CaMg(CO_3)_2 * \frac{184kg}{kg\ mole} \rightarrow 1kg\ mole\ CO_2 * \frac{23.644m^3(ST)}{kg\ mole}$$

184 kg $CaMg(CO_3)_2$ → 23.644 m^3 (ST) CO_2

$$1\ kg\ CaMg(CO_3)_2 \rightarrow \frac{23.644m^3(ST)}{184\ {}^{kg}/_{kg\ mole}} * \frac{1{,}000\ l(ST)}{m^3(ST)}$$

1 g $CaMg(CO_3)_2$ → 0.1285 l(ST)

For Test one the total original packed mass was 19,720.6 g of core and the unpacked mass was 19,673.1 g of core. The measured mass loss was therefore 47.4 g or 0.24 mass percent of the initial core mass. The volume of CO_2 that would be generated if the total mass loss was due to decomposition of the dolomite is

$$CO_2\ generated = (19{,}720.6g - 19{,}673.1g) * \frac{0.1285\ l(ST)}{g}$$

$$CO_2 generated = (47.5\ g) * \frac{0.1285\ l(ST)}{g} = 6.1\ l(ST) of\ CO_2$$

As for Test two, the original packed mass was 19,411.6 g and the unpacked mass was 19,381.2 g of core, hence the mass loss was 30.4 g or 0.16 mass percent.

$$CO_2 generated = (30.4g) * \frac{0.1285\ l(ST)}{g} = 3.9\ l(ST) of\ CO_2$$

While making the above calculations, it was recognized that some core mass can be lost during the unpacking operation, hence the predicted CO_2 generated due to core decomposition are order of magnitude only.

Table 6.8 shows the liquid balance for both tests, and it is appreciated that most of the initial liquids inside the core were displaced from the core due to the combination of the gas flood downstream of the combustion front and the displacement action associated with the combustion front. Small concentrations of oil and water remained in the post-test core but they were primarily downstream from the location which was swept by the combustion zone during the air injection period.

From Figure 6.11 it is appreciated that the embedded core plugs after Test one had no water saturation, while the embedded core plugs after Test two, experienced a high level of oil desaturation but they did have some water imbibed into them.

Even though the two CT tests were performed on light oil, due to oxidation reactions some asphaltenes were formed. This can be seen in Tables 5.21 and 5.38. Although, the amount produced is low, from these tables it is noticed that the overall asphaltenes' productions were 1.38 mass percent for Test one and 1.60 mass percent for Test two.

Table 6.9 summarizes the oil recoveries which were 91.7 and 79.45 mass percent of OOIP for Test one and Test two respectively. The lower oil recoveries reflect the lower initial oil saturation for Test two compared to Test one.

Tables 5.22 and 5.39 show that the pH of the original synthetic brine reduced dramatically for Test one for the brine produced when establishing the initial brine saturation and for the brine displaced during the initial oil flood. Produced water pH for the samples produced between 4.82 and 14.55 hours fell in the same range. The same behavior was observed for Test two for the last two sample bottles. pH values in the range of 4.39 to 4.65 relate to the HCO_3^{3-} concentrations. The reduced pH for the brine flood and oil flood is believed to be related to the sulfur content in the outcrop rock used. The rock was not tested for sulfur, but while the rock was being crushed a strong sulphur smell was detected. It is also apparent that for both tests the calcium did not increase for successive water samples collected, but magnesium, HCO^{-3} and SO_4^{2-} did increase in successive samples. The last samples had the highest values, although for Test one after the initial brine floods the pH showed the lowest value of 3.95 and the highest magnesium content of 1,800 mg/l.

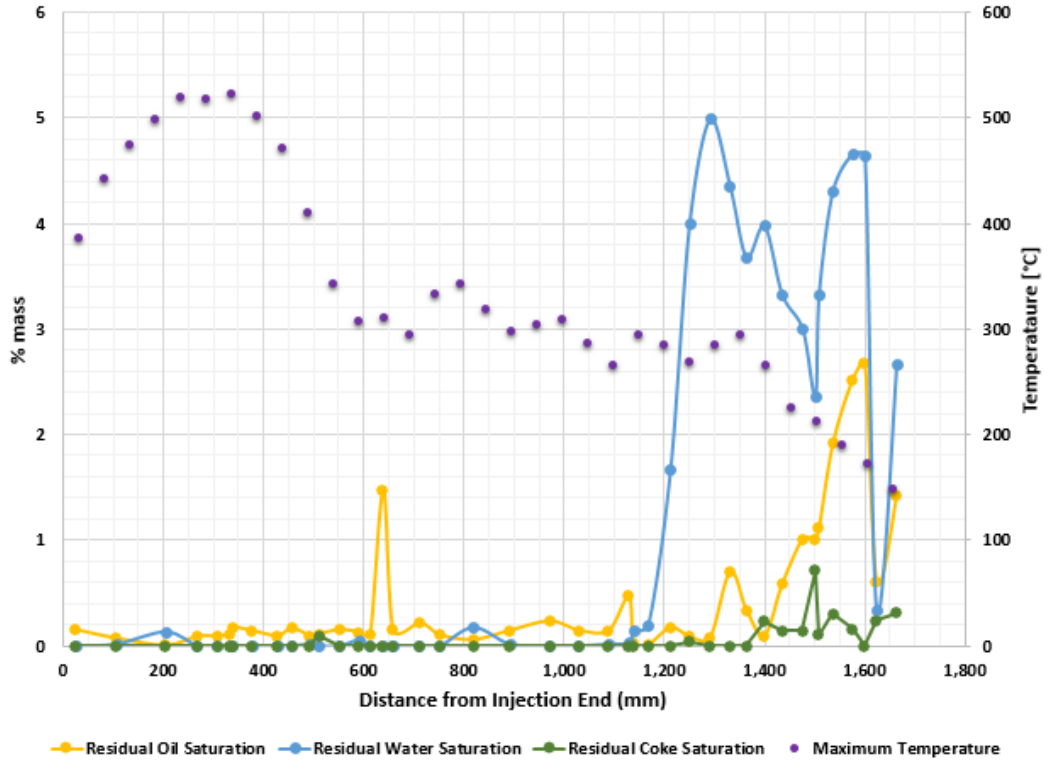

Test One

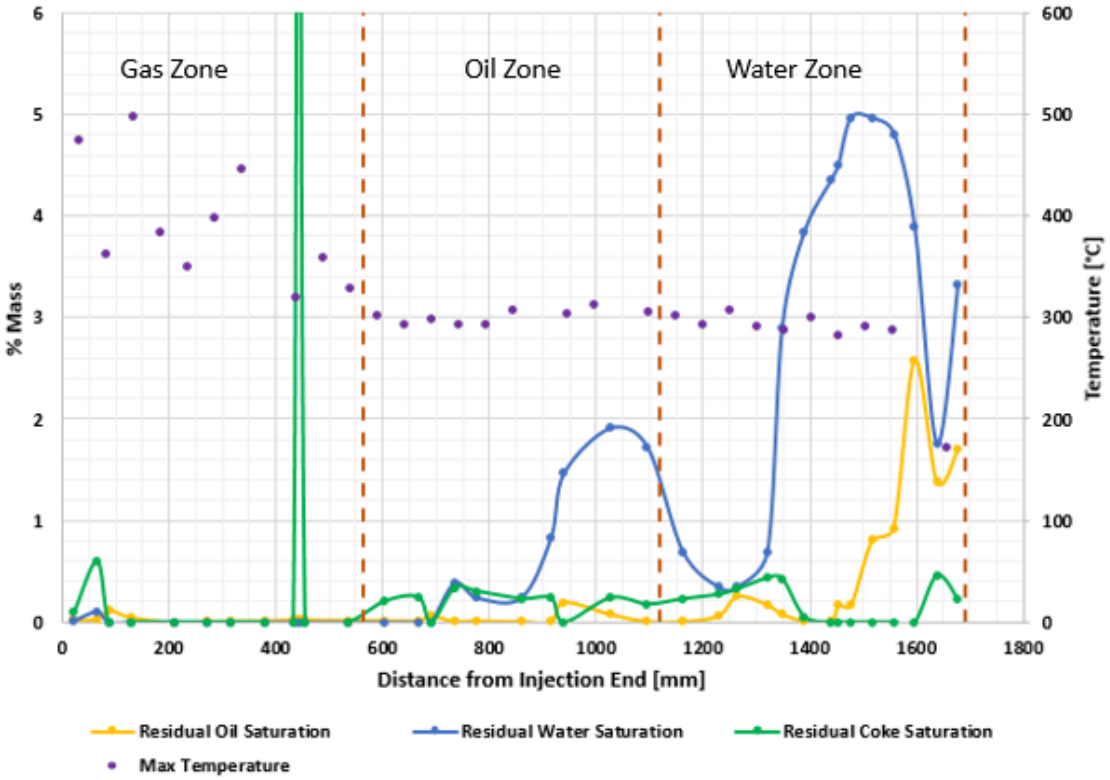

Test Two

Figure 6.10 Residual Oil, Water and Coke in the Post-Burn Crushed Core

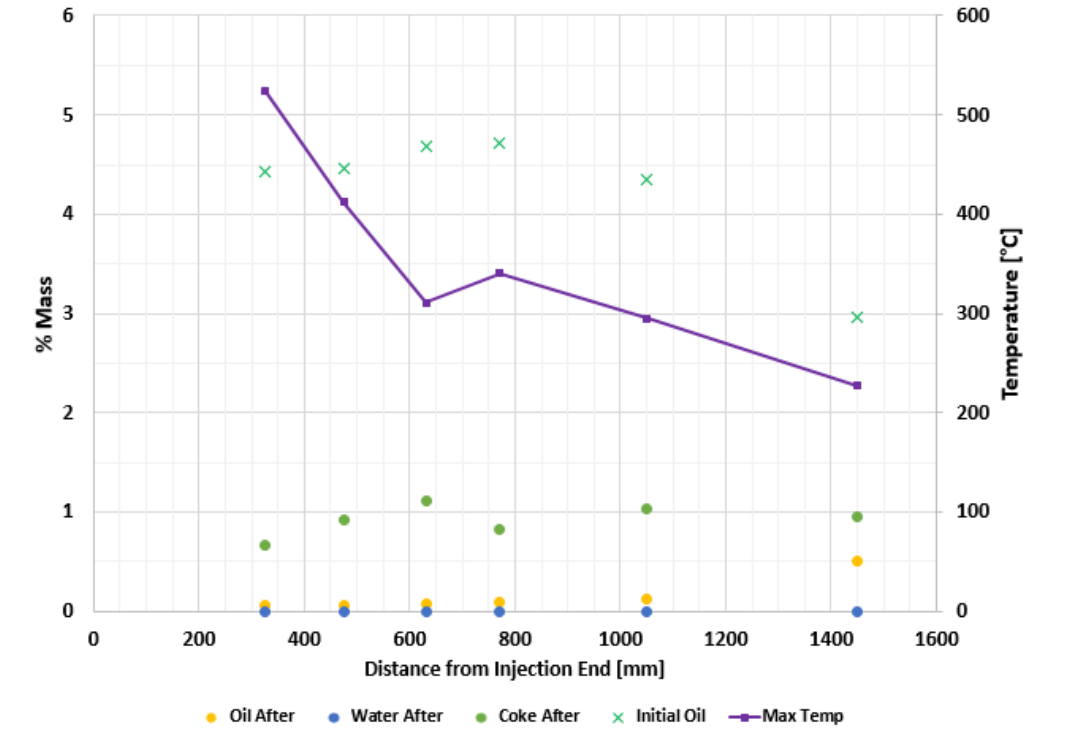

Test One

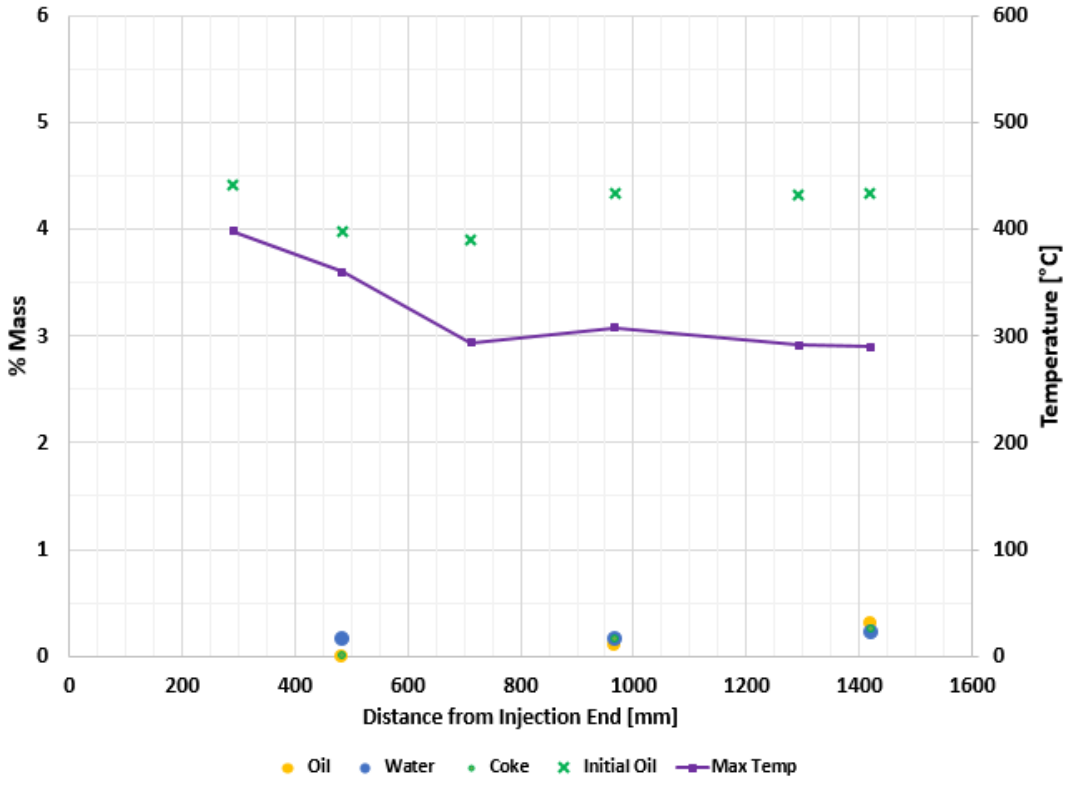

Test Two

Figure 6.11 Mass Saturation for Core Plugs Before and After Combustion Tests.

Oil Balance [g]	Test One	Test Two
Initial Oil in System	2,837.1	1,524.6
Oil Produced as Liquid	2,600.7	1,212.7
Oil Produced as Gas	117.2	142.6
Fuel Produced as Gas	10.6	155.7
Residual Hydrocarbon in Pack	83.0	90.9
Total Produced	2,811.5	1,601.9
Difference	25.6	-77.3
Percent Error	0.9	-5.0
Water Balance [g]		
Initial Water in System	1,704.5	1,575.3
Water Injected	0.0	0.0
Water Generated by Combustion	90.4	140.3
Total In	1,794.9	1,715.6
Water Produced as Liquid	1,554.8	1,405.1
Water Produced as Gas	22.0	18.9
Residual Water in Pack	232.8	241.7
Difference	-14.7	50
Percent Error	-0.8	2.9

Table 6.8 Liquid Mass Balance

The oil recoveries for each test are shown in Table 6.9, which are based in the OOIP

	Test One	Test Two
Initial Oil [g]	2,837.1	1,524.6
Produced Liquid Oil [g]	2,600.7	1,212.7
Recovery [%]	91.67	79.54

Table 6.9 Oil Recoveries Based on OOIP

CHAPTER 7

CONCLUSIONS

Two combustion tests were performed on a Mexican light oil at an air injection flux of 30 $m^3(ST)/m^2h$ at a pressure of 2,213 psia (15.26 MPa) and at the native reservoir temperature of 149°C, the highlights of the results and conclusions are as follows:

- The main difference between the two combustion tube experiments was the initial fluid saturations. For Test one the CT was saturated as a restored state core with oil and brine (liquids), while for Test two there were three saturation zones, which were premixed to represent the actual state with different fluid saturation zone in the reservoir (gas cap, oil interval and aquifer). Another main difference between the two tests was the size and the number of core plugs used. Test one involved seven core plugs of different sizes, while Test Two had six core plugs of the same size. The dolomite core plugs, pre-saturated with dead oil were placed at specific intervals in the recombined core pack, for both tests.
- The target Mexican reservoir is a NFR, due to this the core pack involved crushed outcrop rock core from a Mexican field which simulated in both tests the reservoir fractures, and core plugs bought in Texas simulated the matrix due to its lower permeability than the crushed outcrop core. The core pack ignited easily at 175°C and burned well at the 2,213 psia (15.26 MPa) test pressure.
- Both tests burned with an overall low air requirement of 130 $m^3(ST)/m^3$ for Test one and 161 $m^3(ST)/m^3$ for Test two. The overall oxygen utilizations were 91.5% for Test one and 96.3% for Test two, resulting in high oil mobilization and production.
- As is evident from the overall air requirement, the combustion front for Test two took more time to sweep the combustion tube. Test two required 1.5 more hours to reach TC 26, which was the pre-specified axial length of the core to be burned prior to terminating the air injection.
- Both tests were highly effective sweeping/pushing the original hydrocarbons out of the crushed core and core plugs. Test one showed two stable combustion front velocity periods, however, only the first period was considered to be representative of the stabilized velocity. Based on the first period the stable air requirements was 107 and the stabilized fuel requirement was 9.86 kg/m^3 of reservoir volume swept by the combustion front. For Test two just one stable velocity period was observed. Based on the air injection rate employed, the stable air requirement was 136 $m^3(ST)$ of air injected per m^3 of reservoir volume swept by the front, and the stabilized fuel requirement was 1.46 kg/m^3.
- Both tests showed a low concentration of water left in the burned core towards the production end. This portion of the combustion tube volume was swept during the helium purge.
- The residual content of fluids inside the core after combustion, were very similar for both tests, no matter the initial amount of fluid saturations.

- For Test two, there was a high level of oil desaturation from the embedded core plugs, however, it appears that some water imbibed into the core plugs.
- An important observation from Test two is the velocity of the 220°C location at the combustion front does not vary to a significant extent as the front moved through the simulated gas, oil and water zones.
- No H_2S was produce during both tests, although the original outcrop rock had a strong smell of sulphur and the crude oil had an initial sulfur content of 0.55 mass percent.
- The overall oil recovery based on the OOIP was 91.7% for Test one and 79.5% for Test two. The difference in oil recoveries is primarily a result in the lower oil saturation for Test two which was 35.1% compared to Test one with 67.3%.
- Based on the overall velocity of the combustion front, and produced gas composition history, there did not seen to be a strong effect on the burning performance between Test one which was intentionally fully saturated with liquids and Test two which had three saturation regimes.
- Based on the initial and final fluid saturations for both tests, it can be suggested that an EOR with HPAI for light oils and in particular for the Mexican target reservoir has good potential.
- The produced water came out with a lower pH than the original and with a higher content of magnesium, HCO^{3-} and SO_4^{2-}.
- The overall mass of asphaltenes produced in both tests was very low, showing a maximum of 0.34 mass percent of the oil sample in the second last collected sample for Test one, and 0.32 mass percent in one collected sample for Test two.
- Nitrogen oxidation was neglected in both tests because all combustion performance was lower than 1,000°C.

RECOMMENDATIONS

- Perform SARA tests on the crude oil, for better knowledge and understanding about the burning performance of the native Mexican oil and the specific SARA fractions that are responsible for asphaltenes produced during combustion of this light oil.
- Perform a mineralogy study on the rock used as core in the tests, in order to better understand the ionic composition of the produced water, as well as the dolomite rock decomposition under high temperatures.

APPENDIX A
PHOTOS FROM COMBUSTION TESTS

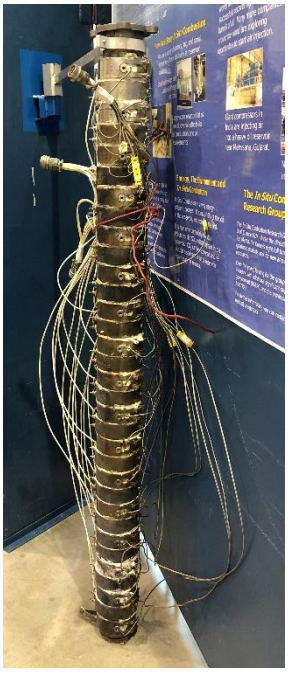

Photo 1. High Pressure Combustion Tube

Photo 2. High Pressure Combustion Tube's jacket with production system in the background (left photo) and jacket cap with flanges (right bottom).

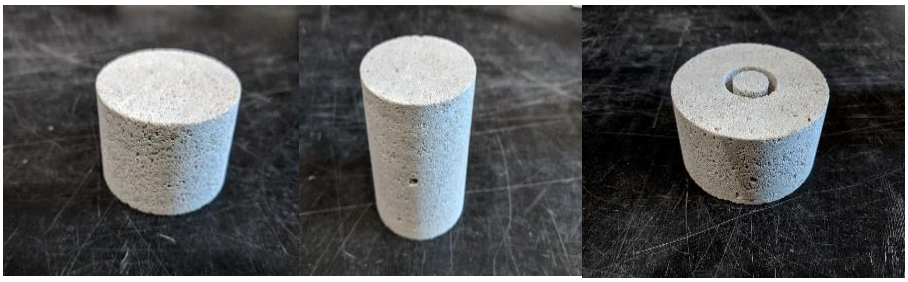

Photo 3. Core Plugs Prior to Oil Saturation

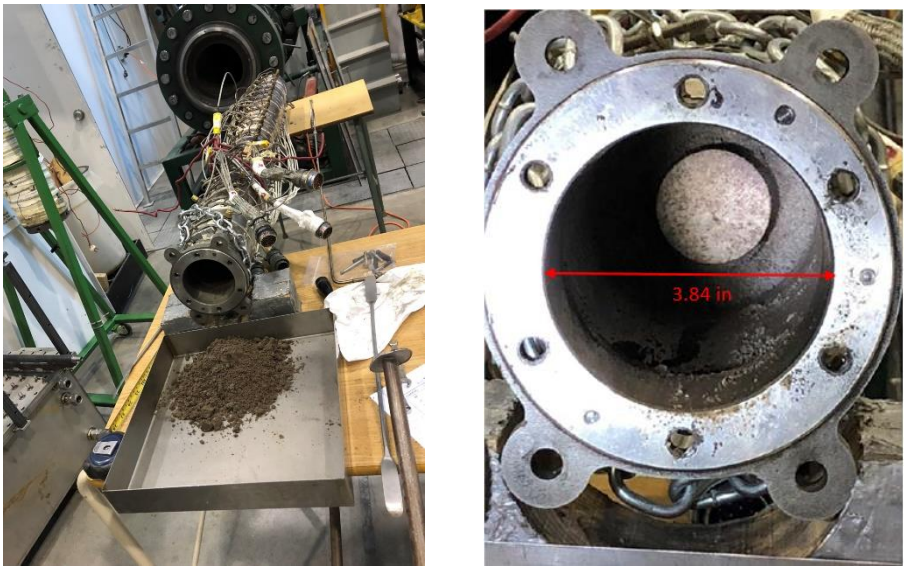

Photo 4. Crushed Core (left) and Core Plug (right) During Unpacking Combustion Tube Test One

Left – Core Plug #1. Located between TC 6 and 7.
Middle – Core Plug #6. Located at TC 22, which was drilled in the center to introduce the TC.
Right – Core Plug #7a. Located between TC 29 and 30.
Photo 5. Core Plugs after Combustion Test One, Prior to Extraction.

Photo 6. Core Plug #4 After Test One. Being Cut Dry Prior Extraction

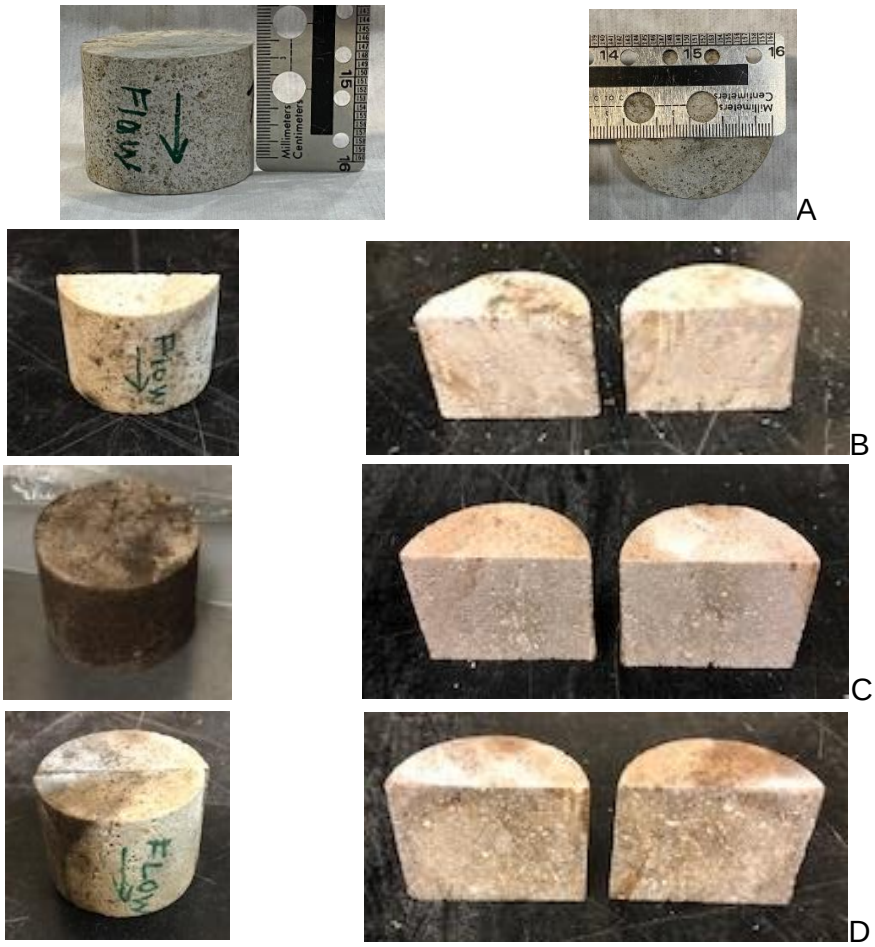

Top (A) – Core Plug #7. Located between TC 6 and 7.
Second (B) – Core Plug #9. Located between TC 9 and 10.
Third (C) – Core Plug #11. Located between TC 19 and 20.
Bottom (D)– Core Plug #16. Located between TC 28 and 29.
Photo 7. Core Plugs after Combustion Test Two, Prior to Extraction.

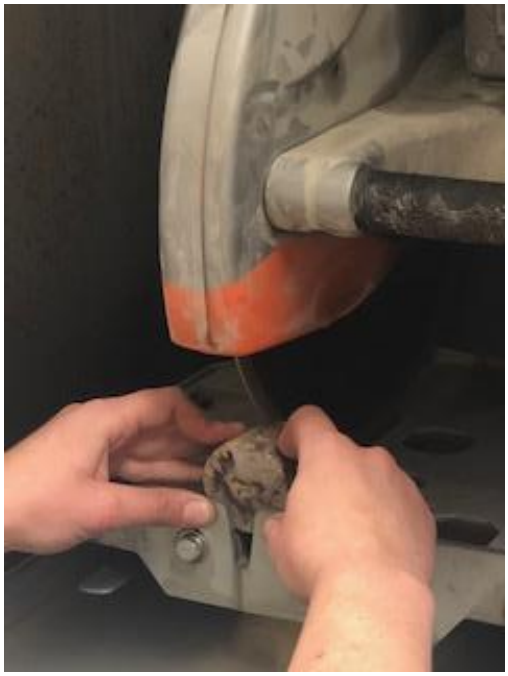

Photo 8. Core Plug #9 After Test Two. Being Cut Dry Prior Extraction

REFERENCES

Adegbesan, K.O., Donnelly, J.K., Moore, R.G., Bennion, D.W. (November, 1987) Low-Temperature-Oxidation Kinetic Parameters for In-Situ Combustion: Numerical Simulation. SPE Annual Technical Conference and Exhibition held in San Francisco, USA. SPE 12004-PA. 573 – 582 p.

Aguilera, R. (1995) Naturally Fractured Reservoirs. Second Edition, PennWell Brooks. Tulsa, Oklahoma.

Alexander, J. D., Martin, W. L., Dew, J. N. (1962). Factors Affecting Fuel Availability and Composition During In Situ Combustion. Society of Petroleum Engineers. SPE 296-PA.

Bae, J. H. (1977). Characterization of Crude Oil for Fireflooding Using Thermal Analysis Methods. Society of Petroleum Engineers. SPE 6173-PA

Balsamo, V., Phan, J., Nguyen, D. (2013) Effect of Diluents on Interfacial Properties and SAGD Emulsion Stability: II. Differential Scanning Calorimeter and Light Scattering Methods. SPE 165384.

Baños T., F.L., Sánchez R., C.A. (2009) Yacimientos Petroleros Debajo de la Sal. Thesis. Universidad Nacional Autónoma de México.

Benham, A. L., Poettman, F. H. (1958). The Thermal Recovery Process - An Analysis of Laboratory Combustion Data. Society of Petroleum Engineers. SPE 1022-G

Bhattacharya, S., Belgrave, J., Mallory, D.G., Moore, R.G, Ursenbach, M.G., Mehta, S.A., (2017) Investigation of Thermal Fingerprint in Accelerating Rate Calorimeter for Air Injection Enhanced Oil Recovery Processes. SPE 178095.

BjØrlykke, K. (2010) Petroleum Geoscience: From Sedimentary Environments to Rock Physics. Springer.

Bousad, I.S., Ramey Jr., N.J. (1968) Oxidation of Crude Oil in Porous Media. SPE 1937-PA.

Burger, J.G., Sahuquet, B. C. (1972) Chemical Aspects of In Situ Combustion – Heat of Combustion and Kinetics. Soc. Pet. Eng. J. 410-422 p. Tras., AIME, 253.

Burger, J. G., Sourieau P., Combarnous, M. (1985). Thermal Methods of Oil Recovery: Editions Technip, France, 430 p.

Chen, X. Chen, Z., Moore, R.G., Mehta, S.A., Ursenbach M.G., Harding, T.G. (2014) Kinetic Modeling of In Situ Combustion Process for Athabasca Oil Sands. SPE 170150-MS

Cinar, M., Castanier, A.R. (2008) Improved Analysis of Kinetic of Crude oil In-Situ Combustion. SPE 113948.

Clara, C., Durandeau M., Quenault, G. (1999) Laboratory Studies for Light Oil Air Injection Projects: Potential Application in Handil Field. SPE 54377

Crain, E.R (1986) Log Analysis Handbook. Tulsa, Oklahoma; PennWell

Dabbous, M.K., Fulton, P.F. (June 1974) Low Temperature Oxidation Reaction Kinetics and Effect on the *In Situ* Combustion Process. Soc. Pet. Eng. Journal. 253-262 p.

Danesh Ali (2003) PVT and Phase Behaviour of Petroleum Reservoir Fluids. ELSEVIER. Heriot Watt University. Edinburgh, Scotland.

Energy Information Administration (2007). Country analysis Briefs

Erickson, A., Legerski J.R.SR., Steece, F.V. (1994) An Appraisal of High Pressure Air Injection (HPAI) or In Situ Combustion Results from Deep, High Temperature, High Gravity Oil Reservoirs. Fiftieth Anniversary Field Conference. Wyoming Geological Association Guidebook. 259-270 p.

Fanchi, J.R. (2010) Integrated Reservoir Asset Management. Elsevier Inc.

Farouq Ali, S.M. (2012) Practical Heavy Oil Recovery. 132-139 p.

Fassihi, M.R., Brighman, W.E., Ramey Jr, H.J. (1984) Reaction Kinetics of In-Situ Combustion: Part I-Observations: SPE 8907-PA, Stanford University.

Fassihi, M.R., Yannimaras, D.V., Kumar, V.K. (1994) Estimation of Recovery Factor in Light Oil Air Injection Projects. SPE 28733

Fassihi, M.R., Yannimaras, D.V., Westfall, E.E., Gillham, T.H. (1996) Economics of Light Oil Air Injection Projects. SPE/DOE 35393

Fazlyeva, R. (2019) Heavy Oil Oxidation/Combustion in Vuggy Porous Media. Thesis. University of Calgary.

Germain, P., Geyelln, J.L. (1997) Air Injection into a Light Oil Reservoir: The Horse Creek Project. SPE 37782.

Gómez S., J.M. (2014) Perforación de un Pozo HPHT: Pache 13 uno de los Pozos mas Profundos de la Región Sur de México. Thesis. Universidad Nacional Autónoma de México.

Greaves, M., Rathbone, R.R, Fishlock, T., Ireland, R. (2000, January) Improved Residual Light Oil Recovery by Air Injection (LTO Process). Journal of Canadian Petroleum Technology. 57-61 p.

Griggs, D.T, Handin, J.W. (1960) Observations of Fracture and a Hypothesis of Earthquakes. Geological Society of America, Mem 9. 347 – 64 p.

Gutiérrez, D., Taylor, A.R., Kumar, V.K., Ursenbach, M.G., Moore, R.G., Mehta, S.A. (2007) Recovery Factors in High Pressure Air Injection Projects Revisted. SPE 108429

Instrument Specialists Incorporated http://instrument-specialists.com/products/thermal-analyzers/pressure-dsc/

Jia, N., Moore, R.G., Mehta, S.A., Ursenbach, M.G., Hancock, M. (June 2003). Kinetic Modelling of Thermal Cracking and Low Temperature Oxidation Reactions. Canadian International Petroleum Conference. University of Calgary. Paper 2003-214.

Lerner, S.L., Fleming G.C., Lara, P.F. (1985) Dominant Processes in In Situ Combustion of Light-Oil Reservoirs. SPE 12003-PA

Mace, C. (1975) Deepest combustion – West Heidelberg, Miss. Oil and Gas Journal, November.

Mallory, D.G., Modaresghazani, J., Ursenbach, M.G., Moore, R.G., Mehta, S.A. (2019) Accelerating Rate Calorimeter (ARC) Tests of Paché Field Oil and Core in Contact with Air. Final Report. University of Calgary.

McNaughton, D.A., Garb, F.A. (1975) Finding and Evaluating Petroleum Accumulations in Fractured Reservoir Rock. *Exploration and Economics of the Petroleum Industry*, Vol. 13. Matthew Bendor & Company Inc.

Mehta, S.A., Moore, R. G. (2018). Air Injection-Based Processes for Improved Oil Recovery. ENCH 647 Thermal Recovery Methods, University of Calgary. Calgary, Canada.

Moore, R. G., Bennion D. W., Belgrave J.D.M., Gie D.N., Ursenbach M.G. (1987). New Insights into Enriched Air *In Situ* Combustion: SPE 16740, Presented at the 62nd Annual Technical Conference and Exhibition of Dallas, TX.

Moore, R. G., Bennion, D. W., Ursenbach, M. G. (1988). A Review of *In Situ* Combustion Mechanisms. Fourth UNITAR/UNDP International Conference on Heavy Crude and Tar Sands, 775–784 p. Calgary, Canada.

Moore, R. G., Belgrave, J. D. M., Mehta, R., Ursenbach, M., Laureshen, C. J., & Xi, K. (1992). Some Insights Into the Low-Temperature and High-Temperature *In Situ* Combustion Kinetics. Society of Petroleum Engineers. SPE 24174-MS

Moore, R.G., Mehta, S.A., Ursenbach, G., Laureshen, C.J. (1998) Strategies for Successful Air Injection – Based IOR Processes. University of Calgary, Calgary, Alberta. Paper 1998-235

Moore, R.G., Ursenbach, M.G., Laureshen, C.J., Belgrave J.D.M., Mehta, S.A. (1999) Ramped Temperature Oxidation Analysis of Athabasca Oil Sands Bitumen. Journal of Canadian Petroleum Technology. Special Edition 1999, Volume 38, No. 13. Paper 95-23.

Moore, R.G., Mehta, S.A., Ursenbach M.G. (2002). A Guide to High Pressure Air Injection (HPAI) Based Oil Recovery. SPE 75207, University of Calgary.

Nelson, R.A. (1985) Geologic Analysis of Naturally Fractured Reservoirs. Gulf Publishing Company, Houston, Texas.

Nelson, T.W., McNeil, J.S. (1961) How to Engineer an In Situ Combustion Project. The Oil and Gas Journal, June 1961.

Olszak-Humienik, M., Jablonski, M. (2015) Thermal Behavior of Natural Dolomite. DOI 10.1007/s10973-014-4301-6

PEMEX (2018) Anuario Estadístico

Penberty, W.L., Ramey, H.J. (1966) Design and Operation of Laboratory Combustion Tubes. SPE. DOI 10.2118/1290-PA

Perry, R.H., Green, D.W., Campebell, J. M. (1960) Reverse Combustion – A New Oil Recovery Technique. SPE 1500-G, The U. Of Oklahoma, Norman, OK.

Poupon, A., Clavier, C., Dumanior, J., Gaymard, R., Misk, A. (1970) Log Analysis of Sand-Shale Sequences. A Systematic Approach. Journal of Petroleum Technology 22(7) 867-881. doi: 10.2118/2897-PA.

Prasad, R.S., Slater, J.A. (1986) High-Pressure Combustion Tube Test. SPE/DOE 14919.

Prats, M. (2005). Thermal Recovery. Monograph Vol.7, Society of Petroleum Engineers.

Ramey Jr, H.J. (1971) In Situ Combustion. Stanford University, California. SPE 14229.

Robinson, C., Smith D.B, (1984) Journal of Hazard Materials, Volume 8, Issue 3, Elservier Inc., p. 199-203

Salazar, M., Cabrera, J.R., Coletta, C.J., Holzberg, B., Balasejus, D., Cortes, C.A. (2009) Anisotropy Identification During a High-Pressure, High-Temperature (HPHT) Drilling Operation in a “Salt-Related” Structure – Real Case in South Mexico. SPE 122745

Sarathi, P (1999) In-Situ Combustion Handbook – Principles and Practices, DOE/PC/91008-0374, National Petroleum Technology Office. Tulsa, Ok.

Satter, A., Iqbal, G.M. (2016) Reservoir Engineering. The Fundamentals, Simulation, and Management of Conventional and Unconventional Recoveries. Elsevier Inc.

Shokoya, O.S., Mehta, S.A., Moore, R.G., Maini, B.B., Pooladi-Darvish, M., Chakma, A. (2001) Does Miscibility of *In Situ* Generated Flue Gases With Light Crude Oils Contribute to Oil Recovery Under High Pressure Air Injection?, Petroleum Society’s Canadian International Petroleum Conference 2001, Calgary, Alberta. DOE 2001-019

Snider, L.C. (1934) Current Ideas Regarding Source Beds for Petroleum. Problems of Petroleum Geology. Bulletin. AAPG. 51 – 66 p.

Tadema, H.J (1959) Mechanisms of Oil Production by Underground Combustion. Fifth World Pet. Cong., New York City, Paper No. 22, 279-287 p.

Thomas, E.C. (1992) 50Th Anniversary of the Archie Equation; Archie Left More Than Just an Equation. The Log Analyst.

Tiabb, D., Donaldson, E.C. (2004) Petrophysics. Oxford Elservier p.1 ISBN 0-7506-7711-2

Tiffin, D.L., Yannimaras, D.V. (1997) The In-Situ Combustion Performance of Light Oils as a Function of Pressure (1000 to 6000 psig). Tulsa, OK. Copyright by Marcel Dekker Inc.

Vossoughi, S., Willliite, G.P., Kritikos, W.P., Guvenier, I.M., El Shoubary, Y. (August 1982). Automation of an In-Situ Combustion Tube and Study of the Effect of Clay on the In-Situ Combustion Process. Soc. of Pet. Eng. Journal. 493-502 p.

Wendlandt, W.WM. (1974) Thermal Methods of Analysis. Second Edition. Volume 198. John Wiley & Sons

Yannimaras, D.V., Sufi, A.H., Fassihi, M.R. (1991) The Case for Air Injection Into Deep Light Oil Reservoirs. 6th European IOR symposium in Stavanger. P. 55-64.

Yannimaras, D.V., Tiffin D.L. (February, 1995) Screening of Oils for In-Situ Combustion at Reservoir Conditions by Accelerating-Rate Calorimetry. Symposium on Improved Oil Recovery, Tulsa, USA. SPE 27791.